Scuola Universitaria Superiore IUSS Pavia

Integrated Seismic and Energy Efficiency Renovation: From Regional to Building-level Strategies

A Thesis Submitted in Partial Fulfilment of the Requirements
for the Degree of Doctor of Philosophy in

EARTHQUAKE ENGINEERING AND ENGINEERING SEISMOLOGY

Obtained in the framework of the Doctoral Programme in
Understanding and Managing Extremes

by

Rita Monteiro Garcia Couto

November, 2025

Scuola Universitaria Superiore IUSS Pavia

Integrated Seismic and Energy Efficiency Renovation: From Regional to Building-level Strategies

A Thesis Submitted in Partial Fulfilment of the Requirements
for the Degree of Doctor of Philosophy in

EARTHQUAKE ENGINEERING AND ENGINEERING SEISMOLOGY

Obtained in the framework of the Doctoral Programme in
Understanding and Managing Extremes

by

Rita Monteiro Garcia Couto

Supervisors: Prof. Ricardo Monteiro
Prof. Rita Bento
Dr. Gianrocco Mucedero

November, 2025

ABSTRACT

The European residential building stock faces a dual challenge of widespread seismic vulnerability and significant energy inefficiency, particularly in Mediterranean countries where a large share of reinforced concrete (RC) buildings was constructed before the implementation of modern design codes and energy standards, leaving communities exposed to elevated safety risks, high energy consumption, and associated carbon emissions. Addressing these deficiencies is essential not only to improve structural safety, but also to reduce energy consumption, supporting climate change mitigation targets, and strengthening community resilience. In fact, earthquake-induced damage not only causes structural and economic losses, but also amplifies social inequities and environmental impacts, highlighting the multidimensional nature of seismic risk. Recognising the interconnected nature of these challenges, recent research has highlighted the need for integrated, multi-sectoral approaches to building performance upgrading.

To address these challenges, this study first develops a national-level prioritisation framework for mainland Portugal as illustrative case-study, combining indicators from three macro-sectors, namely seismic vulnerability, energy deficiency, and socioeconomic vulnerability. By leveraging recent fragility models, energy consumption data, and regional social indicators, the framework identifies the areas of greatest need for combined renovation efforts, providing actionable insights for resource allocation and equitable policy development aligned with national and European climate targets.

Then, to analyse specific priority areas more in detail and support efficient large-scale evaluations of building performance, the thesis proceeds with developing generalised storey loss functions (SLFs) and storey environmental impact functions (SEIFs) for poorly detailed RC buildings, typically the building class more in need for seismic renovation. Such storey-based functions are developed for typically existing RC buildings in Europe, built before the introduction of modern seismic codes. The storey-based methodology integrates building typology characterisation, identification of damageable components, fragility curves, and consequence functions for both repair costs and embodied carbon impacts. Country-specific adaptations for Portugal are also

derived using national cost conversion factors. Application to a case-study building confirms that the proposed storey-level functions provide rapid, reliable estimates of economic and environmental consequences while maintaining sufficient accuracy relative to more robust analysis.

At the building level, determining the optimal combination of seismic and energy interventions is complex, involving multiple technical, economic, social, and environmental decision variables. To facilitate practical decision-making, this study applies a multi-criteria decision-making (MCDM) framework to a case study RC school building. Twelve retrofit scenarios, combining four seismic and three energy retrofit interventions, are assessed under three climate zones and three seismic hazard levels. Both simplified practice-oriented seismic assessment methods, such as cloud-based capacity spectrum method (CB-CSM) and the Italian Sismabonus guideline, and detailed research-based procedures are used to estimate keys variables, including the annual probability of failure, and expected seismic and environmental impacts. Comparison of the resulting retrofit rankings demonstrates the reliability and applicability of simplified approaches for engineering practice while maintaining consistency with more detailed methods.

Together, these contributions deliver a coherent suite of methodologies supporting integrated seismic and energy retrofitting, scalable regional prioritisation, and simplified yet reliable, decision-making tools. The outcomes of this thesis enable policymakers and practitioners to implement more equitable, sustainable, and resilience-enhancing renovation strategies across diverse European contexts.

SOMMARIO

Il patrimonio edilizio residenziale europeo è caratterizzato da una duplice criticità: una diffusa vulnerabilità sismica e una marcata inefficienza energetica. Tale problematica risulta particolarmente rilevante nei Paesi mediterranei, dove una quota significativa degli edifici residenziali è stata realizzata prima dell'introduzione delle moderne normative di progettazione sismica e degli standard energetici. Ciò ha lasciato ampie porzioni di popolazione esposte a elevati livelli di rischio per la sicurezza, a consumi energetici elevati e alle conseguenti emissioni climalteranti. Risulta pertanto imprescindibile affrontare tali carenze non solo per aumentare la sicurezza strutturale, ma anche per ridurre i fabbisogni energetici, contribuire al raggiungimento degli obiettivi climatici e rafforzare la resilienza socio-territoriale. I danni indotti dai terremoti non si limitano a generare perdite strutturali ed economiche, ma amplificano anche le disuguaglianze sociali e gli impatti ambientali, evidenziando la natura intrinsecamente multidimensionale del rischio sismico. Alla luce dell'interconnessione tra queste sfide, la letteratura recente ha sottolineato la necessità di adottare approcci olistici e multisettoriali per il miglioramento e l'adeguamento prestazionale del costruito.

Per fronteggiare tali problematiche, questo studio ha sviluppato un quadro di prioritizzazione nazionale per il Portogallo, integrando indicatori provenienti da tre macrosettori: vulnerabilità sismica, deficienze energetiche e vulnerabilità socioeconomica. Attraverso l'impiego dei più recenti modelli sismici di danno–conseguenza, congiuntamente a dati sui consumi energetici e a indicatori sociali su base regionale, è stato possibile identificare le aree maggiormente critiche, ovvero quelle che evidenziano la necessità più urgente di interventi integrati di riqualificazione sismica ed energetica. Inoltre, si sono investigati diversi scenari di rinforzo sismico a scala regionale, per identificare gli impatti in termini di riduzione del rischio sismico. Tale analisi ha fornito elementi operativi utili per orientare l'allocazione delle risorse e la definizione di politiche di intervento eque e coerenti con gli obiettivi climatici nazionali ed europei.

Inoltre, al fine di supportare future valutazioni su larga scala delle prestazioni sismiche del costruito mediante un approccio computazionale meno oneroso, sono state sviluppate funzioni generalizzate di perdita di piano (Storey Loss Functions, SLFs) e

funzioni di impatto ambientale di piano (Storey Environmental Impact Functions, SEIFs) per edifici residenziali in calcestruzzo armato. La metodologia adottata ha integrato la caratterizzazione tipologica degli edifici, l'individuazione delle principali componenti strutturali e non strutturali, l'utilizzo di modelli di fragilità e le relative funzioni di conseguenza, considerando sia i costi di riparazione sia gli impatti ambientali. Ulteriori adattamenti specifici per il contesto portoghese sono stati ottenuti mediante l'impiego di fattori nazionali di conversione dei costi. L'applicazione delle funzioni a un edificio caso studio ha confermato che le stime ottenute consentono valutazioni rapide e affidabili delle conseguenze economiche e ambientali, mantenendo un livello di accuratezza coerente con analisi più dettagliate.

A livello del singolo edificio, la determinazione della combinazione ottimale di interventi sismici ed energetici risulta particolarmente complessa, poiché implica la valutazione congiunta di numerose variabili decisionali di natura tecnica, economica, sociale e ambientale. Inoltre, differenti condizioni climatiche e di pericolosità sismica possono comportare strategie di intervento ottimali diverse. Per supportare tale processo e investigare l'influenza delle diverse condizioni climatiche e di pericolosità sismica sulla strategia di rinforzo ottimale, è stato implementato un framework decisionale multicriterio (Multi-Criteria Decision Making, MCDM) applicato a un edificio scolastico in calcestruzzo armato. Dodici scenari di intervento, ottenuti combinando quattro strategie di miglioramento sismico con tre misure di riqualificazione energetica, sono stati analizzati considerando tre distinte zone climatiche e tre livelli di pericolosità sismica. Per la quantificazione delle principali variabili decisionali associate alle prestazioni sismiche, quali la probabilità annua di collasso, le perdite economiche e gli impatti ambientali attesi, è stato inoltre proposto un approccio mirato a supportare l'applicazione in ambito non scientifico, integrando e sfruttando metodologie semplificate disponibili in letteratura, così da ottenere stime affidabili con un onere computazionale ridotto. Parallelamente, approcci di tipo "research-based" sono stati utilizzati per confrontare i risultati ottenuti sia a livello delle variabili decisionali, sia in termini di ranking finale delle soluzioni di rinforzo. Il confronto ha evidenziato una buona coerenza tra i risultati derivanti dai metodi semplificati e quelli prodotti dagli approcci più complessi, confermando l'affidabilità e l'adeguatezza delle procedure semplificate per il loro impiego nell'ingegneria strutturale.

Complessivamente, i contributi di questa ricerca forniscono un insieme coerente di metodologie a supporto della riqualificazione integrata sismica ed energetica, della prioritizzazione nazionale su ampia scala e dell'adozione di strumenti decisionali semplificati ma affidabili. I risultati ottenuti offrono indicazioni utili a decisori politici e

professionisti per l'implementazione di strategie di rinnovo del patrimonio edilizio più eque, sostenibili e orientate al miglioramento della resilienza nei diversi contesti europei.

ACKNOWLEDGEMENTS

As the end of my PhD approaches, it would be impossible to not pause and acknowledge all those who made it possible.

Above all, no achievement in my life can be mentioned without acknowledging my parents. They have always encouraged me to aim higher and made sure I had everything I needed to get there. For this and for more, I am endlessly grateful.

As I stepped into the academic world, I was equally fortunate in those who guided me along the way. I would like to express my deepest gratitude to my supervisors, without whom this journey would not have been possible. To Professor Ricardo Monteiro, for his continuous guidance, and his constant encouragement to strive for excellence. His mentorship has left a lasting imprint on the way I approach research and problem-solving. To Professor Rita Bento, who highly contributed for my passion for the world of seismic engineering. Her expertise and dedication have been guiding me even before the PhD and her warmth and care extended well beyond the boundaries of academic life and for that I am especially grateful. To Dr. Gianrocco Mucedero, who was far more than a co-supervisor. A true mentor in every sense of the word, always approachable and generous with his time, offering not only invaluable research guidance but also enriching conversation about life and the many quirks of living in Italy.

A special appreciation also goes to Besim, for his incredible support throughout the PhD, both in terms of research problems, accurate music recommendation for every working mood, or complaining about the many struggles of PhD life. To Rita Peres, my first research colleague in Portugal, and now a friend, who enthusiastically convinced me to come to Pavia, a decision I will always be grateful for. And to Madalena, whose presence in my life has spanned more chapters than either of us probably expected. What started as an academic mentorship naturally grew into a true friendship.

Doing a PhD, especially abroad, goes way beyond research. It is also about the people you meet along the way, the ones who show up at the right moment, who make a foreign city feels like home, and who slowly turn the "saudades" from home into something softer, more bearable, and eventually into new memories worth missing. During my PhD

years in Pavia, I found that most people pass through briefly, friendships form fast and run deep, and then life inevitably pulls everyone in different directions. Yet, somehow, these fleeting encounters become lifelong bonds, and for that I am truly grateful. I am especially thankful to Başar, Bhanu, Diego, Giorgio, Mari, and Öykü, whose company has followed me since the first days in Pavia. To Lana, Nevena, and Maithree, for the conversations, the laughs, and the kind of support that goes beyond words and the unique way each one of them left a mark on me. To Savvinos, for being the perfect companion, especially on the ski slopes. And to all the others, who crossed my path through the PhD and left their mark in their own way: Cata, Mostapha, Ale, Vicky, Anirudh, Nesma, Karim, Sebastian, and Naveen.

To all my friends in Portugal, in particular Catarina, Mariana, Guga, Rita, Pipa, Cristiana, Carol, Batão, David, and Domi, who were not physically present in my daily PhD life, but constantly there in spirit, checking on me, and making the distance feel smaller. You always found new ways to stay close, even when we were thousands of miles apart.

And finally, Mouayed, my home away from home, my comfort when everything felt too heavy, and my celebration when everything felt just right. A constant through every challenge and every triumph. Thank you for being my anchor.

TABLE OF CONTENTS

LIST OF FIGURES

LIST OF TABLES

LIST OF SIMBOLS AND ABBREVIATIONS

A	Floor area (m^2)
AAEL	Average Annual Economic Loss
AACEL	Average Annual Carbon Emission Loss
$AACEL_{/bldg}$	Average Annual Carbon Emission Loss per Building
$AACEL_R$	Average Annual Carbon Emission Loss Ratio
AAEnL	Average Annual Energy Loss
$AAEnL_{/bldg}$	Average Annual Energy Loss per Building
$AAEnL_{/CDD}$	AAEnL normalised by the cooling degree days (CDDs)
$AAEnL_{/HDD}$	AAEnL normalised by the heating degree days (HDDs)
$AAEnL_R$	Average Annual Energy Loss Ratio
AALL	Average Annual Economic Loss
$AALL_R$	Average Annual Carbon Emission Loss
AAEI	Average Annual Carbon Emission Loss Ratio
AEC	Annual Energy Cost
ADO	Adobe
ADRS	Acceleration-Displacement Response Spectrum
AML	Lisbon Metropolitan Area
AHP	Analytic Hierarchy Process
APF	Annual Probability of Failure
AvgSA	Average Spectral Acceleration
BCJ	Beam-Column Joint
BOM-LCA	Bill of Materials Life Cycle Assessment
C	Collapse
CB-CSM	Cloud-Based Capacity Spectrum Method
CBR	Cost-Benefit Ratio
CDH	High Code Design Level
CDL	Low Code Design Level
CDM	Moderate Code Design Level
CDN	No Code Design Level
CEc	Carbon emission cost (€/kg)
c_f	Collapse factor
CFRP	Carbon Fibre Reinforced Polymer
C_i	Decision Variable i
Ci*	Relative Closeness

CLS	Collapse Limit State
CoV	Coefficient of Variation
CO_2e	Carbon Dioxide Emissions
C_{prod}	Labour Productivity of the Construction Sector
CR	Reinforced Concrete (building material classification)
C_{rel}	Daily relocation cost per person
C_{ret}	Retrofit cost
C_{repl}	Total replacement cost (€)
CSM	Capacity Spectrum Method
CDD	Cooling Degree Days
DGEG	Directorate-General of Energy and Geology (Portugal)
DLLS	Damage Limitation Limit State
DNO	Non-Ductile
DCR	Demand-Capacity ration
DS	Damage State
DHU	High Ductility
DUL	Low Ductility
DUM	Moderate Ductility
DTR	Damage-to-Repair Time Ratio
DV	Decision Variable
E	Unit energy cost (€/kWh)
EAC	Expected Annual Cost
EAD	Expected Annual Downtime
EAEL	Expected Annual Economic Loss
EAEI	Expected Annual Environmental Impact
EAL	Expected Annual Loss
EBCJ	Exterior Beam-Column Joint
EC8	Eurocode 8
EDP	Engineering Demand Parameter
EI	Environmental Impact
EIO	Economic Input-Output
EPBD	Energy Performance of Buildings Directive
EPC	Energy Performance Certificate
EPD	Environmental Product Declaration
$EP_{gl,nren}$	Non-renewable primary energy consumption (kWh/m^2/year)
ERA	Earthquake Risk Awareness
ERM	Energy Retrofit Measure
ESM	European Seismic Motion
ESHM20	European Seismic Hazard Model 2020
EU-SPI	European Social Progress Index

FC	Concrete Structural Floor System
f	Inflation rate
f_{lab}	Labour cost fraction
f_{mat}	Material cost fraction
$f_{m,p}$	Margins and preliminaries cost fraction
FR	Functional Recovery
FRP	Fibre Reinforced Polymer
FW	Wood Structural Floor System
GEM	Global Earthquake Model
GNI	Gross National Income
GRI	Green and Resilient Indicator
GVA	Gross Value Added
H	Storey level
HDD	Heating Degree Days
HDI	Human Development Index
HVAC	Heating, Ventilation, and Air Conditioning
IBCJ	Interior Beam-Column Joint
IDA	Incremental Dynamic Analysis
ICE	Inventory of Carbon and Energy
I_E	Energy performance indicator
IEI	Installation Environmental Impact
$I_{G,SVI}$	Global socioeconomic vulnerability indicator
$I_{I,E-G}$	Integrated energy-socioeconomic indicator
$I_{I,S-E}$	Integrated seismic-energy indicator
$I_{I,S-E-G}$	Integrated seismic-energy-socioeconomic indicator
$I_{I,S-G}$	Integrated seismic-socioeconomic indicator
IM	Intensity Measure
IPS	Infills, Partitions, and Services
IRA	Iterative Retrofitting Algorithm
I_S	Seismic risk indicator
LCA	Life Cycle Assessment
LCEI	Life Cycle Environmental Impact
LDUAL	Dual Frame-wall System
LFINF	Infilled Frame
LLRS	Lateral Load Resisting System
LSLS	Life Safety Limit State
LWAL	Wall Frame
MC	Maintenance cost
MCDM	Multi-Criteria Decision Making
MEI	Total Maintenance Environmental Impact

MEVI	Municipal Energy Vulnerability Index
MRF	Moment Resisting Frame
MSA	Multiple Stripe Analysis
MUR	Unreinforced Masonry
N_{bldg}	Number of buildings
NoC	Non-Collapse
NPV	Net Present Value
NUTS	Nomenclature of Territorial Units for Statistics
OLS	Operational Limit State
OOP	Out of plane
P	Seismic risk perception
PACT	Performance Assessment Calculation Tool
PB	Payback Time
PBEE	Performance-Based Earthquake Engineering
PEER	Pacific Earthquake Engineering Research Center
PEC	Primary Energy Consumption
$P_{entrapment}$	Entrapment rate
PFA	Peak Floor Acceleration
PGA_C	Capacity Peak Ground Acceleration
PGA_D	Demand Peak Ground Acceleration
PGA	Peak Ground Acceleration
$P_{i,24}$	Average number of occupants over 24 hours
$P_{lethal\|DS4}$	Probability of fatality given collapse damage state
$P_{LL\|entrapment}$	Loss of life given entrapment
PNEC	National Energy and Climate Plan (Portugal)
PP	Performance Point
PSD	Peak Storey Drift
PSHA	Probabilistic Seismic Hazard Analysis
RC	Reinforced Concrete
RCCF	Repair Cost Conversion Factor
RCJ	Reinforced Concrete Jacketing
ReT	Replacement Time
r	Discount rate
r_{lab}	Labour cost ratio (target vs. reference country)
r_{mat}	Material cost ratio (target vs. reference country)
r_{prod}	Labour productivity ratio
RNC	Roadmap for Carbon Neutrality
RO	Re-Occupancy
RSA	Regulamento de Segurança e Acções (Portuguese design code, 1983)

RSCCS	Regulamento de Segurança das Construções Contra os Sismos (1958)
RSEP	Regulamento de Solicitações em Edifícios e Pontes (1961)
$SA(T_1)$	Spectral Acceleration at Fundamental Period
SC-GHG	Supply Chain Greenhouse Gas Emission Factors
SD	Significant Damage
SDOF	Single Degree of Freedom
SEIF	Storey Environmental Impact Function
SI-LS	Building Safety Index (Life Safety)
SiP	Shelter-in-Place
SL	Service life (years)
SLC	Collapse Limit State (Italian code)
SLD	Damage Limitation Limit State (Italian code)
SLF	Storey Loss Function
SLO	Operational Limit State (Italian code)
SLV	Life Safety Limit State (Italian code)
SRM	Seismic Retrofit Measure
STJ	Steel Jacketing
SVI	Socioeconomic Vulnerability Index
TOPSIS	Technique for Order of Preference by Similarity to Ideal Solution
t	Planning period
T0	Impeding time
T_{el}	Elastic Period
Tgeo	Geometric mean period
T_r	Return period (years)
Tx	Fundamental period in x-direction
Ty	Fundamental period in y-direction
UNK	Unknown (building material classification)
URM	Unreinforced Masonry
$V_{S,30}$	Shear Wave Velocity at 30 m Depth
θ	Median value (fragility or consequence function)
β	Logarithmic standard deviation
β_{DS}	Dispersion due to damage state threshold uncertainty
β_{inter}	Inter-building dispersion
β_{intra}	Intra-building dispersion
β_T	Taxonomy-level dispersion fragility parameter
θ_T	Taxonomy-level median fragility parameter
ΔAAEL	Reduction in Average Annual Economic Loss

CHAPTER 1

Introduction

1 INTRODUCTION

1.1 MOTIVATION

Earthquakes undoubtfully pose a critical threat to modern societies, repeatedly exposing the vulnerability of the built environment and the consequences that follow. Past seismic events have shown that damage to buildings extends well beyond immediate structural losses: they disrupt communities, compromise essential services, generate substantial economic burden, and trigger environmental impacts. From a holistic perspective, seismic risk must be evaluated as a multidimensional problem whose impacts extend far beyond building damage, casualties, or direct economic losses. While these metrics remain essential for quantifying the immediate consequences of an earthquake, they represent only part of the overall risk. A comprehensive assessment of risk must also consider the underlying conditions of social fragility and community resilience, which strongly influence how populations absorb, respond to, and recover from seismic events (Carreño et al. 2012; Thomas et al. 2019). Socioeconomic vulnerability plays a crucial role in explaining why some communities experience the consequences of earthquakes in a more severe or disproportionate manner, despite being exposed to similar levels of hazard (Burton and Silva 2016). Environmental consequences further expand this multidimensional risk. For example, (Gonzalez et al. 2021) demonstrated that post-earthquake decisions in Christchurch largely overlooked environmental considerations, resulting in substantial embodied carbon losses. Similarly, the aftermath of the 2011 Great East Japan earthquake and tsunami released approximately 26 million tons of CO_2e, from housing reconstruction, debris removal and land conversion (Pan et al. 2014). Research quantifying average embodied carbon in building replacement found that the typical reinforced concrete building generates around 375 kg CO_2e/m^2, while reinforced masonry buildings generate around 420 kg CO_2e/m^2. At the European scale, embodied carbon resulting from post-earthquake repair and reconstruction amounts to 6.4 million tonnes of CO_2e per year, with the largest contributions coming from countries combining high seismic hazard and extensive vulnerable building stocks (i.e. Turkey, Italy, Romania, Greece, Spain, and Bulgaria) (Caruso et al. 2024). Moreover, beyond the direct embodied carbon losses from demolition, earthquake-triggered reconstruction generates cascading environmental consequences across extended supply chains and recovery processes. Therefore, integrating environmental impact assessment into seismic loss estimation is essential for guiding more sustainable and resilient planning. These cascading effects highlight the urgent need for a deeper and more holistic

understanding of seismic risk by not only quantifying economic losses but also incorporating human environmental and societal dimensions.

From both seismic and environmental perspectives, seismic risk can be expressed through the average annual economic loss and average annual environmental impact, which represent the expected yearly consequences of earthquake damage in monetary terms and embodied carbon, respectively. While substantial progress has been made in seismic loss modelling (FEMA 2003; Pagani et al. 2014; Gusella et al. 2025), particularly at the building level (FEMA 2018a, p. 1; Cosenza et al. 2018; Aljawhari et al. 2023a), few models are available to be used in large scale and in a simplified way. Storey loss functions (SLFs) (Ramirez and Miranda 2009; Shahnazaryan et al. 2021; Mucedero et al. 2024a), however, provide a useful mean to estimate relative losses within a building when only limited structural or component-level data are available, making them especially valuable for regional applications where detailed inventories are often lacking (O'Reilly and Shahnazaryan 2024). Nevertheless, although the SLF approach offers clear advantages, such as scalability and low data requirements, further work is required to expand SLF datasets to a broader range of building typologies and to systematically incorporate post-earthquake repair cost data. At the same time, although some studies have focused on quantifying the environmental impacts associated with earthquake damage (Aljawhari et al. 2024; Caruso et al. 2024), these approaches generally required detailed information on component quantities and repair cost, data that is often unavailable in large-scale. To address this limitation, (Simonen et al. 2018) developed a comprehensive framework to estimate the environmental impact of earthquake-induced damage by linking repair costs to environmental impacts through sector-specific EI factor, which quantifies EIs per unit of economic output. Nevertheless, this study is based on the US construction sector using dollars.

Recognising seismic risk as a multidimensional phenomenon also shifts attention towards the underlying conditions that amplify both its physical and societal impacts: the vulnerability of the built environment, which often dictates the scale and distribution of these cascading consequences. Focusing on the European built environment, a large share of the building stock, particularly masonry-infilled RC structures, was constructed following outdated design practices and are highly vulnerable to earthquakes. On top of it, around 75% of Europe's buildings are energy inefficient contributing substantially to the EU's total energy consumption and carbon emissions. These challenges are particularly significant in southern Europe, where a substantial portion of the existing building stock was constructed during the 1950s-1970s before modern seismic codes and energy standards were established (Ademovic et al. 2022). For example, more than

55% of the residential RC buildings in Italy were built without seismic provisions, and 88% of both masonry and RC buildings fail to meet modern energy requirements (Gkatzogias et al. 2023). Similar patterns exist in Portugal, Greece, Spain and other Mediterranean countries. As a result, a large share of the population lives in buildings that are simultaneously unsafe, energy-inefficient, and socially vulnerable, making these regions high-priority targets for renovation (Gkatzogias et al. 2022a). Achieving the ambitious targets of the European Green Deal and the Fit-for-55 package requires large-scale renovation efforts that address both seismic safety and energy performance (Pohoryles et al. 2022). Until recently, renovation efforts and related policies have focused predominantly on improving energy efficiency alone, driven by the immediate benefits in reducing heating and cooling demands, lowering household energy costs, and contributing to policy objectives. Energy-only upgrades lead to buildings that are thermally efficient yet remain unsafe where both human safety and prior investments are at stake. Likewise, seismic retrofit conducted without energy considerations miss the opportunity to align building renovation with climate targets and long-term performance improvements. In recent years, the scientific community has recognised the need to address these vulnerability dimensions together. Research on combined seismic and energy retrofitting has expanded rapidly, demonstrating clear benefits for structural safety, environmental performance, financial returns, and long term resilience (Caruso et al. 2021; Marini et al. 2022; Clemett et al. 2023). Among the recent research studies that have addressed the topic, some assessed the benefits of eliminating seismic and energy performance deficiencies of existing buildings through a single intervention (Takeuchi et al. 2006, 2009; Calvi et al. 2016; Manfredi and Masi 2018; Bournas 2018; Pohoryles et al. 2020; Marini et al. 2022) while others studied combined interventions (Clemett et al. 2023; Caruso et al. 2023b).

At a building level, a further challenge lies in the decision-making process regarding optimal renovation strategies. When a broad range of structural and energy retrofitting options are available to be integrated, it becomes crucial to employ decision approaches that can identify the most effective combination of retrofit solutions. Some of those methods, such as seismic resilience-based assessments (Cimellaro 2013), index-based methods (Requena-García-Cruz et al. 2020), cost-benefit analyses (Sousa and Monteiro 2018a), green and resilient indicator (GRI) (Calvi et al. 2016), or multi-criteria decision-making (MCDM) approaches, often consider a range of economic, social and technical decision variables (DVs) that are typically of interest to decision-makers when evaluating and selecting an option from a set of alternatives. For what concerns MCDM approaches, many studies have pointed out the advantages of this methodology on the

selection of seismic (Caterino et al. 2008; Asadi et al. 2019; Requena-Garcia-Cruz et al. 2022), energy (Daniel and Ghiaus 2023) or combined interventions (Caruso et al. 2021; Clemett et al. 2023). Indeed, by considering different decision variables, chosen to capture the essential aspects of the decision problem (e.g. economic costs, social benefits and technical feasibility), decisionmakers can make more informed and balanced decisions. Moreover, the need for context-sensitive, multi-criteria frameworks for integrated building renovation stems from the fact that optimal solutions vary across different regions, exposed to different levels of hazard and climate conditions.

Most methodologies used to estimate the decision variables related to the seismic performance of buildings rely on detailed, data-intensive procedures that usually require extensive information, significant computational resources, and specialised technical expertise. As a result, these approaches are difficult to apply at large scale, impractical for time-sensitive analysis, and largely inaccessible to practitioners or general decision makers. In turn, simplified approaches that are already available, despite their inevitable approximative nature, may provide a more accessible and efficient way to evaluate the performance of existing buildings, favouring the adoption of MCDM methods by practitioners, who usually need to make decisions in a short period of time with limited resources.

1.2 RESEARCH OBJECTIVES AND ORGANISATION

Given the limitations of currently available, highly detailed assessment methodologies, there is a clear need for approaches that balance accuracy, efficiency, and practical applicability. This dissertation aims to help fill this gap by developing streamlined, scalable frameworks that integrate seismic vulnerability, energy performance, and socioeconomic considerations, enabling more informed and equitable decision making. With a view to addressing the multidimensional challenges outlined in the previous section, the main objectives of this dissertation are summarised as follows:

1) Address the lack of integrated regional-scale methods for identifying priority areas for combined seismic and energy retrofitting, by formulating a framework that incorporates technical, socio-economic and equity criteria.
2) Support national- or regional-scale renovation planning by analysing how targeted interventions in the most critical regions and within them (on the most vulnerable building taxonomy classes), identified through a regional prioritisation framework, can alter and reduce seismic risk.

3) Overcome the limitations of existing refined loss assessment approaches, which are often building-specific and not scalable, by proposing generalised functions capable of estimating seismic economic and environmental impacts.
4) Understand how different seismic hazard levels and climate conditions affect and potentially alter the choice of the most suitable combined seismic–energy retrofitting alternatives for existing RC buildings, by employing an MCDM approach to account for technical, economic, environmental, and social trade-offs.
5) Bridge the gap between advanced academic methodologies and engineering practice needs, by developing a simplified, practice-oriented decision-making approach that can be applied by practitioners for real-world retrofitting projects.

Based on these objectives, the dissertation is organised in different chapters, each briefly outlined below and extensively based in published peer-reviewed journal articles:

- **Chapter 2:** a comprehensive framework is proposed and applied to characterise the seismic, energy and socioeconomic needs of the residential building stock across mainland Portugal, with the objective of identifying the regions of highest priority for combined renovation. An indicator-based approach is adopted to address such a complex goal, which is crucial for effective resource management and risk mitigation in an equitable manner. The employed multidisciplinary methodology is scalable to other countries or regions and shares, in fact, the principles of an analogous analysis carried out for the Italian residential building stock (Mucedero and Monteiro 2024a). By integrating indicators from the aforementioned seismic, energy and social sectors, the resulting prioritisation pattern identified the regions more in need for intervention and serves as a tool for policymakers and planners to make informed decisions and develop resilient and equitable response plans to reduce seismic risks and assist communities in coping with challenges related to energy inefficiency and socioeconomic disparities.
- **Chapter 3:** building on the findings of Chapter 2, which highlighted the regional disparities in Portugal and identified key areas for intervention in building retrofitting and renovation efforts across the country, Chapter 3 investigates the impact of retrofitting different building taxonomies, assessing both the financial return and the improvements in occupant safety. By quantifying these outcomes, this section provides a comprehensive understanding of the benefits associated with upgrading the building stock, thereby supporting informed decision-making and guiding national policies for sustainable, resilient and

equitable building renovations in Portugal. The evaluated retrofitting strategies include RC jacketing combined with FRP wrapping and steel jacketing combined with FRP wrapping, representing two feasible interventions for the Portuguese RC building stock.

- **Chapter 4:** following the need to develop regional assessment in terms of economic losses and environmental impacts in a faster and more efficient way, this chapter develops generalised storey loss and EI functions, SLFs and SEIFs, respectively, for different types of poorly detailed RC buildings. The methodology combines building typology characterisation, identification of damageable components, and the integration of state-of-the-art fragility curves with both repair cost and EI consequence functions. Regarding building characterisation, the focus is on buildings with none to limited seismic design, as these structures represent a significant portion of the existing European building stock. These generalised functions are then tailored to Portugal through the development of country-specific cost conversion factors, exemplifying their relevance to national applications. The same rationale and procedure can be applied to other European countries. To end this chapter, the applicability of the proposed SLFs and SEIFs is illustrated through a case study RC building, to which both the storey- and component-based approaches are applied.
- **Chapter 5:** building on the findings of the previous chapters and given that seismic and energy retrofit decision are sensitive to both hazard intensity and climatic conditions, this chapter investigates how changes in seismic hazard and climate influence the preferential ranking of combined seismic and energy retrofit alternatives, while also assessing the consistency between detailed and simplified seismic assessment methodologies. To this end, an RC building is used as a case study and assumed to be located in nine different sites with varying hazard levels and climatic condition. Subsequently twelve combinations of seismic and energy interventions are examined, and the optimal combined retrofitting intervention is evaluated following a previously validated MCDM framework. The considered seismic strategies include FRP, steel bracing, and viscous dampers, while the energy interventions range from roof insulation and LED upgrades to full envelope insulation and photovoltaic systems.
- **Chapter 6:** in this chapter, a brief overview of the main results obtained from Chapter 1 to Chapter 5 is presented, along with final remarks and suggestions for future works.

The main outputs of this dissertation, each directly linked to the objectives outlined above, are summarised as follows:

- A regional prioritisation framework integrating seismic, energy, and socioeconomic indicators, applied to mainland Portugal, producing district-level priority maps to guide renovation investment (Objective 1 → Chapter 2).
- A set of regional-scale renovation scenarios quantifying the seismic risk reduction and financial returns achievable through seismic retrofit across the Portuguese building stock (Objective 2 → Chapter 3).
- Generalised storey loss functions (SLFs) and storey environmental impact functions (SEIFs) for poorly detailed RC buildings, adopted to the Portuguese context throufh country-specific cost conversion factors (Objective 3 → Chapter 4).
- A multi-criteria decision making (MCDM) framework for the selection of optimal combined seismic and energy retrofit strategies, assessed across varying hazard and climate conditions (Objectives 4 and 5 → Chapter 5).
- A simplified practice-oriented seismic assessment procedure validated against detailed methodologies, demonstrating its reliability for engineering practice (Objective 5 → Chapter 5).

Figure 1.1 provides a graphical overview of the thesis structure and the connection between chapters.

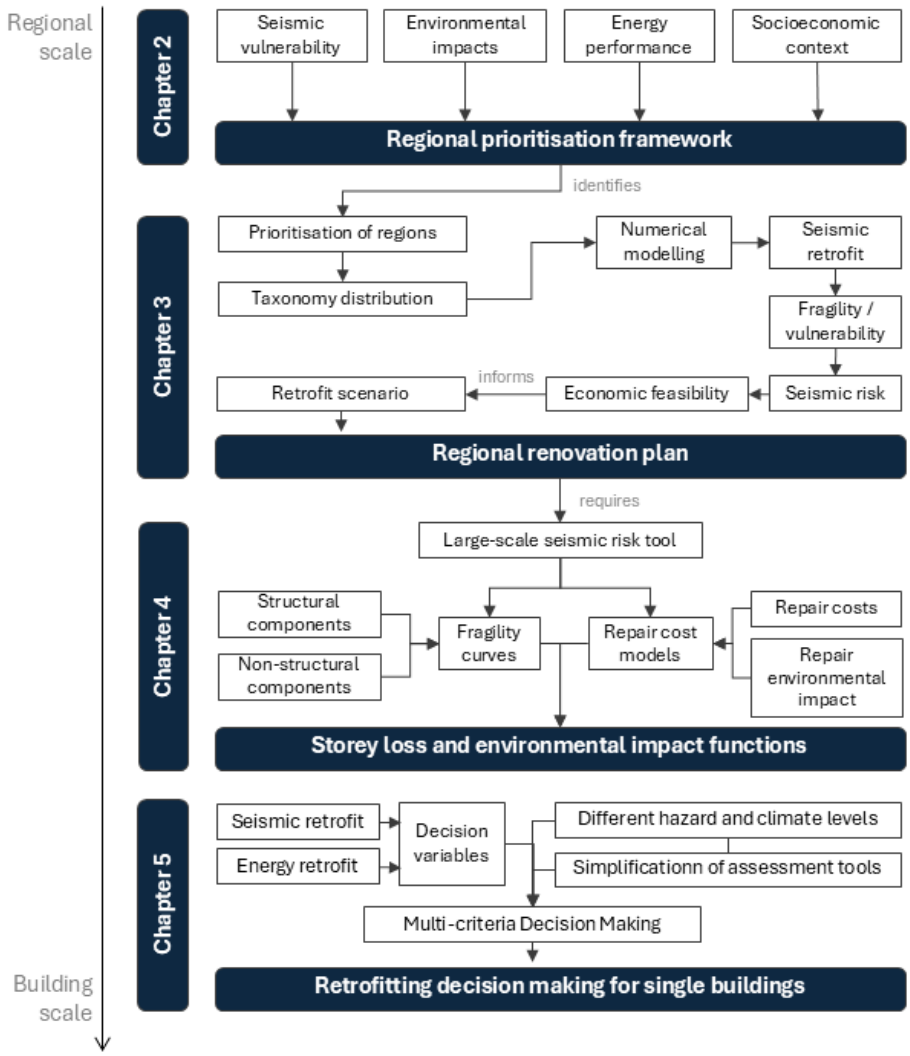

Figure 1.1 Graphical overview of the thesis structure

CHAPTER 2

Priority analysis framework for equitable seismic and energy-efficiency renovation of residential buildings applied to mainland Portugal

This chapter is extensively based on the following publication:

Couto R*, *Mucedero G, Bento R, Monteiro R. (2025) Priority analysis framework for equitable seismic and energy-efficiency renovation of residential buildings applied to mainland Portugal. Earthquake Spectra 41(3):1941-1976. doi: 10.1177/87552930251335282*

**Author Contribution: conceptualisation, methodology, software, validation,* data curation, *writing.*

2 PRIORITY ANALYSIS FRAMEWORK FOR EQUITABLE SEISMIC AND ENERGY-EFFICIENCY RENOVATION OF RESIDENTIAL BUILDINGS APPLIED TO MAINLAND PORTUGAL

2.1 INTRODUCTION

The construction sector in Europe is experiencing a crucial change related to new perspectives and challenges, especially those concerning seismic risk and energy inefficiency, prevalent in many European buildings. While past earthquakes have underscored the vulnerability of the European building stock (Verderame et al. 2011; Ruiz-Pinilla et al. 2016; Ozkula et al. 2023), energy inefficiency remains a widespread issue across Europe, with roughly 75% of buildings performing poorly in energy consumption, leading to significant environmental impacts. Indeed, it is well known that the building sector is responsible for 40% of the total energy consumption in the European Union (EU) and 36% of its CO_2 emissions. The combined challenge of seismic risk and energy inefficiency in the European building stock highlights an urgent need for enhanced community resilience (Gkatzogias et al. 2022a; Pohoryles et al. 2022). Addressing such a problem requires a comprehensive approach that strengthens structural performance while advancing energy efficiency. Up to now, renovation efforts and policies have mainly targeted the energy upgrading of buildings alone, without considering their structural performance. Directly foreseeing energy renovation measures alone at the European level might lead to short-term benefits only (e.g., reduced energy costs for heating/cooling), or even be jeopardized in case of seismic events, especially for highly seismic regions. In this sense, numerous studies have been conducted to proposed procedures and integrated frameworks for upgrading both seismic and energy performance simultaneously (Takeuchi et al. 2006, 2009; Calvi et al. 2016; Manfredi and Masi 2018; Bournas 2018; Pohoryles et al. 2020; Marini et al. 2022; Clemett et al. 2023; Caruso et al. 2023b; Couto et al. 2024). Nevertheless, achieving the ambitious goal of upgrading the European building stock requires a comprehensive prioritisation plan that integrates multiple domains, such as the seismic risk mitigation and economic-energy savings. By identifying high-priority regions and crafting a long-term investment strategy, resources can be allocated more effectively to address the most critical areas. Recent studies have explored integrated frameworks for regional assessment and prioritisation of existing residential and commercial buildings. For instance, Gkatzogias et al. (2022)

proposed an integrated prioritisation framework, which encompassed several metrics and indicators (e.g., loss of life, economic impacts related to seismic repairs, space heating costs, overall energy consumption) to identify priority regions within the EU. Similarly, Mucedero and Monteiro (2024a) conducted a prioritisation analysis focused on the Italian territory, incorporating seismic, energy, and socioeconomic metrics to inform targeted seismic strengthening and energy renovation interventions on existing residential buildings, for increased social equity. These studies further confirm the importance of a multifaceted approach in addressing the complexities of building renovation across Europe, contributing to safer, more efficient, and sustainable living environments.

In line with the EU objectives, Portugal is committed to achieving carbon neutrality by 2050 through its Roadmap for Carbon Neutrality (RNC 2050) (Ministery of the Environment and Energy Transition 2019) and the National Energy and Climate Plan 2021-2030 (PNEC 2030) (Portuguese Republic 2019). The latter outlines the framework for national climate and energy policy, setting ambitious targets for reducing greenhouse gas emissions across various sectors while promoting renewable energy and energy efficiency. These initiatives aim to reduce carbon emissions across all sectors of society and facilitate energy transition, aligning with the goals of the RNC 2050. Such transition is even more challenging given that existing Portuguese residential buildings often suffer from poor energy performance, high maintenance requirements, and outdated materials and technologies; thus, a renovation plan to retrofit these structures and fulfil modern energy efficiency standards is crucial for reducing emissions, enhancing living conditions, and meeting national climate targets. To this end, several strategies have been implemented, including emphasizing energy efficiency renovations under PNEC 2030, which involve upgrading insulation, windows, and HVAC systems, along with providing financial incentives, grants, and tax breaks for homeowners and businesses. Moreover, Portugal has adopted the Energy Performance of Buildings Directive (EPBD), mandating energy performance certificates (EPCs) during the sale or lease of properties, thereby encouraging property owners to improve their buildings' energy ratings. Despite these measures, which were nevertheless applied without a solid equity ground, a significant portion of the Portuguese building stock still requires renovation to meet current energy and environmental standards.

At the same time, the seismic risk of Portuguese buildings is high, even if, in the recent years, the country has been spared from large magnitude earthquakes, such as the devastating 1755 Lisbon earthquake (M_w = 8.5), the 1909 Benavente earthquake

(M_w = 6.3) or the 1969 Algarve earthquake (M_w = 7.8). While recent research on seismic hazard (Vilanova and Fonseca 2007), risk assessment (Costa et al. 2010; Silva et al. 2015a; Sousa 2016; Lopes et al. 2024a; Xofi et al. 2024), and energy performance of Portuguese buildings (Reis et al. 2024) has been carried out, a comprehensive, national-wide assessment of priority regions in need for seismic risk mitigation and energy performance upgrading measures has yet to be conducted. It is more and more consensual that the susceptibility of Portuguese buildings to seismic activity, combined with their energy inefficiency, leads to the critical need for a renovation strategy that addresses both concerns. Simultaneously, it is crucial to consider how socioeconomic conditions influence both seismic risk and energy vulnerability, as growing evidence suggests that the combined effects of seismic vulnerability, energy inefficiency, and social disparities, such as income levels, housing conditions, and demographic composition, aggravate the risks faced by certain communities (Rovai 1994; Mahbubur Rahman et al. 2023). In particular, lower-income households tend to experience longer recovery periods and face more severe long-term consequences following disasters (Hallegatte and Walsh 2021). As a result, a comprehensive renovation strategy, which simultaneously addresses the seismic vulnerability, energy inefficiency, and socio-economic vulnerability of Portuguese buildings, is essential for reducing risk, improving energy performance, and promoting social equity.

While recent studies have integrated seismic risk with socio-economic characteristics (Burton and Silva 2016), a more comprehensive assessment is still lacking. In line with recent research studies (Gkatzogias et al. 2022a; Mucedero and Monteiro 2024a), this chapter proposes and applies a framework that characterises the seismic and energy needs of the residential building stock across mainland Portugal, while also accounting for socioeconomic vulnerability as a factor that exacerbates deficiencies and limits the capacity for improvement, to identify the regions of highest integrated priority. An indicator-based approach is adopted to address such a complex goal, which is crucial for effective resource management and risk mitigation in an equitable manner. The employed multidisciplinary methodology is scalable to other countries or regions and shares, in fact, the principles of an analogous analysis carried out for the Italian residential building stock . By integrating indicators from the aforementioned seismic, energy and social sectors, the resulting prioritisation pattern identified the regions more in need for intervention and serves as a tool for policymakers and planners to make informed decisions and develop resilient and equitable response plans to reduce seismic risks

and assist communities in coping with challenges related to energy inefficiency and socioeconomic disparities.

2.2 METHODOLOGY

The implemented methodology foresees the individual characterisation of three macro sectors, such as seismic risk, energy performance, and socio-economic vulnerability, through several metrics. Such metrics are subsequently used to quantify specific indicators for each sector, to understand the vulnerabilities of eighteen different regions of mainland Portugal. Each region is subdivided in districts, municipalities and parishes, as further described in Section 2.3.2.

The seismic metrics were quantified through seismic risk assessment of the Portuguese residential buildings. To do so, a detailed seismic hazard analysis, using OpenQuake (Pagani et al. 2014) along with the most recent hazard model for mainland Portugal, included in the European Seismic Hazard Model (ESHM20—Danciu et al. 2021), was carried out. This first step was followed by the characterisation of the residential building stock through the most updated exposure model for Portugal. With detailed information on building characteristics, the most recent fragility and vulnerability models available in the literature were selected and combined using a logic tree approach. Finally, the seismic risk estimation was conducted for each parish to quantify the seismic metrics, which were then merged into a single indicator used to define a regional seismic risk-based prioritisation pattern. For the energy domain, instead of conducting energy consumption estimation using available assessment methodologies based on intelligent data analysis (as performed, for instance, in a recent study by Gkatzogias et al. (2022)), specific official data on actual energy consumption (DGEG 2022a, b) and demand for optimal performance (Eurostat 2023a) in Portugal was retrieved. Then, combining this data with the exposure data for residential buildings, several energy performance metrics were quantified and integrated into an overall energy performance indicator to establish an energy-based prioritisation pattern across regions. The socioeconomic indicator encompasses regional strengths and weaknesses in social and environmental dimensions, measured through worldwide and European indices, as well as energy poverty and earthquake risk awareness. These metrics were then combined to obtain a socioeconomic-based prioritisation pattern.

The combination of the seismic, energy, and socioeconomic indicators provides a nuanced understanding of integrated needs across regions, helping to allocate

resources more effectively, support resilience-building efforts, and promote equitable improvements in living conditions. As a result, the prioritisation map identifies areas where interventions can have the most significant impact on safety, energy efficiency, quality of life and social fairness.

2.2.1 Seismic risk metrics and global indicator

The adopted seismic prioritisation metrics are based on two variables: the average annual economic loss (AAEL) and the average annual loss of life (AALL), whose quantification is explained in Section 2.3.4. From AAEL and AALL, three seismic risk metrics were defined:

i. Average annual economic loss per building ($AAEL_{/bldg}$), given by the ratio of the Average Annual Economic Loss (AAEL) at regional level and the total number of buildings (N_{bldg}) within the same region.
ii. Average annual economic loss ratio ($AAEL_R$), which corresponds to the normalisation of AAEL to the total replacement cost (C_{repl}) of all the buildings within a region.
iii. Average annual loss of life ratio ($AALL_R$), which corresponds to the ratio between the average annual loss of life (AALL) and the average number of occupants over a 24-hour period ($P_{i,24}$) of all buildings within a region.

The three different seismic risk metrics are then merged into a single seismic risk indicator (I_S), assuming the same weight, hence relevance, for each metric. The merging into a single indicator is preceded by a scaling to the interval [0,1] according to the minimum and maximum values obtained for all districts within the same region. The equations to compute the seismic metrics and indicator are provided in Table 2.1.

Table 2.1 Seismic risk metrics and prioritisation indicator

Metric/Indicator	Equation
$AAEL_{/bldg}$	$AAEL\ [€]/N_{bldg}$
$AAEL_R$	$AAEL\ [€]/C_{repl}[€]$
$AALL_R$	$AALL\ [€]/P_{i,24}$
I_S	$\frac{1}{3}\left[\overline{AAEL_{bldg}} + \overline{AAEL_R} + \overline{AALL_R}\right]$

2.2.2 Energy metrics and indicator

Six energy-based regional prioritisation metrics were considered, focusing on various aspects of energy performance, namely the energy consumption (kWh/year) and the carbon emissions (CO_2/year), and energy demand, as a function of the climatic conditions, of buildings within each district. The six energy-based metrics are:

i. Average Annual Energy Loss per building ($AAEnL_{/bldg}$), which consists of the average annual energy loss (AAEnL), given by the total consumed energy ($EP_{gl,nren}$) multiplied by the unit energy cost (E [€/kWh]), normalised with respect to the total number of buildings within the considered region (N_{bldg});
ii. Average Annual Energy Loss ratio ($AAEnL_R$), which consists of the AAEnL normalised with respect to the total replacement cost (C_{repl}) of the building assets within the region.
iii. Average Annual Carbon Emission Loss per building ($AACEL_{/bldg}$), which consists of the monetary yearly loss of carbon emissions (CO_2) normalised with respect to the total number of buildings (N_{bldg}) within the considered region.
iv. Average Annual Carbon Emission Loss Ratio ($AACEL_R$), which corresponds to the $AACEL_{/bldg}$ normalised with respect to the total replacement cost (C_{repl}) of the building assets within the considered region.
v. Average Annual Energy Loss per HDD ($AAEnL_{/HDD}$), which represents the AAEnL normalised by the heating degree days (HDDs) of the region under study.
vi. Average Annual Energy Loss per cooling degree days (CDD) ($AAEnL_{/CDD}$), which represents the AAEnL normalised by the CDDs of the region under study.

The energy performance prioritisation indicator (I_E) is then estimated by averaging (equal weights) all the normalised (scaled to the interval [0,1]) energy performance metrics. The equations to compute the energy metrics and indicator are provided in Table 2.2.

2.2.3 Socioeconomic vulnerability metrics and indicator

With respect to traditional regional needs assessment frameworks, the one used herein also accounts for equity concerns (through socioeconomic vulnerability metrics), since it is well-known that economic/financial and social issues might affect the retrofitting/renovation process. In this sense, in line with the studies by

Gkatzogias et al. (2022) and Mucedero and Monteiro (2024a) socioeconomic vulnerability metrics were included in the definition of the retrofitting and renovation needs prioritisation pattern, for more robust and equitable measures. The considered socioeconomic vulnerability metrics are:

i. Socioeconomic vulnerability index (SVI), which is composed by two variables: the human development index (HDI) and the European Social Progress Index (EU-SPI).
ii. Energy Poverty, measured through the Municipal Energy Vulnerability Index (MEVI), and refers to the condition where households are unable to afford adequate energy services, such as heating, cooling, and electricity, due to high energy costs relatively to their income.
iii. Earthquake Risk Awareness (ERA), referring to how individuals understand and respond to the risk posed by earthquakes, influencing their willingness to take preventive measures. ERA is calculated by summing the product of the average number of occupants at the smallest available administrative level (j) over a 24-hour period ($P_{j,24}$) with the corresponding seismic risk perception (P), within the area of interest. This value is then normalised with respect to the average number of occupants over a 24-h period ($P_{i,24}$) of all buildings within a district (i).

Finally, the global socioeconomic vulnerability indicator ($I_{G,SVI}$) is defined by averaging the normalised socioeconomic vulnerability metrics (again scaled to the interval [0,1]). The equations employed to compute the metrics, and the indicator are provided in Table 2.3.

Table 2.2 Energy performance metrics and prioritisation indicator.

Metric/Indicator	Equation
$AAEnL_{/bldg}$	$\left(EP_{gl,nren}[kWh/m^2/year] \cdot A_{dwellings}\,[m^2] \cdot E[€/kWh]\right) /N_{bldg}$
$AAEnL_{R}$	$AAEnL\ [€]/C_{repl}[€]$
$AACEL_{/bldg}$	$\left(CO_2[kg/m^2/year] \cdot A_{dwellings}[m^2] \cdot CEc[€/kg]\right) /N_{bldg}$
$AACEL_{R}$	$AACEL_{/bldg}[€]/C_{repl}[€]$
$AAEnL_{/HDD}$	$AAEnL\ [€]/HDD$
$AAEnL_{/CDD}$	$AAEnL\ [€]/CDD$

I_E	$\frac{1}{6}\left[\overline{AAEnL_{/bldg}} + \overline{AAEnL_R} + \overline{AACEL_{/bldg}} + \overline{AACEL_R} + \overline{AAEnL_{/HDD}} + \overline{AAEnL_{/CDD}}\right]$

Table 2.3 Socioeconomic vulnerability metrics and prioritisation indicator.

Metric/Indicator	Equation
SVI	$1 - \frac{1}{2}\left(HDI + \frac{EU - SPI}{100}\right)$
MEVI	Values obtained from Carvalho et al. (2023)
ERA	$ERA = \frac{\sum_j^n P_{j,24} \cdot P}{P_{i,24}}$
$I_{G,SVI}$	$I_{G,SVI} = \frac{1}{3}[\overline{MEVI} + \overline{SVI} + \overline{ERA}]$

2.2.4 Multi-sectoral integrated prioritisation

The final step of the prioritisation framework foresees the combination of the individual indicators of each macro-sector to obtain a multi-sectoral integrated prioritisation pattern, characterised by four multi-sectoral integrated indicators. The first indicator ($I_{I,S-E}$), prioritises different regions by combining, with an equal weight, the seismic-risk and energy performance indicators. It represents an engineering parameter that emphasises regions where both seismic and energy challenges are more prominent. The second indicator ($I_{I,S-G}$) incorporates seismic and socioeconomic vulnerability while the third one ($I_{I,E-G}$) incorporates energy performance and socioeconomic vulnerability. These two indicators assume that seismic retrofitting and energy renovation are independent and are used to explore how the prioritisation patterns shift when seismic and energy interventions are considered separately, while accounting for the socioeconomic vulnerability of each region. Finally, the fourth indictor ($I_{I,S-E-G}$) provides the most comprehensive perspective, by equally weighing the seismic risk, the energy performance and the socioeconomic vulnerability indicators. It helps directing resources to regions with higher challenges on the three sectors. It is noted that the weights assigned to each indicator or metric can significantly affect the results. Their determination is subject to the discretion of the decision-maker. The Venn diagram illustrated in Figure 2.1 depicts how the indicators are interrelated, showing the intersections between seismic risk, energy performance, and socioeconomic vulnerability.

Seismic + Energy
$I_{I,S-E} = (I_S + I_E)/2$

Seismic and energy performance indicators are combined, highlighting regions with prominent seismic and energy challenges, focusing purely on engineering factors

Energy + Socioeconomic
$I_{I,E-G} = (I_E + I_{G,SVI})/2$

Energy and socioeconomic performance indicators are combined, identifying regions facing both energy efficiency challenges and socioeconomic vulnerabilities.

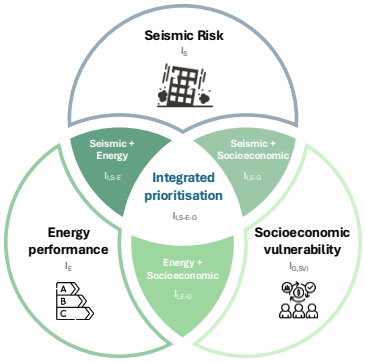

Seismic + Socioeconomic
$I_{I,S-G} = (I_S + I_{G,SVI})/2$

Seismic and socioeconomic indicators are combined, highlighting regions where both seismic vulnerability and socioeconomic challenges are more pronounced.

Integrated prioritisation
$I_{I,S-E-G} = (I_S + I_E + I_{G,SVI})/3$

The three domains are combined, providing a more holistic understanding of vulnerability and enabling more effective risk mitigation strategies.

Figure 2.1 Integrated regional prioritisation.

2.3 SEISMIC RISK ASSESSMENT

2.3.1 Hazard

The seismic hazard characterisation in Portugal began with the comprehensive assessment conducted by Oliveira and Costa (1984), which laid the ground for the seismic hazard map incorporated in the Portuguese design code of 1983 (RSA 1983). Such work was further expanded by Sousa et al. (2006) and Vilanova and Fonseca (2007), who introduced a probabilistic seismic hazard model specifically for mainland Portugal. On a broader scale, the SHARE project created the 2013 harmonised European Seismic Hazard Model (ESHM13) (Woessner et al. 2015). This model was subsequently updated to the European Seismic Hazard Model (ESHM20) (Danciu et al. 2021) as part of the SERA project. The ESHM20 provides two maps that will serve as a reference for the upcoming revision of the European Seismic Design Code (CEN EC8) and provides input to the first earthquake risk model for Europe (Crowley et al. 2021a; Danciu et al. 2024).

In this study, the ESHM20 (Danciu et al. 2021), representing the most up-to-date available seismic hazard model, was adopted to conduct a classical probabilistic seismic hazard analysis (PSHA), carried out in OpenQuake (Pagani et al. 2014). The hazard calculations were performed for each Portuguese parish (for a total of 4049 points) obtaining a hazard curve for each. The intensity measure (IM) levels of the hazard curves are aligned with the IM of the selected representative fragility curves (detailed in Section 2.3.3), namely the Peak Ground Acceleration (PGA) and the Spectral Acceleration conditioned at the fundamental vibration period ($SA(T_1)$). For

what concerns the local site characteristics and site response amplification, the $V_{S,30}$ (shear wave velocity at 30 m depth) map for Portugal, obtained through ESHM20 (Danciu et al. 2021), was used, as illustrated in Figure 2.2(a). Figure 2.2(b) depicts the geographic distribution of the Peak Ground Acceleration (PGA) with a 10% exceedance probability in 50 years (return period of 475 years). The southern and central-west regions of mainland Portugal have the highest seismic hazard, while the northern part of the country is characterised by low to moderate seismic hazard.

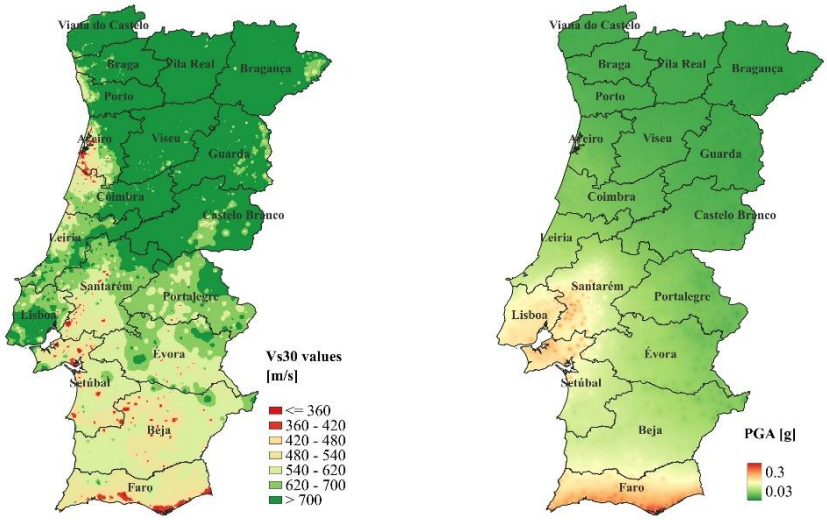

(a) (b)

Figure 2.2 (a) $V_{S,30}$ map for Portugal according to ESHM20 and (b) seismic hazard map in terms of Peak Ground Acceleration (PGA) for a probability of exceedance of 10% in 50 years.

2.3.2 Building Exposure

The current version of the Global Earthquake Model (GEM) Foundation building exposure model for Portugal was adopted (Yepes-Estrada et al. 2023), which updates the previously available exposure model, originally developed using 2011 census data, with data from the 2021 census. Although more recent, the 2021 data still lack critical information regarding building construction types, which is essential for determining building vulnerability. Therefore, both datasets were combined to compute the new GEM exposure model, as explained in detail by Lopes et al. (2024). Although the exposure model incorporates commercial and industrial buildings, following the outcomes of the European Horizon 2020 project SERA (Crowley et al. 2020), only the residential building stock was considered herein. The exposure model

defines the geographic distribution of buildings and dwellings, as well as the number of occupants (in transit, night, day, and average), floor area, and replacement costs (total, structural, and contents) across mainland Portugal. The residential buildings were categorised according to the GEM Building Taxonomy (Brzev et al. 2013), as described in Table 2.4.

Table 2.4 Residential building taxonomy of the exposure model for Portugal.

Material type	LLRS	Seismic Design Code Level	Floor material	Number of storeys
CR	LFINF LDUAL	CDM, CDL, CDM, CDH	FC	H1 – H6 HBET:7-20
MUR	LWAL	CDM, CDL, CDM, CDH	FC FW	H1 - HBET:7-20 H1 – H5
MUR + ADO	LWAL	CDM, CDL, CDM, CDH	FW	H1 – H3
UNK	-	CDM, CDL, CDM, CDH	-	H1 - HBET:7-20

Material type refers to the material of the structural members that are part of the lateral load resisting system (LLRS). In the Portuguese context, the buildings were categorised as follows: reinforced concrete (CR), unreinforced masonry (MUR), unreinforced masonry with adobe blocks (MUR+ADO), and other/unknown typologies (UNK). The lateral load resisting system (LLRS) corresponds to the structural system that provides resistance against horizontal earthquake forces through vertical and horizontal components and can be either a wall (LWAL), infilled frame (LFINF) or dual frame-wall system (LDUAL). The floor material categorises the structural floor systems based on construction materials and methods, such as concrete (FC) or wood (FW). The number of storeys indicates the storeys above ground. For example, H1 indicates a building typology with one storey, while HBET:7-20 indicates a building typology with a number of storeys ranging from 7 to 20. The seismic design code level corresponds to the levels of lateral forces to which these buildings were designed, indicating their capacity to withstand seismic forces. This level is associated with year of construction, as design regulations evolved over time. In the Portuguese context and following previous studies (Silva et al. 2015a; Crowley et al. 2021b; Lopes et al. 2024a), four classes, as a function of the seismic design code level, were identified: i. CDN – no seismic design; ii. CDL – low code; iii. CDM – moderate code and iv. CDH – high code. The first regulations with seismic provisions in Portugal were introduced in 1958 (RSCCS) (RSCCS 1958a) and 1961 (RSEP)

(RSEP 1961a), therefore, buildings built before 1960 were designed to withstand gravity loads only and are designated as CDN. In 1983, an improved seismic design regulation (RSA 1983) (RSA 1983) was introduced, thus, buildings built between 1960 and 1983 are defined as CDL and are the first generation of seismic design codes. CDM buildings are those built between 1981 and 2010, which marks the enforcement of EC8 in Portugal. The fourth and more recent typology buildings are CDH, which were constructed after 2011. It is important to note that although the Eurocodes have been available in Portugal since 2010, EC8 only became the Portuguese seismic code in 2019 (Decree–Law No 95/2019 of 18 July 2019). For the first two generations of seismic designs, the design lateral force coefficient (LFC), which corresponds to the fraction of the weight of the building defining the lateral force, depends on the location of the building. This implies that buildings belonging to the same building class can have different LFC and, consequently, different seismic capacities.

Figure 2.3 shows the evolution of the seismic zonation in Portugal according to the regulation in force. Considering RSEP (RSEP 1961a), Portugal was divided in three seismic zones: A, B, and C, with corresponding LFC values of 0.1, 0.05 and 0, respectively. With the introduction of RSA (RSA 1983), Portugal was divided in four seismic zones: A, B, C, and D, with corresponding LFC values of 0.165, 0.12, 0.09, and 0.045, respectively. Additional information on the LFC for Portugal can be found in Crowley et al. (2021b).

Based on the seismic zonation and LFC, the building exposure model was refined. For this purpose, a seismic zone was assigned at each building based on its construction period and geographic location. Subsequently, a LFC value (0.0, 0.05, 0.10 and 0.15) was assigned to the taxonomy code. These values align with the taxonomy code used for fragility curves in SERA models (Romão et al. 2021) and approximate the LFC values specified in the Portuguese regulations, namely RSEP (RSEP 1961a) and RSA (RSA 1983). The revised exposure model provides a more refined characterisation of the building features, enabling more precise assessments of potential damage.

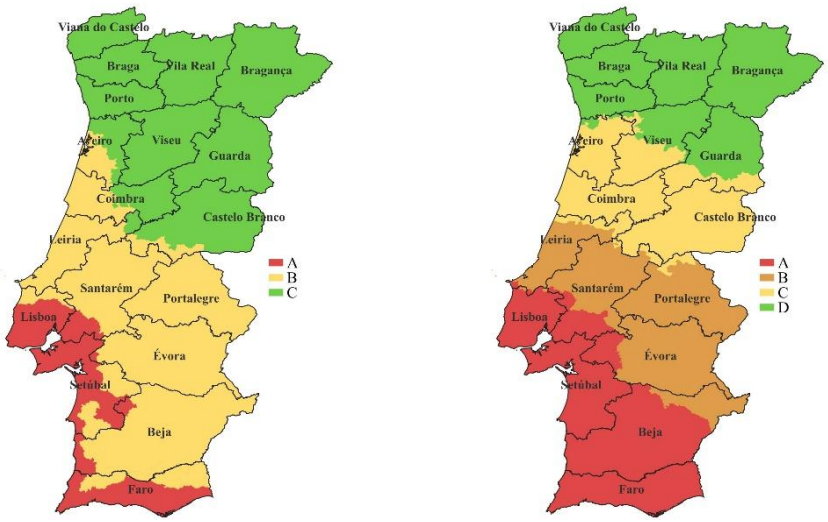

Figure 2.3 Evolution of the seismic zonation in Portugal according to different design codes: (a) RSEP, (b) RSA.

Portugal's administrative divisions are organised into three levels: districts, municipalities and parishes. The seismic metrics were quantified at the highest available resolution (i.e., parishes), while the prioritisation pattern was displayed at the district level. The districts have been grouped according to the NUTS-2 classification, which divides Portugal into larger regional units such as Alentejo, Algarve, Centro, Lisbon Metropolitan Area (AML) and Norte. In Figure 2.4, different colours are used to represent each of the NUTS-2 regions, thus allowing to clearly identify them and facilitating regional comparisons in the prioritisation analysis. In the NUTS-2 classification, the AML includes parts of both Lisbon and Setúbal districts but not their entirety. However, for practical reasons related to the decision-makers tasks, the entire Lisbon and Setúbal districts were considered herein as part of the AML, which also helps the results visualisation.

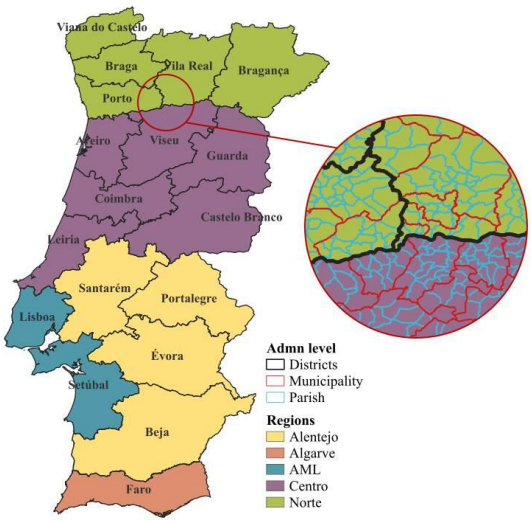

Figure 2.4 Administrative regions of Portugal - district, municipality and parish – and considered regions for this study.

Figure 2.5 provides the spatial distribution of specific attributes of the Portuguese residential building stock, along with the construction material and design code level distribution of each district, while Figure 2.6 summarises some of the attributes at the district level. Mainland Portugal consists of 3,366,797 buildings, with 51% being reinforced concrete, 43% masonry, 5% masonry with adobe, and 1% unknown. At the district level, most districts along the western and southern coastal areas follow a similar distribution of building materials, with a higher proportion of reinforced concrete structures. In contrast, central and eastern districts have a greater percentage of masonry buildings compared to reinforced concrete ones. Regarding the seismic design code levels, 26% of buildings are classified as CDN, 11% as CDL, 48% as CDM, and 14% as CDH.

From an economic point of view, the total replacement cost of the residential building stock in mainland Portugal is estimated at around 673 billion euros, with Lisboa, Porto, Setúbal and Braga representing almost 50% of this value. The replacement cost refers to the value of replacing a building in accordance with the latest building codes applicable to a country, and it includes the cost of the structural, non-structural components and content (excluding the cost of land). In Portugal, the construction cost per square meter is adjusted annually by a coefficient determined by the National Statistics Institute. According to Presidência do Conselho de Ministros (2024), three distinct construction costs were defined in 2024 based on

the building location: buildings in the district capitals, major cities, and islands are included in Zone I (846.63 €/m^2), while those located in urban (740.08 €/m^2) and rural areas (670.50 €/m^2) are classified in Zone II and Zone III, respectively.

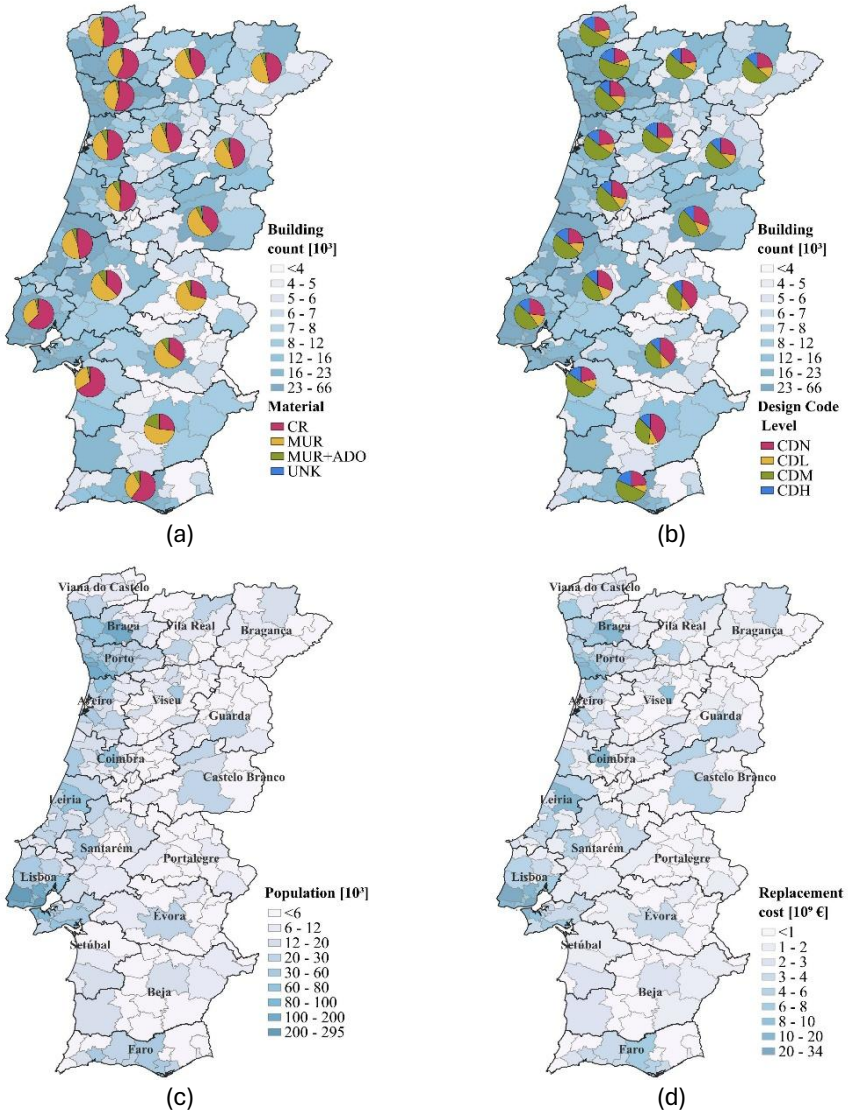

Figure 2.5 Geospatial distribution of (a) building count at municipality level and material distribution at district level; (b) building count at municipality level and design code distribution at the district level; (c) average occupants; and (d) replacement cost of the building assets.

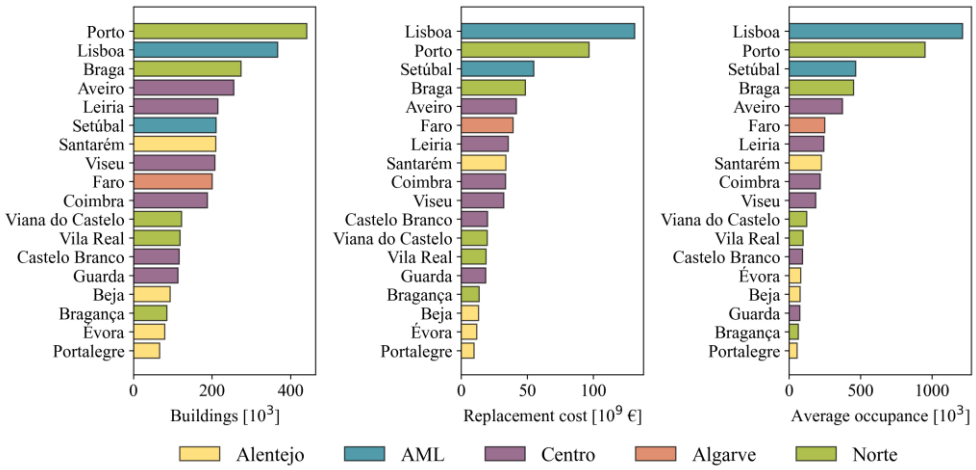

Figure 2.6 Summary of the specific peculiarities of the Portuguese residential building stock, grouped by district.

2.3.3 Fragility and Vulnerability

In the recent decades, significant efforts have been made to develop fragility and vulnerability curves for seismic risk assessment at regional and national scales for large building stocks (Rosti et al. 2021; Manfredi et al. 2023a; Mucedero et al. 2024a). These large-scale approaches aim to account for the variability in geometrical and material properties representative of buildings in the area of interest while addressing different sources of uncertainty. In Portugal, several fragility curves specifically tailored to the Portuguese building stock have been developed. Notable examples include those by LNEC (2005), Costa et al. (2010), Sarchi et al. (2018), Simões et al. (2019), Ilic et al. (2020), Bernardo et al. (2022), Lovon et al. (2023), Varela et al. (2024). These curves address both masonry and RC buildings located mostly in Lisbon, but also covering other regions of Portugal. However, most of this fragility curves are not suitable for direct use in seismic risk applications, as they do not relate directly to a probabilistic seismic hazard model via a conventional IM such as the PGA or SA(T_1). This gap makes it challenging to fully capture the seismic vulnerability of buildings in the different regions and highlights the need for more research. In this study, the fragility curves developed by Silva et al. (2015b) and Silva et al. (2015c) were the ones adopted due to their specificity and relevance to Portuguese buildings. Such fragility functions were derived considering representative reinforced concrete and masonry building typologies, selected based on key attributes in terms of seismic response. These attributes include the construction period (reflecting changes in

design codes), the number of storeys (low-rise to mid-rise), and the seismic zonation, which affects the design level. In addition, the fragility curves developed by Martins and Silva (2021), as part of the Global Seismic Risk Model, and within the SERA project (Romão et al. 2021) were also collected and used herein, with the view to account, although in a simplified way, for the epistemic uncertainty surrounding the derivation of fragility curves. In particular, Martins and Silva (2021) have identified the most common building classes at a global scale and nearly 500 fragility curves were developed to represent various combinations of construction material, building height, lateral load-resisting systems, and seismic design levels. These functions were derived using nonlinear time-history analyses on single-degree-of-freedom oscillators, using ground motion records from different tectonic environments. As regards the study carried out by Romão et al. (2021), a database of existing capacity curves, fragility functions, damage-to-loss models and vulnerability functions for European building classes (classified using the GEM Building Taxonomy v3.1) was collected, and an improved vulnerability analysis framework was developed, with a new set of capacity curves, fragility functions, damage-to-loss models and vulnerability models covering a large number of vulnerability classes in the European exposure model.

Table 2.5 presents a summary of the fragility models used in this study, detailing the construction material, lateral load-resisting system (LLRS), construction period, lateral load coefficient or ductility level and number of storeys. The fragility curves from Silva et al (2015a; 2015b) refer to reinforced concrete buildings (RC), masonry buildings with concrete or timber floors (M0) and weak masonry buildings (M3), comprised of adobe, rubble stone or rammed earthen units. CDN buildings were categorised as pre-code (PC), CDL buildings as mid-code (MC), and CDM and CDH buildings as post-code (C). Moreover, the ductility level of the RC buildings is directly related to the seismic zonation defined by the design code in force for a certain period of construction: MC establishes three zones (A, B, C), whilst C defines four zones (A, B, C, D). Regarding the number of storeys, six height categories were considered: 1, 2, 3, 4, 5-7, >8 storeys.

The fragility curves proposed by Martins and Silva (2021) consider reinforced concrete, masonry and masonry with adobe structures. To reflect different levels of seismic design, in addition to the period of construction labels, three levels of ductility were established: low ductility (DUL), representing structures designed with very limited seismic provisions (CDN structures) or structures in low seismic hazard regions; moderate ductility (DUM), corresponding to structures incorporating some

seismic design but with regulations deemed less rigorous than modern codes, such as CDL buildings; and high ductility (DUH), referring to buildings designed according to contemporary seismic standards, such as CDM or CDH buildings. Unreinforced masonry and earthen constructions are classified as non-ductile (DNO) due to their expected poor performance. In terms of building height, reinforced concrete (RC) structures range from 1 to 7 storeys, masonry buildings vary from 1 to 5 storeys, and masonry with adobe buildings range from 1 to 3 storeys.

Finally, those proposed by Romão et al. (2021), which are fully compatible with the refined exposure model, account for the different levels of seismic design through the LFC, which is assumed as 0, 5, 10 or 15% of the weight of the structure, for Portuguese buildings, as reported in Crowley et al. (2021b). Regarding the number of storeys, six discrete classes were determined, considering buildings of 1 to 6 storeys.

The main differences between the three sources of fragility are related to the type of numerical analysis and damage criteria used, as well as the selected case-study buildings. Martins and Silva (2021) and Romão et al. (2021) share the same methodology to convert capacity curves into fragility curves, apply the same damage state thresholds, and use IMs of the same type. However, the structural models used to represent different building taxonomies differ. To account for the differences and increase the completeness of the fragility model, this study employs a logic tree model, featuring the same weights in all the branches for simplicity, to integrate the various fragility function sources, as they are considered equally representative of the Portuguese building stock.

Each building taxonomy class was linked to its corresponding fragility curve through pre-established correlations (see Table A.1 in Appendix A.1). Regarding the construction material, adobe (MUR + ADO) or unreinforced masonry buildings (MUR + FW or MUR + FC) were always considered to have no ductility (DNO), while unknown buildings (UNK) with a seismic design code level of CDM or CDH were considered as retrofitted masonry (MR). Additionally, the mapping of the seismic design code level to the corresponding ductility level was carried out based on the methodology outlined by Crowley et al. (2021b), which established a relationship between seismic design code level, lateral force coefficients and ductility level. Whenever the building taxonomy specified a number of storeys exceeding those covered by the available fragility models, the maximum number of storeys represented in the fragility models was applied.

Table 2.5 Selected fragility models

Fragility model	Construction material	Period of construction	Ductility level	Storeys
Silva et al. 2015 (Silva et al. 2015a)	CR	pre-code (PC)	-	1, 2, 3, 4, 5-7, >8
		mid code (MC)	A, B and C	
		code (C)	A, B, C and D	
Silva et al. 2015 (Silva et al. 2015b)	M0 and M3	pre-code (PC)	-	
		mid code (MC)	-	
		code (C)	-	
(Martins and Silva 2021a)	CR	CDN	DNO	1 – 7
		CDL	DUL	
		CDM	DUL, DUM	
		CDH	DUH	
	MUR+STDRE	-	DNO	1 – 5
	MUR +ADO		DNO	1 – 3
	MR		DUM	1 – 5
SERA (Romão et al. 2021)	CR	CDN	-	1 – 6
		CDL	0, 5 and 10	
		CDM	0, 5, 10 and 15	
		CDH	0, 5, 10 and 15	
	MUR	-	DNO	1 – 5
	MUR +ADO		DNO	1 – 3
	MR		DUM	1 – 5

The fragility models were then used to derive vulnerability curves, following a building-based approach, according to which, by creating a relation between a measure of damage and a quantity of loss, achieved through a damage-to-loss model, vulnerability curves are derived. Loss ratios (repair costs normalised to the replacement cost) of 0.05, 0.20, 0.60 and 1.00 were assumed for slight, moderate, extensive, and complete damage limit states, respectively, in line with other studies (e.g., (Martins and Silva 2021a; Lopes et al. 2024a)).

In addition to the physical vulnerability model to quantify average annual losses (AAEL), a fatality vulnerability model was employed to quantify the average annual

loss of life (AALL). Equation 2.1 defines the expected loss of life for a given intensity measure level (E[LL|IM]), and is computed by integrating a set of variables: (i) the likelihood that a damaged building ($P(DS_4|IM)$) will collapse to the extent that could cause loss of life ($P_{lethal|DS4}$); (ii) the entrapment rate ($P_{entrapment}$), which depends on the occupancy rate at the time of the earthquake and considers the possibility of evacuating occupants before significant damage or collapse occurs, as well as buildings that leave spaces and gaps that may allow for escape; (iii) the entrapment fatality rate ($P_{LL|entrapment}$), which is related to the people who perish, before being rescued, given the entrapment; and (iv) the collapse factor (c_f), tailored to the specific building class, used (in case of entrapment) as a judgement-based correction of $P_{collapse} \cdot P_{lethal|ds,collapse}$ to implicitly account for the effect of the building collapse mechanism on the LL.

$$E[LL|IM] = P(DS_4|IM) \cdot P_{lethal|DS4} \cdot c_f \cdot P_{entrapment} \cdot P_{LL|entrapment} \quad (2.1)$$

While $P(Ds_4|IM)$ comes from the selected fragility model, the remaining variables are obtained from both past observations and expert judgment. $P_{lethal|DS4}$ is currently taken as an average of 1.0% based on the data from recent earthquakes, while the collapse factor varies between 0.5 and 5 as a function of the building class (Crowley et al. 2021a). $P_{entrapment}$ and $P_{LL|entrapment}$ are obtained following the work of Reinoso et al. (2018). As observed from past earthquakes, the time of occurrence and the number of storeys influence the entrapment rate and the loss of life given entrapment. Hence, different entrapment rates were assumed for day and night, assuming higher values for the latter. Table A.2 (see Appendix A.2) summarises the damage to loss model parameters employed for each building taxonomy, employed in this study. Figure 2.7 shows the vulnerability and fatality functions for some of the most common building typologies in mainland Portugal, as a function of the different selected fragility models.

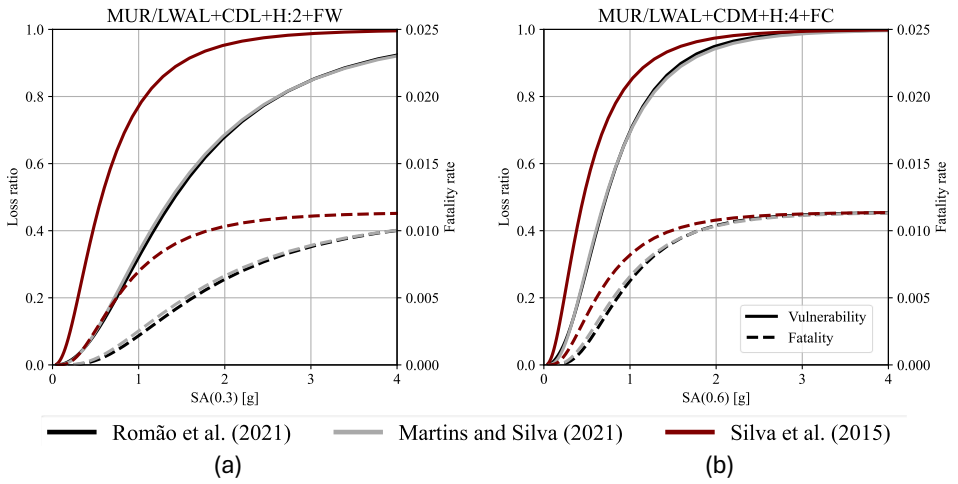

Figure 2.7 An example of fatality (solid line) and vulnerability (dashed line) functions obtained using different fragility models: (a) MUR/LWAL+CDL+H:2+FW and (b) MUR/LWAL+CDM+H:4+FC.

2.3.4 Seismic risk assessment

Following the seismic hazard analysis performed in Section 2.3.1 and the selected vulnerability and fatality functions (Section 2.3.3), two seismic risk metrics, AAEL and AALL, were obtained convoluting each hazard curve (obtained for the centroid of each parish) with the vulnerability and fatality curve, respectively, assigned to each building class available in the Portuguese exposure model. Equal weights were assigned to the selected vulnerability fatality models; thus, the AAEL and AALL, for each building class, were obtained by averaging the results obtained with those models. By summing the calculated AAEL and AALL for all building classes within each parish, the total AAEL and AALL for that parish could be determined. Similarly, this approach was applied to calculate the total AAEL and AALL for each municipality and subsequently for each district. Figure 2.8(a) illustrates the AAEL at the municipality level, while Figure 2.8(b) shows the total AAEL per district. Figure 2.8(a) shows higher losses in the south of Portugal as well as in the Lower Tagus Valley. Figure 2.8(b) shows that the highest AAEL values are concentrated in the districts of Lisbon, Faro, Setúbal and Santarém. This is related to the high seismic hazard in these regions (as detailed in Section 2.3.1), together with a high density of buildings and corresponding replacement cost, as detailed in Figure 2.6. Similar trends have been observed in past studies, such as Sousa (2007) and Lopes et al. (2024). Table 2.6 summarises the seismic risk results obtained according to each fragility model.

Table 2.6 Seismic risk results as a function of the fragility source model.

Fragility source model	Replacement cost (10^9 €)	EAL		Fatalities		
		M€	%	day	night	average
(Silva et al. 2015b)	673	357	0.053	1.43	11.71	6.57
(Silva et al. 2015a)		614	0.091	1.21	10.46	5.83
(Martins and Silva 2021a)		58	0.086	0.24	2	1.12
(Romão et al. 2021)		23	0.034	0.13	0.88	0.5
Average		263	0.066	0.75	6.26	3.5

Past studies assessing seismic risk in mainland Portugal have reported varying estimates of AAEL: Sousa (2006) estimated an AAEL of €257 million, while Silva et al. (2015c) reported a higher estimate of €288.1 million. Shortly after, Sousa and Costa (2016) calculated a lower AAEL of €147 million. In all these studies, only direct economic losses due to structural damage were considered and costs from non-structural damage, contents, or indirect losses, such as business interruption, were not included. The time of the occurrence of an earthquake highly influences the number of fatalities. For residential buildings, a higher number of fatalities might be expected during nighttime as there are more occupants and people react slower (Reinoso et al. 2018). Figure 2.9(a) displays the AALL at the municipality level, whereas Figure 2.9 (b) presents the total AALL for each district in the country. The AALL results present a trend similar to the AAEL one.

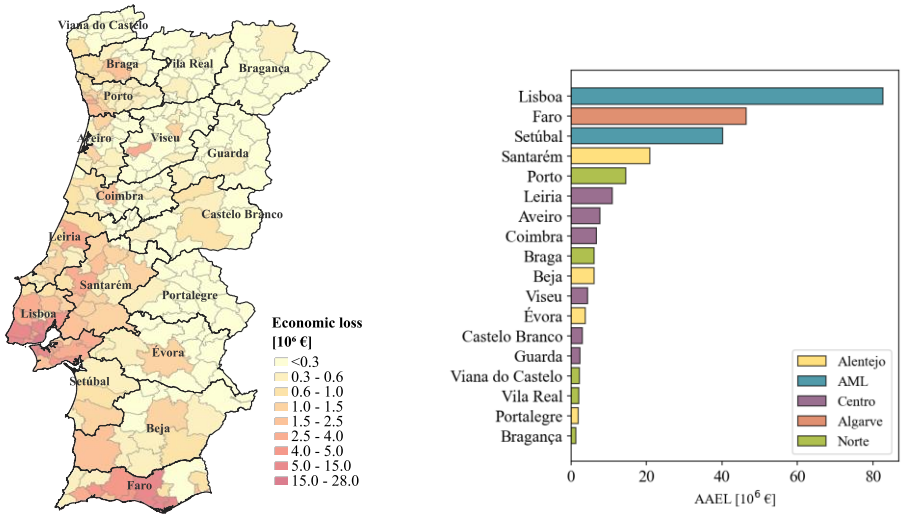

(a) (b)

Figure 2.8 Annual average economic losses summarised for the (a) second and (b) first administrative level.

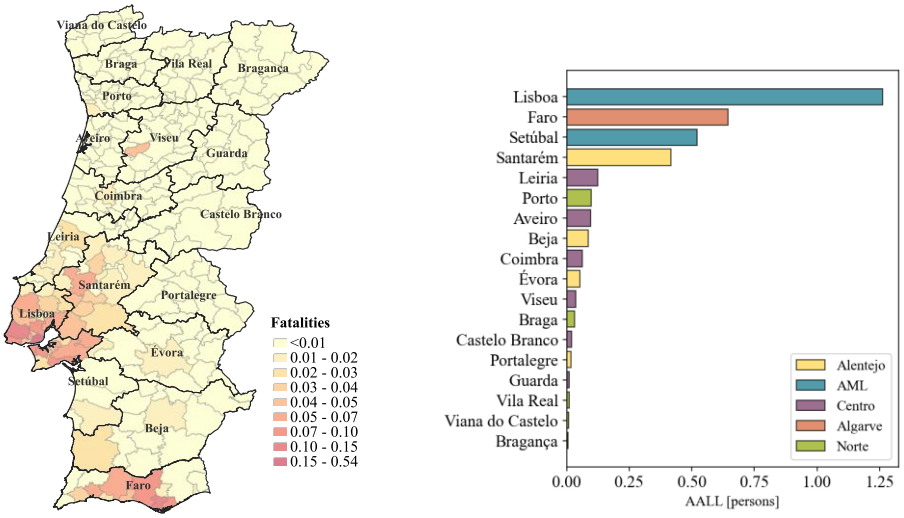

(a) (b)

Figure 2.9 Annual average annual loss of life summarized for the (a) second and (b) first administrative level.

2.3.5 Seismic risk metrics and indicator

The first three seismic risk metrics, the Average annual loss per building ($AAEL_{/bldg}$), the Average annual loss ratio ($AAEL_R$) and the Average annual loss of life ratio ($AALL_R$), are illustrated in Figure 2.10, together with their statistical distributions (33rd and 66th percentiles). Based on these metrics, a rough subdivision of the Portuguese districts into three prioritisation groups can be considered. The rankings for $AAEL_{/bldg}$ and $AAEL_R$ are quite similar, with districts like Faro, Lisbon, Setúbal, Santarém, Beja, and Leiria ranking highest. Conversely, the Norte and Centro regions, with their low seismic hazard levels, come at the end. These findings align with the seismic risk metrics obtained previously (Figure 2.8(b)). Nevertheless, a notable shift in some positions is observed. While $AAEL_{/bldg}$ prioritises regions with fewer buildings, $AAEL_R$ instead prioritises regions with a lower reconstruction cost. With respect to the ranking shown in Figure 2.8 (b), Faro and Beja move up in the $AAEL_{/bldg}$ - and $AAEL_R$ - based rankings, given the lower number of buildings and reconstruction cost when compared, for example, with Lisboa (district with the higher AAEL). Simultaneously, districts like Porto are downgraded, due to the higher building density and reconstruction cost in the region. When considering both metrics, it can be acknowledged that a region with more buildings does not necessarily have a higher total reconstruction cost.

The results obtained for $AALL_R$ indicate a higher ratio of annual fatalities for Faro, Santarém, Setúbal, Lisbon, Beja and Évora with respect to all the other districts. Since this metric prioritises the regions with less occupants, the differences between Figure 2.9 (b) with Figure 2.10 (c) can be justified by the lower population of Faro and Santarém when compared with Lisbon. Moreover, both for $AAEL_R$ and $AALL_R$, Faro stands out significantly from other districts within the 66th percentile, indicating a markedly higher economic loss and fatality rate. In contrast, the differences among districts below the 33rd percentile and those between the 33rd and 66th percentiles are generally smaller, except for Leiria, which aligns with the seismic hazard mapping of the country.

The previously discussed risk metrics were combined to define the seismic risk indicator (I_S), which, as introduced in Section 2.2.1, is obtained as the mean of the three normalised risk metrics. Figure 2.11(a) presents the seismic risk–based prioritisation map, while Figure 2.11(b) illustrates the I_S value per district. Faro emerges prominently as the top priority district, followed by the Lower Tagus region and the central-southern part of Portugal. In similarity with Figure 2.10, the regions of

Norte and Centro exhibit a lower priority position, reflecting the spatial variation in seismic hazard across the country.

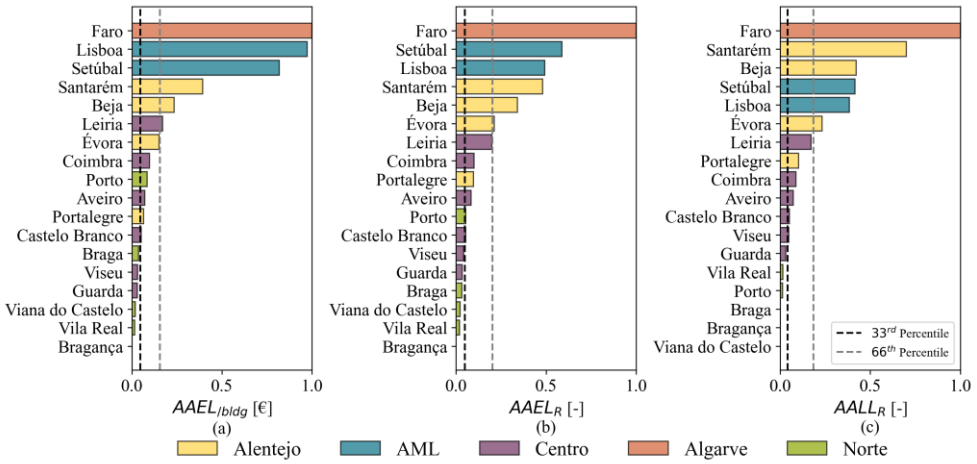

Figure 2.10 Seismic risk-based rankings, as a function of different seismic metrics: (a) average annual loss per building ($AAEL_{/bldg}$), (b) average annual loss ratio ($AAEL_R$) and (c) average annual loss of life ratio ($AALL_R$).

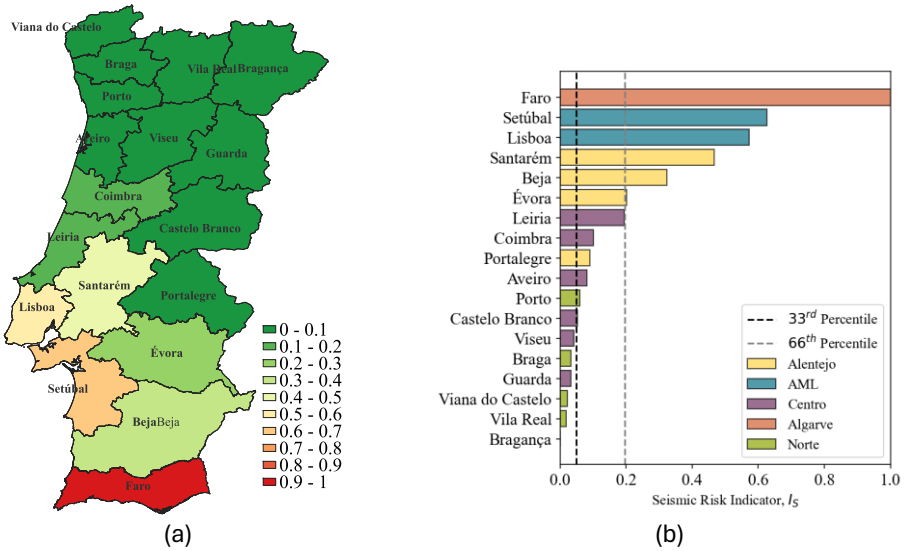

Figure 2.11 (a) Seismic risk-based prioritisation map and (b) seismic risk indicator (IS) value per district.

2.4 ENERGY PERFORMANCE ASSESSMENT

2.4.1 Climatic conditions

The energy consumption related to building thermal comfort is correlated with heating degree-days (HDDs) and cooling degree-days (CDDs), which represent the heating and cooling energy requirements to attain a building-specific baseline temperature (between 18°C and 25°C). Figure 2.12 illustrates the HDD and CDD maps for mainland Portugal, in terms of the mean HDD and CDD patterns for the period 1979-2023 (Eurostat 2024a). The geographic distribution reveals that the northeast and east areas experience high heating and cooling demands, respectively. On the other hand, the southern and northern coastal areas do not experience significant heating or cooling demands, respectively, when compared to the more extreme conditions found in the northeast and southeast areas.

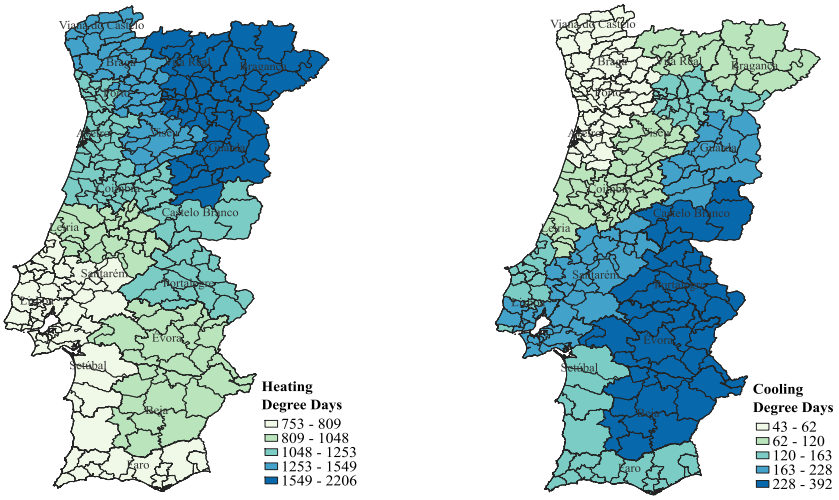

Figure 2.12 Heating (HDD) and cooling (CDD) degree-days per municipality.

2.4.2 Annual energy consumption and carbon emissions

The annual electricity (DGEG 2022a) and gas (DGEG 2022b) consumption data, disaggregated by municipality and economic activity sector, are provided by the General Direction of Energy and Geology (DGEG), which is the responsible body for regulating, overseeing, and promoting activities in the field of energy and geology within Portugal. The data provided in DGEG (2022a, 2022b) are aggregated, i.e., combining both cooling and heating consumptions by sector and administrative

levels (NUTS I, NUTS II, district, and municipality). This aspect makes it impractical to determine, for each district, whether the highest energy consumption is due to heating or cooling of buildings. The annual energy consumption is thus obtained summing the annual electricity and the gas consumption obtained at the district level, as illustrated in Figure 2.13 (a). Lisbon and Porto are the districts with the highest energy consumption, contributing with around 41% to the total energy consumption of mainland Portugal. This was expected as these are the districts with the higher number of occupants. In contrast, Guarda, Beja, and Portalegre are those with the lowest energy consumption, in line with the presence of less buildings and occupants (as previously shown in Figure 2.5).

To estimate the annual CO_2 emissions, the annual energy consumption was multiplied by the greenhouse gas emission factor of fuel and by the carbon emission cost (CEc). The Portuguese Environment Agency (APA) publishes, every year, a report on the greenhouse gas emission factor (in tons of CO_2 equivalent per MWh of electricity produced) for electricity produced in Portugal. The latest available data for the emission factor obtained for mainland Portugal corresponds to the year 2022 hence, an average value for the last five years (2018 – 2022), was assumed – 0.198 tCO_2e/MWh (APA 2024). The carbon emission cost (CEc) was considered to be 0.185 €/kg according to Rennert et al. (2022). Figure 2.13 (b) presents the annual CO_2 emission in Portugal, at the district level. As this parameter is derived by multiplying the annual energy consumption by a fixed coefficient, the distribution of CO_2 emissions per district follows the same trend as the one in Figure 2.13 (a).

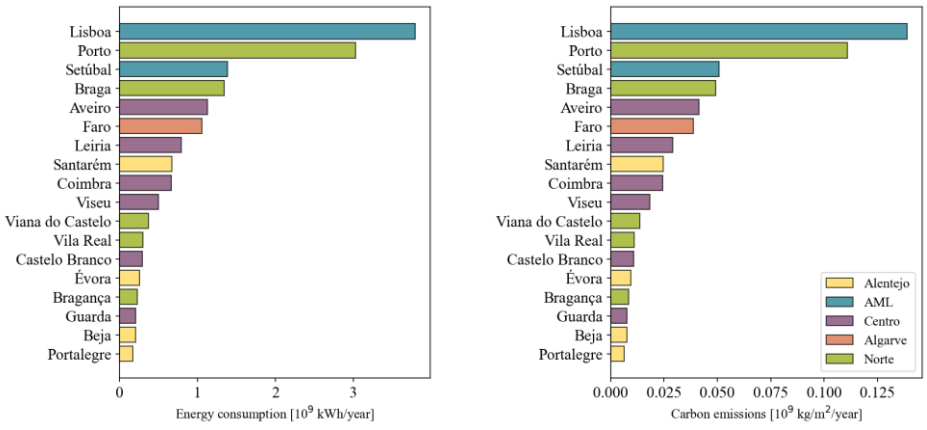

(a) (b)

Figure 2.13 Annual (a) energy consumption and (b) carbon emission per district.

2.4.3 Energy performance metrics and indicator

Following the gathering of the energy performance variables, the energy performance metrics, previously introduced in Section 2.2.2, are computed. Regarding the energy price, a value of 0.218€/kWh was used, which corresponds to the Portuguese average domestic electricity price in Portugal for 2022, as reported by DGEG (2024). When compared to other European countries, Portugal is ranked on the 19th position with the highest electricity price.

Figure 2.14 shows the Average Annual Energy Loss per building ($AAEnL_{/bldg}$), the Average Annual Energy Loss ratio ($AAEnL_R$), the Average Annual Carbon Emission Loss per building ($AACEL_{/bldg}$), the Average Annual Carbon Emission Loss Ratio ($AACEL_R$), the Average Annual Energy Loss per HDD ($AAEnL_{/HDD}$), and the Average Annual Energy Loss per CDD ($AAEnL_{/CDD}$).

By normalising the total energy consumption (Figure 2.14(a)) and carbon emissions (Figure 2.14(c)) to the total number of buildings within a certain region, Lisboa and Porto remain the prioritised districts, whereas the less critical ones are Viseu, Beja and Guarda. Considering the $AAEnL_R$ (Figure 2.14(b)) and AACELR (Figure 2.14(d)), the resulting rankings change, and the most critical regions become the districts in Alentejo and Norte regions. The least priority districts are Lisbon, Viseu and Porto. This can be justified by the higher replacement cost of Lisbon, Porto and Viseu, when compared with the areas of Alentejo and Norte (Figure 2.6). When examining the metrics of $AAEnL_{/HDD}$ (Figure 2.14(e)) and $AAEnL_{/CDD}$ (Figure 2.14 (f)), notable shifts in the ranking of districts become apparent. For $AAEnL_{/HDD}$, districts such as Lisboa, Setúbal, Faro, and Porto, which report the lowest heating degree days (HDD) in the country, exhibit a mismatch between energy consumption and the corresponding heating demand. This indicates that, despite their lower heating needs, energy usage in these areas remains disproportionately high, leading to inefficiencies. In contrast, districts like Viseu, Bragança, Vila Real, and Braga, which have higher HDD values indicating greater energy demand for heating, rank as the least critical in terms of energy consumption. This suggests that these regions are managing their energy needs more effectively, aligning consumption more closely with actual demand. A similar pattern emerges when assessing $AAEnL_{/CDD}$. Districts with lower CDD - such as Porto, Braga, and Aveiro - are categorised as critical, implying that their energy consumption is not adequately meeting the cooling demands of their populations. Conversely, districts that experience higher cooling demands, indicated by higher CDD values, are considered the least critical. These findings underscore the intricate

connection among energy demand, consumption patterns, and efficiency in various regions, identifying opportunities for targeted improvements to ensure energy use more closely matches actual requirements. Social factors, such as socioeconomic conditions, average income, access to education, and awareness of energy-saving practices, also very likely influence consumption behaviours, building occupancy patterns, and energy efficiency levels, contributing to regional disparities in energy use. Detailed correlation analysis between different variables can be addressed in more specific subsequent studies, supported by the results of the framework proposed herein.

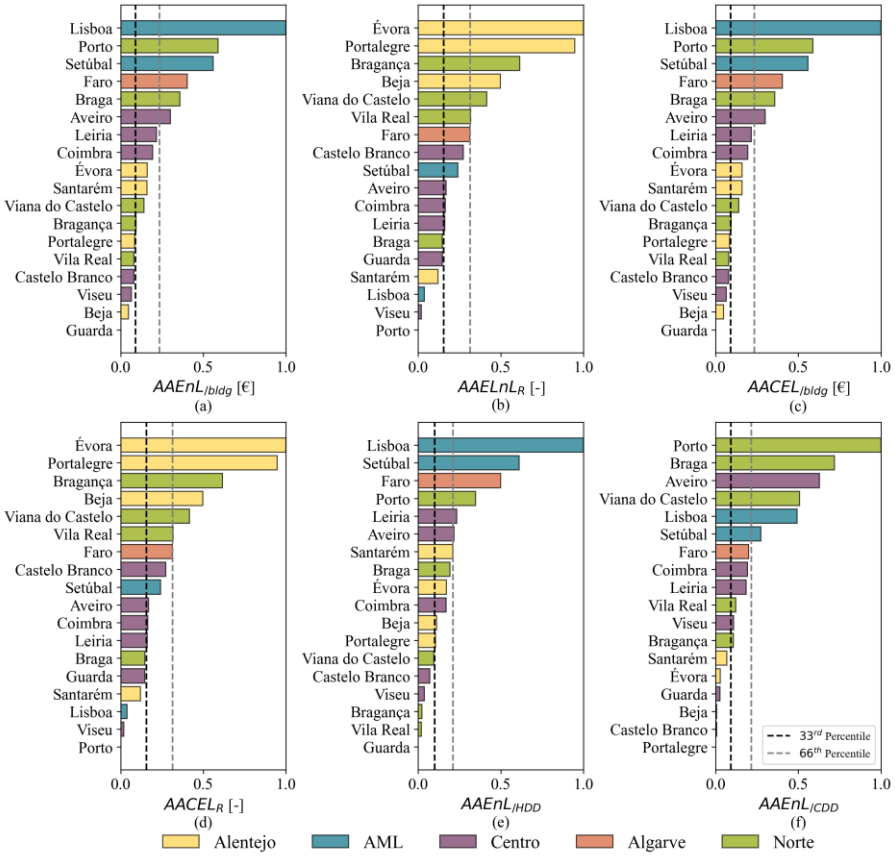

Figure 2.14 Energy performance-based rankings for each of the selected metrics: (a) Average Annual Energy Loss per building ($AAEnL_{/bldg}$), (b) Average Annual Energy Loss ratio ($AAEnL_R$), (c) Average Annual Carbon Emission Loss per building ($AACEL_{/bldg}$), (d) Average Annual Carbon Emission Loss Ratio ($AACEL_R$), (e) Average Annual Energy Loss per HDD ($AAEnL_{/HDD}$), and (f) Average Annual Energy Loss per CDD ($AAEnL_{/CDD}$).

Finally, by merging all the energy-metrics (as shown in Table 2.3), the energy performance prioritisation indicator (I_E) was obtained. Figure 2.15(a) illustrates the I_E-based prioritisation map, while Figure 2.15(b) exhibit the I_E value for each district. It can be seen how Lisbon is the most critical district, followed by Porto, Setubal, Faro, Braga and Aveiro, whereas Guarda is the last in the ranking, preceded by Beja, Viseu, Castelo Branco, and Vila Real. Nevertheless, I_E-based results show a narrower distribution within the [0,1] range, with values across regions being more similar and generally lower. This is largely due to the exceptionally high value recorded for the top-ranking region, Lisbon, which skews the distribution of other results following the application of the min-max scaling approach. Overall, most regions on the eastern side of Portugal exhibit lower priority in terms of energy needs compared to those in the western side of Portugal.

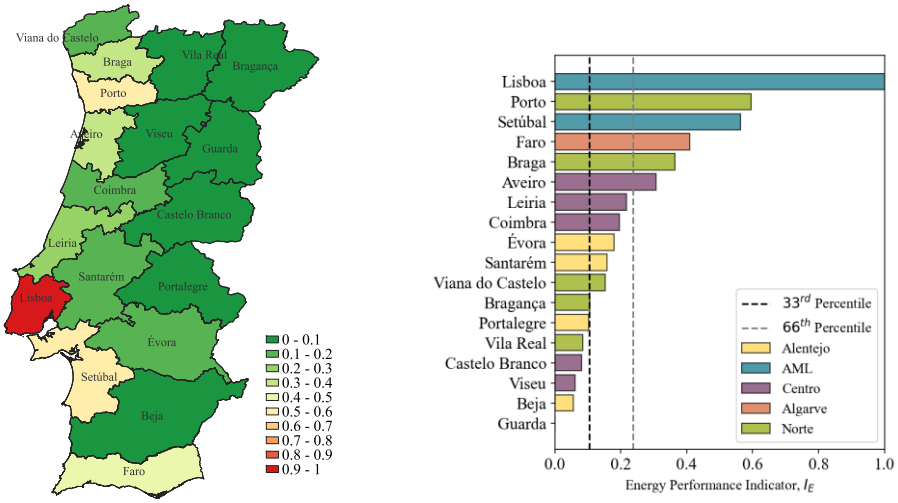

(a) (b)

Figure 2.15 (a) Energy performance-based prioritisation map and (b)energy performance indicator (I_E) per district.

2.5 SOCIOECONOMIC ASSESSMENT

Natural hazards pose significant threats to human lives and properties, often resulting in widespread social and economic disruptions. However, experiences from past events reveal that not all members of society are equally affected by such disasters. Certain groups, often marginalised or disadvantaged, are more vulnerable to the immediate impacts, such as death, injury, and economic loss, as well as the long-term challenges of recovery. Socioeconomic vulnerability plays a crucial role in

explaining why some communities experience the consequences of natural events, such as earthquakes, in a more severe or disproportionate manner, despite being exposed to similar levels of hazard (Burton and Silva 2016). In addition, populations living in buildings characterised by higher seismic vulnerability may struggle to cope during and after a disaster, further amplifying such a vulnerability. This highlights the need to consider the social dimensions of vulnerability when planning for disaster risk reduction and recovery. In line with recent research studies (Gkatzogias et al. 2022a; Mucedero and Monteiro 2024a), three metrics to perform the regional socioeconomic assessment of mainland Portugal were adopted herein: the Socioeconomic Vulnerability Index (SVI), the energy poverty and the seismic risk awareness. These metrics are used in the framework to introduce equity principles when identifying priority regions.

2.5.1 Human Development Index (HDI) and European Social Progress Index (SPI)

The Human Development Index (HDI), introduced in 1990 by the United Nations Development Programme (UNDP), is a composite index used to measure and compare the overall socioeconomic development of countries worldwide. It is comprised of three components: (i) health, measured by life expectancy at birth; (ii) education, measured through the mean years of education for adults aged ≥25 and the total number of years of schooling that a child entering the education system is expected to receive; and (iii) standard of living, measured by the Gross National Income (GNI) per capita, adjusted for purchasing power parity (PPP). Each of these components is scaled between 0 and 1, and their average is then used to calculate the overall HDI, providing a comparative measure of development levels across regions and countries. It is widely used by governments and organisations to inform policy decisions focused on improving overall human development. Unlike strictly economic indicators, the HDI incorporates health, education, and income, offering a more comprehensive view of development (Mucedero and Monteiro 2024a). While a higher HDI value reflects greater development, it does not capture all aspects of well-being, such as income inequality, environmental sustainability, or political stability. As a result, the HDI is often used alongside other measures, such as the European Social Progress Index (EU-SPI), to provide a more complete analysis of the development of a region.

The EU Regional Social Progress Index (EU-SPI) was developed to support the "Beyond GDP" agenda in Europe, offering a tool to benchmark social and

environmental progress across EU regions. It is designed to help policymakers and stakeholders assess the strengths and weaknesses of regions, focusing on aspects such as basic services (healthcare, education, water, waste management), access to ICT, energy efficiency, education, skills, and environmental sustainability. The index complements traditional economic measures, like GDP, providing a more holistic view of regional development by evaluating 53 socio-economic and environmental indicators. These are grouped into 12 components, which are further aggregated into three dimensions: basic, intermediate, and more subtle aspects of social progress. EU-SPI scores are presented on a 0-100 scale, where 100 represents the best performance. The index is particularly aligned with EU cohesion policy goals, aiming to inform investment decisions in key areas of social and environmental improvement.

The most recent available data was gathered for both parameters and is illustrated in Figure 2.16. The 2022 HDI data for each Portuguese NUTS II region was sourced from the Global Data Lab (2023) while the 2024 EU-SPI values were obtained from the European Comission (2024). The obtained values are very close for all Portuguese regions, which suggests a relative homogeneity in the overall level of development and social progress across Portugal. The HDI and the EU-SPI were averaged into a single metric – the Socioeconomic Vulnerability Index (SVI). Since the SVI should measure vulnerability, the mean value was subtracted from unity.

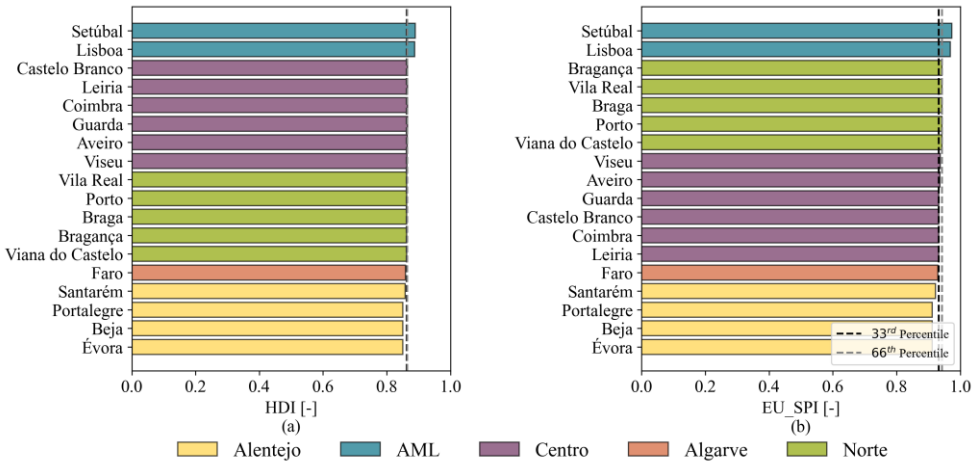

Figure 2.16 (a) Human Development Index (HDI) and (b) European Social Progress Index (EU-SPI) values.

2.5.2 Energy Poverty

Energy poverty is defined as the lack of access by a household to essential energy services, such as adequate heating, hot water, cooling, lighting and power, which provide basic and dignified living and health standards. Energy poverty impacts millions of people worldwide and presents a significant challenge to building an equitable and sustainable energy society. It is a complex, multidimensional issue with wide-ranging effects on social well-being, quality of life, and health. This issue might be exacerbated by a combination of factors, such as unaffordable energy prices, insufficient disposable income, high energy expenses, and poor energy efficiency in homes, all while considering the national context, social policies, and other relevant national policies (European Union 2023). According to Eurostat data (Eurostat 2023b), 10.6% of the European Union population is unable to keep their homes adequately warm. In Portugal, this percentage rises to 20.8% of its population, with the country being on the 1st position, along with Spain, on the list of those in which more citizens are unable to keep their homes adequately warm. Moreover, according to the National Long-Term Strategy for Combating Energy Poverty for 2023-2050, 35.7% of the population in 2012 lived in homes that are not comfortably cool during the summer. To deal with these issues, four strategic action axes have been recently proposed in Portugal (Presidência do Conselho de Ministros 2024), to promote: i) housing energy and environmental sustainability; ii) universal access to essential energy services; iii) integrated territorial action; and iv) knowledge and informed action. The Municipal Energy Vulnerability Index (MEVI), defined at a municipality level by Carvalho et al. (2023), was used to quantify the energy poverty in each Portuguese district. MEVI is an indicator designed to assess the susceptibility of municipalities to energy poverty by estimating the likelihood that individuals in a given municipality are unable to afford adequate heating for their homes. It is computed by incorporating individual and household characteristics, such as income, household composition, and other social and economic variables, from the Survey on Income and Living Conditions, along with municipal-level data from Census or the National Statistics Institute (INE). A higher MEVI value indicates a higher probability of energy poverty within a given region.

2.5.3 Earthquake Risk Awareness (ERA)

Risk perception, regardless of its nature, is critical in shaping individuals' responses and decisions regarding prevention measures. In the context of natural hazards like earthquakes, understanding the dynamics of risk perception and the influencing

factors is vital for mitigating the consequences of such events and developing effective mitigation strategies. Therefore, any prioritisation framework should incorporate risk awareness as a key metric, since lower risk perception may lead to reduced willingness among residents to invest in safety measures for their homes and assets. This understanding can significantly impact prioritisation patterns and resource allocation. Risk awareness is shaped by multiple factors, with the likelihood, frequency, and potential impact of an event being key in raising public consciousness. In mainland Portugal, despite the relatively high probability and frequency of earthquakes, most are of low magnitude, which may reduce the perception of the population to seismic risk. In societies with a limited number of significant disasters, it is often difficult to convince people of the need for effective measures related to awareness, management, and communication (Vicente et al. 2015).

In this study, the earthquake risk perception (P) was derived from a national survey conducted in Portugal (Tavares et al. 2011), which assessed the risk perception and the level of institutional trust in a representative sample of 1200 adult Portuguese citizens. The perception scale ranges from 1 (no awareness) to 5 (maximum awareness). For mainland Portugal, the following P values were gathered: Western-side (2.1), Eastern-side (1.4), North (1.3), Lisbon and Tagus Valley (2.8), South (2.3). Although generally low, the regional distribution of earthquake risk awareness aligns with the seismic hazard of Portugal, with urban areas, such as Lisbon, and the coastal regions showing higher levels of perception. The prolonged absence of a significant earthquake in mainland Portugal may contribute to the low levels of seismic risk perception among the general population. To account for these findings within the socioeconomic vulnerability indicator, the values were normalised to a 0-100 scale, where 0 corresponds to a perception level of 5 and 100 to a level of 1. The metric was then calculated according to the equation included in Table 2.3, for each Portuguese district.

2.5.4 Socioeconomic vulnerability metrics and indicator

The resulting rankings, considering the single socioeconomic metrics (SVI, MEVI and ERA), are presented in Figure 2.17, together with their statistical distributions (33rd and 66th percentiles). The SVI metric (Figure 2.17(a)) highlights significant disparities in socioeconomic conditions across Portugal, with Alentejo and Algarve emerging as the most critical regions. In contrast, the Metropolitan Area of Lisbon demonstrates the strongest performance, followed by the Norte region. Based on the MEVI metric

(Figure 2.17(b)), the most critical districts are in the Norte region, while the regions of Alentejo and the Metropolitan Area of Lisbon are the less critical. This suggests that socioeconomic vulnerability and energy poverty do not necessarily align across regions, indicating that areas with lower social vulnerability might still face significant energy poverty issues, and vice versa. The ERA metric is the one with the most heterogeneous results, showing that earthquake perception is not grouped by region. Nevertheless, the least aware regions, Viana do Castelo and Castelo Branco, are simultaneously characterised by lower hazard levels while the most aware regions are the Metropolitan Area of Lisbon and Santarém.

The global socioeconomic vulnerability prioritisation indicator ($I_{G,SVI}$) was then derived. Figure 2.18(a) illustrates the $I_{G,SVI}$-based prioritisation map, while Figure 2.18 (b) exhibits the $I_{G,SVI}$ for each district. The results are highly heterogeneous, as districts within the same regions of Portugal show significant variations in rankings, indicating a lack of uniformity in socioeconomic vulnerability across the country. Viana do Castelo, Castelo Branco, and Bragança exhibit the highest $I_{G,SVI}$ scores, while Santarém, Lisboa, and Aveiro show the lowest ones.

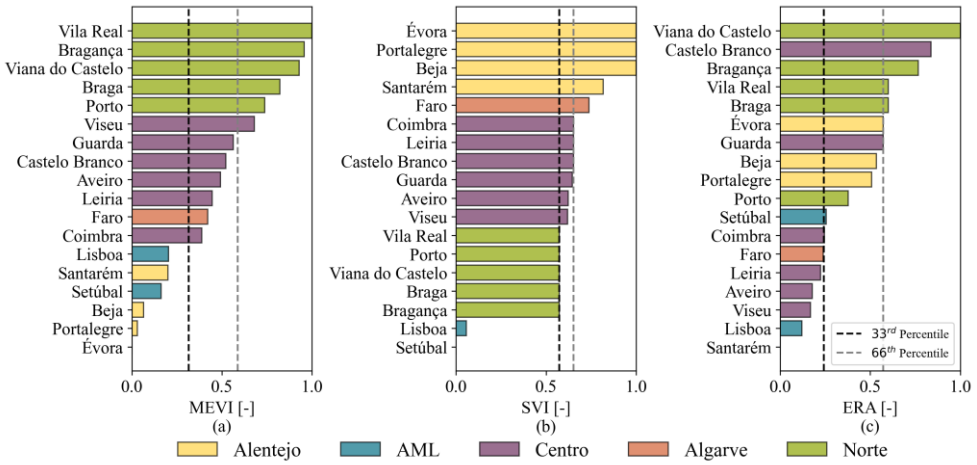

Figure 2.17 Socioeconomic vulnerability-based rankings for different metrics: (a) Socioeconomic vulnerability index (SVI), (b) Municipal Energy Vulnerability Index (MEVI) and (c) Earthquake Risk Awareness (ERA).

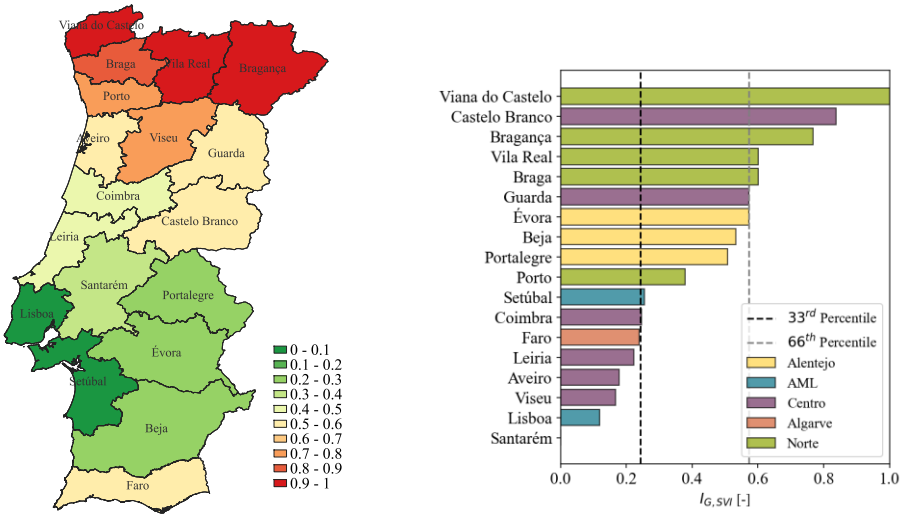

Figure 2.18 Global socioeconomic-based prioritisation map and indicator.

2.6 INTEGRATED PRIORITISATION

Finally, the four multi-sectoral integrated indicators ($I_{I,S-E}$, $I_{I,S-G}$, $I_{I,E-G}$, and $I_{I,S-E-G}$), introduced in Section 2.2.4, were quantified and are presented in Figure 2.19, Figure 2.20, Figure 2.21, and Figure 2.22. Considering a purely engineering-based prioritisation scenario, which would focus solely on seismic risk and energy performance metrics ($I_{I,S-E}$) (Figure 2.19), the results indicate that the AML region and the Algarve region are the most critical areas. These regions rank poorest in terms of seismic and energy performance, as found in Figure 2.11 and Figure 2.15. In contrast, the districts of Guarda, Viseu and Vila-Real emerge as the least critical, exhibiting lower vulnerability in both seismic and energy performance aspects. Even though these are very climatically cold districts, their very low energy consumption, when compared to the other districts, makes their overall performance higher than expected. When considering the seismic retrofitting and energy renovation as two independent strategies, but including the socioeconomic vulnerability, corresponding to the $I_{I,S-G}$ and $I_{I,E-G}$ integrated indicators, different prioritisation patterns are obtained. According to the $I_{I,S-G}$ indicator (Figure 2.20), the district of Faro exhibits the highest vulnerability, far exceeding the 66th percentile of the distribution across the regions. Interestingly, Viana do Castelo and Castelo Branco, which rank lower when only seismic vulnerability is assessed, become critical when social vulnerability is accounted for. Such shift in the ranking highlights the importance of

considering not just physical risks but also equity concerns in regional earthquake risk mitigation programs. In contrast, most districts in the Centro region, such as Viseu, Aveiro, Leiria, and Coimbra, are less critical according to the $I_{I,S\text{-}G}$ indicator. While having moderate or low seismic vulnerability, their socioeconomic resilience is also higher, reducing the urgency for immediate intervention. However, this approach might leave energy inefficiencies unaddressed, leading to continued high energy consumption and costs.

Based on the $I_{I,E\text{-}G}$-based prioritisation pattern (Figure 2.20), most districts in the Norte region, along with Lisboa, and Castelo Branco, emerge as areas of priority. Districts such as Lisboa and Porto do not demonstrate high socioeconomic vulnerability, but they rank at the top given their significant energy inefficiency (as shown in Figure 2.15). On the other hand, most of the districts in the Norte region as well as Castelo Branco show high levels of socioeconomic vulnerability (as shown in Figure 2.18), thus strongly influencing the $I_{I,S\text{-}E}$ values and bringing them up in the rankings, even though their I_E values are below the 33th percentile. In contrast, most districts in the Centro region are ranked at the end, indicating high energy efficiency and higher socioeconomic resilience. This suggests they are less urgent targets for energy renovation interventions compared to the more vulnerable districts in the Norte region and major urban centres.

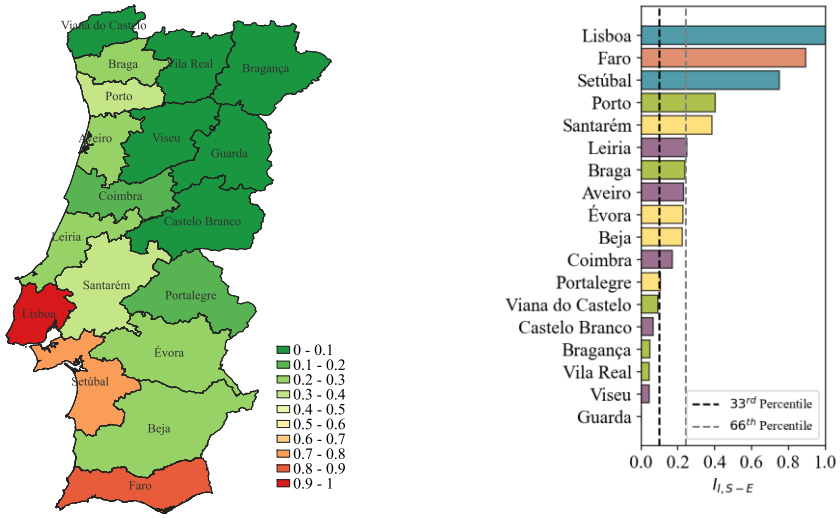

Figure 2.19 Multi-sectoral integrated prioritisation patter: seismic and energy-based prioritisation ($I_{I,S\text{-}E}$)

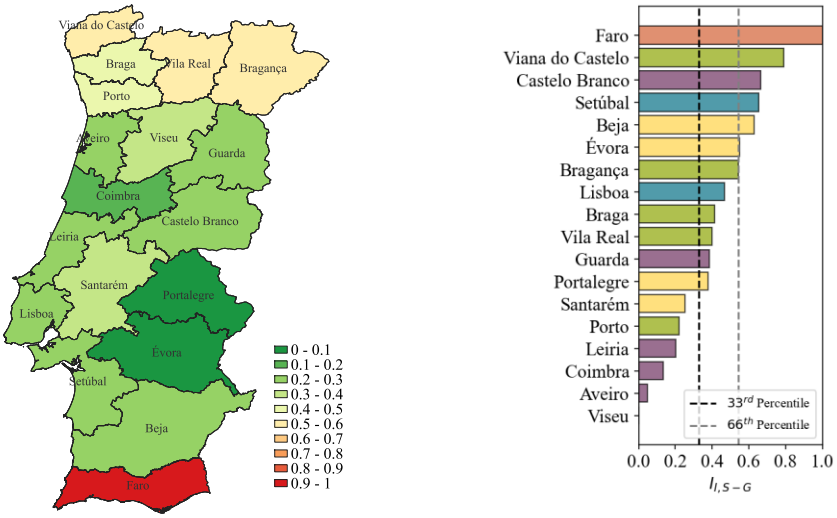

Figure 2.20 Multi-sectoral integrated prioritisation patterns: seismic and socioeconomic-based prioritisation ($I_{I,S-G}$)

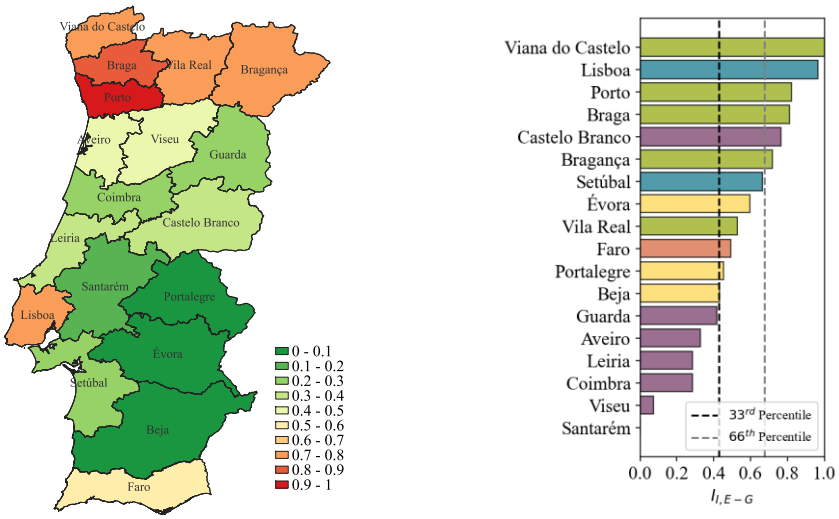

Figure 2.21 Multi-sectoral integrated prioritisation patterns: energy and socioeconomic-based prioritisation ($I_{I,E-G}$)

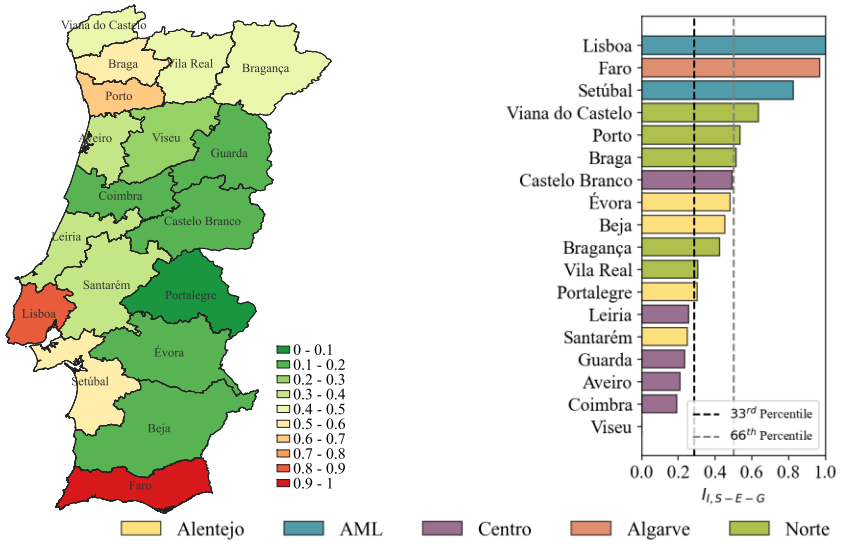

Figure 2.22 Multi-sectoral integrated prioritisation patterns: seismic, energy and socioeconomic-based prioritisation ($I_{I,S-E-G}$).

Finally, when the three macro sectors - seismic, energy and socioeconomic - are integrated within a single prioritisation indicator ($I_{I,S-E-G}$) (Figure 2.22), a clearer and more comprehensive view of the most critical needs of mainland Portugal can be obtained. It is specifically conceived to support regional-based financial strategies to the allocation of funds in regions with higher needs, in terms of seismic and energy deficiencies, but also with socioeconomic levels that can interfere with achieving the transition to a more resilient and sustainable community. Districts such as Faro, Porto, and the AML region rise to the top of the prioritisation list, reflecting high vulnerability across multiple domains. These areas are not only exposed to significant seismic risk but also struggle with energy inefficiency and socioeconomic challenges, making them priority targets for retrofitting and renovation interventions. Viana do Castelo and Castelo Branco also stand out as critical areas, driven largely by their socioeconomic vulnerability, despite performing better in other metrics. In contrast, most districts in the Centro, and the district of Santarém show lower vulnerability across the three macro sectors, as they ranked at the end of the prioritisation scheme, indicating a relatively higher socioeconomic resilience, better energy performance, and lower seismic risk.

2.7 CONCLUDING REMARKS

This chapter presented a comprehensive prioritisation framework for building retrofitting/renovation in mainland Portugal, integrating three macro sectors, namely seismic risk, energy performance and socioeconomic vulnerability. Such a framework can guide decision-maker efforts to efficiently define national-scale intervention strategies. The framework encompasses single and multi-sectoral indicators, and the primary indicators (seismic risk, energy performance and global socio-economic vulnerability) were estimated according to solid, state-of-the-art engineering-based research. The framework is scalable to other regions or countries, provided the information on the three sectors is available.

The resulting prioritisation patterns showed substantial variation depending on the considered multi-sectoral indicators. From a purely engineering-based prioritisation perspective, focused on seismic risk and energy performance metrics, the Lisbon Metropolitan Area and the Algarve regions emerged as the most critical areas, ranking highest for both seismic and energy vulnerability. In contrast, the Norte region (apart from the district of Porto) and some districts in the Centro region, were identified as the least critical, exhibiting lower levels of vulnerability in both aspects. When incorporating socioeconomic vulnerability, different prioritisation patterns arise. When seismic risk and socioeconomic vulnerability are coupled (neglecting the energy renovation), Faro was identified as the most vulnerable district, while Viana do Castelo and Castelo Branco became critical due to their social vulnerabilities, despite lower seismic risk. In contrast, districts in the Centro region showed moderate to low seismic vulnerability and greater socioeconomic resilience, reducing the urgency for intervention. Conversely, considering energy renovation and socioeconomic vulnerability, the Norte region, along with the districts of Lisboa and Castelo Branco, became critical due to significant energy inefficiency, despite not exhibiting high socioeconomic vulnerability. In turn, the Centro region ranked lower, indicating better energy efficiency and resilience, thus lessening the immediate need for retrofitting interventions. Decoupling the retrofitting process allows more flexible allocation of resources, enabling regions to focus on the most pressing vulnerabilities. However, such an approach also requires careful planning to ensure that long-term sustainability is not compromised by focusing on one aspect at the expense of another. For instance, addressing seismic retrofitting without considering energy efficiency might lead to buildings that are safer but still inefficient in terms of energy consumption, thereby limiting the overall benefits of the intervention. Similarly, improving energy performance without addressing seismic risks could

leave buildings vulnerable to future earthquakes, undermining the resilience of communities.

By integrating the three macro sectors, Algarve, the Lisbon Metropolitan Area, and some districts in the Norte region ranked at the top, pointing out the need for a balanced retrofitting/renovation strategy that addresses not only physical risks but also energy inefficiencies and socioeconomic challenges. Conversely, lower levels of vulnerability across these domains were found in the Centro region districts, such as Coimbra and Viseu, suggesting that allocation of funds for renovation/retrofitting strategies may be less urgent in these areas. This comprehensive prioritisation scheme highlighted the regional disparities in mainland Portugal, allowing decision makers and policy makers to tailor interventions as a function of the specific needs of each region. By integrating seismic risk, energy efficiency, and socioeconomic vulnerability, the prioritisation scheme and the resulting financial planning strategies can improve the seismic safety and energy performance of the existing Portuguese building stock in a more consistent and accurate manner and promote equitable social development, contributing to a more resilient and balanced national response plan.

This chapter set the foundation for the need to understand how retrofitting strategies perform at national scale. While the prioritisation framework identifies where seismic and energy interventions are most urgently needed, Chapter 3 will expand the scope of the analysis by exploring retrofitting scenarios and impact assessment for the Portuguese building stock. Moreover, while vulnerability models are appropriate for regional-scale prioritisation and the evaluation of retrofitting scenarios across building portfolios, when the focus shifts to individual buildings, for instance, to assess alternative retrofitting strategies and determine the optimal solution, component-based methodologies become computationally intensive and do not permit rapid assessments. To overcome this limitation, generalised storey loss functions (SLFs) and storey environmental impact functions (SEIFs) will be introduced in Chapter 4. Owing to their flexibility and ease of implementation, these functions can also be employed in professional practice to provide rapid estimates of key decision variables within the multi-criteria frameworks presented in Chapter 5.

CHAPTER 3

Regional renovation scenarios for seismic upgrading of RC buildings in mainland Portugal

3 REGIONAL RENOVATION SCENARIOS FOR SEISMIC UPGRADING OF RC BUILDINGS IN MAINLAND PORTUGAL

3.1 INTRODUCTION

As demonstrated in the previous chapter, large-scale renovation programmes require prioritisation frameworks to allocate limited resources to the areas of greatest need. While retrofitting existing buildings is essential for enhancing seismic resilience, energy efficiency, and overall sustainability of the built environment, it must be approached in a way that maximises combined benefits across multiple dimensions. A key challenge lies in the optimal allocation of available resources to achieve the greatest risk reduction at the community level (Sediek et al. 2024). Focusing only on the effect of earthquakes, this requires a thorough assessment of seismic risk, since the retrofit solutions applicable at a territorial scale strongly depend on hazard, vulnerability, and exposure. To this end, understanding how building typology and construction period influence seismic behaviour is a crucial preliminary step, requiring vulnerability assessments to be carried out for buildings in their as-built state and afterwords for assessing feasible retrofitting strategies. Moreover, to evaluate the effectiveness of seismic mitigation strategies, it is necessary to estimate the potential reduction in vulnerability achievable through retrofit. Despite the recognised seismic exposure of Portugal and the urgent need for retrofit interventions, the availability of fragility and vulnerability functions derived specifically for the Portuguese building stock remains limited (Couto et al. 2025). Most existing fragility curves applicable to Southern European RC frames have been developed for Italian and Greek building typologies, for both as-built (Kappos et al. 2006; Kappos 2013; Da Porto et al. 2021; Dolce et al. 2021; Anelli et al. 2023; Manfredi et al. 2023b; Nafeh and O'Reilly 2024a) and retrofitted buildings (Gentile and Galasso 2021; Aljawhari et al. 2022; Follador et al. 2023), and their direct transferability to the Portuguese context is not straightforward, given differences in construction practice and material properties. While some studies have proposed fragility functions for Portuguese RC buildings in their as-built condition (Silva et al. 2015c, a; Romão et al. 2021; Martins and Silva 2021b), the availability of post-retrofit fragility and vulnerability models remains particularly scarce.

Regarding large scale renovation scenarios and impact assessment, different studies have investigated the post-intervention behaviour of RC buildings subjected to

different strengthening techniques. Most of these studies accounted for the effect of retrofit by horizontally shifting the as-built fragility curves along the intensity measure axis, either by scaling the median of each damage state by a performance improvement factor (Harati and Van De Lindt 2024; Sediek et al. 2024) or by transitioning a building's fragility curve from a lower to a higher code level (Kappos and Dimitrakopoulos 2008; Gkatzogias et al. 2022b). This approach, however, carries inherent limitations, as it assumes that the dispersion of the fragility function remains unchanged after retrofitting, and that the percentage shift is uniform across all damage states and retrofit strategies, neither of which generally holds. As demonstrated by Aljawhari et al. (2022), while the change in dispersion is typically minor, the shift in median intensity is not identical across damage states and varies with the type of intervention.

The influence of retrofitting on the seismic performance of building stocks can be quantified through seismic risk metrics (e.g., average annual economic losses (AAEL), average annual loss of life (AALL)). Reductions in these metrics between the as-built and retrofitted states provide a direct measure of the achieved risk mitigation and form the basis for quantifying the annual benefit of intervention. In this context, it is important to recognise that losses following earthquakes extend beyond direct physical damage to include downtime, housing displacement, business interruption, and broader impacts on livelihoods and supply chains (Donà et al. 2019; Calvi et al. 2021; Gentile and Calvi 2023; Mucedero et al. 2025b, a). Accounting for these indirect effects is therefore essential for a comprehensive seismic risk assessment and cost-benefit analysis, as focusing solely on direct repair costs may underestimate the true benefit of intervention and could bias the final decision-maker's choices. AALL complements the economic dimension by capturing life safety aspects and ensuring that the assessment extends beyond financial metrics thus, at least in some way, addressing the human dimension of seismic risk.

When combined with the cost of the retrofit intervention, these risk-based estimates, encompassing both direct and indirect losses, form the basis for retrofit feasibility assessment. Economic and cost-benefit analyses are central to evaluating the viability of seismic retrofit interventions, providing a structured means of comparing the cost of a mitigation measure against the benefits achieved through improved seismic performance. Multiple studies have employed this approach to assess retrofit strategies for older RC frame buildings, demonstrating that the effectiveness of an intervention must be gauged not only by its capacity to reduce seismic risk but also by its economic viability, given the finite resources available for mitigation

(Kappos and Dimitrakopoulos 2008; Liel and Deierlein 2013; Sousa and Monteiro 2018b; Cardone et al. 2019; Natale et al. 2021). However, these efforts have been conducted predominantly outside the Portuguese context, and equivalent assessments for the Portuguese building stock remain largely absent. Moreover, while considerable research has been devoted to fragility assessment and retrofit design at the building level, frameworks that integrate risk quantification with economic viability and phased intervention planning at the territorial scale remain scarce. To the Authors' knowledge, only a handful of studies have attempted such an integrated approach at a regional scale, notably in the Italian context (Sousa and Monteiro 2018b; Cardone et al. 2019; Carpanese et al. 2025), where vulnerability assessment, seismic risk quantification, and economic evaluation have been combined for a regional building stock. Equivalent efforts remain largely absent in the Portuguese context, where seismic retrofit policy still lacks the quantitative, risk-informed foundation needed to guide investment prioritisation at the national or regional level.

Building on the prioritisation framework developed in Chapter 2, which identified the Lisbon Metropolitan Area (AML) as one of the most critical regions in mainland Portugal in terms of combined seismic, energy, and socioeconomic vulnerability, this chapter proposes a comprehensive methodology for the seismic risk assessment and retrofit evaluation of the Lisbon RC building stock, the major municipality within AML. Eighteen building taxonomies are defined to represent the most at-risk segment of the building stock, and numerical models are subjected to nonlinear static analysis to derive fragility and vulnerability functions using the cloud-based capacity spectrum method (Nettis et al. 2021a). To avoid the approximations inherent in shift-based approaches, fragility curves for the retrofitted building models are derived directly from nonlinear static analysis, ensuring that both the median and dispersion of each damage state reflect the actual post-retrofit structural behaviour. Three retrofit strategies, namely0fibre-reinforced polymer (FRP) wrapping, steel jacketing (STJ), and reinforced concrete jacketing (RCJ), are designed in compliance with EC8-3 (CEN 2005) and evaluated against the as-built condition. The resulting vulnerability functions, incorporating direct losses, indirect relocation costs, and fatalities, are combined with the seismic hazard of the Lisbon municipality to estimate AAEL and AALL. The economic viability of each strategy is then assessed through cost-benefit ratios and payback time analyses, and a phased intervention scenario is also developed to guide possible incremental investment across the building stock, providing a transparent and replicable basis for seismic retrofit policy in Portugal.

3.2 METHODOLOGY

The seismic risk of the Lisbon RC building stock was estimated, and the effectiveness and economic viability of the proposed retrofit strategies were evaluated following five steps. First, the building taxonomies representative of the most at-risk segment of the Lisbon stock are defined. Second, numerical models are developed for each taxonomy to simulate structural behaviour under seismic loading. Third, the retrofit strategies and their associated parameter variations, costs, and environmental impacts are described. Fourth, the seismic hazard of Lisbon is characterised. Finally, the seismic assessment procedure, encompassing damage state definition, fragility and vulnerability function derivation, and loss estimation, is presented. The outputs of this methodology feed directly into the results and economic assessment discussed in Sections 3 and 4.

3.2.1 Taxonomy definition

Following the prioritisation study (Chapter 2) integrating three macro-sectors of vulnerability, seismic, energy, and socioeconomic, Lisbon was identified as the region in most need of intervention, exhibiting the highest combined vulnerability scores across the country. To better understand the drivers of these vulnerabilities, a detailed examination of the building stock and exposure in these regions was carried out, with the aim of identifying which building classes are most susceptible to seismic damage and which contribute most substantially to potential losses.

The building stock of Lisbon comprises 367,022 buildings, of which 63% are reinforced concrete (RC) structures and 37% are masonry buildings. Within the RC inventory, 76% are low-rise buildings (one to three storeys), whereas only 7% correspond to high-rise buildings with seven or more storeys. Based on the seismic design code level, four structural classes were identified: CDN (no seismic design), CDL (low-code design), CDM (moderate-code design), and CDH (high-code design). Among these, CDM constitutes the largest share of the RC stock (52%) followed by CDN (18%), CDH (17%), and CDL (14%).

As this chapter focuses exclusively on seismic risk, the identification of the most critical building classes was informed by the seismic risk indicator (I_S), introduced in Chapter 2. This indicator is derived from three seismic sub-indicators: Average annual economic loss per building ($AAEL_{/bldg.}$), Average annual economic loss ratio ($AAEL_R$), and Average annual loss of life ratio ($AALL_R$), which incorporate outputs from seismic risk assessment, namely the annual economic losses and annual fatalities,

as well as key exposure variables namely the number of buildings, its replacement costs, and the number of occupants.

Figure 3.1 shows the relative contribution of each code level to the total seismic risk across the four indicators. CDN consistently represents the largest share across all metrics, with a particular dominance for the $AALL_R$, concentrating, alone, over three quarters of the total risk, reflecting the extreme life-safety consequences associated with the absence of seismic detailing in older RC buildings. CDL represent the second largest contributor, with shares ranging between 23% and 36% depending on the indicator. CDM and CDH jointly account for less than 25% across all indicators, confirming that buildings designed to more modern seismic codes contribute marginally to the overall risk. The variation in CDN dominance across indicators, lower for economic metrics and highest for life-safety, suggests that while non-ductile buildings do not necessarily have the highest replacement costs, their structural fragility results in disproportionately severe consequences in terms of human casualties. These results tend to identify CDN and CDL as the priority targets for seismic risk mitigation strategies in Lisbon.

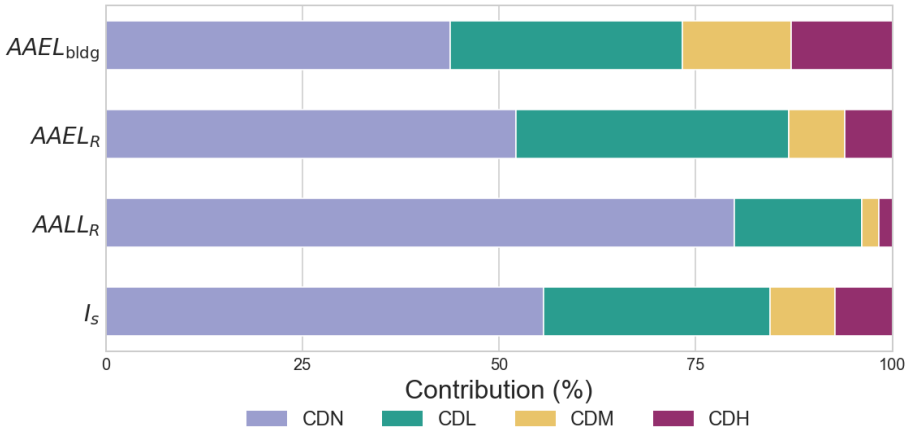

Figure 3.1. Contribution of each code-level building to seismic risk metrics and indicator

Figure 3.2 disaggregates the contribution of each building height class to the seismic indicators within each code level group. Several patterns emerge consistently across indicators and code levels. For $AAEL_{bldg}$, mid-to-high-rise buildings (≥4 storeys) dominate within all code levels, reflecting the larger losses associated with taller and more expensive buildings. In contrast, $AAEL_R$ and $AALL_R$ show a more balanced

distribution across storeys, with low-rise buildings (1 to 3 storeys) contributing more substantially to losses, particularly within CDN and CDL classes. This suggests that while taller buildings drive aggregated economic losses, lower-rise non-ductile buildings exhibit comparatively higher loss ratios relative to their replacement cost and occupancy, a consequence of their higher seismic vulnerability. As regards I_S, the storey distribution reflects a combination of these patterns, with mid-rise buildings (4 to 6 storeys) emerging as consistent contributors across all code levels. It is also noticeable that for the lower code-compliance levels (CDN and CDL), the risk is broadly distributed across all storey classes from 1 to 6, confirming that the vulnerability in these classes is not confined to a narrow height range. Within CDH and CDM, the contribution of 7–20 storey buildings is notably more prominent, which may be explained by the fact that modern code-compliant tall buildings, despite their better design, accumulate larger economic losses due to their size and value. Overall, these results highlight that seismic risk prioritisation cannot rely solely on the ductility class but must also account for building height, as the interaction between structural system, code level, and number of storeys determines the dominant risk profile.

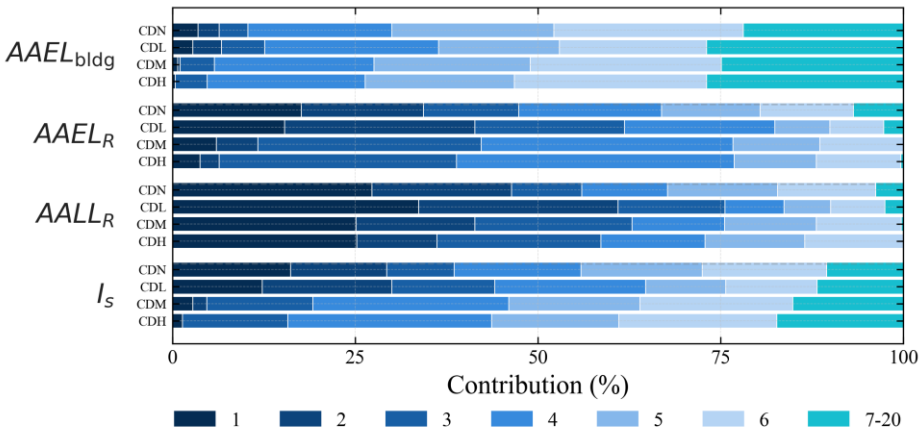

Figure 3.2. Contribution of the number of storeys to each seismic risk metrics and indicator

Furthermore, these results are used to define the scope of the renovation scenarios investigated in this chapter. Given that CDN and CDL buildings jointly account for most of the seismic risk across all indicators, these two ductility classes are selected as the primary targets for seismic retrofitting interventions. Within these classes, the analysis of storey contributions reveals that buildings of 1 to 6 storeys represent the

dominant share of risk, while the 7+ storey category constitutes a comparatively small fraction of the CDN and CDL stock in Lisbon. Accordingly, the renovation scenarios developed in this chapter focus on CDN and CDL RC buildings with 1 to 6 storeys, which represent the most prevalent, most vulnerable, and highest-risk segment of the building stock in Lisbon. For each of these classes, buildings were modelled with lateral force coefficients (LFC) of 5% and 10% of the building weight, in line with the values adopted in the Portuguese exposure model, ensuring consistency between the modelled building stock and the broader risk assessment framework within which the retrofit scenarios are evaluated.

3.2.2 Numerical modelling

Following the selection of building taxonomies of interested, the SimDesign tool (Ozsarac et al. 2025) was employed to generate building models. Firstly, probability distributions describing the geometric characteristics of Portuguese buildings, as published by Silva et al. (2015a) and Furtado et al. (2016), were incorporated into SimDesign to ensure that the generated structures are aligned with the characteristics of the Portuguese building stock. Secondly, three key parameters were defined for each building class: code level, lateral force coefficient (LFC), and number of storeys.

Regarding the LFC, it is noted that CDN buildings, by definition, were not designed with any seismic lateral load provision as they were mainly designed for gravity loads only, and therefore no LFC is assigned to this class. For CDL buildings, the LFC reflects the seismic design coefficient applicable at the time of construction. Given that the analysis is focused on Lisbon, two LFC values were considered for CDL buildings, namely 5% and 10%, consistent with the range of coefficients prescribed by the Portuguese seismic codes (RSCCS 1958b; RSEP 1961b; REBA 1967). Combined with the six storey classes, this results in a total of 18 building classes: 6 for CDN (one LFC level × six storey counts) and 12 for CDL (two LFC levels × six storey counts). For each building class, 10 building layouts were generated, yielding a total of 180 building models.

The buildings were then modelled in OpenSees (McKenna et al. 2010a) through the CAD2Sees tool (Yükselen et al. 2025a), which automates the translation of simulated design structural information into ready-to-run OpenSees models. The numerical model of each building comprises structural elements (i.e. beams and columns), beam-column joints (BCJs), and masonry infills, simulating the structural

behaviour of older Portuguese RC frames. More information of the modelling can be found in Yükselen et al. (2025b, a). Concrete and steel material properties were taken directly from the output of the SimDesign tool (Ozsarac et al., 2025). The effect of the exterior masonry infills on the response of the structure was modelled by incorporating a system of equivalent diagonal struts that represent the behaviour of the infills. The openings' height and length were defined as 1.43 m and 1.8 m respectively, based on the study of (Furtado et al. 2016). The mechanical and geometry properties of the infills correspond to the weak masonry infill typology as per the macro-level classification proposed by Mucedero et al. (2020, 2021). This typology consists of a single-leaf wall made of horizontal hollow lay bricks, with a thickness of 80 mm and finished with 10 mm tick plaster layers on both external faces. This configuration is consistent with experimental observations and common construction practices reported for Portuguese masonry infills (Akhoundi et al. 2018). The strut models used in these analyses are only capable of modelling the in-plane behaviour of the infills. To simplify the analysis and the post-processing, the out-of-plane (OOP) behaviour of the infills was not included.

3.2.3 Retrofit strategies

Three widely adopted seismic retrofit techniques were selected: fibre-reinforced polymer (FRP) wrapping, steel jacketing (STJ), and RC jacketing (RCJ). These strategies were selected based on their prevalence in literature and their practical applicability to the case study building stock. An illustrative example of each seismic retrofit technique is illustrated in Figure 3.3. These retrofit strategies are applied within the Iterative Retrofitting Algorithm (IRA) framework developed by Yükselen et al. (2025a), which reproduces the approach commonly followed in engineering practice for the design of local seismic interventions. IRA operates by identifying structural members that fail to meet the prescribed performance criteria following assessment of the as-built building, and progressively applying interventions until full compliance is achieved. Even though IRA does not produce an optimised design as it seeks a feasible retrofit scheme rather than minimising an explicit objective function, namely cost or disruption, it can be considered representative of common engineering practice. In this context, the resulting structure is designed to satisfy code requirements without further optimisation of the retrofit strategy or combination of different retrofit interventions. It is also worth noting that the initial constraints imposed on member-level interventions can occasionally lead to an ill-conditioned problem, where the algorithm becomes entrapped and no solution is

found. Despite this, IRA provides a practical and transparent baseline that is representative of current engineering practice, and the resulting designs can serve as a starting point for more refined optimisation if needed.

Two strategies combining the different retrofitting techniques were considered: i) RC jacketing applied to the columns and FRP wrapping applied to the beams and ii) steel jacketing applied to columns while FRP wrapping is applied to beam elements. For each retrofit strategy, the key geometric and material parameters governing structural performance were varied systematically to generate an ensemble of retrofitted structural variants, capturing the range of practically feasible intervention levels. For FRP wrapping, the number of fibre layers and the strip width (w) were varied across a discrete set of combinations, alongside the edge bonded fibre width at beam ends, capturing configurations ranging from light confinement to full-section wrapping. For RC jacketing, the jacket thickness (t_j) applied to the columns was varied, with longitudinal and transverse reinforcement properties held consistent with current practice. For steel jacketing, three parameters were varied simultaneously: the angle section leg length (L), the batten plate height (h_b), and the batten spacing (s_b), reflecting the main design variables controlling confinement effectiveness and composite action. Material properties, including steel yield strength, FRP elastic modulus, ultimate strain, and characteristic tensile strength, were held constant across variants, consistently with commonly available commercial products. For each combination of parameters, the updated cross-section strength, stiffness, and deformation capacity were computed, and the full assessment was re-executed. Further details on the modelling approach of these retrofitting strategies can be found in Yükselen et al. (2025a). For each retrofit configuration, the associated installation cost and embodied carbon were then estimated by identifying the required actions, aggregating unit costs and $eqCO_2$ values per action, and summing across all intervention components. Cost data were drawn from Italian sources as a comparable proxy for the Portuguese context, while embodied carbon values were obtained from Environmental Product Declarations (EPD) sourced via the EC3 platform and producer declarations, with Southern European equivalents used where Portuguese data were unavailable. Only the production stage (A1–A3) was considered, and mean $eqCO_2$ values were adopted for computational consistency. Further details can be found in Yükselen et al. (2025b).

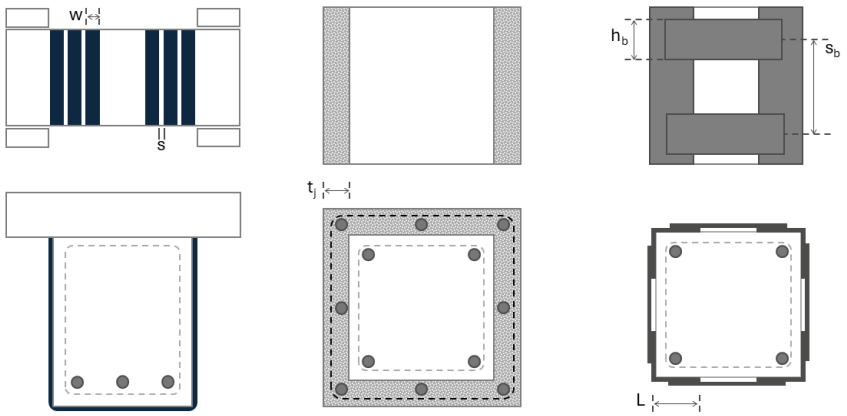

Figure 3.3. Illustrative example of the selected seismic retrofit techniques: (a) FRP, (b) RC jacketing and (c) steel jacketing.

3.2.4 Seismic Hazard

The seismic hazard analysis was performed using the European Seismic Hazard Model, ESHM20 (Danciu et al. 2021), within the OpenQuake engine (Pagani et al. 2014), following a classical probabilistic seismic hazard analysis (PSHA) approach. Hazard curves were computed for each parish in Lisbon. For what concerns local site conditions, the $V_{S,30}$ map for Portugal derived from ESHM20 (Danciu et al., 2021) was adopted to account for site response amplification effects. The average spectral acceleration (AvgSA) was selected as intensity measure (IM), defined over a period range representative of the fundamental vibration periods of the building stock under consideration. For each taxonomy, the fundamental periods in both horizontal directions were extracted from the 10 building layouts. The period range for each taxonomy was then defined by the minimum and maximum period across the 10 layouts, for each direction. The geometric mean of these four values (T_{geo}) was then computed for each building. The period range used to define the AvgSA was set to $[0.2T_{geo}, 2.0T_{geo}]$ to ensure that such an IM captures both higher-mode contributions (through the lower bound) and elongated-period effects due to nonlinear behaviour and damage accumulation (through the upper bound). Moreover, since this study encompasses both as-built and retrofitted buildings, which exhibit different stiffness characteristics hence different fundamental periods, the selected period ranges vary across the building set. This variability ensures that the AvgSA definition remains structure-specific and captures the relevant frequency content for each case,

making it a more stable and efficient IM when compared to $S_a(T_1)$, for example, when dealing with a heterogeneous building portfolio. Table 3.1 summarises the minimum and maximum periods of vibration obtained for each horizontal direction, along with T_{geo}.

Table 3.1 Minimum and maximum fundamental periods obtained for each set of storeys in both principal directions, along with the selected period range for the calculation of the average spectral acceleration.

Number of storeys	T_x (s)		T_y (s)		T_{geo}	Period range
	min	max	min	max		
1	0.18	0.42	0.15	0.27	0.25	0.05 – 0.5
2	0.30	0.68	0.27	0.42	0.42	0.08 – 0.8
3	0.46	0.82	0.39	0.58	0.56	0.11 – 1.1
4	0.54	0.98	0.44	0.66	0.65	0.13 – 1.3
5	0.62	1.14	0.55	0.88	0.80	0.16 – 1.6
6	0.86	1.65	0.63	1.02	1.00	0.20 – 2.0

Figure 3.4 shows the obtained hazard curves for all the parishes in Lisbon, as a function of the selected IM. The hazard curves exhibit a consistent shape across all sites and all period ranges, reflecting the relatively uniform seismotectonic setting of the region.

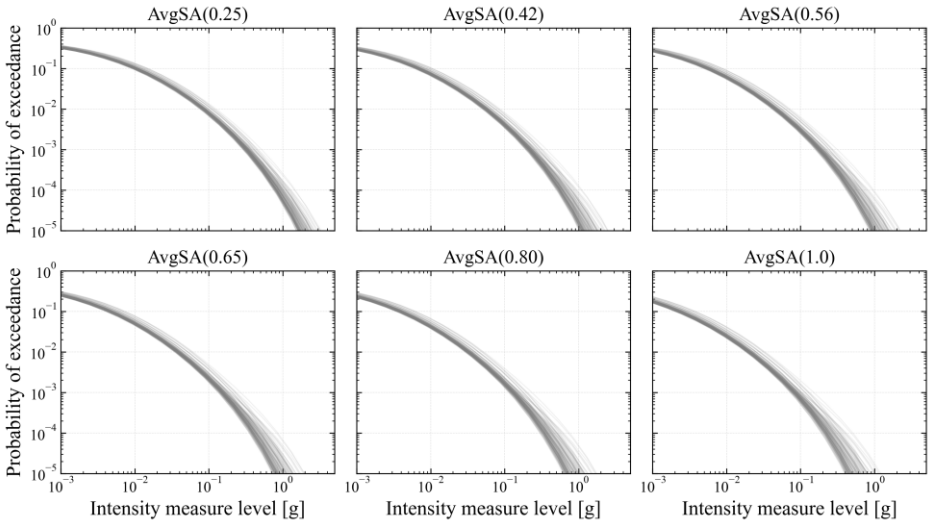

Figure 3.4 Hazard curves for the location and IM considered

3.2.5 Seismic assessment and fragility analysis

The seismic performance of the buildings of each taxonomy, in both the as-built and retrofitted configurations, was evaluated through nonlinear static (pushover) analysis carried out independently in both principal directions using a modal load pattern. Analyses were performed up to a target roof drift of 10%, ensuring that the full nonlinear response is captured, including the post-peak degradation regime, which is particularly relevant for the collapse assessment. The pushover results served as the foundation for two distinct assessment workflows: i) a code-compliance verification, in which the performance point was determined via the N2 method in accordance with EC8 and used to design each retrofit intervention and ii) a probabilistic fragility analysis based on the Cloud-Based Capacity Spectrum Method (CB-CSM), through which intensity-dependent fragility functions were derived for each taxonomy and used as input for the subsequent seismic risk quantification.

Regarding the first point, for each retrofit configuration, the displacement demand was determined using the extended N2 method, proposed for infilled frames (Dolšek and Fajfar 2008). For each pushover analysis, the capacity curve was idealised and converted into spectral coordinates, and the performance point was identified as the intersection with the seismic demand spectrum. The seismic demand was defined for importance class II buildings at the Significant Damage (SD) limit state, corresponding to a return period of 308 years (15% probability of exceedance in 50 years). For the selected site of Lisbon, this corresponds to a peak ground acceleration (PGA) of 75% of the 475-year return period value (0.15g), using the Type-1 elastic response spectrum from the Portuguese Annex (CEN 2009). At the performance point, all primary structural members have to be checked through the procedures established in Part 3 of Eurocode 8 (CEN 2005), which foresees the evaluation of the shear strength and flexural deformation. A retrofit configuration was considered valid only if all frame members satisfied both checks. If any member was found non-compliant in any direction or loading case, the configuration was rejected.

Seismic fragility was then characterised for both the as-built structure and the code-compliant retrofit configurations using the Cloud-Based Capacity Spectrum Method, implemented within the CAD2Sees tool (Yükselen et al. 2025a). Unlike the N2 method, which targets a single performance point at a prescribed hazard level, the CB-CSM evaluates structural response across a suite of ground motion records scaled to multiple intensity levels, yielding a cloud of EDP–IM pairs. Damage state thresholds were defined directly from the idealised capacity curve in spectral

displacement coordinates capturing the full range of structural behaviour from yielding through to collapse. The pushover curve was idealised, adopting either a bilinear or multi-linear form depending on the shape of the capacity curve and the presence of infill degradation. For each ground motion, the performance point was determined iteratively in the ADRS format using the equivalent viscous damping approach. The resulting cloud of EDP–IM pairs was used to derive fragility functions for each damage state through the total probability theorem, distinguishing between collapse and non-collapse cases. For non-collapse cases, a Power Spectral Demand Model (PSDM) was established by log-log linear regression of EDP on IM, with logarithmic dispersion computed using two degrees of freedom. Collapse probability as a function of IM was estimated through logistic regression using a generalised linear model with binomial family and logit link, applied to the binary collapse indicator. The combined fragility curve was subsequently fitted to a lognormal cumulative distribution function by nonlinear least squares, yielding the median intensity measure (α) and logarithmic standard deviation (β) for each damage state. This procedure was applied independently to each building class and retrofitted configuration, enabling a direct comparison of fragility parameters across as-built and retrofitted buildings.

3.2.5.1 Damage state definition

For the definition of damage state thresholds, four damage states were considered, ranging from slight (DS1) to complete damage (DS4). The threshold for DS1 was set at 75% of the yield displacement, reflecting the onset of damage in non-structural elements, namely masonry infill walls, which typically exhibit cracking prior to the yielding of the main structural system. DS4 was defined as the point at which the structure reaches its ultimate displacement capacity, beyond which collapse is considered imminent. The two intermediate damage states, moderate (DS2) and extensive (DS3), were defined by equally spacing the displacement thresholds between DS1 and DS4, following the approach proposed by Martins and Silva (2021b).

The ultimate displacement capacity of each building was identified directly from the pushover curve using a combination of local and global criteria: (i) shear demand-capacity ratio (DCR) exceeding unity for more than 50% of columns in any storey; (ii) rotation DCR exceeding unity for more than 50% of columns in any storey; (iii) inter-storey drift ratio exceeding 2.5%; and (iv) base shear dropping below 85% of its peak value. The most conservative criterion governs in each case, ensuring a definition of

collapse that is sensitive to both localised brittle failure and global structural degradation. Infill panel failure was additionally tracked through a panel-level DCR criterion, with the corresponding displacement used to define the transition point in the idealised capacity curve. The adoption of multiple criteria is motivated by the recognised limitations of any single global parameter in capturing all possible failure mechanisms across several building layouts (Silva et al. 2015a).

3.2.5.2 Taxonomy based fragility functions

Once building-specific fragility parameters were obtained for each damage state and for each analysed building, taxonomy-based fragility functions were derived by aggregating the lognormal parameters across all buildings within each taxonomy. The taxonomy-level median, θ_T, was computed as the geometric mean of the building-specific medians, defined in the logarithmic space as represented in Eq. 31. The taxonomy-level dispersion, β_T, was obtained by applying the law of total variance, which accounts for both intra (β_{intra}) and inter (β_{inter}) building variability.

A further contribution to the total dispersion arises from the uncertainty inherent in the definition of the damage state thresholds. As discussed above, no single criterion is universally capable of capturing all relevant failure mechanisms across a heterogeneous building population, and the choice of the threshold inevitably introduces epistemic uncertainty into the fragility model. To account for this, an additional dispersion term β_{DS} = 0.4 was added following the recommendations of (FEMA 2024), such that the total taxonomy-level dispersion β_T combines all three contributions: β_{intra}, β_{inter}, and β_{DS}

$$\theta_T = \frac{1}{N}\sum_{j}^{N_{bdgs}} \eta_{IM|EDP,j,DS_i} \tag{3.1}$$

$$\beta_{intra} = \sqrt{\frac{\sum_{i=1}^{N}\beta_i^2}{N}} \tag{3.2}$$

$$\beta_{inter} = \sqrt{\frac{\sum_{i=1}^{N}\left[ln\left(\eta_{i,50}\right) - ln\left(\eta_{all,50}\right)\right]^2}{N}} \tag{3.3}$$

$$\beta_T = \sqrt{\beta_{intra}^2 + \beta_{inter}^2 + \beta_{DS}^2} \tag{3.4}$$

3.2.5.3 Loss estimation

The fragility functions derived in the previous section were converted into vulnerability functions, which were subsequently convolved with the seismic hazard curve of the site to compute two key risk metrics: the Average Annual Economic Loss (AAEL) and the Average Annual Loss of Life (AALL). These metrics provided a basis for comparing the seismic risk of the as-built and retrofitted building stock and for evaluating the viability of each retrofit strategy. Three distinct vulnerability functions were derived for each building taxonomy: direct economic losses, indirect economic losses, and fatalities, each described below.

Direct losses: Direct economic losses were quantified by converting the fragility curves into vulnerability functions through a consequence model, which assigns a mean loss ratio to each damage state representing the fraction of the total replacement cost required to restore the building to its pre-damage condition.

Indirect losses: Indirect losses were limited to occupant relocation costs, evaluated following the simplified procedure proposed by Calvi et al. (2021), and expressed in Equation 3.5. The relocation cost was obtained by multiplying the daily relocation cost per person (C_{rel}) by the average number of occupants in 24 hours ($P_{i,24}$) and the total expected downtime. The latter was computed as the sum over all damage states of the probability of being in each damage state multiplied by the corresponding damage-to-repair time ratio (DTR), which expresses the time required to restore the building from a given damage state as a fraction of its total replacement time (ReT). An impeding time T_0 was included to account for preliminary activities namely mobilisation, financing, bidding, and permitting, which precede the onset of physical repairs. Relocation was assumed to be triggered only when buildings reach or exceed extensive damage (DS3), below which occupant displacement is not considered necessary.

$$LR_{ind}(IM) = \frac{C_{rel}P_{i,24}}{ReC}\sum_{i=3}^{n} P(DS = DS_i|IM)(DTR_i \cdot ReT + T_0) \qquad (3.5)$$

Fatalities: Fatality vulnerability functions were derived following the same methodology described in Chapter 2. The expected loss of life for a given IM level was computed by combining: (i) the probability of collapse and the conditional likelihood that collapse results in fatalities, (ii) the entrapment rate, accounting for building occupancy and the possibility of evacuation prior to significant damage, (iii) the entrapment fatality rate, representing the fraction of trapped occupants who perish

before rescue, and (iv) a collapse factor, correcting for the influence of the building collapse mechanism on loss of life.

3.3 RESULTS AND DISCUSSION

Following the methodology described in Section 3.2.5 for the as-built and two retrofit strategies (STJ+FRP and RCJ+FRP), the results are presented sequentially, starting with the structural response characterised through the pushover analysis, followed by the fragility and vulnerability functions, and concluding with the seismic risk metrics.

As described in Section 3.2.3, two retrofit strategies were considered in this study: RC jacketing of columns combined with FRP wrapping of beams (RCJ+FRP), and steel jacketing of columns combined with FRP wrapping of beams (STJ+FRP). For each strategy, the key design parameters governing structural performance are varied systematically to generate an ensemble of retrofitted structural configurations, and the full pushover-to-fragility pipeline is executed for each configuration. The design is carried out iteratively, with each candidate configuration assessed against the EC8-3 compliance criteria described in Section 3.2.5. Configurations that fail any verification are rejected and the design parameters are updated accordingly. For RCJ+FRP, the iterations covered varying RC jacket thicknesses (75, 100, and 150 mm) applied to columns, combined with FRP edge distances of 100, and 200 mm. For STJ+FRP, the parameter space was broader, combining steel angle sizes (50, 75, and 100 mm), batten heights (50, 75, and 100 mm), batten spacing (ranging from 100 to 400 mm), and FRP edge distances. For each parameter combination, an independent structural simulation was carried out, producing a comprehensive set of retrofit configurations whose performance could subsequently be evaluated and compared against EC8-3 compliance criteria.

3.3.1 Structural performance

The nonlinear static (pushover) analyses were carried out for all eighteen building taxonomies considering the as-built condition and the two retrofit strategies. The pushover curves, shown in Figure 3.5 to Figure 3.7, illustrate the base shear versus roof displacement response of all building samples within each taxonomy, together with the mean curves. Three building typologies are distinguished according to the seismic design level: CDN (solid line), CDL+LFC:5.0 (dashed line) and CDL+LFC:10.0 (dotted line). The influence of masonry infill panels is visible in the

lower-rise archetypes (H:1 and H:2), where many individual curves exhibit a sudden drop in base shear at small roof displacements (approximately 0.02 to 0.05 m), characteristic of brittle infill failure once cracking initiates. In taller archetypes, the frame contribution becomes increasingly dominant, and the infill failure no longer produces a clearly distinguishable drop in the global pushover response. As expected, the as-built buildings exhibit the lowest lateral resistance, with base shear capacity generally increasing with building height. The STJ+FRP retrofit yields only a marginal improvement in lateral strength over the as-built condition, with median curves remaining close to those of the as-built buildings across most archetypes, suggesting that this strategy has a limited effect on the global lateral capacity, while the infill-driven softening behaviour is still clearly present. In contrast, the RCJ+FRP strategy produces more noticeable improvements, with substantially higher base shear capacity, a more gradual post-peak degradation, and a reduced influence of infill failure on the global response, as the RC jacketing causes the strengthened frames to carry a larger share of the lateral load. The effect of the design code level is evident across all strategies, becoming increasingly pronounced for taller buildings (H:3-H:6), where CDL yield a notably higher lateral resistance compared to CDN. This trend is less visible for lower-rise archetypes (H:1 and H:2), for which the three code levels produce similar responses.

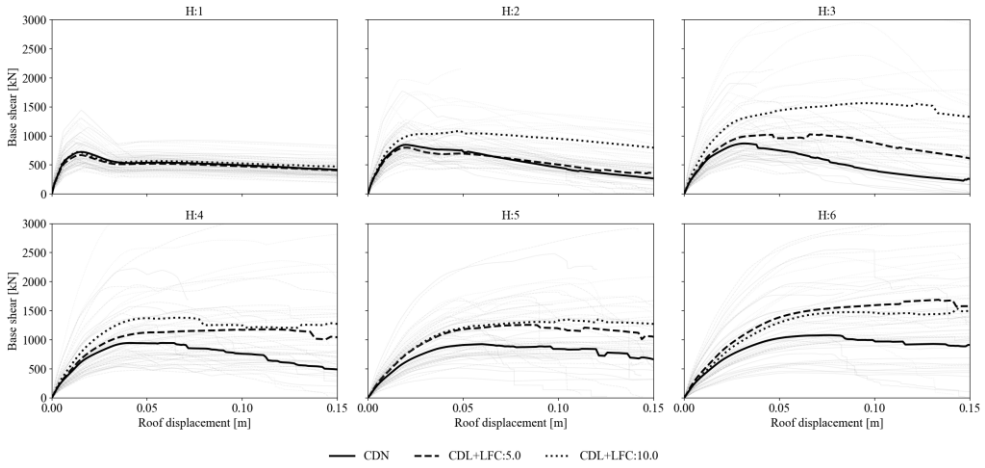

Figure 3.5 Pushover curves for the as-built building archetypes in function of the number of storeys

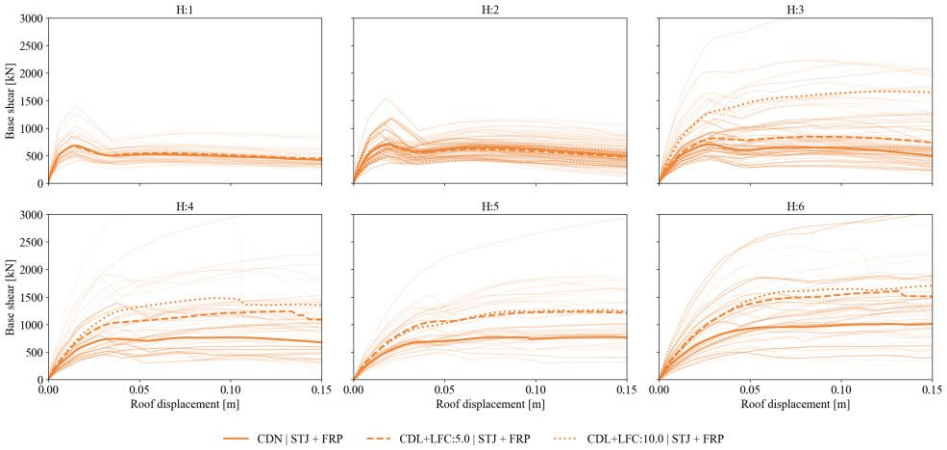

Figure 3.6 Pushover curves for the STJ+FRP retrofitted building archetypes in function of the number of storeys

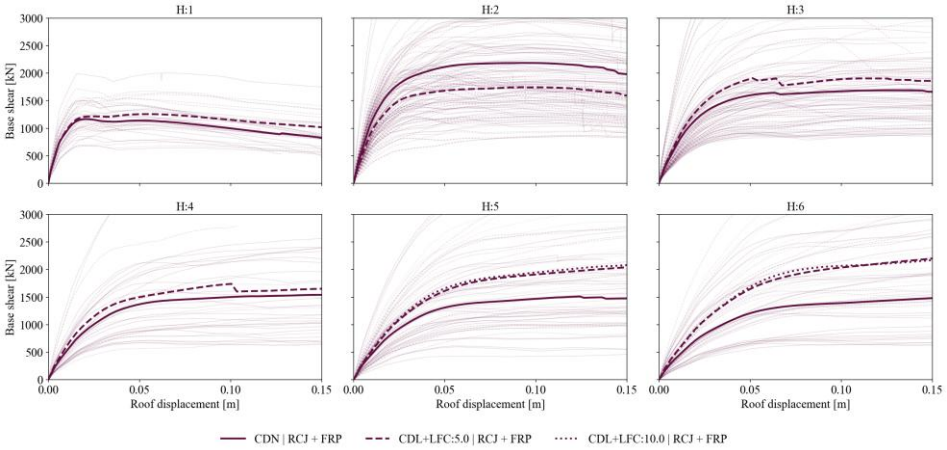

Figure 3.7 Pushover curves for the RCJ+FRP retrofitted building archetypes in function of the number of storeys

3.3.2 Fragility and vulnerability curves

Following the initial seismic assessment, the CBCSM was employed to derive the fragility parameters of each damage state of the several building samples of each building taxonomy. To do so, a set of 200 ground motions covering a wide range of magnitudes were selected from the ESM ground motion database (Luzi et al. 2020) and converted into the ADRS format for application of the CSM (Applied Technology Council (ATC) 1996). The fragility curves derived for the as-built, STJ+FRP, and

RCJ+FRP building taxonomies are presented in Figure 3.8 to Figure 3.10, respectively. As discussed in Section 3.2.4, the adopted IM for each building taxonomy was defined as the average spectral acceleration (AvgSA) over a period range representative of its fundamental period, which varies with the number of storeys. Consequently, fragility curves corresponding to different numbers of storeys are expressed in different IM ranges and a direct comparison is not meaningful. For the as-built and STJ+FRP cases, the CDL code level leads to slightly better performance than CDN, with the difference becoming more noticeable from H:2 onwards, where the curves shift marginally towards higher IM levels, indicating a small but consistent reduction in damage probability. This is in line with the modest strength gains seen earlier in the pushover curves. For RCJ+FRP, the two code levels behave more similarly to each other, which suggests that once the columns are substantially strengthened through RC jacketing, the design code level plays a less decisive role in the fragility response. Looking across all three configurations, the retrofitted taxonomies show a clear shift of the fragility curves towards higher IM levels compared to the as-built case, with RCJ+FRP producing a considerably more pronounced improvement than STJ+FRP across all archetypes and damage states.

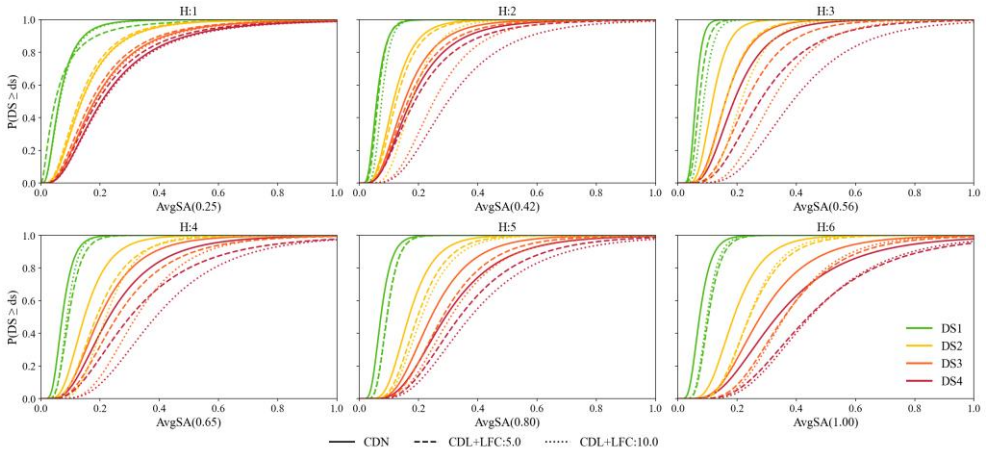

Figure 3.8 Fragility curves for the as-built building taxonomies

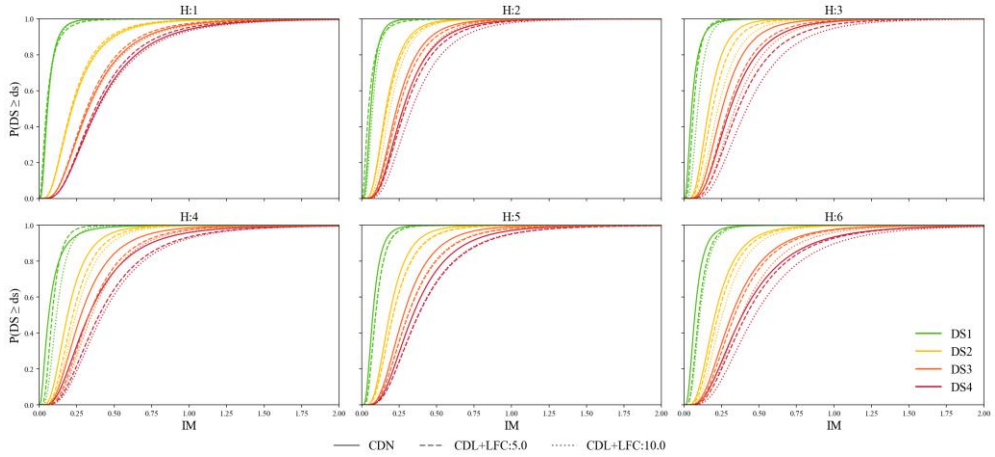

Figure 3.9 Fragility curves for the STJ+FRP retrofitted building taxonomies

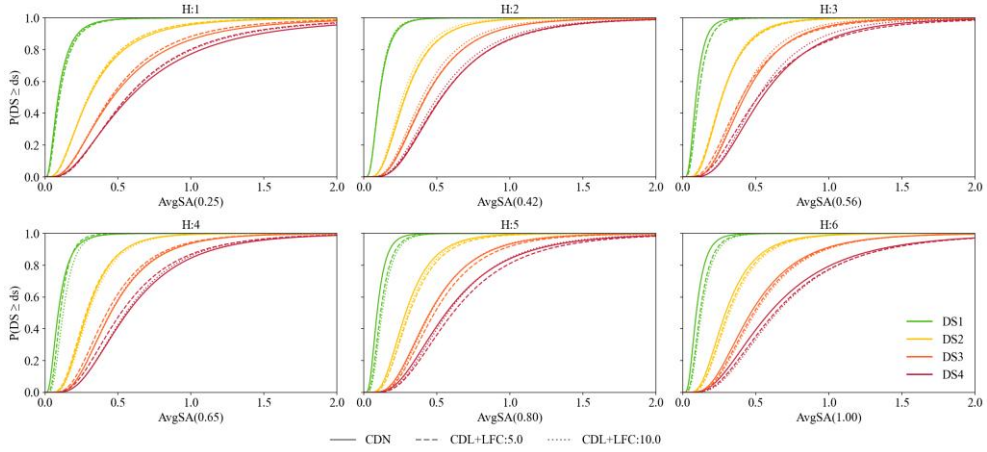

Figure 3.10 Fragility curves for the RCJ+FRP retrofitted building taxonomies

Following the derivation of the fragility functions, three vulnerability functions are computed for each building taxonomy and retrofit configuration: direct economic losses, indirect economic losses, and fatalities. Direct losses are obtained by convolving the fragility curves with a consequence model assigning loss ratios of 0.05, 0.20, 0.60, and 1.00 to DS1 through DS4, respectively, consistent with values adopted in the literature (Martins and Silva 2021b; Lopes et al. 2024b). Indirect losses were calculated according to Equation 3.5. The number of occupants is taken directly from the exposure model for each building taxonomy, based on night-time occupancy. A daily relocation cost of 35 €/person/day is adopted following (Calvi

2025), and the damage-to-repair time ratios (DTR) are obtained from Aljawhari et al. (2023b). The building replacement time is estimated in 730 days (two years) and an impeding time T0 of 100 days is assumed to account for permitting, financing, and bidding activities. In the absence of standardised Portuguese guidance on this parameter, the value adopted here is consistent with that used in comparable Italian studies (Aljawhari et al. 2025), noting that the actual value may be higher depending on local bureaucracy and administrative procedures. For what regards the fatality vulnerability model, the same damage-to-loss model parameters adopted in Chapter 2 are employed for the as-built taxonomies. For the retrofitted configurations, the consequence model was updated to a high code level (CDH) to reflect the improved structural performance. For the sake of brevity, only the direct loss vulnerability curves are presented in the following section, as these constitute the dominant component of total losses across all taxonomies. The indirect and fatality vulnerability functions follow the same structure and are used directly in the risk calculations presented in the following sections.

Figure 3.11 presents vulnerability curves depicting the loss ratio as a function of the seismic IM for the multiple taxonomies, comparing the as-built condition with each retrofit condition. Across all heights, CDN buildings (solid black curve) systematically exhibit the highest loss ratios at any given IM level, establishing no-code structures as the most vulnerable configuration and serving as a lower bound reference. Both retrofit strategies effectively reduce vulnerability compared to the as-built structure, represented by a shift of the curves towards higher IM levels, with RCJ performing better. For STJ, at higher storeys, the vulnerability of certain taxonomies is not considerably better than the as-built structure.

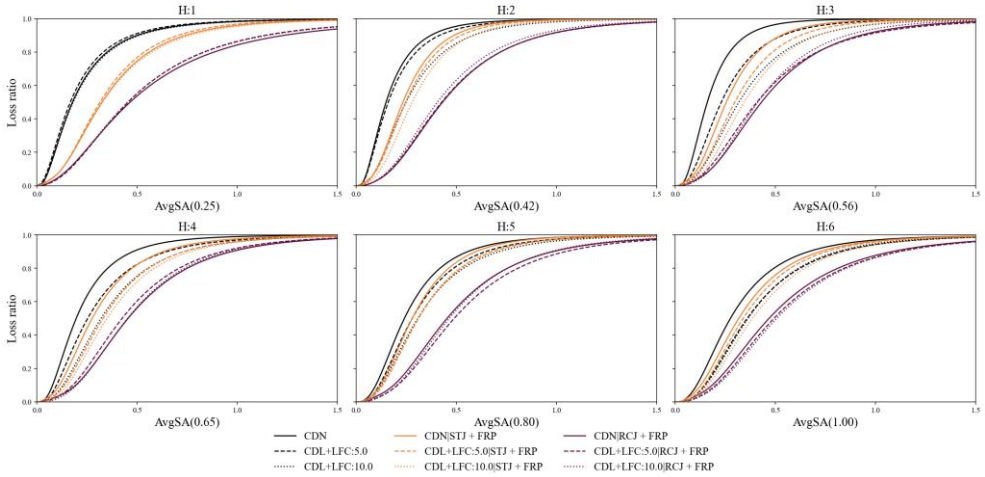

Figure 3.11 Vulnerability curves for the as-built, STJ+FRP, and RCJ+FRP

3.3.3 Retrofit cost

Figure 3.12 presents the investment cost and environmental impact (EI) per unit floor area for the STJ+FRP and RCJ+FRP strategies across all six-storey buildings and three design code levels. The cost accounts for material and labour requirements of each intervention type and varies across classes primarily as a function of the number of storeys and the extent of deficiency of the as-built structure. The RCJ+FRP strategy consistently incurs significantly higher costs and environmental impact than STJ+FRP across all archetypes. For both strategies, costs and EI show a general increasing trend with building height, which can be attributed to the greater number of structural elements requiring intervention in taller buildings. The influence of the design code level is also evident, with CDN yielding the highest costs and EI within each retrofit strategy, followed by CDL+LFC:5.0 and CDL+LFC:5.0, consistently across all taxonomies. This is consistent with the more demanding reinforcement requirements prescribed by higher code levels, which translate directly into greater material quantities and associated costs. While STJ+FRP exhibits relatively modest variability, it is notably larger for RCJ+FRP, particularly for taller archetypes, reflecting the greater sensitivity of this strategy to the variability in building geometry and structural configuration across the buildings stock.

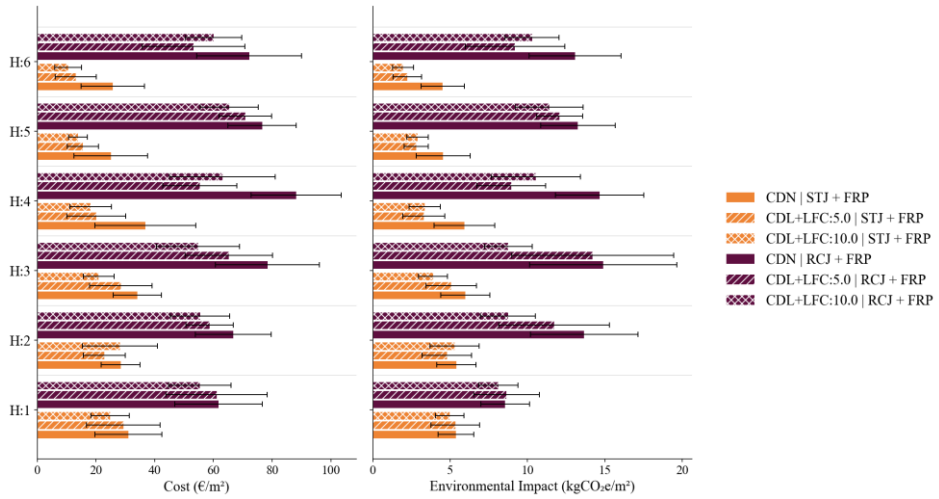

Figure 3.12 Direct retrofit cost (€/m²) and environmental impact (kgCO₂e/m²) per unit floor area for the STJ+FRP and RCJ+FRP retrofit strategies across building archetypes

3.3.4 Seismic risk

The fragility and vulnerability functions are then assigned to the building stock, whose scale and composition is summarised in Figure 3.13, in terms of number of buildings, total floor area, and retrofit cost as a percentage of replacement cost, per taxonomy. This overview provides additional context for the risk and cost-benefit results that will follow.

The building stock is dominated by lower-rise buildings, with H:1-2 taxonomies accounting for the largest number of buildings and floor area across all code levels, while taller archetypes (H:5-6) represent a comparatively small fraction of the total stock. RCJ+FRP consistently requires a higher investment than STJ+FRP, with retrofit costs ranging from 4 to 8% and 1 to 3%, respectively, of the replacement cost, both increasing modestly with building height, reflecting the greater number of structural elements requiring intervention in taller buildings. This metric provides a normalised measure of the financial burden associated with each intervention, regardless of the absolute building value and confirms that both strategies represent a relatively modest upfront investment relative to the total replacement value of the stock.

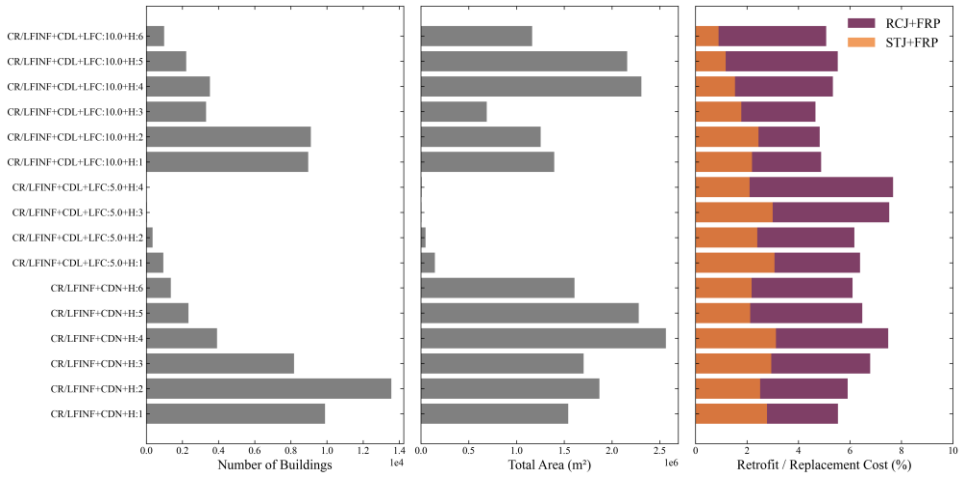

Figure 3.13 Characterisation of the building stock by taxonomy: number of buildings, total floor area, and retrofit cost as a percentage of the replacement cost for RCJ+FRP and STJ+FRP.

The seismic risk of the building stock was then quantified by convolving the vulnerability curves with the seismic hazard curve. Three metrics are evaluated for each building taxonomy and retrofit configuration: the average annual economic loss (AAEL), disaggregated into direct and indirect components, and the average annual loss of life (AALL). For the retrofitted configurations, the total replacement cost of each taxonomy is updated to include the retrofit cost.

Figure 3.14 illustrates the AAEL per unit floor area, disaggregated into direct and indirect components, for the as-built and retrofitted configurations across all taxonomy classes. Normalising by the floor area allows meaningful comparisons across taxonomies with significantly different building stock sizes. Single-storey buildings (H:1) consistently exhibit the highest losses, decreasing with building height. Direct losses dominate across all taxonomies, while indirect losses remain small, as most buildings remain in early damage states where occupant relocation is not required. The indirect component is relatively more significant for H:1, where a larger fraction of the stock reaches higher damage states. The influence of the design code level becomes clearer with increasing height, with CDL+LFC:10.0 consistently yielding lower losses than CDL+LFC:5.0 and CDN from H:2 onwards, while differences are negligible for H:1. Both retrofit strategies produce substantial loss reductions, with H:1 losses dropping from approximately 10-11 €/m^2 to below 4-5 €/m2, corresponding to a reduction of 60-70%. For taller buildings the absolute

benefit is more modest but remains consistent. RCJ and STJ yield broadly comparable results, with STJ showing marginally higher residual losses for some typologies.

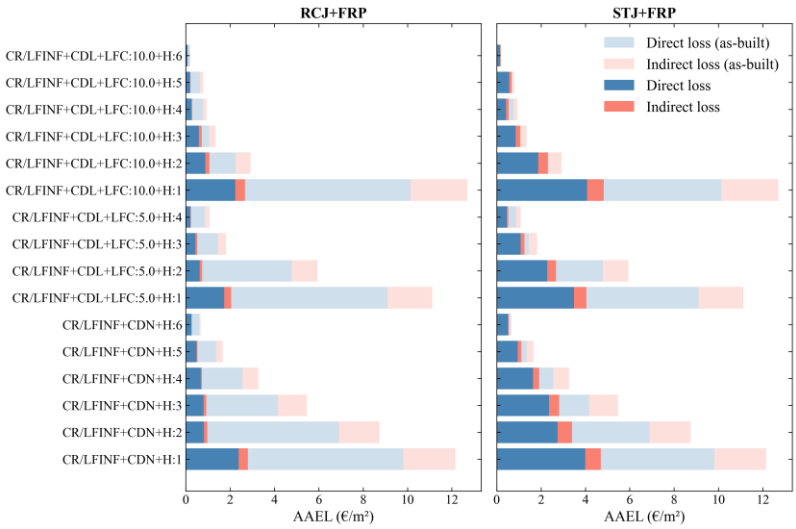

Figure 3.14 Average annual economic loss per unit floor area disaggregated into direct and indirect losses, for the as-built, RCJ+FRP, and STJ+FRP configurations across all building taxonomies

Figure 3.15 presents the AALL, computed as the average of the day and night occupancy scenarios, to account for the variability in building occupancy over time per unit floor area. As was observed for the economic losses, single-storey buildings (H:1) exhibit the highest fatality rates across all code levels, reflecting their higher seismic vulnerability and the greater proportion of the stock expected to reach severe or collapse damage states. The CDN taxonomies consistently show the highest as-built fatality rates, with values decreasing progressively for higher code levels, particularly from H:2 onwards, where the structural response becomes more sensitive to the design code level. Both retrofit strategies produce a substantial reduction in annual fatalities relative to the as-built condition, with RCJ+FRP performing marginally better, in line with its superior structural performance observed in the pushover and fragility analyses.

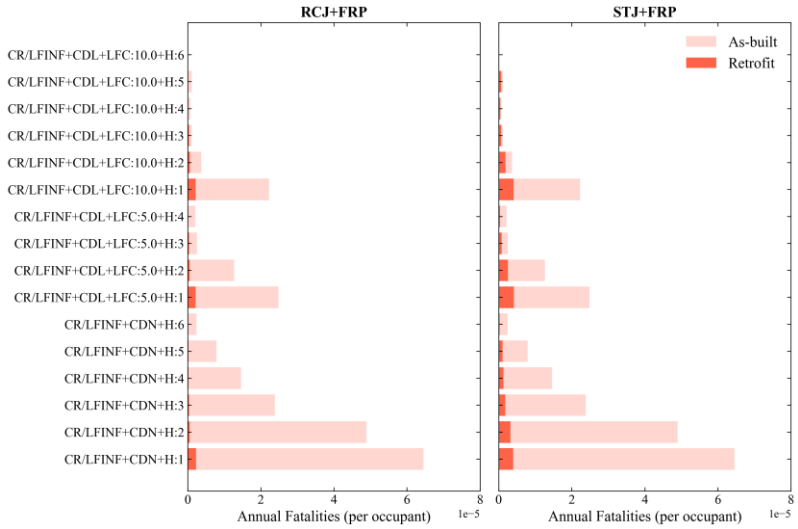

Figure 3.15 Expected annual fatalities per unit floor area, for the as-built and retrofitted (RCJ+FRP and STJ+FRP) building taxonomies across all building taxonomies

3.4 ECONOMIC ASSESSMENT

Building upon the results obtained so far, the cost of each intervention (Figure 3.13) can be analysed together with the corresponding reduction in risk metrics values (Figure 3.14 and Figure 3.15). STJ+FRP requires a lower upfront investment but also delivers a more modest reduction in AAEL, particularly for mid-to-high-rise buildings, raising questions about whether the risk reduction justifies the cost. RCJ+FRP is more expensive but achieves substantially greater loss reductions, suggesting a more favourable cost-effectiveness profile, especially for lower-rise buildings. For both strategies, the benefit of retrofit is most pronounced for single-storey CDN buildings (H:1) and diminishes progressively with building height. To quantitatively gauge the trade-off between intervention cost and risk reduction benefit, two complementary indicators were evaluated: the Cost-Benefit Ratio (CBR), which measures the cumulative economic benefit relative to the upfront cost over a given planning period, and the Payback Period (PBT), which identifies how quickly the accumulated savings offset the initial investment. Together, the two indicators provide a more comprehensive assessment of the economic feasibility of the mitigation strategies, which becomes even more relevant considering the uncertainty in the remaining service life of the building stock.

3.4.1 Cost-benefit ratio

The cost-benefit ratio (CBR), expressed in Equation 3.6, represents the economic benefit accumulated from the retrofit intervention, characterised by the reduction of the economic loss due to retrofit (ΔAAEL), over the planning period (t), normalised by the cost of renovation (C_{ret}) of the retrofit and replacement cost of the investigated building taxonomy (C_{rep}) (Gkatzogias et al. 2022b). A CBR of zero indicates no economic benefit of the retrofit, a CBR of one means the benefit exactly offsets the retrofit cost, and a CBR greater than one indicates a net economic gain over the planning period.

$$CBR = \frac{\Delta AAEL / C_{rep}}{C_{ret} / C_{rep}} \cdot t \tag{3.6}$$

Figure 3.16 presents the CBR for each building taxonomy under both retrofit strategies across five planning periods, ranging from 10 to 50 years. The upper bound of 50 years was set as the maximum residual service life that could be reasonably expected for the retrofitted buildings, originally built before the 1960s. The range of planning periods is intended to reflect such a residual service life uncertainty, allowing the CBR to be evaluated across a spectrum of realistic remaining lifespans.

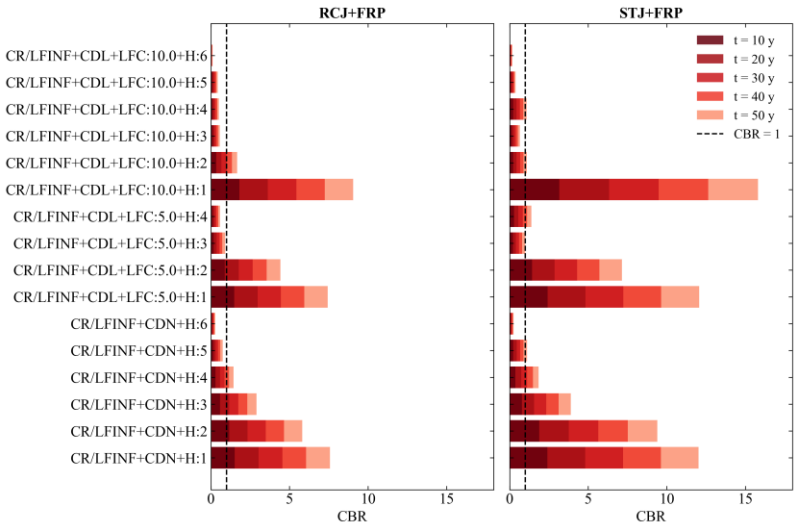

Figure 3.16 Cost-Benefit Ratio (CBR) per building taxonomy for the RCJ+FRP and STJ+FRP retrofit strategies

As expected, the CBR increases with the planning period for all taxonomies. For the RCJ+FRP retrofit strategy, most taxonomies reach CBR > 1 within 20 to 30 years, with single-storey CDN buildings (H:1) consistently showing the highest values due to their high as-built vulnerability and large absolute loss reductions. Mid-to-high-rise building taxonomies and higher code levels yield lower CBR values, as their as-built losses are already modest with respect to the retrofit cost. STJ+FRP generally produces higher CBR values than RCJ+FRP, primarily a consequence of its lower upfront cost, while the absolute loss savings remain considerably smaller than those achieved by RCD+FRP.

3.4.2 Payback time

The payback time (PB) is calculated by finding the point in time where the cumulative discounted savings equal the initial retrofit cost, i.e. where the Net Present Value (NPV) curve crosses zero. For each building taxonomy, the NPV at time t is computed by accumulating the annual risk reduction savings (ΔAAEL), discounted to present value using a discount rate *r* and adjusted for cost inflation at rate *f*, and subtracting the initial retrofit cost (C_{ret}) (Equation 3.7). Building taxonomies for which the NPV does not reach zero within the analysis time horizon are considered economically non-viable under the assumed financial parameters. In this study, a discount rate of r = 2% and an inflation rate of f = 1% were adopted, in line with past studies on seismic retrofitting (Sousa and Monteiro 2018b; Cardone et al. 2019).

$$NPV(t) = -C_{ret} + \sum_{y=1}^{t} \frac{\Delta AAEL \cdot (1+f)^y}{(1+r)^y} \tag{3.7}$$

Figure 3.17 presents the NPV recovery curves for all building taxonomies under the RCJ and STJ retrofit strategies over a 200-year time horizon. Each curve represents the cumulative discounted cash flow of a given retrofit investment, starting from a negative value at year zero (corresponding to the upfront retrofit cost) and evolving as annual loss savings accumulate over time. Curves crossing the zero line indicate taxonomies for which the retrofit investment is eventually recovered, with the crossing point corresponding to the PB, translated into a bar chart in Figure 3.18.

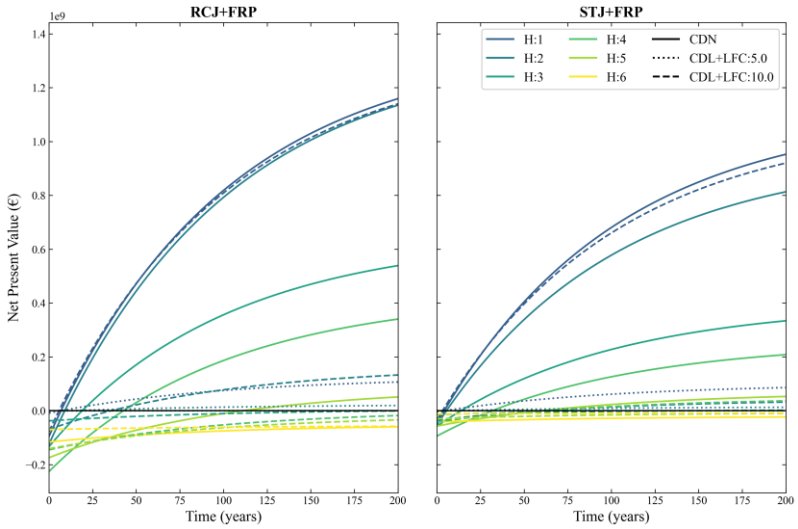

Figure 3.17 Net Present Value (NPV) recovery curves for each building taxonomy under the RCJ+FRP and STJ+FRP retrofit strategies.

Results are colour-coded according to the time threshold within which the investment is recovered, using the same red shade family adopted for the CBR analysis: dark red indicates taxonomies with PB below 10 years, progressively lighter shades correspond to payback times within 20, 30, 40, and 50 years respectively, and grey bars indicate taxonomies for which the retrofit investment is not recovered within the 50-year analysis horizon.

A clear dependence on both the design code level and the number of storeys is observed, consistent with the results presented so far. CDN taxonomies consistently exhibit the shortest payback times, particularly for low-rise configurations (H:1-3), where both retrofit strategies recover their costs within the analysis horizon. As the number of storeys increases, payback times grow substantially, with H:5 and H:6 CDN buildings exhibiting payback times that approach or exceed the analysis horizon under both strategies. For CDL+LFC:10.0, the retrofit investment is rarely recovered within the 50-year horizon regardless of the number of storeys or retrofit strategy applied, reflecting the limited marginal loss reduction achievable for these already better-performing structures. CDL+LFC:5.0 buildings show intermediate behaviour, with low-rise typologies achieving payback within acceptable timeframes while mid- and high-rise configurations remain economically marginal or unfeasible. Both retrofit strategies show broadly similar trends in payback time, with economic viability primarily confined to low-rise, low-code (CDN) buildings. STJ+FRP tends to

recover its cost more quickly for these typologies owing to its lower upfront investment, while RCJ+FRP exhibits greater variability across the full range of taxonomies.

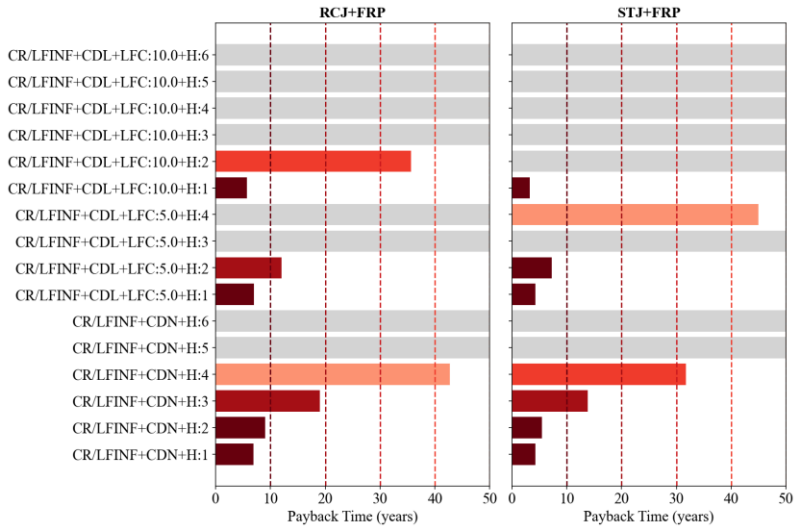

Figure 3.18 Payback time (PB) for each retrofit strategy and building class.

3.4.3 Example of a retrofit scenario

Using the taxonomy-level results, a long-term intervention scenario is developed in which taxonomies are prioritised according to their PB, reflecting common financial constraints faced by policymakers who cannot retrofit the entire stock simultaneously. PB is preferred over CBR as the prioritisation criterion because while both metrics indicate economic viability, PB additionally conveys when the investment breaks even, a more actionable criterion for policymakers operating within fixed planning horizons. The time *t* provides a more intuitive and policy-relevant metric for sequencing investments under financial constraints. Moreover, PB provides finer discrimination among viable interventions (those with CBR > 1), allowing the most financially efficient ones to be prioritised first. Five phases are defined based on PB thresholds of 10 (P1), 20 (P2), 30 (P3), 40 (P4), and 50 (P5) years, with each taxonomy assigned to the earliest phase for which its PB falls below the corresponding threshold. Taxonomies with PB exceeding 50 years are considered economically non-viable and excluded from the analysis. Within each phase, the total retrofit investment, AAEL reduction, and covered fraction of stock are computed

by aggregating the taxonomy-level results multiplied by the number of buildings in each taxonomy.

Figure 3.19 presents the cumulative AAEL reduction as a function of the cumulative retrofit investment for both retrofit strategies, with the corresponding percentage of retrofitted buildings. The curves show clear diminishing returns, with the steepest risk reduction achieved in the early phases. For RCJ+FRP, P1 alone covers approximately 49% of the stock at an investment of around 300 M€, delivering approximately 44 M€/yr in AAEL reduction. The full viable retrofit renovation, corresponding to 80% of the building stock and 750 M€ investment achieves an AAEL reduction of approximately 61 M€/yr. For STJ+FRP, the investment is considerably lower, around 300 M€, but so is the risk reduction with approximately 42 M€/y, with P1 again dominating. RCJ+FRP achieves a 45% higher cumulative risk reduction than STJ+FRP at approximately 2.5 times the cost, making STJ+FRP the more affordable entry point and RCJ+FRP the better option when maximum risk reduction is the objective. In both cases, a fraction of the stock remains outside the viable retrofit renovation (approximately 20% for RCJ+FRP and 33% for STJ+FRP), representing buildings whose retrofit investment cannot be recovered within the 50-year horizon under the assumed financial parameters.

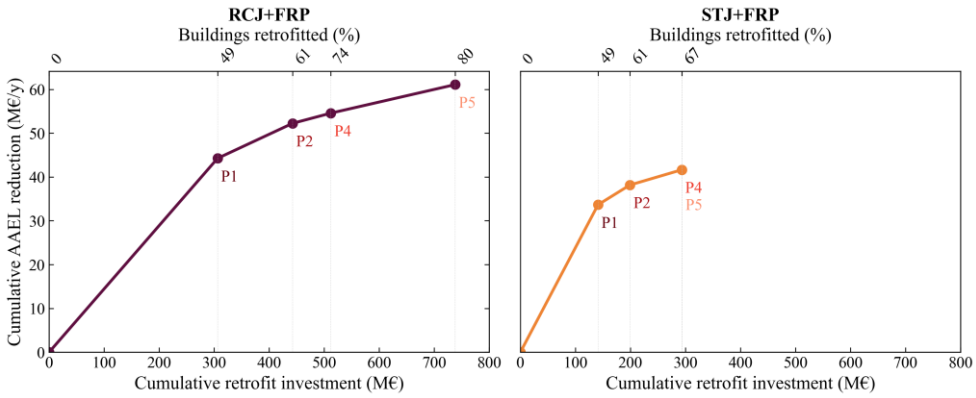

Figure 3.19 Cumulative AAEL reduction (M€/y) as a function of cumulative retrofit investment (M€) for the RCJ+FRP and STJ+FRP phased intervention scenarios.

3.5 CONCLUDING REMARKS

This chapter presented a comprehensive assessment of the benefits associated with seismic retrofitting of different taxonomies within the Portuguese building stock, thereby supporting informed decision-making for building renovations in Portugal.

Following the prioritisation patterns (Chapter 2), Lisbon was identified as the region most in need for intervention, exhibiting the highest combined vulnerability scores across all indicators considered. To better understand the drivers of these vulnerabilities, a detailed examination of the building stock in the region was carried out, to identify which building classes were most susceptible to seismic damage and which contributed most substantially to potential losses. No code (CDN) and low code (CDL) reinforced concrete buildings of one to six storeys were identified as the primary targets for seismic intervention. Accordingly, eighteen building taxonomies were defined by varying the code level, the lateral load coefficient, and the number of storeys. For each taxonomy, a set of building models representative of the case-study region was generated and subjected to nonlinear static analysis, from which fragility and vulnerability functions were derived using the cloud-based capacity spectrum method (CB-CSM). Considering the vulnerability of these buildings, two retrofit strategies: RC jacketing of columns combined with FRP wrapping of beams (RCJ+FRP), and steel jacketing of columns combined with FRP wrapping of beams (STJ+FRP), - were designed iteratively for each taxonomy following Eurocode 8 -Part 3EC8-3 compliance criteria, and the nonlinear static analysis, fragility, and vulnerability assessment procedure was repeated for the retrofitted configurations. The resulting vulnerability curves for both as-built and retrofitted buildings, incorporating direct losses, indirect relocation costs, and fatalities, were combined with the seismic hazard of each parish in Lisbon to estimate the average annual economic loss and average annual loss of life for each taxonomy. The economic viability of each strategy was then assessed through cost-benefit ratio and payback time analyses, and a phased intervention scenario was developed to identify the most effective sequencing of investments, from a strictly economic viewpoint, across the building stock.

The results demonstrate that both retrofit strategies effectively reduce seismic risk across all taxonomies, with RCJ+FRP consistently outperforming STJ+FRP in terms of structural improvement, loss reduction, and fragility performance. Single-storey CDN buildings emerged as the most vulnerable and, consequently, the most responsive to intervention, exhibiting the highest reductions in average annual economic losses and fatalities following retrofit. The economic assessment confirmed that retrofit viability is strongly governed by the design code level and building height, with low-rise CDN buildings offering the most favourable cost-benefit ratios and shortest payback periods, while mid- and high-rise CDL buildings remain economically marginal or unfeasible within the assumed planning horizon. Although

STJ+FRP recovers its investment more rapidly due to its lower upfront cost, RCJ+FRP achieves substantially greater risk reduction and should be preferred where maximum loss mitigation is the objective. The phased intervention scenario further showed that the greatest risk reduction per unit of investment is concentrated in the earliest phases, confirming the importance of prioritising the most vulnerable taxonomies first.

Overall, the findings of this chapter provide a basis for guiding seismic retrofit policy in Portugal, with the derived fragility and vulnerability functions directly applicable to national risk models, and the phased retrofit scenario offering a practical tool for urban planning. The methodology is also transferable to other regions facing similar challenges of ageing building stocks and elevated seismic exposure. It is important to note, however, that these results do not provide a single definitive answer, but rather offer quantitative information that, alongside additional other technical and social variables, can assist decision-makers in guiding seismic retrofit policies. Moreover, the analysis is confined to Lisbon and extending it to other high- or medium-risk regions of Portugal would provide a more complete national picture. Only two retrofit strategies were considered, and the inclusion of additional or hybrid interventions could increase the decision space and potentially identify more cost-effective solutions for certain taxonomies. Finally, the retrofit viability evaluation is based solely on economic metrics, and the incorporation of environmental impacts and fatality reduction as explicit decision criteria would offer a more comprehensive basis for intervention prioritisation.

CHAPTER 4

Storey loss and environmental impact functions for existing reinforced concrete buildings

This chapter is extensively based on the following publication:

Couto R*, *Mucedero G, Yükselen B, Bento R, Monteiro R. (2025) Storey loss and environmental impact functions for existing RC buildings, Bulletin of Earthquake Engineering (under review).*

**Author Contribution: conceptualisation, methodology, software, validation,* data curation, *writing.*

4 STOREY LOSS AND ENVIRONMENTAL IMPACT FUNCTIONS FOR EXISTING REINFORCED CONCRETE BUILDINGS

4.1 INTRODUCTION

Past earthquakes have repeatedly demonstrated their capacity to inflict severe damage to societies, leading to extensive damage and economic losses. These events highlight the importance of accurately estimating seismic losses to support risk assessment, prioritising retrofitting interventions, and informing polices that target community resilience. However, the consequences of seismic events extend beyond direct economic damage, as they also entail significant environmental impacts driven by material consumption, waste generation, and carbon emissions associated with repair and reconstruction activities. For instance, Gonzalez et al. (2021) showed that post-earthquake decisions in Christchurch largely overlooked environmental considerations, resulting in substantial embodied carbon losses. Incorporating environmental impacts as a complementary seismic performance metric is therefore crucial to capture the full extent of earthquake consequences and to guide more sustainable recovery and risk mitigation strategies.

To quantify the consequences of earthquake-induced damage, loss estimation methodologies often rely on empirical or analytical relationships that link engineering demand parameters (EDPs) to chosen decision variables. Building on this concept, the component-based loss assessment methodology introduced by the Pacific Earthquake Engineering Research (PEER) Performance-based Earthquake Engineering (PBEE) framework (Moehle and Deierlein 2004) represented the first systematic attempt to quantify losses at the component level, accounting for both structural and non-structural components. FEMA P-58 (FEMA 2018a) subsequently operationalised this approach, providing standardised procedures and databases to calculate repair costs, downtime, and casualties for individual buildings. While highly detailed and accurate, these component-based approaches are computationally intensive and require extensive input data, which can limit their practical applicability for large-scale studies. To address this, storey loss functions (SLFs), initially developed by Ramirez and Miranda (2009), have rapidly emerged as one of the most refined, yet practical, tools for estimating seismic metrics, effectively replacing more computationally demanding methods. They offer an acceptable compromise between simplicity and accuracy, lying between the component- and building-level

approaches that are currently used in loss assessment. Among their key advantages, SLFs allow the disaggregation of losses into drift- or acceleration-sensitive structural and non-structural components. This allows for a faster and more efficient identification of loss contributions, which can help decision-makers and stakeholders in selecting effective retrofitting strategies to reduce overall seismic risk. Moreover, SLFs can be integrated with simplified single-degree-of-freedom (SDOF) building models, enabling faster and computationally feasible seismic loss assessment studies at a large scale O'Reilly and Shahnazaryan (2024). Several studies have explored the development and application of simplified seismic loss estimation methods, particularly through the use of SLFs, to estimate seismic economic losses. Shahnazaryan et al. (2021) introduced a Python-based toolbox designed to facilitate the creation of SLFs, offering a streamlined alternative to traditional tools (FEMA 2018a; Elkady and Lignos 2020; Zsarnoczay et al. 2024). The practical application of SLFs was demonstrated through a case study, highlighting their ability to provide accurate results while being more time-efficient and user-friendly for practitioners. Papadopoulos et al. (2019) expanded on the concept of SLFs by leveraging resources from FEMA P-58 (FEMA 2018a). Through a case study of low- to mid-rise steel office buildings, the study demonstrated how this simplified method can efficiently quantify potential seismic losses without requiring exhaustive data on individual building components. Nafeh and O'Reilly (2024) employed SLFs as the core of a simplified seismic loss assessment framework based on static pushover analysis for infilled RC buildings in Italy. A comparative study with the FEMA P-58 component-based assessment demonstrated the robustness and accuracy of such a framework, while also showing improved performance over other simplified loss assessment methodologies. Mucedero et al. (2024) focused on the development of generalised SLFs for existing reinforced concrete (RC) residential buildings in Italy, using post-earthquake damage data from the 2009 L'Aquila earthquake. The proposed SLFs were then applied to a portfolio of Italian buildings, and the expected annual loss results were compared to those obtained in other studies, showing consistency. The same study also demonstrated the SLFs potential for widespread application in academic research, the (re)insurance field, and practice assessments. While most of the existing studies have derived SLFs for a given building or building typology, for which detailed information for each damageable component was available, SLFs can also be effectively employed for regional risk assessment by grouping different building typologies into representative categories with known component characteristics. However, their development

remains limited across many seismic-prone European countries, restricting their use in large-scale applications.

The SLF underlying formulation, originally set to estimate the economic impact of earthquake damage, can be extended to the evaluation of associated environmental consequences. This requires establishing a damage-to-impact conversion for each damage state and corresponding repair activity. Recent efforts have been made to include environmental impact (EI) assessment methods within seismic loss estimation approaches, such as the PEER-PBEE framework (Moehle and Deierlein 2004). As summarised by Hasik et al. (2018), existing studies typically estimate EI either through life cycle assessment (LCA) tools (Chhabra et al. 2018), by applying greenhouse gas emission factors (Arroyo et al. 2015; Belleri and Marini 2016; Wei et al. 2016; Aljawhari et al. 2024), from Input-Output LCA (Comber et al. 2012), or from Economic Input-Output-LCA (EIO-LCA) (Simonen et al. 2018; Clemett et al. 2022). These estimates can then be used to quantify the total embodied carbon associated with repairing earthquake damage, allowing for component-specific or building-level assessments. However, while detailed models can quantify the EI of repairing earthquake damage, their complexity often limits their practical application in both single-building and large-scale risk assessments. Although simplified metrics, such as the mean damage-to-embodied carbon ratios, were recently proposed by Aljawhari et al. (2024) for common building types in Mediterranean countries, storey EI functions, which are not available, can facilitate a quick estimation of earthquake-induced EI, particularly for regional seismic assessment.

To address the two identified gaps, this chapter develops generalised storey loss and EI functions, SLFs and SEIFs, respectively, for different types of poorly detailed RC buildings. The methodology combines building typology characterisation, identification of damageable components, and the integration of state-of-the-art fragility curves with both repair cost and EI consequence functions. Regarding building characterisation, this study focuses on buildings with none to limited seismic design, as these structures represent a significant portion of the existing European building stock. In the case of seismically designed buildings, the proposed SLFs and SEIFs for non-structural components can still be employed, while new ones should be derived for structural components. Fragility curves for each damageable component were collected from different studies and regional contexts to better represent the epistemic uncertainty associated with the variability in the building inventory. To overcome the challenges of limited component-level data, the approach employs consequence functions derived from post-earthquake repair cost

data collected after the 2009 L'Aquila earthquake and an economic input-output life cycle assessment (EIO-LCA) model to estimate EI. These generalised functions are then tailored to Portugal through the development of country-specific cost conversion factors, exemplifying their relevance to national applications. The same rationale and procedure can be applied to other European countries. Finally, the applicability of the proposed SLFs and SEIFs is illustrated through a case study RC building, to which both the storey- and component-based approaches are applied. The application shows a good agreement between both approaches in terms of loss curves and annualised metrics, confirming the robustness of the storey-based approach as a practical and computationally efficient alternative.

4.2 METHODOLOGY

Generalised SLFs and SEIFs establish a relationship, per storey, between engineering demand parameters (EDPs), typically expressed in terms of peak storey drift (PSD) or peak floor acceleration (PFA), and the corresponding repair costs or EI associated with different building components. The process begins with detailed data collection of damageable components located at each storey, classifying them according to the EDP to which their damage is sensitive. Further categorisation of components into functional groups (i.e., structural, non-structural) facilitates a clearer understanding of the contribution of each category to the overall losses and supports the development of more generalised and transferable storey-based functions. Subsequently, the methodology integrates fragility functions, consequence models, and probabilistic simulations to generate a robust dataset of loss and impact values across an EDP range, which are subsequently fitted using parametric regression techniques. The following subsections detail the individual steps of the employed methodology, namely: (i) building characterisation, (ii) damageable components, (iii) fragility functions, (iv) repair consequence functions, and (v) environmental impact consequence functions.

4.2.1 Building characterisation

Building characterisation provides essential information on structural systems, materials, age, and seismic code compliance. This study focuses on RC buildings, which account for more than 30% of the approximately 145 million residential, commercial, and industrial buildings in Europe . According to Crowley et al. (2021b), RC buildings can be classified in four seismic design categories based on their design level: CDN - no seismic design, corresponding to the buildings built with no seismic

provisions; CDL - low code, referring to buildings designed according to the first generation of seismic design codes, CDM - moderate code, corresponding to buildings designed following the second generation of seismic design codes; and CDH - high code, representing buildings constructed in compliance with the latest generation of seismic design codes. It is estimated that 60% of the RC buildings in Europe have been seismically designed. Among these, approximately 60% were designed to low code standards, 25% to moderate code standards and 15% to high code standards (Crowley et al. 2021b). Within the RC class, this study focuses on CDN and CDL buildings, as these structures were constructed with none or limited seismic design criteria, therefore, more vulnerable to seismic actions and consequently, key contributors to significant economic losses during earthquake events. The seismic assessment of these buildings is thus crucial, not only to estimate potential economic impacts but also to support effective seismic risk mitigation strategies. From a social perspective, these buildings often house a large portion of the population and are integral to community functioning, meaning their poor performance can lead to severe consequences in terms of safety and post-event disruption. From an economic perspective, their higher vulnerability can result in substantial direct and indirect losses, emphasising the importance of prioritising their assessment and retrofitting within seismic risk reduction policies (Mucedero and Monteiro 2024a; Couto et al. 2025). Although the periods of transition between different code levels vary across countries, it is generally assumed that buildings designed under the same code level exhibit similar performance. Owing to the similarities among buildings in southern Europe, they are often characterised together. Figure 4.1 illustrates the distribution of buildings across the European Union countries and other European countries with high seismic risk (Crowley et al. 2021a), categorised by code level and based on the European exposure model developed by Yepes-Estrada et al. (2023). CDN and CDL buildings dominate in most countries (except for a few: Albania, Germany, Montenegro, Portugal, Serbia, Slovenia, and Spain), indicating that a large part of the existing European building stock was constructed before the widespread enforcement of modern seismic design standards. This trend is particularly pronounced in high seismic risk countries such as Croatia, Italy, Malta, and Turkey. CDM and CDH buildings represent a smaller share, though countries like Greece, Romania, and Spain display a relatively higher proportion of CDH structures. Nevertheless, it is highlighted that periods of rapid urban expansion, such as the case of Albania (Freddi et al. 2021) or Turkey (Ilki and Celep 2012; Hasanoğlu et al. 2025), were accompanied by limited public awareness of seismic risk and insufficient enforcement of construction standards, including

inadequate supervision and inspection during both the design and execution phases, leading to the widespread development of low-quality buildings.

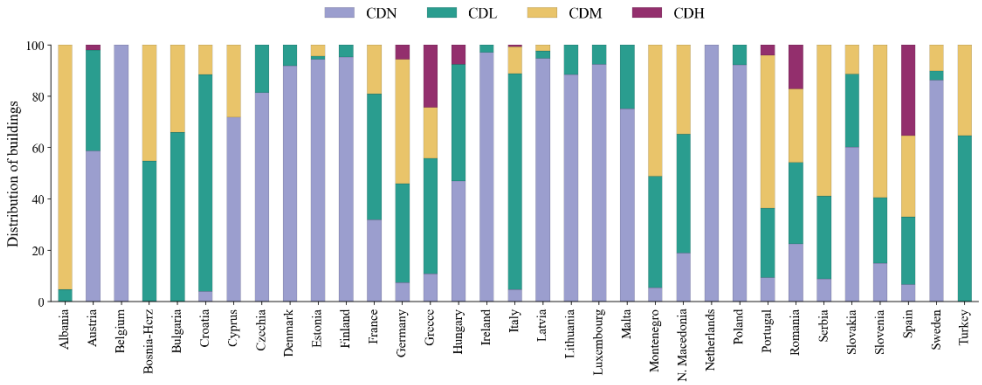

Figure 4.1 Distribution of buildings by code level in European Union countries and other countries with significant seismic hazard

4.2.2 Damageable components

Five performance groups were identified based on the different damageable component groups in existing buildings: (1) structural components, which include brittle columns and interior and exterior beam-column joints, (2) infills and partitions, (3) plumbing and electrical systems, (4) windows and doors, and (5) other non-structural components, which comprise floor finishes, chimneys and sanitary equipment. This categorisation, based on the work of Del Vecchio et al. (2020), facilitates the subsequent methodological steps by organising components according to their functional roles and seismic sensitivity. Table 4.1 provides a summary of the categories, the specific components included within each, and the corresponding EDP.

Regarding the structural typology, RC buildings in Europe are mainly moment-resisting frames, with significant geometric and structural irregularities. Vertical irregularities include columns tapering along their height, while horizontal irregularities stem from asymmetric column layouts and frames oriented mainly in one direction. Structural irregularities, such as indirect beam-beam supports, eccentric beams, and irregular column spacing, are also common. Reinforcement detailing is generally poor, with insufficient transverse reinforcement, inadequate beam-column detailing, use of smooth rebars and insufficient anchorage of vertical reinforcement into the foundations (Ricci et al. 2011; Xavier et al. 2022).

Table 4.1 Classification of building components into macro-categories (Cat.) and associated engineering demand parameters (EDP).

Cat.	Component	EDP
1 - Structural	Interior beam-column joints (IBCJ)	PSD
	Exterior beam-column joints (EBCJ)	
	Brittle columns	
2 - Infills and partitions	Infill walls	PSD/PFA
	Partitions	
3 - Plumbing and electrical	Plumbing and electrical systems	PSD/PFA
4 - Windows and doors	Windows and Doors	PSD
5 - Other non-structural components	Sanitary waste piping	PFA
	Floor slabs and tiles	
	Lighting	

The materials themselves have low mechanical properties, with concrete of low compressive strength and steel with low yield strength (Repapis and Zeris 2019; Mucedero et al. 2021; Xavier et al. 2022; Nafeh and O'Reilly 2022; De Risi et al. 2025). Recent earthquakes, such as Kocaeli (Turkey) in 1999 (Ilki and Celep 2012), L'Aquila (Italy) in 2009 (Ricci et al. 2011), Lorca (Spain) in 2011 (Ruiz-Pinilla et al. 2016), Emilia (Italy) in 2012 (Manfredi et al. 2014), and Kahramanmaraş (Turkey) in 2023 (Binici et al. 2023) have demonstrated the deficiency of these components and consequent vulnerability, particularly due to shear failure in beams, columns, and beam–column joints. Moreover, the local interaction between infills and adjacent columns can reduce the effective column height, increasing shear demand and potential brittle failure at the point of contact (Hak et al. 2014; Di Trapani et al. 2024). It can also lead to shear concentration at the column end and subsequent brittle failure caused by the diagonal compression forces from the infill panel. These buildings are typically enveloped by masonry infill walls and contain internal masonry partitions, which are often used to separate acoustically adjoining apartments. Evidence from past earthquakes has shown that masonry infill walls and internal partitions are the largest contributors to seismic losses (Ricci et al. 2011; Del Vecchio et al. 2020). Infill walls are often discretised into a macro classification based on their thickness and construction period, ranging from weak to strong types

(Hak et al. 2012; Mucedero et al. 2020). The first type of infill walls consisted of a single masonry layer, most commonly built with solid bricks and, in some cases, stone (weak infills). With the widespread adoption of RC structures and increasing thermal and acoustic insulation requirements, infills evolved into two unconnected masonry layers (cavity wall) with a total thickness of about 30 cm. These walls had an external solid brick layer and an internal hollow brick layer, separated by an air cavity, and were placed within RC frames with little attention to their connection to the structure. Over time, the air spacing between the leaves was filled with thermal insulation (medium infills). Strong infills correspond to the most recent type, where wall systems have become ticker, with smaller cavities and ticker hollow brick leaves, especially the external one. In many recent buildings, cavity walls have been replaced by single-leaf walls with external thermal insulation (Braga et al. 2011; Silva et al. 2021). Interior partitions are generally made up of thin hollow clay blocks (8–10 cm thick). In a few cases, particularly in public buildings, partitions are built using rather large gypsum blocks. (Braga et al. 2011). External infills consist of either solid walls or walls with window openings, while internal partitions are either solid or include door openings (Bal et al. 2008; De Risi et al. 2020; Nafeh and O'Reilly 2022; Aljawhari et al. 2024). In most cases, the internal infill is fixed at all four corners of the RC frame, while the external infill is usually restrained only at the top and bottom by a small horizontal support. This construction technique weakens the interaction between the RC frame and the external infill under both in-plane and out-of-plane seismic actions and usually causes damage to the external layer as observed in previous earthquakes (Ricci et al. 2011; Ruiz-Pinilla et al. 2016). . In the Mediterranean construction system, plumbing and electrical systems, which include electrical cables, pipes, lighting, and rain drainage systems (Del Vecchio et al. 2020), are typically embedded with hollow clay brick infills and partitions in residential buildings (Del Vecchio et al. 2020; Aljawhari et al. 2024). As a result, their damage is closely correlated with the damage states experienced by the infill walls. Since it is often difficult to determine whether these systems are installed within infills or attached externally to walls or roofs, they are classified in this study as both acceleration- and drift-sensitive components. This allows the decision maker to select, for a specific building, the appropriate EDP that controls the damage. Windows and doors represent another significant source of non-structural damage and associated economic losses. Window systems typically consist of wood, aluminium, PVC, or mixed materials (e.g., PVC–aluminium, PVC–wood, wood–aluminium) frames with single or double glazing, anchored to the surrounding partition or infill wall through mechanical or adhesive connections. Door frames are

usually made of similar materials, with either solid or hollow cores, and are embedded in the masonry or infill partitions. Both windows and doors may experience glass breakage, frame distortion, or loss of operability even under moderate drift demands. Accordingly, these components are modelled as drift-sensitive non-structural components, with their fragility functions correlated to the deformation levels of the corresponding infill or partition walls. Finally, in addition to the above-mentioned components, there are also roofs and chimneys, stair finishes, floor finishes, lighting, sanitary equipment, and communication and security components (Del Vecchio et al. 2018).

4.2.3 Fragility functions

Following the detailed characterisation of structural and non-structural components, multiple component-specific fragility functions were collected from a wide range of studies, under the assumption that these components are representative of those described in Section 4.2.2. Furthermore, by collecting fragility curves from different studies and regional contexts, a better representation of the epistemic uncertainty associated with the variability in the building inventory is achieved. Table B.1 (see Appendix B.1) provides a summary of the fragility functions used in this study, including their associated EDP and source. For Category 1 components, i.e. brittle columns and interior and exterior beam-column, the adopted fragility functions were specifically chosen to address the common deficiencies present in existing gravity load-designed RC buildings in Europe. These deficiencies include inadequate detailing of interior and exterior beam-column joints (Aslani and Miranda 2005; Cardone 2016a; Ruiz-García and Ramos-Cruz 2024) and the presence of slender, short, and brittle columns with insufficient transverse reinforcement (Pagni and Lowes 2006; Cardone 2016a). The fragility functions adopted for the masonry infill walls were selected from previous experimental studies that extensively investigated the seismic behaviour of infilled RC frames under various configurations, materials, and boundary conditions. As the vulnerability of these components involves both in-plane and out-of-plane behaviours, PSD and PFA fragility functions were considered. The selected studies include tests om exterior and interior walls with and without openings (Cardone and Perrone 2015), as well as solid and hollow clay bricks, concrete blocks, and other masonry units tested across different regions (Sassun et al. 2016a; Del Gaudio et al. 2017; Chiozzi and Miranda 2017; Rossi et al. 2021). The fragility functions for partitions were selected from experimental studies covering both masonry and gypsum-board systems (Aslani and Miranda 2005; Retamales et

al. 2013; FEMA 2018a). To specifically consider the out-of-plane damage of infills and partitions, the fragility functions developed by Cardone and Perrone (2015) and FEMA (FEMA 2018a) were employed. Considering the specific construction typologies, damage to plumbing and electrical systems (Category 3) was assumed to be correlated to the damage of masonry infills and partition walls (Category 2). Similarly, damage to windows and doors (Category 4) was assumed to be correlated with the failure of the envelope infill/partition wall. As a result, the fragility parameters assigned to Category 4,are considered identical to those of the infill/partition walls, in line with the assumptions made in previous research studies (Rossi et al. 2021; Mucedero et al. 2024a). Nevertheless, considering the possibility of plumbing and electrical systems being located within the suspended ceilings, their vulnerability to acceleration demands was also considered by adopting the PFA-based fragility functions proposed in FEMA (2018). Finally, for other non-structural components (such as under-floor cavity and floor undercoats, sanitary fixtures, and lighting), the fragility functions from (FEMA 2018a) were employed.

4.2.4 Repair consequence functions

Typically, the computation of storey loss functions requires detailed information on the quantities of individual building components, which can be challenging when only aggregated or general data are available. In addition, it is necessary to assign consequence functions to each component, which quantify the monetary losses associated with different levels of damage. These functions need to be developed for each component, often based on unit cost data derived from public works price lists. This can be particularly challenging when publicly available information on the repair costs of common civil structures is limited or inaccessible. An alternative can be using repair costs per square meter of building (€/m^2), which offers a more straightforward approach to estimate losses, as it enables loss calculations even when detailed component data are uncertain or unavailable. These costs are usually available in the format of post-earthquake data. Ideally, repair cost data for building components should be sourced directly from the country under analysis to ensure contextual accuracy. However, such data are rarely available hence it becomes necessary to rely on repair cost data from other countries. For this reason, the consequence functions developed by Del Vecchio et al. (2020) for different component categories, derived from actual repair costs incurred for repairing RC residential buildings damaged by the 2009 L'Aquila earthquake, were employed. The consequence functions are expressed in terms of the mean repair cost and

corresponding standard deviation for six damage states (DS0 to DS5). Since each component category encompasses multiple elements, separate consequence models were derived for each individual component by distributing the category-level consequence functions according to predefined cost ratios. To align the several fragility functions collected for each component, each with a varying number of DSs, with the selected consequence model, a harmonisation process was carried out. This involved mapping the damage states from the fragility functions to those defined in the consequence functions, using the damage descriptions provided in each source. Where direct correspondence was not possible, the consequence data were rescaled to align with the fragility model, ensuring that each damage state was associated with an appropriate consequence value. For example, given a fragility function with four damage states, the original (Del Vecchio et al. 2020) DS4 and DS5 were merged into a single, broader damage state. Given that the repair costs reflect construction prices in Italy in 2011, an adjustment was required to account for inflation, adjusting the repair costs to 2022 price levels, using an inflation value of 1.23. The updated repair cost consequence models for each subcomponent are summarised in Table 4.2.

Table 4.2 Summary of repair costs consequence models adopted for each component.

Cat	Component	DS0		DS1		DS2		DS3		DS4	
		θ	CoV	θ	CoV	θ	CoV	θ	CoV	θ	CoV
1	Interior BCJ	1.4	1.8	3.3	1.5	6.8	2.4	5.3	1.4	8.3	2.3
	Exterior BCJ	1.4	1.8	3.3	1.5	6.8	2.4	5.3	1.4	8.3	2.3
	Brittle columns	0.7	1.8	1.6	1.5	3.4	2.4	2.7	1.4	4.2	2.3
2	Infill walls	20.8	1.0	55.1	0.5	65.4	0.7	75.7	0.5	73.7	0.3
	Partitions	20.8	1.0	55.1	0.5	65.4	0.7	75.7	0.5	73.7	0.3
3	Plumbing and electrical syst.	8.1	1.2	27.1	0.6	42.7	0.9	54.4	0.8	59.8	0.7
4	Windows and Doors	5.3	1.4	12.7	1.6	27.8	0.9	41.3	0.7	48.5	0.6
5	Sanitary waste piping	5.7	0.6	8.5	0.8	15.7	0.8	20.5	0.8	27.7	0.4
	Lighting	5.7	0.6	8.5	0.8	15.7	0.8	20.5	0.8	27.7	0.4
	Floor slabs and tiles	5.7	0.6	8.5	0.8	15.7	0.8	20.5	0.8	27.7	0.4

Note: θ: mean repair cost value, in €/m2; CoV: repair cost coefficient of variation

4.2.5 Environmental impact consequence functions

Environmental impact consequence functions provide a means to quantify these effects by linking damage states to corresponding EIs. These functions can be estimated through several approaches, distinguished by their level of detail. The most detailed method for estimating EIs is the Bill of Materials Life Cycle Assessment (BOM-LCA), which evaluates the EI of all materials and components required for repair across their fill life cycle. While accurate, it requires precise identification and quantification of all materials, making it a time-intensive process. Moreover, it depends on access to professional LCA databases (Gervásio and Dimova 2018; Aljawhari et al. 2024). A simpler approach uses embodied carbon factors (f_{CO_2eq}) to quantify the carbon emissions associated with the production of construction materials. These factors can be obtained from environmental product declarations (EPDs) issued by construction-material manufacturers, or through databases such as the Inventory of Carbon and Energy (ICE) (Hammond et al. 2011), which provides cradle-to-gate embodied carbon values per kilogram of material. Total embodied carbon is calculated by multiplying the material quantities required for each damage state by their carbon factors. Although easier to apply, this method is less precise than BOM-LCA due to regional variations in production and challenges in estimating repair material quantities (Arroyo et al. 2015). In the context of this study, where detailed material quantities cannot be directly determined, EIs can be estimated using Economic Input-Output Life Cycle Assessment (EIO-LCA), which associates EIs with economic activities. In this approach, each repair activity is disaggregated into a list of services, materials, or components, which are then mapped to specific economic sectors. Once each activity is assigned an economic sector, the repair cost associated with that activity is multiplied by the sector-specific EI factor, which quantifies EIs per unit of economic output (i.e., $kgCO_2e$ per dollar spent). These factors are derived from national EIO databases, such as the Carnegie Mellon EIO-LCA model, and cover a broad range of indicators, including greenhouse gas emissions, energy consumption, water use, and toxic releases. While it provides comprehensive coverage and ease of use, it features some limitations. It operates at an aggregate level, relying on average sectoral technologies and supply chains, restricting its resolution when compared to other methodologies and possibly reducing accuracy when applied to specific or innovative construction practices that differ from typical sector averages. Additionally, the resulting EI relies heavily on the repair cost estimation, the choice of the industrial sectors assigned to each repair activity, and the corresponding costs distribution. Uncertainty also grows as the

assessment moves further from the dates of the construction cost data and the default geographic region (Simonen et al. 2018).

The EI data used in this analysis were sourced from the Supply Chain Greenhouse Gas Emission (SC-GHG) factors v1.33 (U.S. Environmental Protection Agency, 2022). The EI estimated in this study focuses solely on embodied carbon, as it has been shown to serve as a representative metric for overall EIs (Simonen et al. 2018). The estimated impact accounts for cradle-to-gate emissions, however, emissions related to the transportation and disposal of waste, as well as the transportation of materials and workers to the site, were not considered. The effects of demolition, waste processing, and disposal were accounted by allocating part of the repair cost to the solid waste collection sector. Following the repair costs presented in the previous sections, a disaggregation of repair activities was performed for each damage state of every component, and, for each repair activity, the relevant materials or/and services were identified and mapped to one or more industrial sectors, using engineering judgement. The repair actions involve a sequence of preparatory, structural and finishing tasks aimed at restoring the integrity of the damaged components. For structural components, the process begins with the installation of scaffolding and shoring systems to ensure safety and accessibility, followed by the removal of furnishings, electrical, and plumbing systems as needed. Damaged or deteriorated areas are then exposed by demolishing partitions and cleaning or removing loosened concrete, after which cracks are prepared and injected with epoxy resin, and, if necessary, reinforcement bars are replaced. Structural defects are repaired using mortar or rheoplastic concrete and the repair cycle ends with restoring finishes, utilities, and removing scaffolding. The extent and material composition of these actions vary with damage severity. For slight damage, interventions are limited to surface-level treatments such as crack sealing, epoxy injection, and protective coatings, with chemicals, coatings, and cleaning products representing the largest share of costs, while concrete, steel, and waste collection play a minor role. In moderate damage, where localised spalling and partial reinforcement exposure occur, repair strategies involve more concrete patching and some steel replacement, increasing the contribution of these materials with respect to chemicals and coatings. In severe damage, characterised by significant concrete loss and reinforcement yielding, major section replacement or jacketing is required. Consequently, concrete and steel dominate the repair costs. For masonry infill walls and partitions, the process typically begins in a similar way to the structural components, followed by the removal of plaster along cracked or damaged areas to

expose the underlying masonry. Depending on the damage severity, the repair may involve localised plaster patching with fiberglass reinforcing mesh, partial wall demolition and reconstruction, or complete wall replacement. Once the damaged areas are addressed, plastering and painting are carried out to restore the original finish and ensure adequate protection. For slight damage, interventions are limited to plaster removal and localised patching using lime- and mineral-based products, following by repainting. These actions mainly involve coatings, plaster, and minor amounts of masonry materials. In moderate damage, where portions of infills are loosened or cracked, repair actions include partial demolition, brick replacement, mesh-reinforcement plastering, and repainting, leading to higher contributions from masonry and plaster materials. For severe damage, the existing wall is fully demolished and rebuilt before finishings, making masonry products (bricks, concrete, and lime) the dominant contributors to repair costs, with finishes playing a secondary role. The type of repair actions for interior gypsum partition walls is similar to those for interior masonry walls; however, gypsum partition repairs typically involve lighter, less material-intensive interventions and focus more on surface treatments and component replacement, such as replacing screws, studs, bracing, join tapes, and gypsum boards, rather than heavy structural reconstruction.

Following the identification of the repair activities and their corresponding sectors for each damage state and component, the cost contribution of each activity within that damage state was quantified. Figure 4.2 presents an example of the cost allocation for the structural components. As it can be observed, for initial damage, epoxy and paint/coating activities account for the largest shares of the total repair costs, while concrete and steel contributions increase progressively with the damage severity, reflecting the growing need for structural replacement and reinforcement in higher damage states. Subsequently, the cost allocation for each activity was multiplied by the EI factor of its sector to estimate its associated EI.

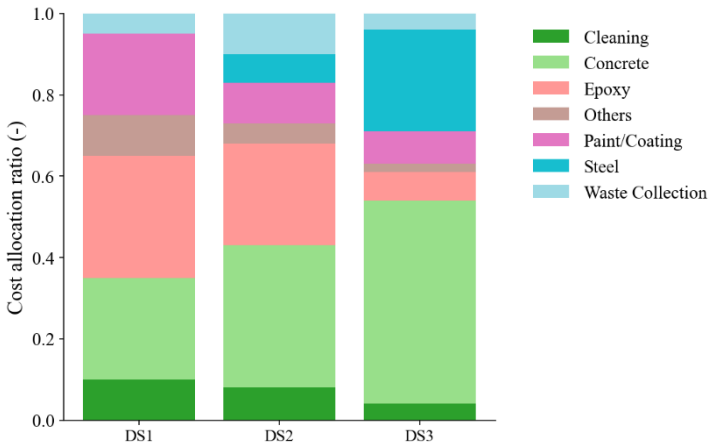

Figure 4.2 Sectoral cost allocation for each damage state of structural components

Since the reference year of the database matches that of this study (2022), no inflation adjustment was required. However, as the repair costs are expressed in euros, a conversion to U.S. dollars was necessary. Figure 4.3 illustrates the average contributions to the total embodied carbon factor ($kgCO_2e/€$) for each component category. It is observed that structural, masonry infills, and gypsum partition components lead to the highest EI. These components feature prominent use of high-impact sectors, such as concrete, mortar, and gypsum. Table 4.3 summarises the EI consequence models adopted for each component.

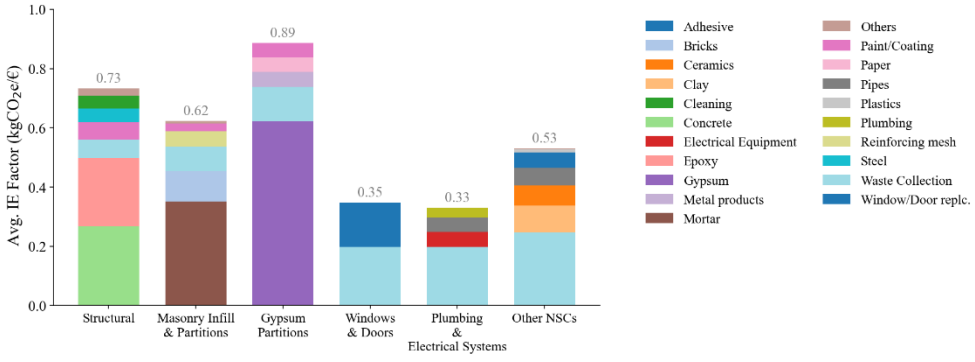

Figure 4.3 Average sector contributions to the embodied carbon factor of each component category.

Table 4.3 Summary of environmental impact consequence models adopted for each component.

Cat.	Component	DS0		DS1		DS2		DS3		DS4	
		θ	CoV	θ	CoV	θ	CoV	θ	CoV	θ	CoV
1	Interior BCJ	1.0	1.8	2.3	1.5	5.0	2.4	3.0	1.4	4.7	2.3
	Exterior BCJ	1.0	1.8	2.3	1.5	5.0	2.4	3.0	1.4	4.7	2.3
	Brittle columns	0.5	1.8	1.2	1.5	2.5	2.4	1.5	1.4	2.4	2.3
2	Infill walls	17.0	1.0	41.8	0.5	34.7	0.6	38.5	0.5	37.5	0.3
	Partitions	17.0	1.0	41.8	0.5	34.7	0.6	38.5	0.5	37.5	0.3
3	Plumbing and electrical syst.	2.8	1.2	9.4	0.6	14.9	0.9	18.9	0.8	20.8	0.7
4	Windows and Doors	1.9	1.4	4.6	1.6	10.2	0.9	15.1	0.7	17.8	0.6
5	Sanitary waste piping	2.3	0.6	3.4	0.8	6.3	0.8	8.2	0.8	11.1	0.4
	Floor slabs and tiles	4.1	0.6	6.1	0.8	11.3	0.8	14.7	0.8	19.9	0.4
	Lighting	2.9	0.6	4.3	0.8	7.8	0.8	10.2	0.8	13.8	0.4

Note: θ: mean EI value, in kgCO2e/m2; CoV: EI coefficient of variation

4.3 DEVELOPMENT OF STOREY LOSS AND ENVIRONMENTAL IMPACT FUNCTIONS

4.3.1 Generalised functions

The storey loss and EI functions were derived for the various component categories introduced in Section 4.2.2, using a modified version of the toolbox provided by Shahnazaryan et al. (2021). Specifically, repair cost and EI values were sampled through Monte Carlo simulations based on the input fragility and consequence functions across different EDP levels. A regression analysis was then performed on the resulting dataset using a Weibull cumulative distribution function to capture the nonlinear relationship between damage and demand. The goodness of the regression was evaluated using two metrics: the maximum relative error ($error_{max}$) (Equation 4.1) and the cumulative relative error ($error_{cum}$) (Equation 4.2), both calculated over the entire EDP range for each component group. The maximum relative error captures the largest discrepancy between observed and predicted loss values, reflecting the worst-case deviation. In contrast, the cumulative relative error provides an

aggregated measure of the overall fitting accuracy across the full range of EDP values. In Equation 4.1 and Equation 4.2, the terms C_{repair}^{EDP} and $\hat{C}_{repair}^{EDP}$ correspond, respectively, to the original and fitted repair costs.

$$error_{max} = max\left(\frac{\left|C_{repair}^{EDP} - \hat{C}_{repair}^{EDP}\right|}{max\left(C_{repair}^{EDP}\right)}\right) \tag{4.1}$$

$$error_{cum} = \int_{0}^{EDP\,=\,\max EDP} max\left(\frac{\left|C_{repair}^{EDP} - \hat{C}_{repair}^{EDP}\right|}{max\left(C_{repair}^{EDP}\right)}\right) dEDP \tag{4.2}$$

Figure 4.4 and Figure 4.5 illustrate the storey-based loss and EI functions, respectively, for the various component categories. The mean, 16th, 50th, and 84th percentiles corresponding to the observed and fitted losses are included, together with the scattered data points corresponding to each Monte Carlo realisation, characterising the variability in repair costs/EI within the same component category. In these figures, the goodness of the regression parameters used to evaluate the performance of the storey-based functions ($error_{cum}$ and $error_{max}$) is also presented. The obtained functions show that, across the entire EDP range, the maximum and cumulative relative regression errors remain consistently low for all component categories: below 11% and 1%, respectively, for the SLFs and below 14% and 1% for the SEIFs. Table B.2 and Table B.3 (see Appendix B.2) summarise the fitting coefficients of the Weibull distribution for all component categories regarding the storey loss and EI functions, respectively.

Structural components

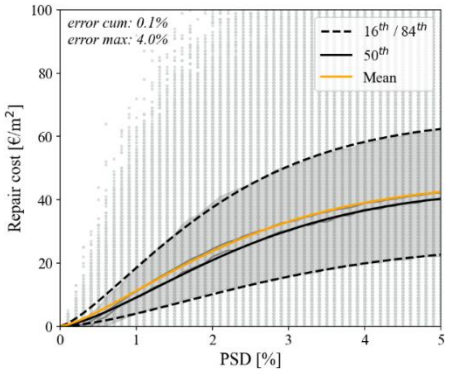

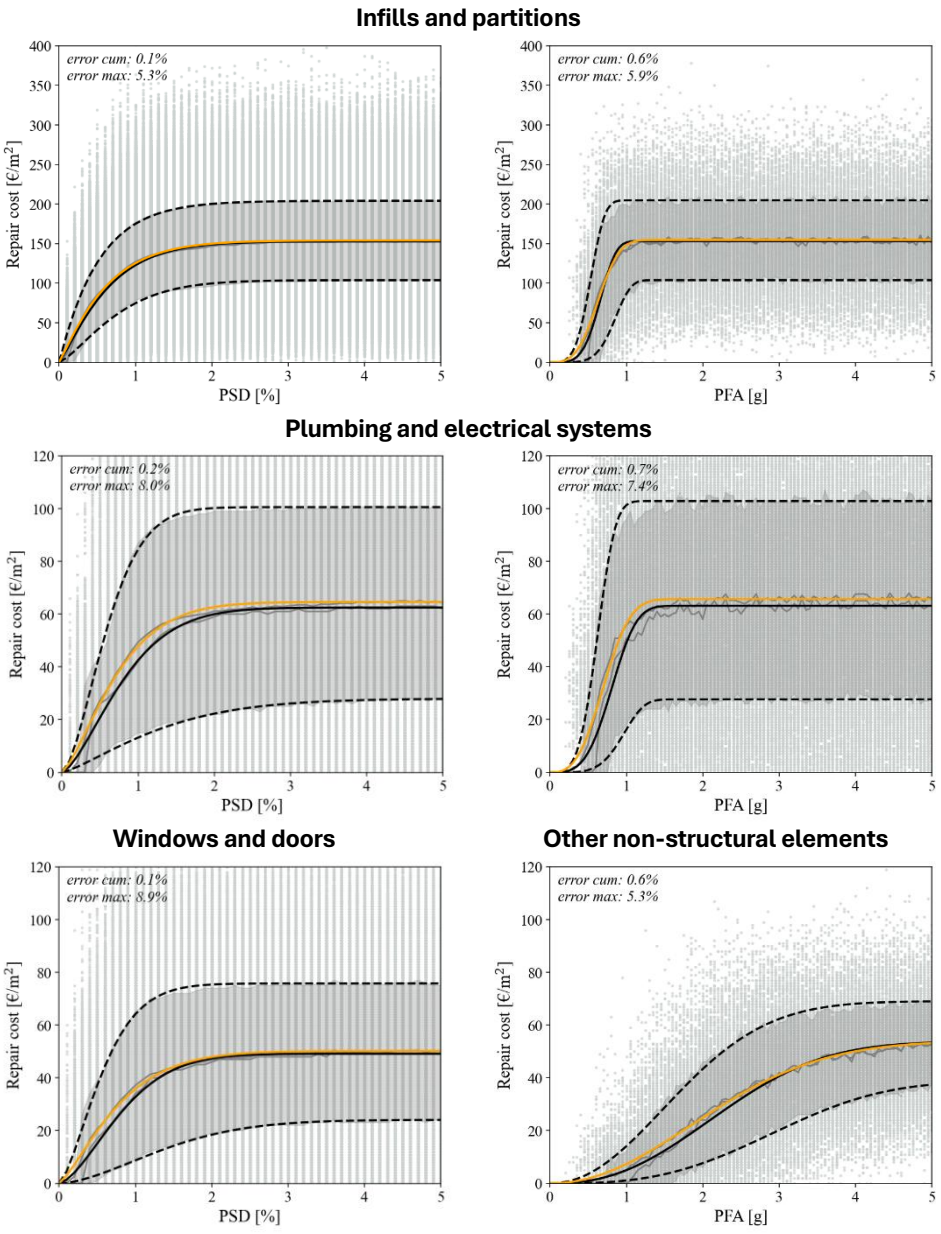

Figure 4.4 Storey loss functions (SLFs) for each component category as a function of the EDP (goodness of regression parameters indicated in each plot).

Structural components

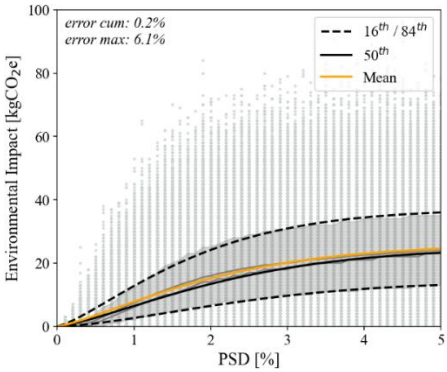

Infills and partitions

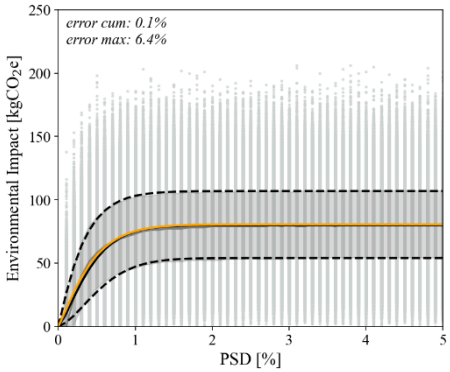

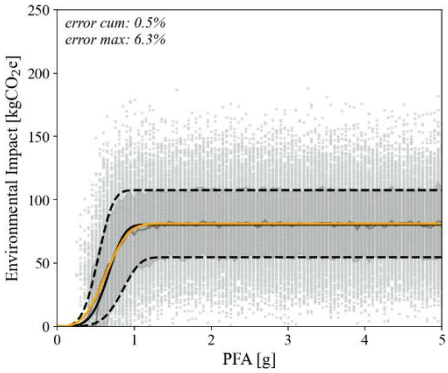

Plumbing and electrical systems

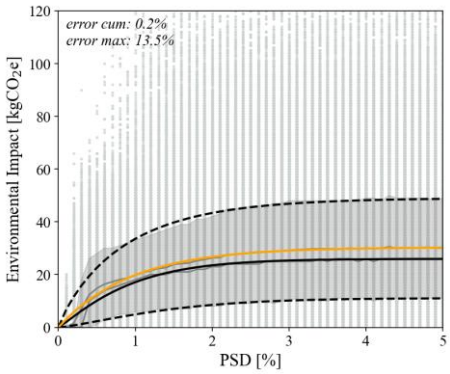

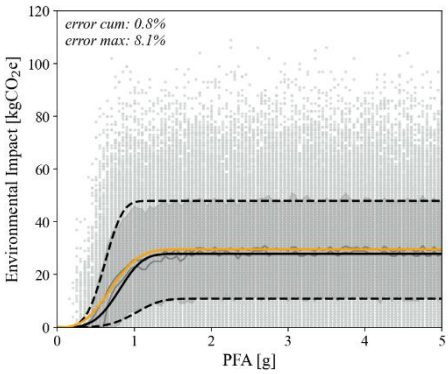

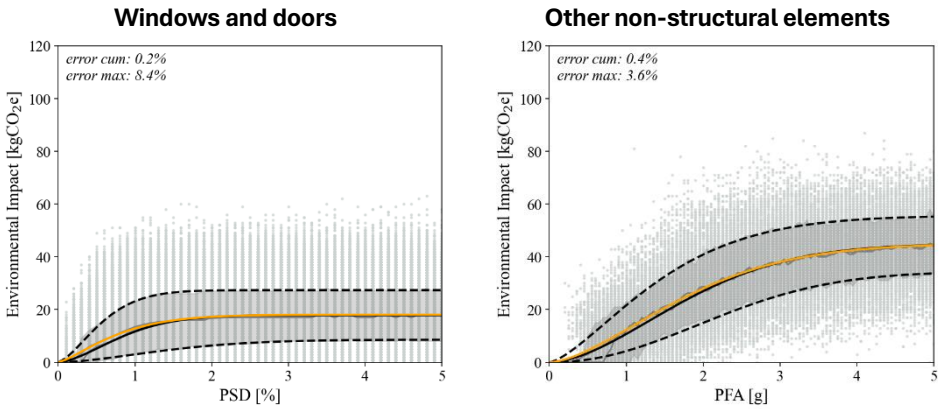

Figure 4.5 Storey environmental impact functions (SEIFs) for each component category in function of the EDP (goodness of regression parameters indicated in each plot).

Overall, the functions reveal a consistent trend of significant uncertainty in both repair cost and EI prediction, with the variability (spread between the 16th and 84th percentiles) increasing notably at higher levels of EDP. Infills and partitions emerge as the dominant driver of financial loss and EI, showing the highest mean and the largest uncertainty. Their functions rise steeply at low EDP values, reflecting their low capacity and proneness to early damage. Since the damage of windows/doors and plumbing/electrical systems is conditioned on the damage of infills and partitions, these associated functions show a similar trend. Conversely, the structural components exhibit a smoother, more gradual increase in repair costs and EI, and generally show the tightest uncertainty band. PFA-sensitive components exhibit a sharp increase in losses followed by a plateau at moderate PFA values (around 1-2g). This behaviour is likely due to the limited number of PFA-sensitive fragility curves available for these components, leading to sparse data coverage across the full range of PFA values, particularly in the critical transition zone where damage escalation typically occurs. Consequently, the introduction of more sources of PFA-sensitive fragilities should be considered in future studies.

4.3.2 Country-specific cost conversion functions

As mentioned in Section 4.2.4, the adopted repair costs are based on actual data from the L'Aquila earthquake. Since these costs reflect construction prices in Italy, adjustments are required to account for specific cost differences to other countries. To address the differences in construction dynamics between the reference country (Italy) and a target country, a country-specific cost conversion should be

implemented. Different approaches exist to account for such variations (Papadopoulos et al. 2019; Silva et al. 2020), typically involving adjustment factors based on labour costs, material prices, and relevant economic indices. In this study, the methodology proposed by Papadopoulos et al. (2024) was adopted, estimating the Repair Cost Conversion Factor (RCCF) using Equation 4.3, allowing for the translation of repair costs from the Italian context to the Portuguese one.

$$RCCF = \left(r_{lab} \cdot f_{lab}/r_{prod}\right) + \left(r_{mat} \cdot f_{mat}\right) + r_{m,p} \cdot f_{m,p} \quad (4.3)$$

In Equation 4.3, f_{lab}, f_{mat}, and $f_{m,p}$ are the proportion of the total repair cost associated with labour, materials, margins and preliminaries, respectively, in the reference country. The terms r_{lab}, r_{mat} and $r_{m,p}$ denotes the estimated cost ratios for labour, material, and margins and preliminaries between the target and reference country. Additionally, r_{prod} represents the difference in labour productivity between the target and reference country. It is calculated using the construction sector's labour productivity (c_{prod}), defined as the gross value added (GVA) of the construction sector per employed person, multiplied by the average worker compensation. Based on official data from different countries (Eurostat 2024b, c), the RCCF between Italy and the remaining EU countries was derived, as illustrated in Figure 4.6, distinguishing between (a) structural and architectural components and (b) non-structural components. Table B.6 (see Appendix B.3) summarises the parameters used to quantify the RCCF for all the considered countries. Specifically, r_{lab} and r_{mat} were obtained through the ratios of worker hourly compensation and construction cost indices between the target and the reference country, respectively. The value of $r_{m,p}$ was set to one, assuming no significant differences in margin and preliminaries among the countries considered in this study. Finally, f_{lab}, f_{mat}, and $f_{m,p}$ were derived based on the judgment of the Authors.

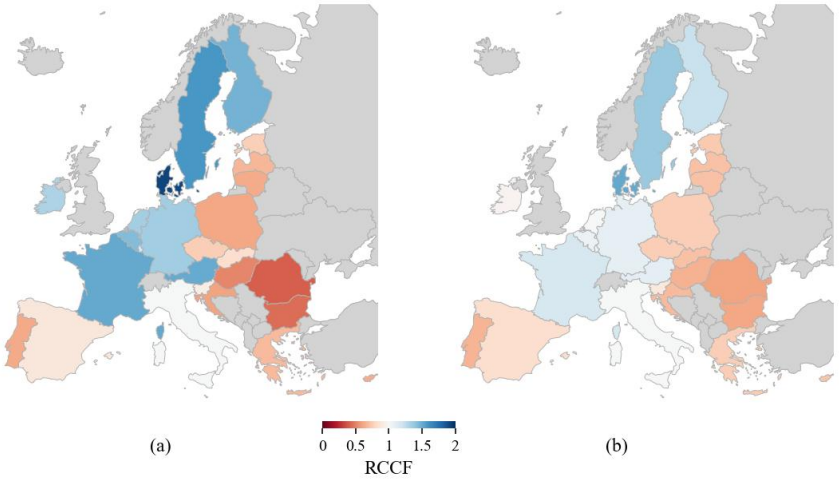

Figure 4.6 Repair Cost Conversion Factor (RCCF) between Italy (reference country) and European Union countries for (a) structural and architectural, and (b) non-structural components.

4.4 TAILORED FUNCTIONS FOR THE PORTUGUESE RC BUILDINGS STOCK

To illustrate the practical application of the proposed generalised functions and to provide country-specific insights, a set of tailored SLFs and SEIFs was developed for the Portuguese RC building stock. The following sections describe the adaptation process in detail and demonstrate how these functions can be used to estimate both economic losses and EI.

4.4.1 SLFs and SEIFs adaptation

Figure 4.7 (a) illustrates the distribution of different building typologies across the districts of mainland Portugal, along with the corresponding distribution of the number of buildings, following the latest exposure model for the country (Yepes-Estrada et al. 2023). RC buildings account for 51% of the total building stock in Portugal, accommodating 63% of the total population and covering 63% of the total built area. Figure 4.7 (b) shows the distribution of each code level (CDN, CDL, CDM, and CDH) in terms of building count, population, and total replacement cost. Overall, approximately 26% of the RC buildings were constructed with none-to-limited seismic design provisions, 57% with moderate seismic design and only 19% with high seismic design standards. CDM buildings account for the majority in terms of building count, population, and total reconstruction cost (≈ 57%). Although CDN and

CDL buildings represent a smaller proportion of the total RC building stock (≈ 26%), they are of particular concern due to their poor seismic performance, stemming from their design with little to no consideration of seismic resistance. These structures are predominantly moment-resisting frame structures, primarily designed to support gravity loads, and are often characterised by geometrical irregularities, slender RC elements, inadequate reinforcement in both quantity and detail, unconfined concrete with low compressive strength, insufficient cover, and smooth reinforcement rebars (Xavier et al. 2022). The majority of these buildings is also characterised by the presence of masonry infill walls (Furtado et al. 2016) that typically feature a cavity wall design, where the external leaf is thicker (usually 0.15 m) than the internal leaf (usually 0.11 m). The two layers of the wall were not connected, and the cavity between them was left empty (Silva et al. 2021). Different studies have addressed the characteristics of reinforced concrete RC buildings in Portugal, focusing on various aspects such as building spatial distribution, period of construction and geometrical properties (Silva et al. 2015a; Furtado et al. 2016).

The generalised storey loss and EI functions from the previous section are adapted herein for the Portuguese building stock, using the country-specific cost conversion factors. Based on the resulting RCCF value obtained in Section 4.3.2, the obtained repair costs presented in Section 4.2.4 should be adjusted by a factor of 0.62 for structural and architectural components (categories 1, 2, 3, and 4) and 0.66 for non-structural components (category 5), as indicated in Table B.6 (see Appendix B.3). To ensure consistency and comparability across all available data, the repair costs were adjusted to 2022 price levels using an inflation value of 1.23.

The Portuguese-specific functions are presented in Figure 4.8 (economic loss) and Figure 4.9 (EI). Each figure displays, for each component's category, both the total loss/EI (left y-axis) and the corresponding normalised value (right y-axis), i.e. the repair costs normalised by the total reconstruction cost or total EI. The total reconstruction cost of residential buildings in Portugal was estimated through the Property Reconstruction Cost Simulator (Cruz and Branco 2020). This publicly accessible tool provides indicative reconstruction cost estimates based on the total floor area of a building, adjusted through a set of multiplicative coefficients that account for construction quality, architectural characteristics, geographic location, and other relevant building-specific attributes. The simulator allows users to specify several input parameters, including the type of property (apartment or standalone housing), the geographic location corresponding to the NUTS II regions of Portugal, and the structural typology, such as reinforced concrete (RC), mixed systems,

concrete blocks, or stone masonry. For RC buildings, it is also possible to indicate the energy performance class, ranging from A+ to F, or "unknown." To derive an average reconstruction cost representative of RC buildings across Portugal, the simulator was used to generate estimates under varying regional conditions, while maintaining RC as the structural typology and a low energy class (C, D, E, or F), to reflect the characteristics (older and less energy-efficient structures) of the building stock under investigation. This process resulted in a median reconstruction cost of €1248/m^2, with a standard deviation of €187/m^2, reflecting the variability associated with regional and architectural differences across the country. Interestingly, the median construction costs obtained in this study are similar to the total funding (1213.40 €/m^2) provided by the Italian government for the demolition and reconstruction of buildings classified as unusable following the 2009 L'Aquila earthquake (Baggio et al. 2007) For the total average EI of building replacement in Portugal, the value of 375 kg CO_2e/m^2 reported by Caruso et al. (2024) was employed. Table B.4 and Table B.5 (see Appendix B.2) summarise the fitting coefficients of the Weibull distribution for all component categories regarding the storey loss and EI functions, respectively.

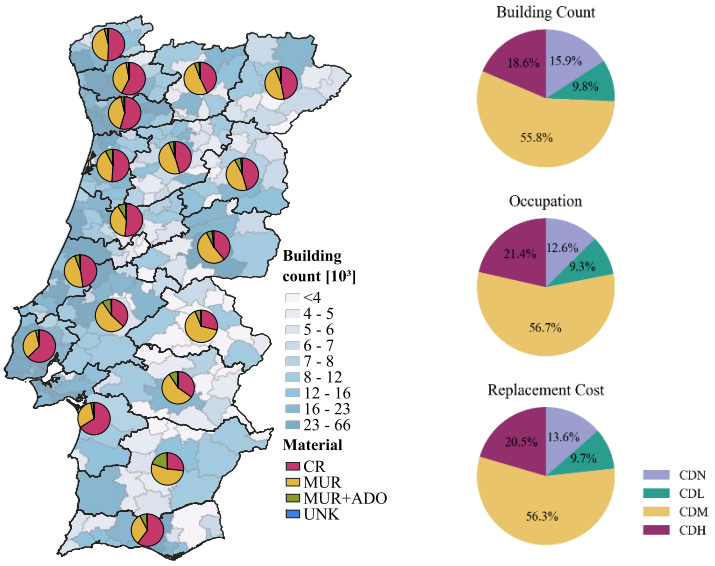

(a) (b)

Figure 4.7 Exposure characteristics of the Portuguese building stock: (a) distribution of building count and construction material by municipality and district, respectively; and (b) variation of exposure variables as a function of code level for the entire country.

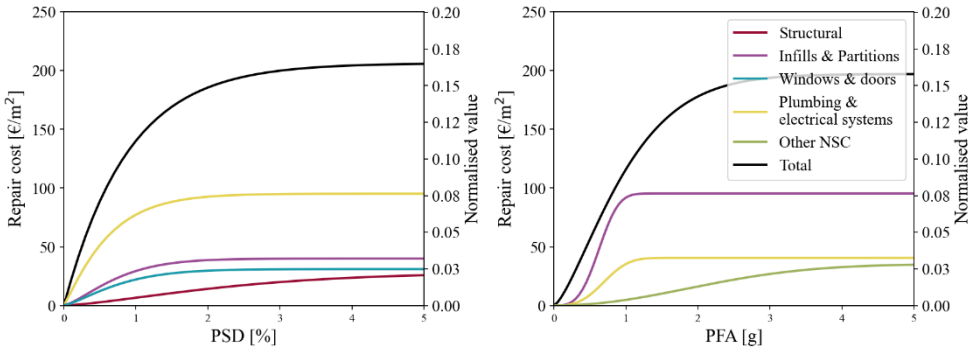

Figure 4.8 SLFs for all the components, as a function of the EDP.

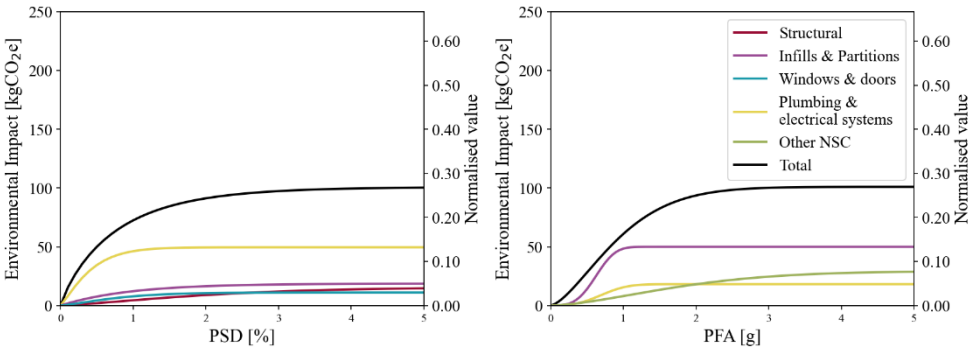

Figure 4.9 SEIFs for all the components, as a function of the EDP.

4.4.2 Loss and environmental impact estimates

Finally, this section illustrates the implementation of economic loss and EI functions to quantify the Expected Annual Economic Loss (EAEL) and the Expected Annual Environmental Impact (EAEI) for a specific building. A comparison between the storey and component-based approaches is also conducted. This analysis is conducted on a six-storey RC moment-resisting frame (MRF) building with unreinforced masonry (URM) infill walls. The structure, typical of residential construction in Europe, built before the introduction of modern seismic regulations, was built in 1966, and is located in Benfica, Portugal. Each storey has a floor area of approximately 200 m^2. Further information regarding the structural characteristics, modelling assumptions, and data sources can be found in Yükselen et al. (2025). It is important to note that the purpose of this example is not to validate the developed storey functions but rather to demonstrate their practical application also in a real single-building scenario.

The EAEL and EAEI, hereafter referred to as decision variables (DV), are estimated following the PEER Performance-Based Earthquake Engineering (PEER-PBEE) framework (Moehle and Deierlein 2004). This approach consists of four sequential stages: hazard analysis, structural analysis, damage analysis, and loss analysis, which are linked through the total probability theorem (Equation 4.4). This equation represents the sum of three mutually exclusive and collectively exhaustive events, conditioned on an IM. Specifically: (i) E[DV|NC∩R,IM] expresses the expected DV given that no collapse (NC) has occurred and the components are repaired (R), conditioned on the IM, (ii) E[DV|NC∩D,IM] expresses the expected DV given that NC has occurred, but the building requires demolition (D) conditioned on the IM, and (iii) E[DV|C] expresses the expected DV when the building has collapsed (C). Each of these components is then multiplied by the corresponding probability: P(NC∩R|IM) is the probability of NC with repair as a function of the IM level, P(NC∩R|IM) is the probability of NC with demolition as a function of the IM level and P(C|IM) is the probability of collapse as a function of the IM level.

$$E[DV|IM] = E[DV|NC \cap R, IM] \cdot P(NC \cap R|IM) + E[DV|NC \cap D, IM] \cdot P(NC \cap D|IM) + E[DV|C] \cdot P(C|IM) \quad (4.4)$$

The seismic hazard at the site of the selected case-study building was characterised through probabilistic seismic hazard analysis (PSHA) using the European Seismic Hazard Model 2020 (ESHM20) (Danciu et al. 2024) implemented in OpenQuake (Pagani et al. 2014). The adopted IM was the average spectral acceleration (AvgSa) over the 0.15–2.25 s period range. Subsequently, a set of thirty hazard-consistent ground motion records was selected from the Engineering Strong-Motion Database (Luzi et al. 2020). Each record comprised two orthogonal horizontal components, and the selection covered 12 intensity levels corresponding to return periods of 30, 45, 73, 100, 200, 308, 475, 712, 975, 1462, 2475, and 4000 years. Then, multiple-stripe analysis (MSA) was performed to assess structural response under the increasing IM levels. The recorded EDPs were the PFA and the PSD. In addition, collapse fragility parameters, namely the median intensity (θ) and dispersion (β), were derived to characterise the probability of exceeding the collapse condition. This condition was defined according to the Portuguese National Annex to Eurocode 8 (EC8 – Part 3) (CEN 2005), which specifies two types of behaviour for existing

buildings, brittle and ductile, to be verified at the Significant Damage (SD) limit state. Specifically, the code stipulates that: (i) the shear demand shall not exceed the shear capacity of the primary structural members; and (ii) the chord rotation of the structural elements shall not surpass their total chord rotation capacity. Figure 4.10 illustrates the PSD and PFA profiles obtained for each individual ground motion record, along with the corresponding mean profile across all records.

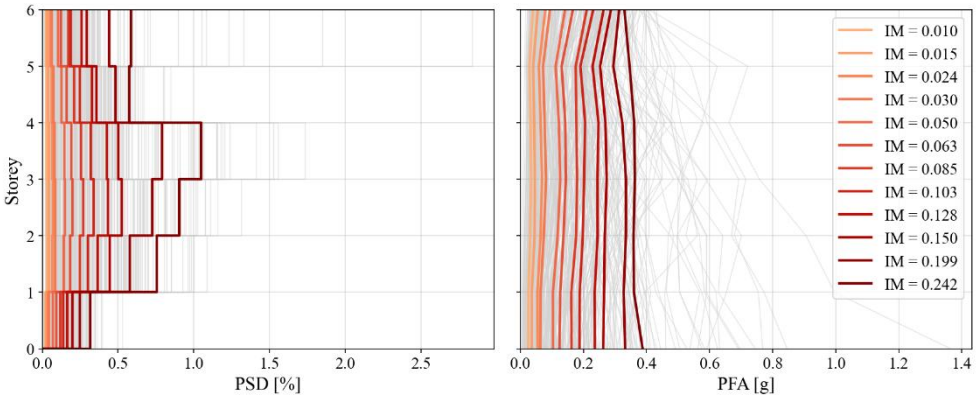

Figure 4.10 Peak storey drift (PSD) and peak floor acceleration (PFA) profiles for the building

Finally, the expected DVs can be obtained through two different alternative procedures. In the first procedure, following the component-based loss assessment methodology of FEMA P-58 (FEMA 2018a), the PELICUN tool (Zsarnoczay et al. 2024) was employed to simulate building damage and losses by generating 250 Monte Carlo realisations. In addition to the structural performance assessment results expressed in terms of EDPs, this methodology requires assembling a detailed inventory of structural and non-structural components and assigning appropriate damage and consequence models to each. Since the architectural plans of the building were available, it was possible to accurately quantify both structural and non-structural components. Then, for each component, a consequence model (covering both economic and EI) was assigned. Table 4.4 provides a summary of the building component inventory, the corresponding EDP, and source of the employed fragility model and consequence data.

In the second approach, the seismic performance assessment results, in terms of EDPs, were interpolated with the SLFs and SEIFs derived in Section 4.4.1. For components sensitive to both drift and acceleration demands, the final DV value was

taken as the maximum value obtained between the drift-sensitive and acceleration-sensitive functions. This procedure was repeated for each IM level, allowing for the quantification of expected DVs across the full range of seismic intensities considered in the MSA. In both approaches, it is necessary to determine the total replacement cost and EI of the case-study building. A unit replacement cost of €1600/m^2 was adopted, with an additional 10% to account for demolition. For the total embodied carbon, a value of 375 kg CO_2e/m^2 proposed by Caruso et al. (2024) was used. An additional 15% of the reconstruction EI was added to include the impacts associated with the demolition and disposal of the damaged structure, following Clemett et al. (2022). Considering an approximate floor area of 200 m^2, the total reconstruction cost and embodied carbon were estimated to be €1,920,000 and 450,000 kg CO_2e, respectively.

Table 4.4 Inventory of damageable components and respective sources of fragility and consequence data.

Component	EDP	Reference
Exterior beam-column joint Interior beam-column joint Brittle weak and short RC columns	PSD [%]	Fragility: (Cardone 2016a) Repair cost: adapted from (Cardone 2016a) Environmental impact: (Aljawhari et al. 2024)
Staircase	PSD [%]	Fragility: (FEMA 2018a) Repair cost: adapted from (FEMA 2018a) Environmental impact: adapted from (Aljawhari et al. 2024)
Masonry infills and partitions (with and without windows)	PSD [%] / PFA [g]	Fragility:(Cardone and Perrone 2015) Repair cost: adapted from (Cardone and Perrone 2015) Environmental impact: (Aljawhari et al. 2024)
Cold/Hot water piping	PSD [%] / PFA [g]	Fragility:(Cardone and Perrone 2015) Repair cost: adapted from (Cardone and Perrone 2015) Environmental impact: (Aljawhari et al. 2024)
Elevator	PSD [%]	Fragility: (FEMA 2018a) Repair cost: adapted from (FEMA 2018a) Environmental impact: adapted from (FEMA 2018a)

Figure 4.11 presents the loss curves, expressed as expected DV versus IM, obtained using the two approaches, with Table 4.5 reporting the corresponding EAEL and EAEI.

Figure 4.11Figure 4.11 shows a very good match between the approaches for the analysed building, which is further confirmed via the estimates of both DVs presented in Table 4.5. To investigate the relative contribution of the component categories to the total losses, the expected DVs were further disaggregated by building component categories. Given the differences between the building inventory used to derive the SLFs and SEIFs and that employed in the FEMA P-58 component-based loss assessment, the only direct comparable categories are the structural components and the infills and partitions. For the selected case study, the latter category already accounts for the presence of windows and doors. Figure 4.12 compares the AAEL and AAEI for structural components and infills and partitions, considering the case where the building is damaged and components are repaired, obtained through both approaches. The storey-based results are presented as mean values along with the 16th, 50th, and 84th percentiles. It should be noted that, in the storey-based approach, the infills and partitions category was merged with the windows and doors category to ensure comparability with the inventory used with the FEMA P-58 approach. This combined category is herein referred to as infills, partitions, and services (IPS). Results show that infills and partitions contribute more to losses with respect to the structural components for both DVs. Among the different approaches, it is observed that, although the mean storey-based results are smaller than those obtained using the component-based approach, the latter consistently falls between the 16th and 84th percentiles, indicating that the storey-based approach can provide upper and lower boundaries of a more accurate estimation of both DVs.

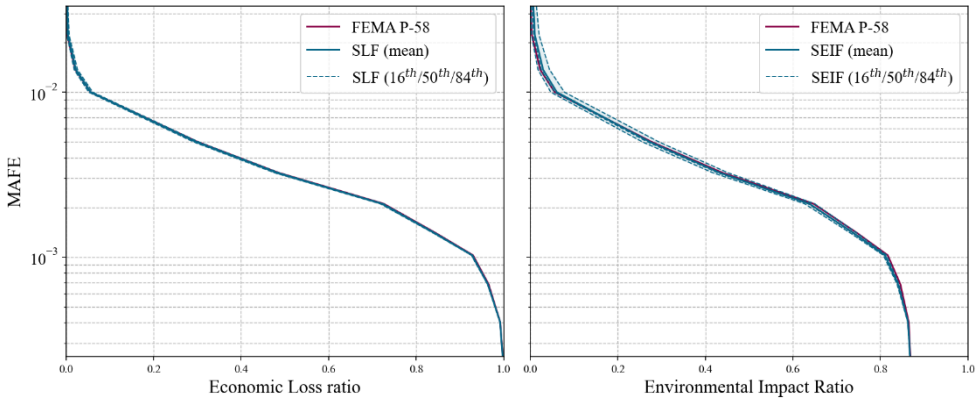

Figure 4.11 Loss curves obtained from each approach

Table 4.5 Average annual economic loss (AAEL) and average annual environmental impact (AAEI) obtained from each approach (in parentheses, the normalised value in relation with the total replacement cost/environmental impact)

Approach	AAEL	AAEI
FEMA P-58	9286 € (0.48%)	2061 $kgCO2_e$ (0.46%)
SLF	9203 € (0.48%)	2027 $kgCO2_e$ (0.45%)

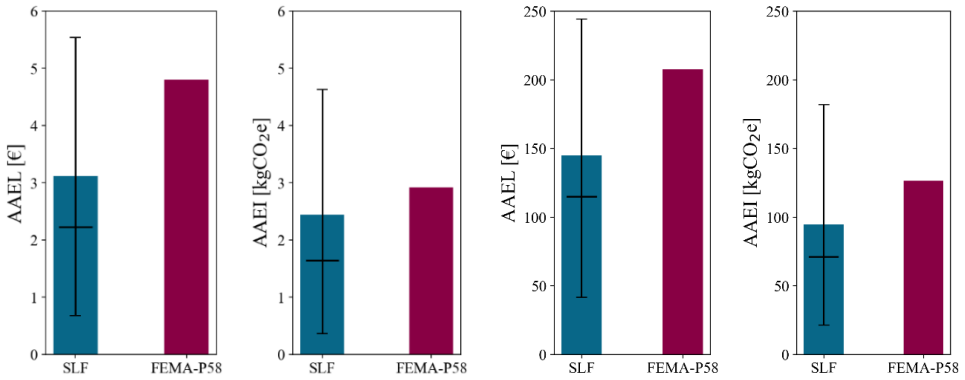

Figure 4.12 Comparison between the AAEL and AAEI estimated with the two approaches for (a) structural components and (b) infills, partitions, and services.

Building on the previous results and considering the stronger contribution of infills, partitions, and services to the total losses, the expected economic losses and EI values obtained through both approaches were compared for each IM level. The results, illustrated in Figure 4.13, show a very good agreement, indicating that the fragility and consequence functions adopted in both approaches are overall consistent. In general, the component-based (FEMA P-58) results fall within the 16th and 84th percentiles of the storey-based results. Nevertheless, some differences can be noted: for lower IM levels, the storey-based approach tends to produce higher DVs, whereas for higher IM levels, the opposite trend is observed. The discrepancies observed for lower IM values are mainly attributed to the difficulty of achieving an exact fit with the selected regression function, which struggles to accurately capture the expected DVs at lower intensities. For higher IM levels, the differences are likely due to the used consequence functions, with those adopted for the case study assigning higher repair costs and EIs to severe damage states.

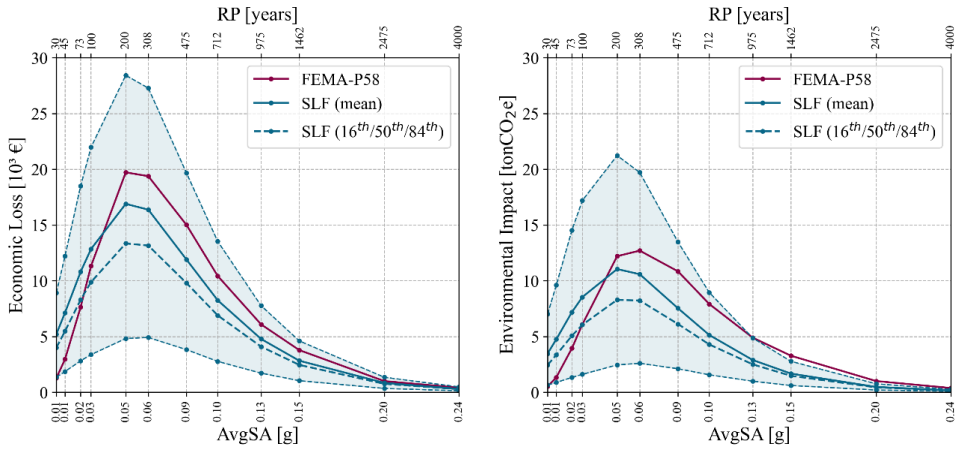

Figure 4.13 Comparison between (a) economic loss and (b) environmental impact as a function of the IM level obtained through both approaches for infills, partitions, and services.

4.5 CONCLUDING REMARKS

This chapter presented the development of generalised storey loss (SLF) and environmental impact (SEIFs) functions for the seismic assessment of reinforced concrete buildings characterised by limited capacity to withstand seismic actions therefore highly vulnerable. The methodology for deriving these functions began with the characterisation of the selected building typologies, followed by the identification of relevant damageable components. Fragility functions describing the seismic vulnerability of these components were then combined with repair costs and environmental impact (EI) consequence functions to derive the storey loss and EI functions. The consequence functions derived from post-earthquake repair cost data collected after the 2009 L'Aquila earthquake were used and disaggregated to the component level through cost ratios and adjusted for inflation. An economic input-output life cycle assessment (EIO-LCA) approach was adopted to generate the EI associated with each repair activity. The generic functions developed within this study serve as a foundation for future large-scale seismic risk assessment studies and can be customised and applied to different European or Mediterranean countries by following the same methodology and the country-specific cost conversion factors also provided.

The adaptation of the derived functions was illustrated for mainland Portugal, ensuring that local construction practices, cost and environmental data were adequately represented. This customisation enhances the relevance and applicability of the generalised storey-based functions for national-scale seismic risk estimation and supports decision-making for both risk mitigations and sustainability goals. The application of the storey-based approach was also demonstrated and compared with the component-based methodology proposed in FEMA P-58. Both assessments were implemented to estimate the expected annual economic loss and the expected annual EI, for a typical Portuguese RC building. The results showed a good agreement between the two approaches, both in terms of loss curves and annualised metrics, confirming the robustness of the storey-based approach. Overall, the example illustrates the practical applicability and consistency of the storey-based approach as an efficient alternative to more data- and computation-intensive component-based assessments, while also emphasising the importance of carefully selecting fitting functions and consequence models to ensure accuracy across all intensity levels.

Whereas Chapters 2 and 3 addressed building assessment at larger scales, identifying critical areas and exploring potential retrofit scenarios with their associated impacts on seismic risk reduction, this chapter introduced storey-level loss and environmental impact functions capable of supporting evaluations at both portfolio and individual building levels. Building on this, Chapter 5 will present a multi-criteria decision-making framework designed to integrate multiple technical, economic, social, and environmental decision variables involved in selecting optimal retrofit strategies for single buildings.

CHAPTER 5

Retrofitting decision making for single buildings

This chapter is extensively based on the following publications:

Couto R*, *Mucedero G, Bento R, Monteiro R (2024), Understanding the Impact of Seismic Hazard and Climate Conditions on Multi Criteria–Based Retrofitting of Existing Buildings, Sustainability, 16(10): 4318, 10.3390/su16104318*

Couto R**, Mucedero G, Bento R, Monteiro R. (2024) A Practice-Oriented Approach for Seismic and Energy Performance Upgrading of Existing Buildings. Journal of Earthquake Engineering, 28(15): 4380-4407, 10.1080/13632469.2024.2382474*

Mucedero G, ***Couto R*****, Yükselen B, Monteiro R (2025), Estimation of seismic downtime for building retrofitting decision-making, Resilient Cities and Structures 4: 15–29, https://doi.org/10.1016/j.rcns.2025.07.001*

**Author Contribution: conceptualisation, methodology, software, validation,* data curation, *writing.*
***Author Contribution: methodology, validation*, *writing.*

5 RETROFITTING DECISION MAKING FOR SINGLE BUILDINGS

5.1 INTRODUCTION

As discussed in Chapter 1, tackling the dual challenge of seismic vulnerability and energy inefficiency is essential not only for reducing risk and environmental impact, but also for promoting well-being, economic growth, and achieving EU climate targets. Building on this, Chapter 2 presented a national-scale prioritisation framework, integrating seismic, energy, and socioeconomic indicators to identify areas with the highest need for combined retrofitting interventions, providing the foundation for large-scale and targeted renovation strategies. While this approach is suitable for identifying priority areas and assessing broad retrofitting scenarios, effectively evaluating alternative retrofit strategies and determining the optimal combination of interventions requires a shift to the single-building scale, where more detailed assessment methods are necessary to support decision-making.

As a result, significant attention has been recently paid to the development and evaluation of combined seismic and energy retrofitting schemes, with a view to minimise economic losses and environmental impacts and promote building renovation (Menna et al. 2021; Caruso et al. 2021; Clemett et al. 2023). Among the recent research studies that have addressed the topic, some assessed the benefits of eliminating seismic and energy performance deficiencies of existing buildings through a single intervention (Takeuchi et al. 2006, 2009; Calvi et al. 2016; Manfredi and Masi 2018; Bournas 2018; Pohoryles et al. 2020; Marini et al. 2022) while others using combined interventions (Clemett et al. 2023; Caruso et al. 2023b). With respect to the combined interventions, there is a broad range of structural and energy retrofitting options available to integrate, making it crucial to use optimisation methodologies that can identify the most effective combination of retrofit solutions. Some of those methods, such as seismic resilience-based assessments (Cimellaro 2013), index-based methods (Requena-García-Cruz et al. 2020), cost-benefit analyses (Sousa and Monteiro 2018a), green and resilient indicator (GRI) (Calvi et al. 2016), or multi-criteria decision-making (MCDM) approaches, often consider a range of economic, social and technical decision variables (DVs) that are typically of interest to decision-makers when evaluating and selecting an option from a set of alternatives. Regarding MCDM, in specific, many studies have shown the advantages of this methodology on the optimization of structural retrofit (Caterino et al. 2008;

Asadi et al. 2019; Requena-Garcia-Cruz et al. 2022), energy retrofit (Daniel and Ghiaus 2023) or the combination of both (Caruso et al. 2021; Clemett et al. 2023). The MCDM approach for selecting the optimal coupled retrofit intervention can become extremely helpful to decision-makers and practitioners because it allows the consideration of multiple criteria when making decisions about retrofitting options. By considering different decision variables, chosen to capture the essential aspects of the decision problem (e.g., economic costs, social benefits and technical feasibility) decision-makers can make more informed and balanced decisions.

From a broader perspective, recent research has shown that optimal renovation priorities differ significantly across regions depending on seismic hazard, energy demand, and socio-economic vulnerability. For instance, central-southern Italy is generally more critical for seismic retrofitting, whereas northern Italy shows higher needs for energy upgrading (Mucedero and Monteiro 2024a). These findings reinforce the need for a holistic approach when addressing combined retrofitting.

However, most of the aforementioned studies make use of refined methodologies, currently used in the research field, to estimate the decision variables related to the seismic performance of the structure, rendering them very computationally expensive and time-consuming, thus, unfeasible to be implemented by practitioners or general decision-makers. In turn, simplified approaches that are already available, despite their inevitable approximative nature, may provide a more accessible and efficient way to evaluate the performance of existing buildings, favouring the adoption of the MCDM methods by practitioners, who usually need to make decisions in a short period of time with limited resources. Building on these considerations, this Chapter focuses on the evaluating the influence of different climate and hazard levels on the preferential ranking of seismic and energy retrofit alternatives while simultaneously comparing the performance of detailed and simplified procedures. To do so, an RC school building is selected as a case study, given the high seismic vulnerability of school buildings in Italy demonstrated by past earthquakes (Saler et al. 2023). Twelve possible combinations of energy and seismic interventions are defined, and the buildings is assumed to be located in nine different sites characterised by varying levels of seismic hazard and climate conditions.

While past seismic events have highlighted the significant social and economic impacts in building downtime, previous proposed MCDM frameworks have neglected recovery time as a DV or design target. To fill this gap, this study investigates the impact of including downtime as a potential DV on the final ranking of different

retrofitting alternatives. Recent frameworks, including FEMA P-58 (FEMA 2018b), the REDi guidelines (Almufti and Willford 2013), and the approaches proposed by (Costa et al. 2021) and (Molina et al. 2022) provide tools to quantify building- and community-level recovery trajectories. Building on these advances, this study integrates an analytical framework to assess post-earthquake downtime into the MCDM framework to assess the preferential ranking among different retrofit measures.

5.2 METHODOLOGY

5.2.1 Decision-making framework

Given the demonstrated need to simultaneously evaluate seismic and energy retrofit alternatives for existing buildings, while accounting for varying seismic hazard and climate conditions, this section presents the framework adopted for selecting the optimal integrated retrofitting solution. The overall methodology corresponds to a structured process for assessing, designing, and selecting retrofit solutions for buildings exhibiting both seismic and energy deficiencies. This methodology comprises five main steps, which are illustrated in Figure 5.1and briefly summarised as follows:

1. Assessment, which is conducted initially on the as-built configuration of the structure to identify its seismic and energy deficiencies. The evaluation is based on a set of predefined parameters and conducted using a suite of available assessment tools.
2. Design, which involves the selection and design of the possible alternative retrofit solutions tailored to the specific structural and energy deficiencies identified in Step 1.
3. Performance, in which the seismic and energy performance of each retrofitted alternative is evaluated. The same assessment tools used in Step 1 are applied to quantify the performance and risk parameters of the building for each retrofit combination.
4. Decision, which includes the identification and compilation of all relevant decision variables (DVs). These include seismic and energy performance (outcomes of Step 3) as well as additional variables reflecting social aspects (e.g., architectural impact, duration of the retrofitting works) and technical considerations (e.g., need for specialized labour, required interventions at the foundations).

5. Selection, in which the optimal combined retrofit alternative is selected, through a multi-criteria decision-making (MCDM) process or other suitable approaches (e.g., seismic resilience-based assessment, index-based methods, cost benefit analysis, among others).

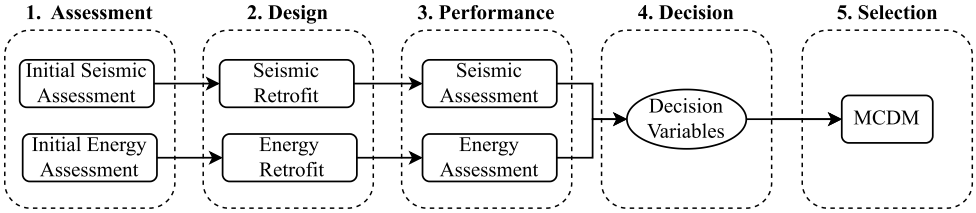

Figure 5.1 Overview of the framework

As regard Step 5, the MCDM framework, as employed by Clemett et al. (2023) and in subsequent studies (Caruso et al. 2023a; Couto et al. 2023; Mucedero et al. 2023), is adopted herein to identify the optimal combination of seismic and energy retrofitting solutions for a building when several combination options are feasible.

Specifically, the method employs the Technique for Order of Preference by Similarity to Ideal Solution (TOPSIS) (Hwang and Yoon 1981), which allows the identification of the optimal alternative based on its proximity to a positive ideal solution and its distance from a negative ideal solution. The TOPSIS method involves several key steps. First, the decision-maker identified a set of relevant DVs to evaluate the performance of each retrofit alternative. Each DV is then assigned a weight reflecting its relative importance (higher weights indicate greater significance compared to other criteria). Next, a decision matrix is created listing the values of each DV for every retrofit alternative. Since these DVs have different units, the matrix is normalised. A weighted normalised decision matrix is then calculated by multiplying each column of the normalised decision matrix by the corresponding weight. Subsequently. the positive and negative ideal solutions are defined by selecting, for each criterion, the best and worst performance values among all alternatives. In this study, the best value corresponding to the minimum value of each DV. Finally, the relative closeness (Ci*) of each alternative to the ideal solution is computed by calculating the Euclidean distance in n-dimensional space. Alternatives with values close to 1 are considered more preferable, while those closer to 0 are less desirable.

The DVs chosen to assess the performance of the building are provided in Table 5.1, along with the corresponding weight factors which are used to quantify the importance of each criterion in the decision-making process, playing a crucial role in

determining the relative importance or priority of different criteria or decision variables within the MCDM framework. As a result, weight factors exert a substantial influence on the ranking of the alternatives (Carofilis et al. 2022a). The weight factors selected in this study are based on the work of Clemett et al. (2023).

Table 5.1 Decision variables and corresponding weights

Group	Decision Variables	Weight
Economic	C_1 Installation cost	0.15
	C_2 Expected annual costs (EAC)	0.19
Environmental	C_3 Expected life-cycle environmental impacts (LCEI)	0.18
Social	C_4 Annual probability of failure (APF)	0.14
	C_5 Duration of works	0.13
	C_6 Architectural impact	0.06
Technical	C_7 Need for specialized labour/design knowledge	0.05
	C_8 Required intervention at the foundations	0.10

The installation cost (C_1) corresponds to the combined cost of the seismic and energy retrofit schemes, considering efficiencies that can be gained simultaneously by implementing both retrofitting schemes. The expected annual cost (EAC) (C_2) includes the maintenance cost (MC) of the structural and energy retrofit interventions, the annual energy cost (AEC), and the expected annual loss (EAL) from seismic damage. The expected annual cost (EAC) is calculated according to Equation 5.1 (Caruso et al. 2020), where the EAL and AEC are multiplied by the nominal design service life of the building (SL) and added to the total maintenance costs. This value is then normalized to SL and the floor area (A).

$$EAC = \frac{MC + (EAL + AEC) \times SL}{A \times SL} \tag{5.1}$$

The Life-cycle environmental impacts (LCEI) (C_3) were chosen as the representative environmental impact (EI) DV because it is a comprehensive parameter that encompasses all the sources of environmental impact over the life of the structure (Caruso et al. 2020; Passoni et al. 2021). The expected LCEI is calculated according to Equation 5.2 (Caruso et al. 2020) where IEI is the installation EI of the retrofit alternative, $EAEI_{post\text{-}retrofit}$ is the EAEI of the retrofitted structure, SL is the expected

service life of the structure post-retrofit, MEI is the total maintenance EI of the alternative over the expected service life, and A is the total floor area of the building.

$$LCEI = \frac{IEI + EAEI_{post-retrofit} \times SL + MEI}{A \times SL} \quad (5.2)$$

The annual probability of collapse (C_4) was included in the assessment as a measure of structural safety and the ability of the structure to prevent loss of life during an earthquake event. Duration of works (C_5) corresponds to the estimated duration of the structural intervention works. Architectural impact (C_6) and the need for specialised labour/design knowledge (C_7) are qualitative variables, determined using the AHP, and engineering judgment. The required interventions at the foundations (C_8) are estimated through the maximum ratio of the vertical support reactions between the as-built case-study building and each of the retrofit alternatives and are used to represent the amount of work eventually required to improve the foundations of the existing structure to cope with the loads transferred from the retrofitting structure. In this specific study, DVs C_1, C_2, and C_3 are considered more relevant to the choice of the optimal retrofit solution, demonstrated by their higher weight, while DVs C_6 and C_7 are considered the less relevant.

Once the values for each DV are obtained (Step 3 in Figure 5.1), a decision matrix (DM) can be assembled, containing the associated values for each retrofit intervention. The values of the DM are then normalized, and the ideal and least ideal solutions for each DV are determined, allowing a comparison with each of the proposed retrofit alternatives. To do so, the n-space Euclidean distance between the DM values for a specific retrofit alternative and the ideal and least ideal solutions is used. Finally, the relative closeness of each alternative to the least ideal solution is calculated and, consequently, the alternative with the highest relative closeness (i.e., the furthest alternative from the least ideal) is chosen as the preferred one. More details on the MCDM framework used herein can be found in Clemett et al. (2023).

5.2.2 Seismic performance assessment methods

As previously mentioned, one of the goals of this study is to compare the use of detailed and simplified procedures to estimate the parameters related to the collapse and loss assessment, namely the EAL and EAEI, which are part of the DVs C_2 and C_3, and the annual probability of failure (APF) (C_4). In this section, a brief description of both procedures is provided.

5.2.2.1 Detailed approach

The detailed approach follows a comprehensive performance-based seismic assessment and loss analysis through the PEER-PBEE methodology (Moehle and Deierlein 2004). The procedure initiates with the characterisation of the seismic hazard at the selected site, followed by a selection of suitable hazard-consistent ground motion sets. Then, nonlinear time history analysis is conducted on the structure under analysis, using the previous set of selected ground motions, through multiple-stripe analysis (MSA), which allows the quantification of the structural response. Through the MSA results, collapse fragility parameters are derived. Expected damage and losses are quantified considering structural and non-structural components; thus, it is necessary to develop an inventory of damageable components in the building, together with the definition of their potential damage states, expected repair cost, and environmental impact consequences. Finally, the detailed seismic loss assessment is performed through PACT (FEMA 2018c, p. 3). The ultimate outcomes needed for the MCDM framework are the EAL, the EAEI, and the APF.

Sismabonus is a relatively recent procedure implemented in Italy to evaluate the seismic risk of buildings and use it to classify them (Cosenza et al. 2018). This guideline provides a simple method for practitioners to assess the building's initial seismic condition and estimate its expected yearly seismic losses. This estimation can also help in evaluating the effectiveness of different retrofitting strategies in improving the building's seismic performance, hence guiding the choice of the retrofitting strategy. Notably, the Sismabonus approach requires only nonlinear static analysis, making it a more practical and quicker method to evaluate seismic annual losses when compared to approaches like the PEER-PBEE (Moehle and Deierlein 2004). Furthermore, when compared to other available simplified procedures for estimating the EAL of a building, Sismabonus holds additional advantages as it is already in use within the Italian engineering practice, even if recent findings show its loss estimates to be more conservative when compared to the ones obtained with more refined methodologies (O'Reilly et al. 2018; Peres et al. 2023). This method requires the computation of two performance indices: the Building Safety Index (SI-LS) and Expected Economic Annual Losses (EAL). The SI-LS is calculated by determining the capacity peak ground acceleration (PGA_C) and demand peak ground acceleration (PGA_D) associated with the Life Safety limit state (LSLS). Concurrently, the EAL is estimated by considering the building's performance for various return periods (T_r) and repair costs expressed as a fraction of the Reconstruction Cost

(%RC). The resulting loss curve, which defines the seismic risk, is represented by a point ($1/T_r$, %RC) for each limit state, whereas the area underneath is the EAL. The overall risk class of the building is defined as the worst between SI-LS and EAL classes. This method integrates structural and economic considerations, providing a comprehensive framework for seismic risk assessment. More details on the procedure can be found in Cosenza et al. (2018)

5.2.2.2 Simplified approach

The simplified counterpart makes use of two readily available tools to estimate the AFP and EAL, namely the cloud-based capacity spectrum method (CB-CSM) and Sismabonus, respectively.

Cloud-based Capacity Spectrum Method (CB-CSM)

The CB-CSM makes use of two known methods, the well-known capacity spectrum method (CSM) (Applied Technology Council (ATC) 1996) and the cloud-based (CB) procedure, proposed by Jalayer et al. (2017a) to obtain the collapse fragility parameters of a given structure. The method starts with the identification of the performance point (PP) of the structure by employing the CSM, which consists of an iterative graphical procedure aimed at determining the intersection (PP) of the structure's capacity curve, in an acceleration-displacement plane, with overdamped real demand spectra. Multiple performance points can therefore be obtained, which is not feasible and representative of the behaviour of the structure, and several recommendations on how to overcome this problem and select the most suitable performance point are given by Nettis et al. (2021). It is worth mentioning that the methodology is quite in line with that employed by engineers for the identification of the PPs, at different limit states, of existing structures. In the present study, in the case of multiple solutions, the adopted PP was the one for which the absolute difference between the geometric average of spectral displacements over an appropriate range of periods (AvgSdk) and each obtained PP (|AvgSdk − ΔPP|) is minimum. This procedure leads to a cloud of Engineering Demand Parameter (EDP) vs Intensity Measure (IM) points for each analysed SDoF system, where the EDP is the target displacement corresponding to the PP calculated via the CSM and the adopted IM is the geometric mean of the average spectral accelerations (AvgSa) computed in the interval $[0.2T_{el} - 1.5T_{el}]$, with being T_{el} the elastic period, as recommended by Nettis et al. (2021). Based on the criteria selected to define the collapse limit state, the cloud data is divided into non-collapse (NoC) and collapse (C) points. Then, the collapse fragility parameters are calculated by applying the total

probability theorem (Equation 5.3), aggregating the probability of reaching or exceeding the DS for the NoC cases, $\mathrm{P}(\mathrm{EDP} > 1|\mathrm{IM}, \mathrm{NoC})$, and the probability that the collapse occurs, P(C|IM). The fragility model related to the NoC cases is expressed by the normal cumulative distribution function ϕ(n) based on the probabilistic seismic demand model for NoC cases, which is in turn calculated by fitting a power-law model, EDP = aIMb, for the non-collapse cases in the log IM− log EDP plane. The parameters a and b are estimated through regression analysis resorting to the least squares method. P(C|IM) is computed by fitting a logistic regression model suitable to binary (collapse-no collapse) variables.

$$\begin{aligned} P(EDP > 1|IM) \\ &= P(EDP > 1|IM, NoC) \cdot \big(1 - P(C|IM)\big) \\ &+ P(EDP > 1|IM, C) \cdot P(C|IM) \end{aligned} \tag{5.3}$$

SPO2FRAG

SPO2FRAG (Baltzopoulos et al. 2017) is a simplified method for assessing the seismic performance of reinforced concrete buildings. It was developed to overcome some of the limitations and drawbacks of more complex and time-consuming nonlinear dynamic analysis. This method considers the building as a 2D frame structure and develops structure-specific seismic fragility curves, using the results of static pushover analysis, by simulating Incremental dynamic analysis (IDA) results. This procedure requires, as input data, the building geometry, the material properties of the structural elements, the seismic hazard of the site, the modal parameters of the structure and the pushover curve. With the latter, an equivalent single-degree-of-freedom (SDoF) representation of the nonlinear structure is obtained and, by employing the SPO2IDA algorithm (Vamvatsikos and Cornell 2005), the probabilistic seismic response of the structure is obtained, enabling the user to generate fragility curves for multiple limit states. Recent studies (Baltzopoulos et al. 2017; Ugalde et al. 2020; Ruggieri et al. 2021) have provided reasonable estimates of the seismic vulnerability of RC structures using this methodology. Moreover, it is available as an interactive open-source MATLAB-coded PBEE tool, making it easier and faster to implement, when compared to more refined methodologies.

Expected Annual Loss - Seismic Risk Classification (Sismabonus)

The Italian government recently approved a law decree (Decreto Ministeriale 2020) foreseeing tax deductions for seismic strengthening interventions on existing buildings. Such a framework is regulated by a guideline describing a procedure, also known as Sismabonus, which is used to estimate the seismic risk of existing buildings

on the Italian territory (Cosenza et al. 2018). The proposed classification system offers practitioners a straightforward approach to assess the initial seismic condition of a building and estimate its expected seismic annual losses, with which the effectiveness of various retrofitting strategies in enhancing its seismic performance can be evaluated. It only requires nonlinear static analysis to be conducted, thus, it is a more practical and faster approach to assess seismic annual losses, in comparison to other methods, such as the PEER-PBEE methodology (Moehle and Deierlein 2004) which requires more detailed information about the building components inventory and the seismic hazard at the site. Furthermore, when compared to other available simplified procedures to estimate the EAL of a certain building, Sismabonus has the advantage of being already currently used in engineering practice in Italy. The choice of using Sismabonus is therefore motivated by the goal of the study and the desired level of practicality that is intended to be achieved, despite the fact that the loss estimation obtained with it have shown to be conservative with respect to the ones obtained with more refined methodologies (O'Reilly et al. 2018; Peres et al. 2023).

A brief overview of the procedure is presented next, whereas more details are provided in Cosenza et al. (2018). The seismic risk class of the building is assigned based on the minimum of two performance indices, namely the building safety index (SI-LS), associated to a life-safety limit state verification, and the EAL. Table 5.2 summarises the range of values and corresponding classes (G to A^+) for both indices. The procedure starts with the computation of the pushover curves in the two horizontal directions and the assessment of two damage limit states: Damage Limitation (DLLS) and Life Safety (LSLS). The attainment of each limit state is then evaluated according to the current Italian building code (MIT 2018). To estimate the first index (SI-LS), it is necessary to calculate the capacity peak ground acceleration (PGA_C), which is defined as that required to cause the building to attain the LSLS, and demand peak ground acceleration (PGA_D), which corresponds to the design PGA at the building location, according to the hazard map, affected by the site amplification factor (MIT 2018). The second index (EAL) is estimated by computing the performance of the building for different return periods (T_r) (expressed in terms of the mean annual frequency of exceedance, $\lambda = 1/Tr$) and the associated repair costs (%RC). The loss curve is hence defined by the points (λ, %RC) representative of each limit state, while the area below the curve represents the EAL (expressed in percentage of the building replacement cost). Once both indices are assessed, the minimum of the SI-LS and EAL classes determines the overall seismic risk class of

the building. The %RC assumed in Sismabonus were calibrated with actual repair costs observed during the L'Aquila reconstruction process (Di Ludovico et al. 2017) thus corresponding to the specific features of typical Italian buildings. Given the location of the case-study building, Sismabonus, favoured for its simplicity over more complex methodologies, is suggested herein as a simplified loss assessment tool to replace the component-based loss assessment methodology. For a simplified loss analysis in other countries, the damage-to-loss models in Sismabonus can be updated with alternative ones, based on post-earthquake observation damage data from those countries or, alternatively, Sismabonus can be replaced with other available simplified loss assessment tools such as storey loss functions (Ramirez and Miranda 2009; Mucedero et al. 2024a).

Table 5.2 Seismic risk classification according to the Sismabonus (Decreto Ministeriale 2020).

Life-safety index (LS-LS)	Expected annual losses (EAL)	Seismic Risk Class
100% < SI-LS	EAL ≤ 0.5%	A^+
80% ≤ SI-LS < 100%	0.5% < EAL ≤ 1.0%	A
60% ≤ SI-LS < 80%	1.0% < EAL ≤ 1.5%	B
45% ≤ SI-LS < 60%	1.5% < EAL ≤ 2.5%	C
30% ≤ SI-LS < 45%	2.5% < EAL ≤ 3.5%	D
15% ≤ SI-LS < 30%	3.5% < EAL ≤ 4.5%	E
SI-LS ≤ 15%	4.5% < EAL ≤ 7.5%	F
-	7.5% ≤ EAL	G

5.3 APPLICATION TO A CASE-STUDY SCHOOL BUILDING

The selected case-study school building is a reinforced concrete (RC) moment resisting frame (MRF) with unreinforced masonry (URM) infills, located in Isola del Gran Sasso d'Italia (Abruzzo, Italy) and built between the 1960s and 1970s. The building has two aboveground storeys with roughly 630 m^2 each and inter-story heights of 3.75 and 4.25 m on the first and second floors. Additionally, there is a small partial basement at the east end. The structural system consists of two-way RC MRFs in the longitudinal and transverse directions, along with URM infills and partitions. More details on the school building, including architectural plans and elevations, together with the material properties of structural members, can be found

in Prota et al., (2020). The masonry infills were assumed to have the same geometry and material properties as the medium-strong masonry infill typology in the macro-level classification as proposed in Mucedero et al. (2020). The numerical model of the building, comprising flexural elements (for beams and columns), beam–column joints (BCJs), a staircase, and masonry infills, was developed in OpenSees (McKenna et al. 2010b), and a three-dimensional representation of the model is presented in Figure 5.2. The beam and column elements were modelled using the force-based beam–column element with a Modified Radau plastic hinge integration scheme (Scott and Fenves 2006). Although the shear behaviour of RC elements was considered elastic, a post-processing analysis was carried out to determine any possible shear failure, similar to the approach adopted by Mucedero et al. (2022a). To capture the nonlinear behaviour of beam–column joints, a scissor model was implemented, characterised by a zero-length spring coupled with a rotational hinge defined according to the backbone curve proposed by O'Reilly (2016). Further details on the numerical modelling of the structure can be found in Carofilis et al. (2021) and Clemett et al. (2023).

To understand the influence of seismic hazard level and climate conditions on the combined retrofitting, the building is assumed to be located in nine different sites in Italy. There are three sets of different hazard levels, namely high (H), medium (M), and low (L), paired with three sites characterised by different climatic conditions, namely cold (C), moderate (M), and warm (W). Choosing real locations in Italy was intended to ensure the results of this study closely reflect actual conditions. However, this decision may introduce uncertainty when assessing and comparing the results due to variations in seismic hazard curves and the corresponding selection of records. The climate and seismic maps of Italy with the indication of the selected locations is illustrated in Figure 5.3. The specific features of each site are summarized in Table 5.3 with the indication of the peak ground acceleration (PGA) for the life safety limit state (SLV), defined according to the Italian code (NTC-2018) (MIT 2018) and the heating degree days (HDD) for each location. The latter is a measure used to estimate the heating energy demand, calculated by summing the number of degrees that the outdoor temperature falls below a certain base temperature on each day over a specified period. It is used to estimate heating energy requirements such as consumption patterns, performance, and costs. Figure 5.4 provides the acceleration response spectrum and the hazard curve for each selected site. Even though the PGA of each location within the same seismic hazard level group is very similar, as anticipated, the corresponding hazard curves show some differences.

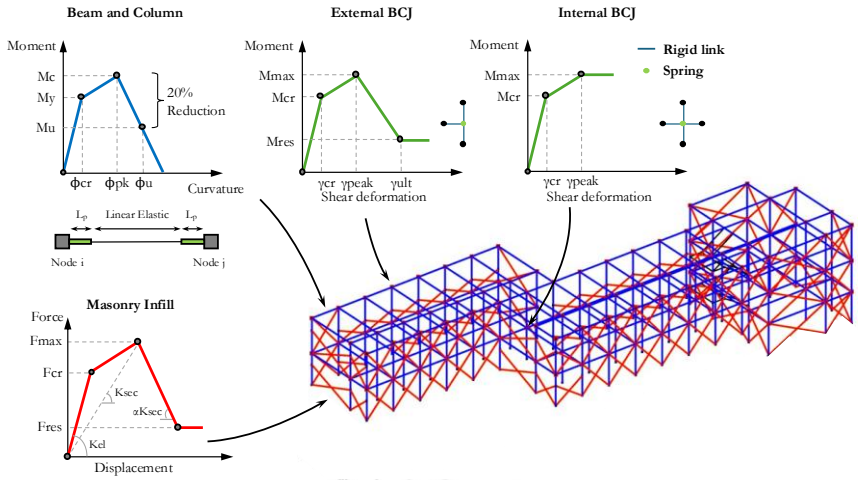

Figure 5.2 Numerical model of the case-study building, developed in OpenSees.

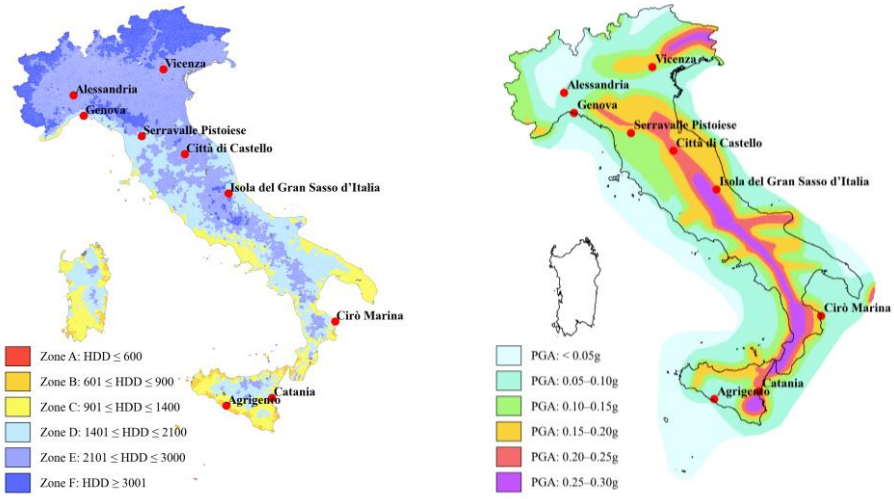

(a) **(b)**

Figure 5.3 Climate and seismic hazard levels maps of Italy, with the indication of the selected locations under study.

Table 5.3 Main features of selected case-study sites.

City	ID	Coordinates	Level of Seismicity	PGA (SLV) [g]	Climatic Zone	Heating Degree Days (HDD)
Città di Castello	H-C	43.4700° N 12.2314° E	High (H)	0.30	Cold (C)	2347
Isola del Gran Sasso d'Italia	H-M	42.5056° N 13.6592° E		0.29	Moderate (M)	2038
Catania	H-W	37.5013° N 15.0742° E		0.29	Warm (W)	833
Vicenza	M-C	45.5455° N 11.5354° E	Medium (M)	0.21	Cold (C)	2371
Serravalle Pistoiese	M-M	43.9059° N 10.8330° E		0.20	Moderate (M)	2010
Cirò Marina	M-W	39.368° N 17.128° E		0.21	Warm (W)	845
Alessandria	L-C	44.9073° N 8.6117° E	Low (L)	0.08	Cold (C)	2559
Genova	L-M	44.4056° N 8.9463° E		0.10	Moderate (M)	1435
Agrigento	L-W	37.3089° N 13.5858° E		0.08	Warm (W)	729

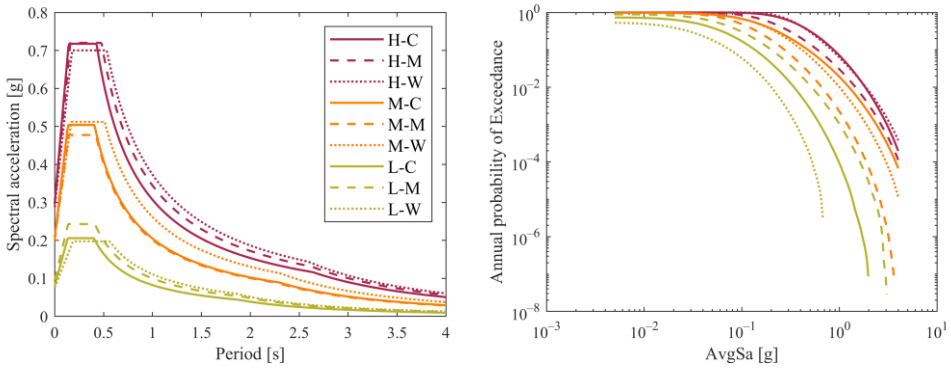

(a) (b)

Figure 5.4 (a) Acceleration response spectra and (b) hazard curves for the nine analysed sites.

5.3.1 Preliminary seismic and energy assessment

A preliminary seismic assessment of the structure was conducted through a nonlinear static procedure, using an inverted triangular load pattern and a control node located at the centre of mass on the top floor, as established in the Italian seismic code (MIT 2018). The target displacements of the structure for the collapse limit state (SLC) using the N2 method (Fajfar 2000) were estimated and compared with the performance point displacements at which the structure attains its capacity for the SLC limit state, considered to be reached as soon as one of the following performance criteria is met:

- The shear force demand exceeds the shear capacity of one or more of the beam or column elements;
- The chord rotation of one or more of the plastic hinges in the beam, column, or wall elements exceeds the collapse limit state deformation limits;
- The shear deformation in one or more of the beam–column joints (BCJs) exceeds 0.02 rad.

The first two performance criteria are the ones prescribed by the Italian seismic code (MIT 2018) for the seismic assessment of columns and beams. The last criterion, regarding the assessment of the BCJs, was adopted following experimental evidence (O'Reilly and Sullivan 2019), given that the one foreseen by the Italian code is very conservative. The pushover curves of the as-built structures, together with the performance points (SLC_C) and target displacements (SLC_D) of the structure for each site, are presented in Figure 5.5. These curves are expressed in the base shear coefficient, given by the ratio between the total base shear and the total mass of the structure. Both directions present pushover curves with similar initial stiffness but different degradation due to the larger number of openings on the masonry infills in the longitudinal direction of the building. For both directions, the main structural weaknesses at the collapse limit state were identified as the shear failure of columns that were not designed to withstand seismic actions. Given the different demands of each set of sites, different target displacements are obtained; for the LH sites, the safety performance of the structure in its as-built condition is achieved in the X direction and almost achieved in the Y direction.

According to the Italian guidelines for the seismic risk classification of constructions (Decreto Ministeriale 2020), the safety index of the structure (SI-LS), defined as the ratio between the capacity peak ground acceleration (PGA_C) and the demand peak

ground acceleration (PGA_D), was calculated and is summarised in Table 5.4. PGA_C was assumed to be the one that caused the collapse of the building, and it is calculated by scaling the code-based response spectrum to intersect the pushover curve on its capacity point for the life safety limit state (SLV). The capacity point is considered to be the one corresponding to the first element collapse within the building in terms of: i) the shear force demand exceeding the shear capacity of one or more of the beam or column elements, ii) the chord rotation of one or more of the plastic hinges in the beam, column, or wall elements exceeds the life safety limit state deformation limits. PGA_D is defined as the PGA of the code-based response spectrum for the location of interest.

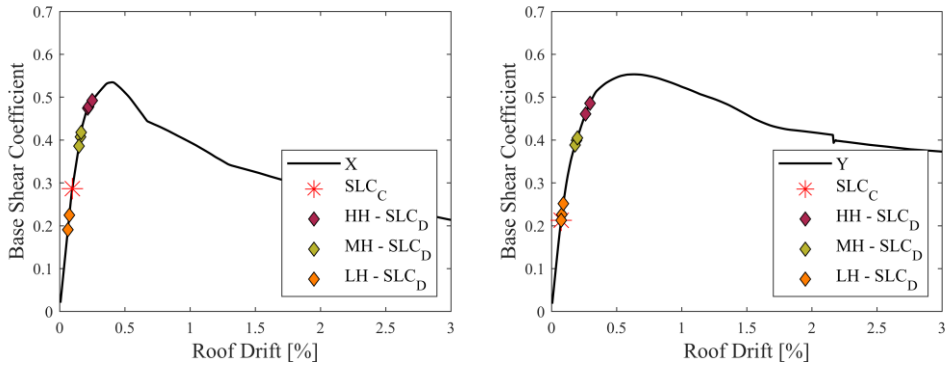

Figure 5.5 Preliminary seismic assessment of the as-built structure pushover curves in the X (left) and Y (right) direction, with the indication of the N2 performance points for the SLC limit state and the target displacement as a function of the hazard level.

The obtained SI-LS values reveal, as anticipated, variations in demand across the different sites, with direction Y emerging as the most critical. Considering the satisfactory performance of the as-built structure for the low-hazard sites, retrofitting was deemed unnecessary; hence, different retrofitting schemes were solely considered for sites with moderate and high hazard levels, as addressed in the next sections.

Table 5.4 Seismic safety index (SI-LS), in percentages, of the as-built structure as a function of the level of hazard and climate conditions (critical direction in bold).

Direction	Low Hazard			Medium Hazard			High Hazard		
	L-C	L-M	L-W	M-C	M-M	M-W	H-C	H-M	H-W
X	135	115	140	55	58	54	39	40	39
Y	**95**	**81**	**98**	**38**	**41**	**38**	**27**	**28**	**27**

5.3.2 Retrofit Interventions

Given the structural deficiencies identified in the preliminary seismic assessment of the building, four different seismic retrofit measures (SRMs) were considered:

- S_1: local strengthening with carbon FRP (CFRP).
- S_2: global strengthening with concentric steel braces.
- S_3: CFRP strengthening combined with concentric steel braces.
- S_4: CFRP strengthening combined with viscous dampers.

Additionally, for all SRMs, a seismic gap between the URM infills and the RC frame was introduced, reducing the column-infill interaction and, thus, the shear forces acting on the columns. The design of the SRMs, conducted following the Italian building code (NTC) (MIT 2018), was carried out to address the weaknesses and improve the performance of the as-built structure as much as possible, with the acknowledgment that the achieved performance was not always that required for new code-conforming buildings due to practical and cost considerations (Calvi 2013).

The seismic response of retrofitted structures is significantly influenced by the location and number of retrofit elements. In the case of S_1, an iterative procedure was implemented wherein CFRP was initially applied to non-compliant elements, followed by successive assessments until all structural elements met safety standards. In S_2, the strategic placement of braces was prioritized to minimise storey drifts. S_3 modelling incorporated the methodologies of both S_1 and S_2. Additionally, for S_4, the procedure from S_1 was adopted while integrating viscous dampers at various locations within the school building. Further details on the design specifications for each retrofit alternative are available in Carofilis et al. (2022b).

Considering the varying seismic hazard levels across each site, the extent of retrofitting interventions implemented for the case-study building was adjusted accordingly. Due to the poor performance of the building under high seismic hazard conditions, each intervention was designed to provide the optimal contribution to the structure, meaning that it was not strictly designed for the same seismic demand. Consequently, it did not strictly achieve the same threshold in terms of capacity between the several alternatives. Table 5.5 provides a summary of the details and quantities of the retrofit components for each retrofit alternative.

Table 5.5 Retrofit components and corresponding amount per alternative for the considered hazard levels.

Retrofit Alternative		Units	Medium Hazard	High Hazard
S_1	Column wrap	m^2	245.1	352.6
	Column bar	m	2972	2972
	Beam wrap	m^2	177.8	256.2
	Joint wrap	m^2	138.2	186
S_2	Braced bays	N_r	9	10
S_3	Column wrap	m^2	5.1	10.2
	Column bar	m	272.0	272.0
	Beam wrap	m^2	11.7	31.22
	Joint wrap	m^2	45.5	45.5
	Braced bays	N_r	10	10
S_4	Column wrap	m^2	-	10.2
	Column bar	m	-	456
	Beam wrap	m^2	-	33.7
	Joint wrap	m^2	53.4	53.4
	Viscous dampers	N_r	36	36

5.3.3 Energy Retrofit Interventions

Subsequently, with a view to improving energy performance, three different energy retrofit measures (ERMs) were considered:

- E_1: roof insulation and installation of efficient LEDs and thermostatic valves on radiators;
- E_2: intervention E_1 coupled with external wall insulation with expanded polystyrene (EPS) panels;
- E_3: intervention E_2 coupled with installation of efficient windows, floor insulation, condensing boiler, lighting control system, and photovoltaic panels.

Each energy retrofitting intervention aims to simultaneously reduce heat losses to the external environment and enhance the energy efficiency of systems within the building. The level of intervention increases from E_1 to E_3, according to the Italian

Ministerial Decree (Economico 2015), which also corresponds to a higher degree of invasiveness.

Finally, the four seismic interventions were coupled with each energy intervention, leading to twelve possible combined retrofit alternatives. Each coupled intervention is designated by S_iE_i, where S_i and E_i correspond, respectively, to the considered seismic and energy retrofit schemes.

5.3.4 Post-Intervention Seismic Assessment

The post-intervention assessment followed the same strategy outlined for the as-built structure (S_0). Nonlinear static analyses were performed for each retrofitted model, and the displacement demand and capacity (according to NTC (MIT 2018)) were computed using the N2 method (Fajfar 2000). The results for the retrofitting scenarios are illustrated in Figure 5.6.

At first glance, it can be observed that the pushover curves for the same type of retrofit intervention between the different levels of hazard are very similar. This can be justified by the similarity of each retrofit intervention between the different sites, both in terms of their layout within the building structure and specific structural elements being retrofitted. When compared with the as-built scenario, all retrofitted models exhibit a decrease in the initial stiffness and lateral strength due to the seismic gap introduced between the infills and the surrounding frame. Moreover, all the retrofit interventions lead to an improvement in the structural performance of the building at the collapse limit state. Given the different design levels of the retrofitting interventions (dictated by the different seismic hazard levels), the displacement for which the structure, with the same type of intervention, reaches its capacity is distinct. Nevertheless, for most of the cases, the type of structural failure, usually a brittle failure on a column or beam as mentioned previously, that dictates the capacity performance is similar.

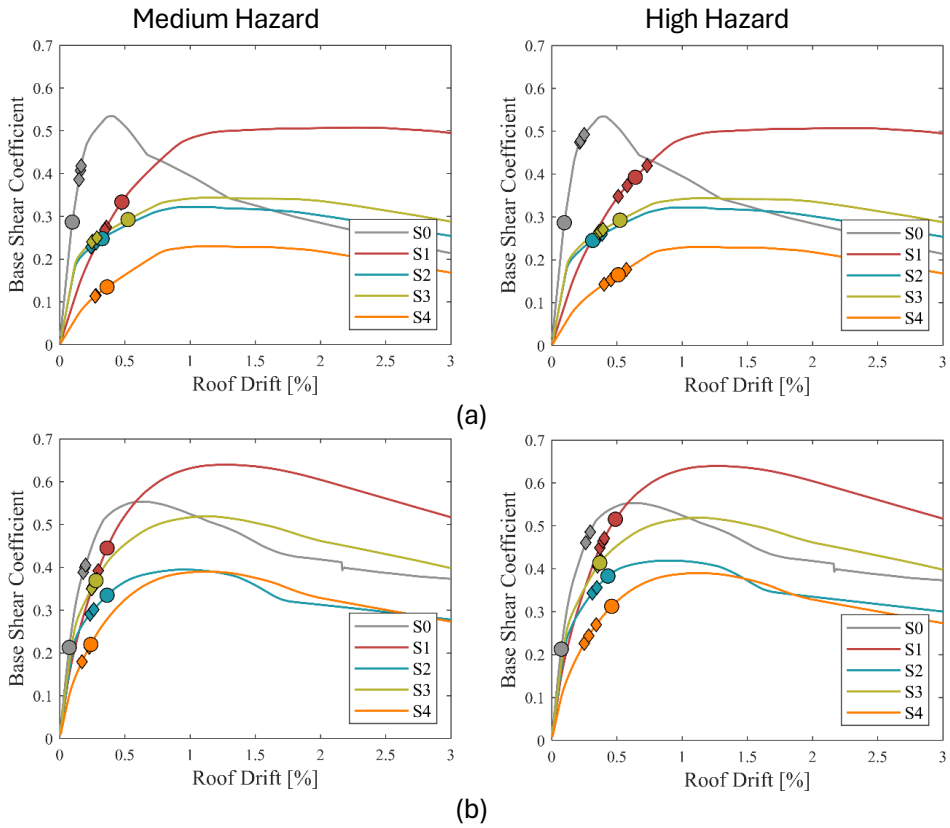

Figure 5.6 Post-seismic intervention assessment of the structural retrofit schemes. Pushover curves in the (a) X and (b) Y direction, with capacity (circles) and N2 performance points (diamonds) for the SLC limit state, as a function of the hazard level: medium (left) and high (right) hazard.

Table 5.6 summarizes the SI-LS values obtained for the retrofitted models in each hazard site. Considering the most critical direction, the effectiveness ranking of the retrofit measures is $S_4 > S_1 > S_3 > S_2$ and $S_1 > S_4 > S_3 > S_2$ for the medium- and high-hazard sites at the LSLS. Comparing the results of Table 5.4 with Table 5.6, an overall improvement is observed in the performance of the retrofitted structures with respect to the as-built structure.

Table 5.6 Seismic safety index (SI-LS) of each structural intervention, Si, for the different levels of hazard and climate conditions (critical direction in bold).

Alt.	Dir.	Medium Hazard			High Hazard		
		M-C	M-M	M-W	H-C	H-M	H-W
S_1	X	**120%**	**123%**	**95%**	**120%**	**108%**	**99%**
	Y	134%	134%	105%	120%	107%	109%
S_2	X	**92%**	**95%**	**73%**	**63%**	**55%**	**50%**
	Y	113%	115%	88%	85%	76%	70%
S_3	X	122%	125%	**96%**	**82%**	**73%**	**68%**
	Y	**111%**	**113%**	99%	87%	77%	76%
S_4	X	**125%**	**128%**	**97%**	**117%**	**105%**	**96%**
	Y	127%	130%	99%	155%	137%	129%

After conducting the initial seismic assessment of the structure in its retrofit conditions, the estimation of all the DVs outlined in Section 5.2.1 can be carried out following the suggestions provided in Clemett et al. (2023). The ones for which the use of simplified procedures is proposed (C_2, C_3, and C_4) are fully described in the subsequent subsections.

5.3.4.1 Annual Probability of Failure

The estimation of APF was carried out using the different approaches described in Section 5.2.2. For the detailed methodology, the first step consisted of characterising the seismic hazard at the site of interest (see Table 5.3) through a probabilistic seismic hazard analysis (PSHA) performed in OpenQuake (Pagani et al. 2014). Then, a selection of 20 pairs of suitable hazard-consistent ground motion records was carried out for each site. The IM adopted in this study, AvgSa, is defined as the geometric mean of the pseudo-spectral acceleration over a structure-specific range of periods, derived from the fundamental periods of the analysed structural models.

Table 5.7 summarizes the relevant dynamic elastic properties of the analysed models, including the fundamental period in both directions (with the first mode highlighted in bold), the participation mass of the first mode of vibration (M_1^*), the geometric mean period (T_{GM}), and the corresponding period range considered in this study ($0.2T_{GM}$–$1.5T_{GM}$). MSAs were then performed, and a set of selected EDPs, namely the absolute Peak Floor Acceleration (PFA), Peak Story Drift (PSD), and Peak Floor Velocity (PFV), were recorded for each stripe. These EDPs served as an input

for the subsequent performance-based loss assessment following the PEER-PBEE methodology. In addition, the MSA outcomes were used to derive the collapse fragility parameters.

Table 5.7 Model parameters of each retrofitted building.

Hazard Level	Model	Fundamental Period [s]		M_1^* [%]	T_{GM}	$0.2T_{GM}$–$1.5T_{GM}$
		Longitudinal	Transverse			
Medium hazard	S_0	0.235	**0.267**	38.0	0.25	0.05–0.38
	S_1	**0.561**	0.454	39.3	0.50	0.10–0.76
	S_2	**0.408**	0.379	47.1	0.39	0.08–0.59
	S_3	**0.405**	0.379	46.1	0.39	0.08–0.59
	S_4	**0.779**	0.565	41.5	0.66	0.13–1.00
High hazard	S_0	0.235	**0.267**	38.0	0.25	0.05–0.38
	S_1	**0.571**	0.454	40.4	0.44	0.09–0.67
	S_2	**0.407**	0.373	44.0	0.39	0.08–0.60
	S_3	**0.405**	0.365	43.9	0.38	0.08–0.60
	S_4	**0.785**	0.563	41.4	0.59	0.12–0.90

Following the simplified methodology, a set of 200 ground motions covering a wide range of magnitudes were selected from the NGA-West2 ground motion database (Ancheta et al. 2014) and converted into the ADRS format for application of the CSM (Applied Technology Council (ATC) 1996), as described in Section 5.2.2.2. For each model, the intersection between the capacity curve of the corresponding SDoF system and the response spectra of the selected ground motions results in a cloud of PPs. These PPs were then classified into non-collapse (NoC) and collapse (C) cases by comparing the resulting displacements with the collapse thresholds previously defined for the preliminary seismic assessment and MSA, ensuring consistency across methodologies. Lastly, the regression parameters required to estimate the conditional probability of exceedance were obtained using the modified cloud analysis procedure proposed by . A slight adaptation of the CB-CSM procedure was necessary to assess the structural performance of S4 to account for the supplemental damping introduced by the viscous dampers. A supplemental damping ratio of 25%, in addition to the initial 5% inherent damping, was considered both in the time history analyses and within the CSM, following the recommendations of Carofilis et al. (2021). Figure 5.7 presents the fitted regression models for both NoC

and C datasets for each retrofitted configuration considering only the high hazard location, together with the respective cloud points (black for NoC and red for C).

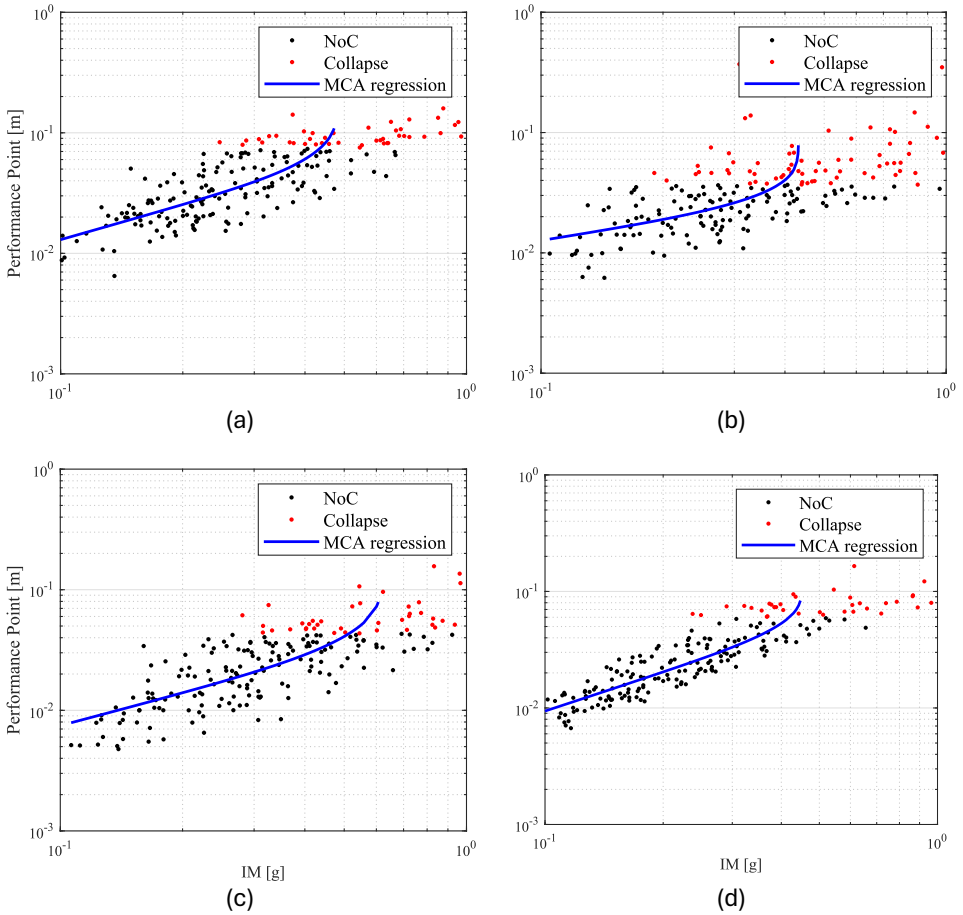

Figure 5.7 Cloud analysis data and regression prediction models for the high-hazard location and for each retrofit alternative: (a) S1, (b) S2, (c) S3, and (d) S4

The collapse fragility curves obtained from both methodologies, incorporating epistemic uncertainties following O'Reilly and Sullivan (2018) and Mucedero et al. (2022b, a), are presented in Figure 5.8 for both the medium- and high-hazard sites. Considering the medium hazard sites, the differences in the median collapse intensities obtained through the detailed approach are likely justified by the different hazard curves observed in Figure 5.4(b). In contrast, the median collapse intensities for the high-hazard sites are very similar. Comparing the simplified with the detailed approach, a closer approximation of the median intensity values is achieved for the

medium hazard, with a difference of about ±15% (excluding S_0 and S_4). This difference increases up to ±80% when considering the high-hazard results. For the S_4 alternative, the simplified approach results in extremely conservative results (an average difference of around 43% and 136% for the medium- and high-hazard sites).

Subsequently, the APF values were obtained, integrating the collapse fragility curve with the hazard curve of each site. Figure 5.9 plots the APF values as a function of the employed methodology (simplified (S) and detailed (D)) for both seismic hazard levels - medium (Figure 5.9 (a)) and high (Figure 5.9 (b)).

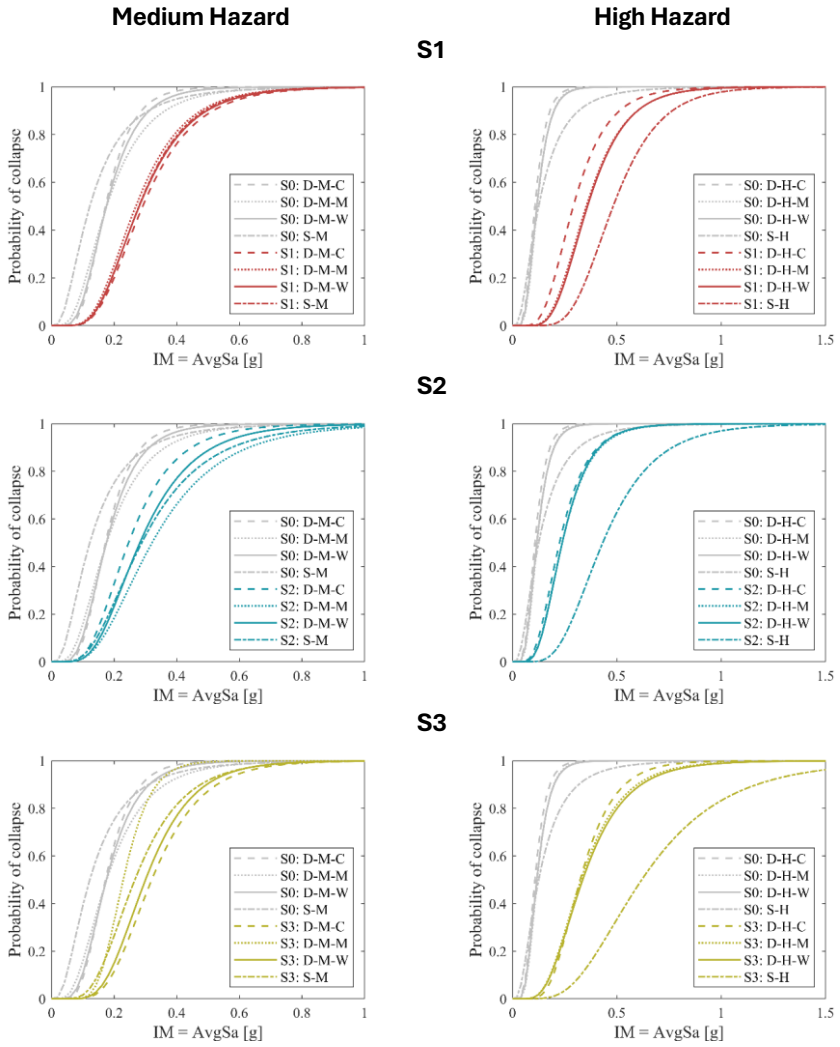

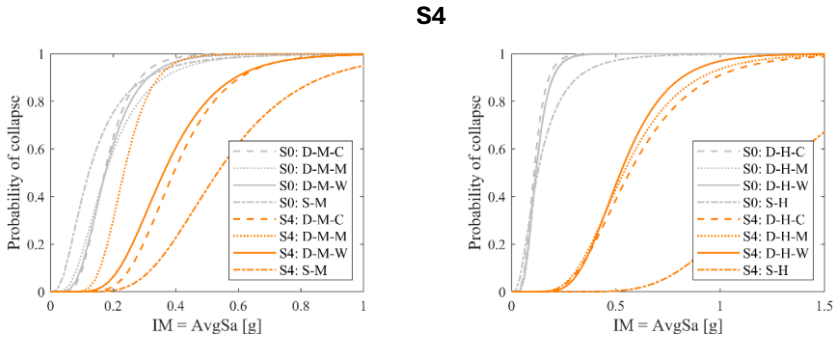

Figure 5.8 Collapse fragility curves for different hazard levels and retrofitted buildings.

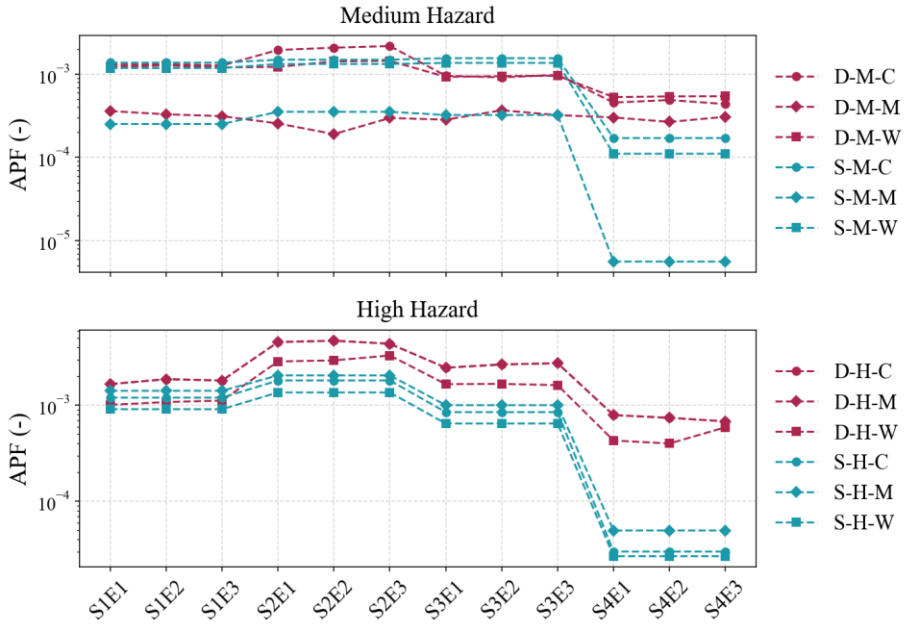

Figure 5.9 Annual probability of failure (APF) obtained employing the detailed and simplified methodologies for medium- and high-hazard sites.

In terms of retrofitting approaches, for medium hazard, solution S_4 has the better seismic performance, followed by S_1, S_2, and S_3, with identical performance. For the high hazard, solutions S_2 and S_4 have the worst and better seismic performance, whereas the performance of S_1 and S_3 oscillates between the second and third positions.

For the medium-hazard sites, overall, both approaches lead to very similar APF results, except for solution S_4, for which the simplified APF estimates result lower

than the detailed ones. On the other hand, for high hazard, regardless of the retrofitting option, the APF results can be considered in two groups, depending on the adopted approach. A general underestimation of the simplified APF values is observed with respect to the detailed ones. Among other possible reasons, it can be related to the fact that the adopted CSM procedure is the one from ATC-40 (Applied Technology Council (ATC) 1996), which has been shown to underestimate the displacement demand (Chopra and Goel 2000; Gencturk and Elnashai 2008), resulting in a lower number of collapses. Still, the differences are never high enough to change the corresponding ranking (when solely based on the APF values) of the different retrofit alternatives.

5.3.4.2 Expected Annual Losses (EAL)

On the detailed approach side, the PEER-PBEE methodology was employed to estimate the EAL and EAEI for each retrofitted model. By handling the EDPs obtained from the MSA and an inventory of damageable components in the building, including their potential damage states and associated repair cost and EI consequences, a detailed loss assessment was carried out in PACT. Table C.1 (see Appendix C.1) provides a summary of the building component inventory for the as-built and each retrofitted model, including details on each fragility model, such as its source, the corresponding EDP and units. The influence of the ERMs was incorporated at this stage by considering additional repair consequences for specific non-structural components, reflecting their significant effect on loss estimates (Calvi et al. 2016; Mauro et al. 2017; Menna et al. 2019). For the as-built configuration, a replacement cost of €2,652,242 and a replacement EI of 1,830,000 $kgCO_2e$ were adopted. To reflect the increased building value resulting from the various energy retrofit schemes, the replacement costs and EIs were adjusted proportionally to the material cost of the ERMs, following the Economic Input-Output Life Cycle Analysis (EIO LCA) approach, which estimates the environmental impact associated with each euro spent on a given economy sector (Simonen et al. 2018) (see Section 4.2.5 for further details). For simplicity, it has been assumed that only the ERMs, and not the SRMs, increase the value of the building above the cost of the as-built configuration. Table 5.8 summarises the replacement costs and EIs adopted for each retrofit configuration. Subsequently, building properties, fragility curve repositories, consequence models, and NRHA outputs were introduced into PACT, and time-based loss calculations were carried out for the 12 retrofit alternatives in each analysed site.

Table 5.8 Replacement costs and EIs for the as-built structure and different retrofit combinations

Alternative	Replacement cost (€)	Replacement EIs ($kgCO_2e$)
S_0	2,652,242	1,830,000
S_iE_1	2,700,684	1,867,485
S_iE_2	2,729,918	1,888,749
S_iE_3	2,858,340	1,982,159

Regarding the simplified approach, the procedure outlined in Section 5.2.2.2 was implemented to determine the seismic risk classification of each retrofitted structure using Sismabonus (Cosenza et al. 2018). The SI-LS index, defined as the ratio between the capacity peak ground acceleration (PGA_C) and the demand peak ground acceleration (PGA_D), previously used to compare the seismic performance of the retrofitted structures, is summarised in Table 5.4 and Table 5.6 for the X and Y directions of the as-built and retrofitted configurations, respectively. The EAL under the simplified approach was then determined by evaluating the structural performance at four limit states, namely the Operational (OLS), Damage Limitation (DLLS), Life Safety (LSLS) and Collapse (CLS) limit states, as defined by the current Italian building code (MIT 2018). For school buildings, the corresponding return periods (T_r) are 45, 75, 712, and 1463 years. The Italian guidelines (Cosenza et al. 2018) were used to compute the return period associated with PGA_C, as a function of T_{rD} and PGA_D for a each limit state. The EAL curve (for both the as-built and retrofitted conditions) was then derived by converting the return period of each limit state into a mean annual frequency of exceedance ($\lambda=1/T_r$) and assigning the corresponding repair cost (%RC). The SI-LS index, EAL, and resulting seismic risk classification for the critical direction of the as-built and retrofitted models are summarised in Table 5.9, along with the overall seismic risk class.

The expected annual environmental impacts (EAEI) are obtained employing the detailed methodology within the loss assessment procedure through PACT. As such, when using the simplified procedure (Sismabonus), which does not enable the direct quantification of the EAEI, the results from the detailed methodology were used to fit a linear regression model between EAL and EAEI. The regression is then used to estimate, in a simplified manner, the EAEI straight from EAL.

Table 5.9 Sismabonus results.

Alt.	Param.	Medium Hazard									High Hazard								
		M-C			M-M			M-W			H-C			H-M			H-W		
		%	Class		%	Class		%	Class		%	Class		%	Class		%	Class	
S_1	SI-LS	120	A^+	**A^+**	123	A^+	**A^+**	95	A	**A**	120	A^+	**A**	108	A^+	**A**	99	A	**A**
	EAL	0.46	A^+		0.48	A^+		0.52	A		0.61	A		0.61	A		0.64	A	
S_2	SI-LS	92	A	**A**	95	A	A	73	B	**B**	63	B	**B**	55	C	**C**	50	C	**C**
	EAL	0.49	A^+		0.51	A		0.59	A		0.80	A		0.82	A		0.60	A	
S_3	SI-LS	111	A^+	**A^+**	113	A^+	A^+	96	A	**A**	82	A	**A**	73	B	**B**	68	B	**B**
	EAL	0.46	A^+		0.46	A^+		0.50	A		0.63	A		0.67	A		0.65	A	
S_4	SI-LS	125	A^+	**A^+**	128	A^+	A^+	97	A	**A**	117	A^+	**A**	105	A^+	**A**	96	A	**A**
	EAL	0.42	A^+		0.43	A^+		0.47	A^+		0.52	A		0.54	A		0.52	A	

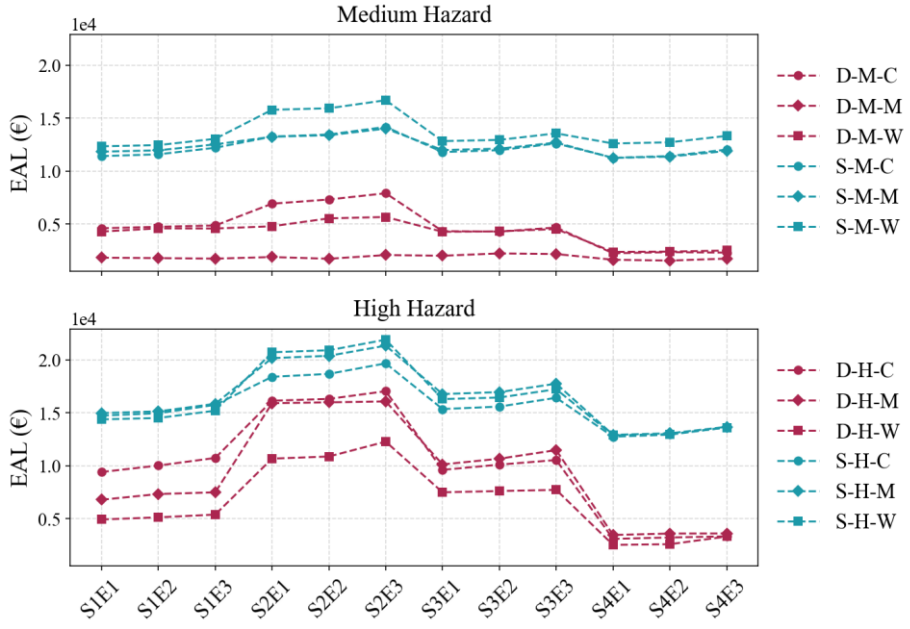

Figure 5.10 Expected annual loss (EAL) values obtained employing the detailed and simplified methodologies for medium- and high-hazard sites.

5.3.4.3 Expected Annual Environmental Impacts (EAEI)

The expected annual environmental impact (EAEI) represents the aggregated environmental impacts associating with the building over its lifetime. Within the

detailed methodology, the EAEI was quantified through the PACT loss assessment procedure, which encompasses the environmental impact of the activities required to repair a given component, in functions of its damage state. Since yje simplified approach (Sismabonus) does not include an equivalent in-built feature, the EAEI values obtained from the detailed methodology were used to calibrate a linear regression model relating EAL to EAEI. This regression model was then employed to estimate EAEI directly from EAL in a simplified manner. As shown in Figure 5.11, the resulting WAEI values are proportional to the corresponding EAL values.

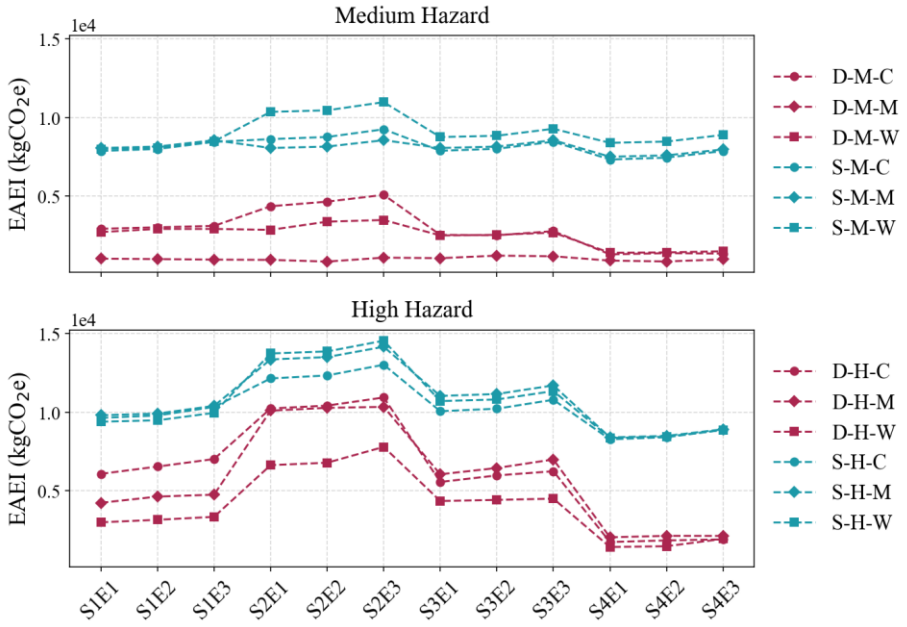

Figure 5.11 Expected annual environmental impacts (EAEI) values obtained employing the detailed and simplified methodologies for medium- and high-hazard sites.

5.3.5 Post-Intervention Energy Assessment

The energy performance of the case-study building was evaluated using the Edilclima software (Edilclima 2022), with monthly weather data derived from UNI 10349:2016 (UNI 2016) to calculate the thermal loads. Most modelling parameters were defined according to national design codes for buildings with occupancy class E.7, which corresponds to school buildings (UNI 2014a, b). The building was divided into four thermal zones, namely the basement, ground floor, first floor, and stairwell, all of which are assumed to be conditioned spaces, with heating and cooling set-point

temperatures of 20°C and 26°C, respectively. An internal heat gain of 4 W/m^2, as recommended in UNI 11300-1 (UNI 2014a), was used to represent heat contributions from occupants. Additional internal gains from domestic hot water and electrical or mechanical equipment were not explicitly included. Natural ventilation was assumed (i.e. no mechanical ventilation system), as its effect was modelled through yhe air-exchange method, adopting a rate of one complete air change per hour (1 Vol./h) to represent the low airtightness of existing buildings before retrofitting (Pohoryles et al. 2020). Lighting power demand was assigned using recommended values for the relevant room typologies, and operational hours were obtained from UNI 11300-2 (UNI 2014b). Emergency lighting and control devices were assumed to consume 6.0 kWh of electricity per year (UNI 2014b).

Regarding the improvement of the energy performance of the building, three ERMs, as described in Section 5.3.3, were considered and modelled in Edilclima using the same base assumptions as the as-built configuration. The additional modelling parameters are described in Clemett et al. (2023). The energy performance results of the as-built and retrofitted configurations are summarised in Table 5.10. The retrofit configurations were compared using primary energy consumption (PEC), equivalent CO_2 emissions (Eq. CO_2), annual energy costs (AEC) and the Italian energy class rating. As expected, all ERMs enhanced the energy performance of the structure, with scheme E_3 exhibiting the greatest improvement, followed by E_2 and E_1. The enhancements occur progressively, highlighting the challenge of selecting the optimal intervention level based solely on direct energy indicators, and emphasising the need for a broader multi-criteria evaluation. Specifically, the first level (E_1) archives a 28% reduction in the annual PEC, while E_2 and E_3 deliver reductions of approximately 50% and 80% respectively; similar trends are observed for Eq. CO_2 and AEC.

Table 5.10 Energy performance assessment results.

Alt.	PEC (kWh/m^2)	Eq. CO_2 (kgCO_2e)	AEC (EUR)	Energy Class
E_0	309	76,651	12,718	E
E_1	221.76 (*−28%*)	52,476 (*−32%*)	8765 (*−31%*)	D
E_2	166.63 (*−46%*)	40,716 (*−47%*)	7121 (*−44%*)	C
E_3	64.92 (*−79%*)	14,982 (*−80%*)	3109 (*−76%*)	A2

Note: In brackets, the reduction (%) of PEC, Eq. CO_2, and AEC for each energy-retrofitting intervention, with respect to the as-built condition.

5.4 DECISION ASSESSMENT AND DISCUSSION

5.4.1 Decision Variable Assemblance

In this section, all DVs are combined to support the final decision-making process. The methods and assumptions used to compute each DV and the corresponding weight factors are described in detail in Clemett et al. (2023).

The total installation cost (C_1) for each retrofit alternative includes, in addition to the cost of the retrofit materials, the removal of internal linings, partial demolition of the existing structural elements and infills, debris removal, installation of the retrofit system, and restoration of infills and finishes. Costs associated with CFRP or steel braces installation were primarily based on data from Mazzolani et al. (2018) and scaled according to the quantities of materials required. The cost of the steel joint enlargement was estimated by multiplying the required steel weight by the average European price of hot-rolled steel products, while the cost of the dampers was obtained directly from a local manufacturer in Italy. For the energy retrofit, the cost of EPS insulation was estimated using data from Formisano et al. (2019), and the prices of the condensing boiler and solar panels were taken from Mauro et al. (2017). Cost related to modifications of existing blockwork, plastering, and finishing were based on Sassun et al. (2016). The cost of window units was estimated using US data (Homewyse 2021) and subsequently converted to Italian euros (June 2020) following the methodology proposed by Silva et al. (2020).

The expected annual cost (C_2), calculated according to Equation 5.1, comprises the EAL, the AEC, and the maintenance costs of the retrofit components. The EAL and the AEC were determined from the seismic and energy performance analyses carried out in the previous sections. The structural maintenance cost over the lifetime of the structure (75 years) was estimated by adapting the interventions proposed by Caterino et al. (2008) and scaling them according to the quantities of materials used in each retrofit.

The expected LCEI (C_3), calculated using Equation 5.2, includes the installation EI of the retrofit alternative, the EAEI of the retrofitted structure and the total maintenance EI of the alternative over the expected service life. The Eis associated with installation and maintenance were estimated using the EIO-LCA procedure. Specifically, the monetary costs associated with materials, labour, and installation activities were multiplied by sector-specific environmental emission factors, which translate euro spent into the corresponding CO_2 emissions. The EAEI values, capturing operational

and damage-related environmental impacts, were obtained from the seismic loss assessment (Section 5.3.4.3). The values of the annual probability of failure (C_4) were determined in Section 5.3.4.1. The duration of works (C_5) was estimated using the intervention durations reported by Mazzolani et al. (2018) as a baseline and scaled according to the quantities of materials and the floor area where appropriate. It was assumed that a maximum of 20 workers could be present on site at any given time. The remaining DVs, architectural impact (C_6), need for specialized labour/design knowledge (C_7), and required interventions at the foundations (C_8), were set according to Clemett et al. (2023).

The DVs directly related to the seismic performance of the structure, namely C_2, C_3, and C_4, are the only DVs whose quantifications depend on the employed methodology. The final values for such DVs are detailed in Table 5.11 and Table 5.12 for the medium- and high-hazard sites, respectively. The remaining DVs (C_1, C_5, C_6, C_7, and C_8), which are independent of the chosen assessment approach, are summarized in Table 5.13.

Table 5.11 Decision variables C2, C3, and C4 for the medium-hazard sites, as a function of the employed methodology

Alt	Detailed									Simplified								
	C			M			W			C			M			W		
	C_2	C_3	C_4	C_2	C_3	C_4	C_2	C_3	C_4	C_2	C_3	C_4	C_2	C_3	C_4	C_2	C_3	C_4
S_1E_1	9.5	25.4	1.22	10.4	43.2	0.36	13.5	52.7	1.30	15.3	29.2	1.19	18.0	48.2	0.25	18.9	56.3	1.38
S_1E_2	9.5	21.6	1.28	9.6	35.3	0.33	12.5	42.5	1.31	15.2	25.3	1.19	17.4	40.4	0.25	18.0	46.1	1.38
S_1E_3	8.8	14.8	1.20	7.4	18.0	0.31	9.9	21.4	1.28	14.8	18.7	1.19	15.6	23.4	0.25	15.7	25.2	1.38
S_2E_1	9.0	23.5	1.14	9.5	41.1	0.26	14.2	51.8	1.95	16.8	28.9	1.33	17.1	46.2	0.35	18.8	54.8	1.49
S_2E_2	9.3	19.9	1.40	8.7	33.2	0.19	13.5	41.7	2.08	16.8	25.0	1.33	16.4	38.4	0.35	17.9	44.6	1.49
S_2E_3	8.6	13.1	1.39	6.7	16.1	0.30	11.1	20.8	2.18	16.5	18.5	1.33	14.6	21.4	0.35	15.6	23.8	1.49
S_3E_1	8.7	22.4	0.93	9.7	40.3	0.28	12.5	49.6	0.96	15.3	26.9	1.37	17.2	45.4	0.32	18.2	53.4	1.56
S_3E_2	8.6	18.4	0.95	9.2	32.6	0.37	11.4	39.3	0.92	15.2	23.0	1.37	16.6	37.6	0.32	17.2	43.3	1.56
S_3E_3	8.0	11.7	0.96	6.9	15.3	0.32	8.9	18.3	0.98	14.9	16.5	1.37	14.8	20.6	0.32	14.9	22.4	1.56
S_4E_1	8.6	21.8	0.53	10.7	40.5	0.30	12.3	49.0	0.46	16.2	26.8	0.11	17.9	45.2	0.006	18.8	53.3	0.17
S_4E_2	8.5	17.9	0.54	9.9	32.6	0.27	11.3	38.7	0.49	16.1	22.9	0.11	17.3	37.4	0.006	17.9	43.1	0.17
S_4E_3	7.8	11.1	0.54	7.9	15.4	0.31	8.5	17.5	0.44	15.8	16.4	0.11	15.4	20.4	0.006	15.6	22.2	0.17

Note: The units of C_2 and C_3 are, respectively, EUR and $kgCO_2e$. C_4 is unitless ($\times 10^{-3}$).

Table 5.12 Decision variables C2, C3, and C4 for the high-hazard sites, as a function of the employed methodology

Alt	Detailed									Simplified								
	C			M			W			C			M			W		
	C_2	C_3	C_4	C_2	C_3	C_4	C_2	C_3	C_4	C_2	C_3	C_4	C_2	C_3	C_4	C_2	C_3	C_4
S_1E_1	12.9	28.4	1.01	16.2	40.4	1.66	18.8	47.5	2.67	19.7	33.0	0.91	22.7	52.3	1.42	23.7	60.3	1.20
S_1E_2	12.9	24.5	1.08	14.3	23.4	1.87	16.5	26.6	2.90	19.6	29.1	0.91	22.1	44.5	1.42	22.8	50.2	1.20
S_1E_3	12.3	17.9	1.12	13.4	42.7	1.81	16.9	52.5	2.94	19.3	22.6	0.91	20.4	27.5	1.42	20.6	29.4	1.20
S_2E_1	13.1	25.0	2.86	18.8	38.7	4.55	19.7	44.6	4.58	20.3	30.1	1.36	22.5	48.9	2.05	22.4	56.2	1.81
S_2E_2	13.1	21.2	2.93	16.6	21.5	4.70	17.1	23.5	4.73	20.3	26.3	1.36	22.0	41.1	2.05	21.5	46.1	1.81
S_2E_3	13.3	15.1	3.30	22.3	47.2	4.37	24.2	55.9	4.69	20.2	19.9	1.36	20.5	24.3	2.05	19.5	25.3	1.81
S_3E_1	13.6	23.9	1.66	17.4	36.3	2.46	17.8	41.7	2.05	19.9	28.5	0.65	22.8	47.7	1.00	23.0	55.2	0.85
S_3E_2	13.5	20.0	1.67	15.5	19.3	2.66	15.4	20.8	2.30	19.8	24.6	0.65	22.2	40.0	1.00	22.1	45.1	0.85
S_3E_3	12.8	13.3	1.62	22.8	45.6	2.74	23.3	53.3	2.24	19.6	18.2	0.65	20.6	23.1	1.00	19.9	24.3	0.85
S_4E_1	13.7	22.6	0.43	16.3	34.2	0.79	16.9	39.8	0.52	21.2	27.6	0.027	23.8	46.6	0.06	24.8	54.7	0.03
S_4E_2	13.6	18.7	0.40	14.2	19.2	0.74	14.2	20.8	0.57	21.1	23.7	0.027	23.2	38.9	0.06	23.9	44.6	0.03
S_4E_3	13.4	14.4	0.59	2.6	1.5	0.68	2.4	1.4	0.54	20.7	19.4	0.027	21.4	24.0	0.06	21.6	25.9	0.03

Note: The units of C_2 and C_3 are, respectively, EUR and $kgCO_2e$. C_4 is unitless ($\times 10^{-3}$).

Table 5.13 Decision variables C1, C5, C6, C7, and C8 for each retrofit alternative per level of hazard

Alt.	C_6	C_7	Medium Hazard									High Hazard								
			Cold			Moderate			Warm			Cold			Moderate			Warm		
			C_1	C_5	C_8	C_1	C_5	C_8	C_1	C_5	C_8	C_1	C_5	C_8	C_1	C_5	C_8	C_1	C_5	C_8
S_1E_1	0.023	0.084	529	38	5.9	525	38	6.2	507	38	7.0	867	60	6.1	881	61	5.7	871	63	5.7
S_1E_2	0.023	0.084	589	38	5.9	568	38	6.2	543	38	7.0	927	60	6.1	925	61	5.7	908	63	5.7
S_1E_3	0.023	0.084	753	42	5.9	692	42	6.2	671	42	7.0	1091	64	6.1	1048	65	5.7	1036	67	5.7
S_2E_1	0.056	0.013	135	21	10.9	131	21	11.3	113	21	12.5	136	22	16.5	132	22	16.5	114	22	16.5
S_2E_2	0.056	0.013	196	23	10.9	175	23	11.3	150	23	12.5	196	24	16.5	175	24	16.5	150	24	16.5
S_2E_3	0.056	0.013	359	28	10.9	298	28	11.3	277	28	12.5	360	29	16.5	299	29	16.5	278	29	16.5
S_3E_1	0.093	0.084	172	23	12.8	168	23	13.4	150	23	13.0	180	37	16.6	213	42	16.6	195	42	16.6
S_3E_2	0.093	0.084	232	23	12.8	211	23	13.4	186	23	13.0	240	37	16.6	257	42	16.6	232	42	16.6
S_3E_3	0.093	0.084	396	27	12.8	335	27	13.4	314	27	13.0	404	41	16.6	380	46	16.6	360	46	16.6
S_4E_1	0.162	0.151	289	14	3.3	284	14	3.5	266	14	3.9	437	44	5.1	419	44	4.8	381	43	4.8
S_4E_2	0.162	0.151	349	27	3.3	328	27	3.5	303	27	3.9	499	44	5.1	463	44	4.8	418	43	4.8
S_4E_3	0.162	0.151	513	31	3.3	451	31	3.5	431	31	3.9	661	48	5.1	586	48	4.8	546	47	4.8

Note: The units of C_1 and C_5 are, respectively, EUR/m^2 and days. C_6, C_7, and C_8 are unitless.

5.4.2 Ranking of the Retrofit Alternatives

The DVs quantified in the previous sections were then used as input for the MCDM framework. The ranking of each alternative is determined by its relative closeness, a measure of proximity to the ideal solution or reference point, typically expressed between 0 and 1. A value of 1 indicates that the alternative is closer to the ideal solution, and thus more desirable, while values closer to 0 indicate lower desirability. This metric enables decision-makers to quantitatively evaluate, and rank alternatives based on specified criteria and their associated weights. Among the twelve retrofit alternatives considered in this study the first ranked option is the most preferred, while the twelfth-ranked is the least preferred. The preferential rankings for each methodology and hazard level are reported in Table 5.14.

Table 5.14 Classification ranking of the retrofit alternatives as a function of hazard level, employed approach, and climate site.

Rank	Medium Hazard						High Hazard					
	Detailed			Simplified			Detailed			Simplified		
	C	M	W	C	M	W	C	M	W	C	M	W
1	S_3E_3	S_2E_3	S_3E_2	S_4E_1	S_4E_1	S_4E_1	S_3E_3	S_4E_3	S_4E_2	S_4E_2	S_4E_2	S_4E_2
2	S_4E_3	S_2E_2	S_4E_1	S_4E_2	S_4E_2	S_4E_2	S_4E_3	S_4E_2	S_4E_1	S_3E_3	S_4E_3	S_4E_1
3	S_4E_2	S_3E_3	S_2E_1	S_4E_3	S_4E_3	S_2E_1	S_4E_2	S_3E_3	S_4E_3	S_4E_3	S_4E_1	S_4E_3
4	S_3E_2	S_2E_1	S_3E_1	S_2E_2	S_2E_2	S_2E_2	S_3E_2	S_4E_1	S_3E_2	S_3E_2	S_3E_3	S_3E_2
5	S_4E_1	S_3E_2	S_4E_2	S_2E_3	S_2E_1	S_4E_3	S_3E_1	S_3E_2	S_3E_3	S_4E_1	S_3E_2	S_3E_1
6	S_3E_1	S_4E_3	S_3E_3	S_2E_1	S_2E_3	S_3E_1	S_4E_1	S_2E_3	S_3E_1	S_3E_1	S_3E_1	S_3E_3
7	S_2E_3	S_3E_1	S_2E_2	S_3E_2	S_3E_2	S_3E_2	S_2E_3	S_3E_1	S_2E_2	S_2E_3	S_2E_3	S_2E_2
8	S_2E_2	S_4E_1	S_2E_3	S_3E_1	S_3E_3	S_2E_3	S_2E_2	S_2E_2	S_2E_1	S_2E_2	S_2E_2	S_2E_1
9	S_2E_1	S_4E_2	S_4E_3	S_3E_3	S_3E_1	S_3E_3	S_2E_1	S_2E_1	S_2E_3	S_2E_1	S_2E_1	S_2E_3
10	S_1E_3	S_1E_3	S_1E_3	S_1E_3	S_1E_3	S_1E_1	S_1E_3	S_1E_3	S_1E_2	S_1E_3	S_1E_3	S_1E_2
11	S_1E_2	S_1E_2	S_1E_1	S_1E_2	S_1E_2	S_1E_2	S_1E_1	S_1E_1	S_1E_1	S_1E_2	S_1E_2	S_1E_1
12	S_1E_1	S_1E_1	S_1E_2	S_1E_1	S_1E_1	S_1E_3	S_1E_2	S_1E_2	S_1E_3	S_1E_1	S_1E_1	S_1E_3

It is first observed that the ranking of retrofit alternatives changes with the seismic hazard level. For high hazard sites, a clear trend emerges: alternatives tend to be grouped according to the structural retrofit scheme, with S4 consistently being the most preferred, followed by S_2, S_3, and S_1. This pattern indicates that the structural

retrofit has a stronger influence on the overall ranking than the energy retrofit, as also highlighted by Clemett et al. (2023). Within each structural retrofit group, however, the energy retrofit scheme influences the ranking according to the energy needs of each site. For example, in colder climates, alternatives with E_3 are favoured, while in warmer climates, E_1 tends to be preferred.

For medium hazard sites, both structural and energy retrofit interventions contribute more equally to the ranking, S3 and S4 are generally preferred as structural retrofit options, except in moderate climate sites, where similar performance values for APF, EAL, and EAEI make it difficult for the MCDM framework to clearly differentiate between alternatives.

When comparing the detailed and simplified approaches, for medium hazard sites, the simplified methodology generally aligns rankings based on the structural retrofit, with S4 ranked first, followed by S2, S3, and S1. The main difference between the two approaches lies in the ranking positions of S2 and S3, reflecting the trends observed in the collapse assessment results. For high hazard sites, despite some differences in the exact DV values estimated by the two approaches, the final ranking of retrofit alternatives is largely consistent, with only minor deviations. In both approaches and for all hazard levels, S1 is consistently the least preferred alternatives, primarily due to its high installation costs, two to six times higher than other options, because it requires numerous CFRP bars, which are costly and labour-intensive to install.

Since the ranking is based on the relative closeness value for each retrofit alternative, its variation with hazard level and the methodological detail was also analysed, providing insights into the reliability of the simplified approach. Figure 5.12 presents the relative closeness values, with alternatives along the X-axis sorted according to the detailed approach ranking. For medium hazard sites, some mismatches between the approaches are observed, although there is a good alignment for alternatives S_1 and S_4 across cold and warm climates. For high hazard sites, the alignment is stronger, with only minor differences in relative closeness values between the two approaches for S_4 in moderate and warm climate conditions, which do not affect the overall classification.

According to the MCDM framework, the first-ranked alternative is considered the optimal solution. However, given the close relative closeness values among several alternatives, it is also possible to identify a group of most preferable alternatives rather than a single top option. To achieve this, the 25^{th} and 75^{th} percentiles of the relative closeness values were quantified for both detailed and simplified

approaches, as shown in Figure 5.12. In this way, three groups of alternatives are obtained, allowing one to identify the less (below the 25th percentile), relatively (between the 25th and 75th percentile), and most (above the 75th percentile) preferable alternatives.

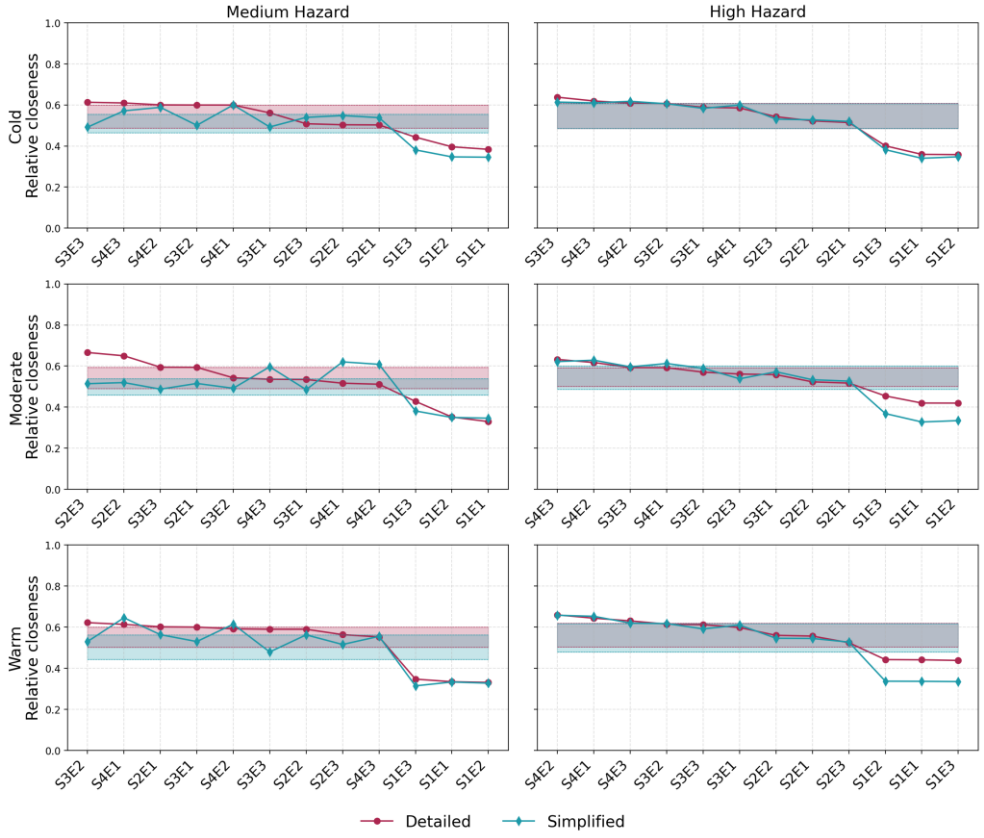

Figure 5.12 Relative closeness obtained through detailed and simplified approaches for different seismic hazard and climate levels.

Table 5.15 categorises the retrofit alternatives into three preference groups: less preferable (red), relatively preferable (yellow), and most preferable (green), based on their relative closeness values. This classification is shown for each seismic hazard level and for both the detailed and simplified assessment approach.

Table 5.15 Less, medium, and most preferable alternatives as a function of the location and employed methodology.

Medium Hazard						High Hazard					
Detailed			Simplified			Detailed			Simplified		
C	M	W	C	M	W	C	M	W	C	M	W
S_1E_1	S_1E_1	S_1E_1	S_1E_1	S_1E_1	S_1E_1	S_1E_1	S_1E_1	S_1E_1	S_1E_1	S_1E_1	S_1E_1
S_1E_2	S_1E_2	S_1E_2	S_1E_2	S_1E_2	S_1E_2	S_1E_2	S_1E_2	S_1E_2	S_1E_2	S_1E_2	S_1E_2
S_1E_3	S_1E_3	S_1E_3	S_1E_3	S_1E_3	S_1E_3	S_1E_3	S_1E_3	S_1E_3	S_1E_3	S_1E_3	S_1E_3
S_2E_1	S_2E_1	S_2E_1	S_2E_1	S_2E_1	S_2E_1	S_2E_1	S_2E_1	S_2E_1	S_2E_1	S_2E_1	S_2E_1
S_2E_2	S_2E_2	S_2E_2	S_2E_2	S_2E_2	S_2E_2	S_2E_2	S_2E_2	S_2E_2	S_2E_2	S_2E_2	S_2E_2
S_2E_3	S_2E_3	S_2E_3	S_2E_3	S_2E_3	S_2E_3	S_2E_3	S_2E_3	S_2E_3	S_2E_3	S_2E_3	S_2E_3
S_3E_1	S_3E_1	S_3E_1	S_3E_1	S_3E_1	S_3E_1	S_3E_1	S_3E_1	S_3E_1	S_3E_1	S_3E_1	S_3E_1
S_3E_2	S_3E_2	S_3E_2	S_3E_2	S_3E_2	S_3E_2	S_3E_2	S_3E_2	S_3E_2	S_3E_2	S_3E_2	S_3E_2
S_3E_3	S_3E_3	S_3E_3	S_3E_3	S_3E_3	S_3E_3	S_3E_3	S_3E_3	S_3E_3	S_3E_3	S_3E_3	S_3E_3
S_4E_1	S_4E_1	S_4E_1	S_4E_1	S_4E_1	S_4E_1	S_4E_1	S_4E_1	S_4E_1	S_4E_1	S_4E_1	S_4E_1
S_4E_2	S_4E_2	S_4E_2	S_4E_2	S_4E_2	S_4E_2	S_4E_2	S_4E_2	S_4E_2	S_4E_2	S_4E_2	S_4E_2
S_4E_3	S_4E_3	S_4E_3	S_4E_3	S_4E_3	S_4E_3	S_4E_3	S_4E_3	S_4E_3	S_4E_3	S_4E_3	S_4E_3

The results presented in Table 5.15 are consistent with observations discussed previously. The optimal group of alternatives varies depending on the climate conditions. For cold climate sites, there is a clear preference for the most demanding energy retrofit combined with the structural retrofit that provides the highest structural performance, in with the findings of Section. In contrast, for warm climate sites, the selection is driven primarily by the structural retrofit performance, with less influence from the energy retrofit. Across all methodologies, alternatives incorporating S1 as the structural retrofit consistently rank as the least preferred option due to their high costs and limited overall efficiency. The shaded area between the 25th and 75th percentiles of relative closeness values in Figure 5.12 further supports the interpretation of the differences between the application of both approaches. While minimal variations are noted in high-hazard locations among the alternatives in each preference group, greater disparities are evident in medium-hazard locations, mostly for the moderate climate, where the results obtained with the simplified approach are different from the ones obtained with the detailed

counterpart. This is likely due to the difference in the hazard curves, as observed in Figure 5.4, which shows how the M-M hazard curve is slightly different from the other medium-hazard locations.

5.5 INCLUSION OF DOWNTIME AS A DECISION VARIABLE

After identifying the optimal alternative and the group of less, moderate and most preferable alternatives based on the initial set of DVs, the study was extended by incorporating downtime as an additional DV. Downtime was not accounted as a DV within the initial MCDM methodology, although it may have an impact on the selection of the optimal retrofitting alternative. Indeed, while the expected annual losses are related to the economic impact of the repair activities, the recovery time as a function of the recovery state indicates the time to reach essential functionality for the owner or tenants. Moreover, as demonstrated in Section 5.4.2, when the relative closeness values obtained through the MCDM analysis are very similar across several alternatives, it becomes appropriate to identify a set of most preferable options rather than relying solely on the top-ranked solution. In such cases, quantifying the downtime and recovery trajectory of each of the most preferable alternatives could highlight which of them would be more efficient in the aftermath of a seismic event, thus limiting the time to access essential functionality.

5.5.1 Downtime-based methodology

The downtime estimation of each retrofit alternative was carried out with the methodology proposed by (Molina et al. 2022). The framework starts with the evaluation of the extent of damage, using a component-based loss assessment methodology, and the corresponding post-earthquake usability of the building, considering five distinct recovery states: stability, shelter-in-place, re-occupancy, functional recovery, and full recovery. The building's condition, including its post-earthquake state of both structural and non-structural elements (NSEs), is associated with each of the five distinct recovery states, which describe the building's status. Moreover, a repair class for each structural and non-structural element is defined for each recovery state, thereby identifying the minimum repair class that hinders achieving the recovery state. While re-occupancy (RO), functional recovery (FR), and full recovery (F) states are also considered in the FEMA P-58 (FEMA 2018b) and the REDi guidelines (Almufti and Willford 2013), (Molina et al. 2022) introduced two additional recovery states. The first is stability (S), which refers to a post-earthquake condition where the building’s structure and facade are deemed

sufficiently stable, eliminating the need for safety cordons. The second is shelter-in-place (SiP), which refers to moderate structural and non-structural damage that does not threaten the safety of residents and where, in line with the (SPUR 2012) resilient city initiative, repair activities can be conducted while keeping people in their homes. The assignment of a recovery state to the building is made according to different damage criteria, described in detail in (Molina et al. 2022).

After identifying the building's recovery state for a given earthquake intensity level, the temporal recovery trajectory to achieve the desired recovery state is estimated, providing downtime estimates for each repair phase. This estimation considers not only the repair duration but also potential delays and impeding factors that may affect the initiation of the repair actions. Within this framework, repair times are estimated based on the repair sequences and worker allocations, while various factors that could hinder the initiation of the repair actions are also incorporated. Such factors are related to the needed time to: (i) perform building inspection, (ii) secure finance, (iii) carry out engineering services, (iv) obtain permits, (v) mobilise the contractor, (vi) perform all the repairs activities, (vii) minimise aftershock collapse risk and falling debris hazard. These steps are repeated for numerous Monte Carlo simulations to address uncertainties in the downtime estimation process.

Subsequently, the building's repair and delay time to achieve the desired recovery state is estimated, based on the repair sequence and the number of workers available, after which the previous estimates (repair and delay time) are used to model the building's temporal recovery trajectory, providing downtime estimates for each storey in the building. To address uncertainties in the downtime estimation process, the previous steps are repeated across thousands of Monte Carlo simulations, generating numerous downtime realisations and recovery trajectories, each equally likely.

Finally, downtime estimates are connected to probabilistic performance measures - such as robustness and rapidity - that aid decision-making for building owners, engineers, and policymakers. The financing delay, which was defined by (Molina et al. 2022) as a function of the economic loss ratio of the building, was distinguished into public loans, private loans and insurance. In the Italian context, the repair and reconstruction process is generally based on public loans and, as opposed to the US or New Zealand, for instance, only 5% of the residential buildings have earthquake insurance coverage (ANIA 2024). It is thus reasonable to assume that the financing

delay is mostly due to secure public loans hence, accordingly, only such a delay is accounted for in this study.

5.5.2 Decision-making framework updated

Possible downtime-based metrics that can be introduced in the MDCM framework are defined herein. Such metrics are essential for establishing design threshold that allow individuals to return to their homes and ensure access to other vital services, including education, healthcare, and commerce. Additionally, the life cycle-based design of retrofitting interventions further increases the interest in identifying downtime metrics, as post-event repair and restoration activities are one of the life cycle assessment steps. While F_R state appears to be too restrictive, the FR state might be an objective to be pursued in the retrofitting design phase. (Molina et al. 2022) proposed two downtime-based metrics, namely robustness and rapidity. The former identifies the immediate post-earthquake usability of the building, such as its ability to withstand seismic forces without loss of functions. The latter quantifies the ability to meet recovery goals in a timely manner. In both cases, a target downtime has to be defined, which can be influenced by various factors and determined by different parties, such as the building owner, relevant codes or standards committees, stakeholders, or emergency plans.

This study adopted expected annual downtime (EAD) as a metric to be used in the MCDM framework. It is computed analogously to expected annual losses, by integrating the expected downtime curve, defined as a function of the rate of exceedance of a given intensity level. It is noted that the definition of downtime within this metric may vary depending on the prescribed target recovery state following an earthquake, reflecting decision-makers' objectives regarding the building's post-earthquake functionality. In this study, being the selected case study a school building, functional recovery was adopted as the target recovery state. Furthermore, the estimation of expected annual downtime was conducted in accordance with the return periods established by the Italian code. Introducing this parameter required recalculating the decision matrix and updating the weighting scheme to account for its relative importance within the overall evaluation. To assess how the inclusion of downtime influences the decision-making process, two scenarios were examined:

i. MCDM-1: this scenario represents the original MCDM framework, which does not account for post-earthquake–related DVs. The DVs used are those presented in Section 5.2, while the weights assigned to each group

of DVs (economic, environmental, technical, and social) are the same, each equal to 0.25.

ii. MCDM-2: this scenario is similar to MCDM-1, but it includes the expected annual downtime (EAD) as an additional DV, along with updated weights (different from those in MCDM-1) for the DVs belonging to the economic group.

Within each group and for both scenarios, the individual DVs were also equally weighted, as shown in Table 5.16. The EAD was then introduced as DV with the economic group of DVs, and, accordingly, the previous weights (0.125), equally assumed for all DVs, were updated to 0.083. The EAD might be also related to the social group of DVs, given the socio-economic implications that a loss of functionality of the building could bring.

Table 5.16 Decision variables and corresponding weights

Group	Decision Variables	Weight	
		MCDM-1	MCDM-2
Economic	C_1 Installation cost	0.125	0.083
	C_2 Expected annual costs (EAC)	0.125	0.083
	C_9 Expected annual downtime (EAD)	-	0.083
Environmental	C_3 Expected life-cycle environmental impacts (LCEI)	0.25	0.25
Social	C_4 Annual probability of failure (APF)	0.083	0.083
	C_5 Duration of works	0.083	0.083
	C_6 Architectural impact	0.083	0.083
Technical	C_7 Need for specialized labour/design knowledge	0.125	0.125
	C_8 Required intervention at the foundations	0.125	0.125

5.5.3 Downtime assessment and results

The downtime estimation framework employed in this study starts with the evaluation of the extent of damage to structural and non-structural components within the inventory of the building, which is later associated with corresponding repair classes. It is hence necessary to identify the repair class (RC) triggered by each damage state at the outset of the procedure. Subsequently, the impedance of the

recovery states is identified by the repair classes obtained for each realisation. Therefore, each repair class (RC_i) is assigned to the damage state of each component based on the definition of the repair needs and recovery state it may hinder: RC1 – Full Recovery, RC2 – Functional Recovery, RC3 – Re-occupancy, RC4 – Shelter-in-PLace, and RC5 – Stability. The case of exterior non-ductile beam-column joint components (B1046.001a in Table C. 1), which foresee three damage states (DS1, DS2, and DS3), is taken as an example to explain the RC_i assignment to each damage state. DS1 represents light cracking at beam/column-joint interfaces, yielding of beam rebars, and possible first inclined crack in the joint, which is tagged with RC_1 and impedes achieving the FR state. DS2 encompasses severe cracking in the beams and joints with possible spalling of joint cover concrete; it is tagged with a repair class RC_4 and hinders achieving the SP state. Finally, DS3 refers to spalling of joint concrete cover, potential crushing of concrete at beam-joint interface, and possible buckling of rebars, which is believed to compromise the load-bearing capacity of the component and is therefore linked to RC_5, hindering the achievement of the S state. In turn, group E (Equipment & Furnishings) components are characterised by a single damage state, with the consequence of replacement assumed to correspond to RC_1, as it is evident that any damage to these components would not impede any recovery state.

Furthermore, it is important to identify the logical repair sequences (RS) at the outset of the procedure, similar to the repair classes. The repair sequence logic proposed by (Molina et al. 2022) has been adopted with some updates considering the case-study building and the Italian context. For instance, RS_6 is defined as staircase repairs, assuming that parallel repair actions will be taken for each stair across the floors, whereas it is described as elevator repairs in (Molina et al. 2022). Moreover, the repair actions for equipment and furnishings (group E components) are considered RS_7. Table 5.17 summarises the repair classes triggered by each damage state and repair sequences of each component considered in the building components inventory, detailed in Table C. 1.

For each repair sequence (RS), a specific number of workers must be allocated based on the required repair type, the number of damaged units, and the floor area. At each floor level, the total number of workers is limited by the maximum number allowed per RS. If a specific RS requires more workers than the allowed maximum, the number of workers is constrained to the limit. Additionally, the same RS cannot be conducted simultaneously on multiple floors if all available workers are assigned to one floor. In this study, worker allocation per RS follows the recommendations of

(Paul et al. 2018): RS_1 – 2 workers (per damaged unit), RS_2 – 1 worker per 1000 sq. ft., RS_3/RS_6/RS_7 – 2 workers (per damaged unit), and RS_4/RS_5 – 3 workers (per damaged unit). The repair time for each RS on each floor consists of the repair time of all components divided by the total number of workers assigned to each sequence. The repair schedule needed to achieve the target recovery state is then obtained by summing the repair times for each sequence and floor.

Table 5.17 Repair class associated with each damage state, together with the repair sequence of each component adopted in the building models.

Component	ID (FEMA P58)	Damage State (DS)						RS
		0	1	2	3	4	5	
Steel braces	B1033	0	1	2	4	5	5	1
RC columns and beams	B1041	0	1	3	5	5	5	1
RC beam-column joints	B1046	0	1	4	5	5	5	1
Interior doors in URM infill	C1021	0	2	2	2	2	2	2
Suspended ceilings	C3032	0	2	3	3	3	3	2
Cold/hot water services	D2021, D2022	0	2	3	3	3	3	2
URM Infills	B1051	0	2	3	4	5	5	3
Windows in URM infill	B2021	0	3	3	3	3	3	3
Curtain walls	B2022	0	2	3	3	3	3	3
Boilers	D3021	0	2	2	2	2	2	4
Air distribution systems	D3041	0	2	2	2	2	2	4
Energy control panels	D3067	0	2	2	2	2	2	4
Pendant lights	C3034	0	2	2	2	2	2	5
Regular stairs	C2011	0	1	4	4	4	4	6
Chairs and desks	E2022.2xx	0	2	2	2	2	2	7
Other equipment and furnishings	E2022.xxx	0	1	1	1	1	1	7

In addition to the time required for repair work, it is equally important to consider the downtime caused by delays, referred to as impeding factor delays, as outlined in Section 5.5.1. While the lognormal cumulative distribution functions, representing these delays, identified in the work of (Molina et al. 2022) were used herein, future investigation should focus on identifying those specifically tailored to the Italian context. As mentioned, the repair and reconstruction process, in the Italian context, is generally based on public loans. Hence, the framework considers that public loans will finance 100% of the realisations. After determining the delays associated with

repairs and impeding factors, the total downtime required to achieve the target recovery state can be calculated.

Figure 5.13 illustrates the median downtime for the re-occupancy and functional recovery states for the considered return periods, as a function of the structural model and hazard level. The return periods for the SLO (45 years), SLD (75 years), SLV (712 years) and SLC (1463 years) limit states are highlighted as these correspond to the return periods foreseen by the Italian code (MIT 2018). As expected, downtime for RO is consistently lower than that for FR across all cases.

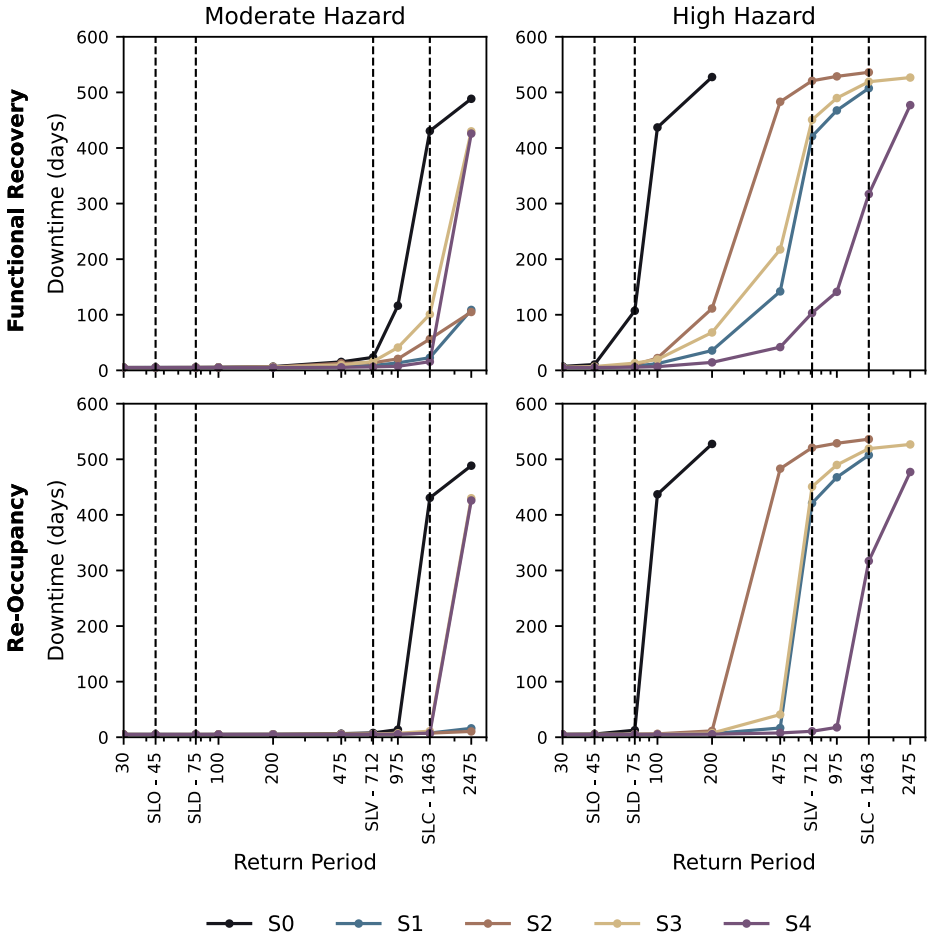

Figure 5.13 Median downtime (in days) for re-occupancy (RO) and functional recovery (FR) states, for different return periods: SLO (45 years), SLD (75 years), SLV (712 years) and SLC (1463 years).

Additionally, buildings located in the MH site experience shorter downtimes than those in HH site. It is also demonstrated that for both sites, regardless of the adopted retrofitting solution, the median downtime estimate is consistently lower than the case of as-built (S0). For the MH site and the RO state, downtime is nearly negligible, less than 10 days, at intensity levels corresponding to the SLO, SLD and SLV limit states. However, S0 exhibits the highest downtime for the SLC limit states, while the retrofitted solutions exhibit near-negligible times, remaining under 15 days. For the HH site and for all retrofitting solutions, median downtime estimates remain minimal for the SLO and SLD limit states for both recovery states, whereas the S0 configuration of the building's median downtime to reach the functional recovery state is estimated at more than 100 days for the 75-year return period (SLD). Moreover, significantly higher downtimes are obtained for both recovery states at the SLV and SLC limit states, with the only exception of the S4 retrofitting solution for the 712-year return period, which still exhibits less than 15 days of downtime for the RO state.

Although downtimes are estimated to be near-negligible for more frequent earthquake intensities, they are not zero due to the necessary inspection time. Conversely, estimated downtimes may reach higher values for longer return periods, typically between 300 and 550 days. These extended downtimes primarily indicate that the median scenario corresponds to irreparable cases. Considering the impedance factors of demolition, financing and engineering, along with the time required for reconstruction, the reconstruction duration falls within this range. For the HH location, S_2 exhibits the highest downtime, followed by S_3, S_1, and S_4, across all intensity levels and recovery states. However, for the MH location, the highest estimated downtime is for S_3, followed by S_2, S_1 and S_4. In addition to the recovery time trajectory, the probability of being in a specific target recovery state, $P(RS = rs_i \mid RP)$, immediately after an earthquake was also evaluated, as shown in Figure 5.14. The analysed recovery scenarios include the five recovery states and the irreparable case. It is observed that, regardless of the site, retrofitting alternative and intensity levels, the full recovery (F_R) state is impeded. For the MH site, all structural configurations guarantee the re-occupancy of the building for 45- and 75-year return periods (corresponding to SLO and SLD limit states). On the contrary, for the HH site, the hindrance of lower-level recovery states becomes more pronounced, with retrofitted models generally exhibiting a higher probability of being limited to the maximum FR state.

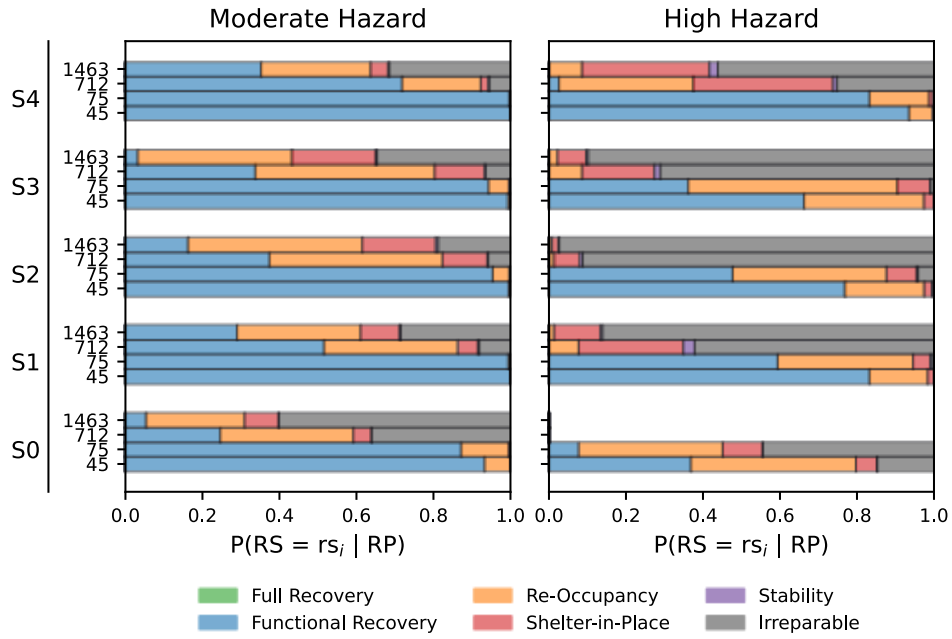

Figure 5.14 Probability of each alternative being in a specific recovery state, per return period (RP) and hazard level.

Additionally, the probability of preventing different recovery states varies more significantly depending on the considered retrofitting option and the return period. By increasing the return period, while slight changes between the retrofitting alternatives in terms of P(RS = rs_i | RP) are noticed at the MH site, significant variations are obtained at the HH site. In particular, the probability of being irreparable in the case of S1 and S3 is much higher than that observed for S_4, as well as the probability of being in RO and SiP states is less than that observed for S_4. It is also noted that probabilities for the S_0 configuration at the HH site for the 712- and 1463-year return periods are not presented, as the building is solely experiencing collapse for such intensity levels, rendering recovery state assessments irrelevant. In order to clearly identify the difference between all the retrofitting alternatives, as a function of the hazard levels, the recovery times for both RO (DT_{RO}) and FR (DT_{FR}) states are summarised in Table 5.18.

Table 5.18 Recovery time to achieve RO (DTRO) and FR (DTFR) states for the different retrofitting alternatives, as a function of the code return periods and hazard levels.

Site	T_r	S1		S2		S3		S4	
	(years)	DT_{RO}	DT_{FR}	DT_{RO}	DT_{FR}	DT_{RO}	DT_{FR}	DT_{RO}	DT_{FR}
MH	45	5	5	5	5	5	5	5	5
	75	5	5	5	5	5	5	5	5
	712	6	9	6	14	6	16	5	6
	1463	8	23	7	56	11	101	7	16
HH	45	5	6	5	6	5	7	5	5
	75	5	8	5	10	5	13	5	6
	712	421	421	521	521	451	451	11	103
	1463	508	508	536	536	519	519	317	317

Note: T_r:return period

5.5.4 Downtime-based optimal interventions

The obtained EAD is presented in Table 5.19. While at the MH site the differences in terms of EAD between the retrofitting alternatives are negligible, they become more significant at the HH site.

Table 5.19 Expected annual downtime (days) for each alternative, as a function of the hazard level.

Alternative	Medium Hazard	High Hazard
S0	1.83	16.70
S1	0.55	3.51
S2	0.66	6.81
S3	0.70	4.54
S4	0.47	1.53

The final ranking of the different retrofitting alternatives, considering both scenarios and per hazard level, is provided in Table 5.20. Regarding the first scenario, and for both MH and HH, S_1 consistently exhibits the lowest relative closeness value, making it the least preferred alternative. On the other hand, S_2, S_3, and S_4 show higher relative closeness values, with S_2 being the optimal alternative for MH and S_3 for HH. Interestingly, the ranking of alternatives varies slightly between the two regions: for MH, the order is $S_2 > S_3 > S_4 > S_1$ (from highest to lowest), while for HH the ranking shifts to $S_3 > S_4 > S_2 > S_1$. It is thus recommended that, before ranking different retrofitting alternatives, each of them should be designed to reach predefined performance objective thresholds, corresponding to the minimum acceptable performance and then, by applying the MCDM, the optimal solution can be identified.

As for the second scenario, S_1 exhibits the lowest relative closeness value, making it the least preferred alternative, regardless of the hazard level. Conversely, S_2, S_3, and S_4 show higher relative closeness values, with S_2 being the optimal alternative for MH and S_4 for HH. When comparing both scenarios, while no changes in the ranking were noticed at the MH site, S_4 became the most preferable solution for HH. As also noticed before, the ranking of alternatives varies slightly between the two regions: for MH, the order is $S_2 > S_3 > S_4 > S_1$ (from highest to lowest), while for HH, the ranking shifts to $S_4 > S_3 > S_2 > S_1$. Finally, while in case of the HH site, the preferable retrofitting alternative (S_4) corresponds to the best performing one in terms of downtime at FR state, S_2 is not the best one in terms of EAD at the MH site; this is due to the small differences between EAD values for the different retrofitting alternatives, making the impact of EAD on the final ranking less relevant.

Table 5.20 Ranking of the different retrofitting alternatives, per hazard level, considering expected annual downtime (EAD) as DV.

Rank	MCDM-1				MCDM-2			
	Medium Hazard		High Hazard		Medium Hazard		High Hazard	
	Alt.	RC	Alt.	RC	Alt.	RC	Alt.	RC
1	S_2	0.708	S_3	0.603	S_2	0.680	S_4	0.588
2	S_3	0.645	S_4	0.595	S_3	0.616	S_3	0.554
3	S_4	0.532	S_2	0.577	S_4	0.530	S_2	0.517
4	S_1	0.374	S_1	0.383	S_1	0.405	S_1	0.425

5.6 CONCLUDING REMARKS

This chapter assessed the influence of different seismic hazard levels and climate conditions on the preferential ranking of combined energy and seismic retrofitting interventions through the employment of a multi-criteria decision-making (MCDM) framework, with the aim of enhancing the sustainability of existing buildings. Additionally, this study assessed the accuracy of employing a practice-oriented approach in the estimation of decision variables related to the seismic performance of a building within the MCDM framework, namely the expected annual losses (EAL), the annual probability of failure (APF), and expected annual environmental impact (EAEI).

To this end, a case-study school building was selected, and four seismic retrofitting solutions, combined with three energy-based interventions, were identified. The

case-study building was assumed as located in six different sites in Italy, characterised by two levels of seismic hazard (moderate (M) and high (H)) and with different climatic conditions, namely cold (C), moderate (M), and warm (W). The performance of the building, in its as-built and retrofitted conditions, was then analysed considering the simplified approach and compared with a more detailed one. Finally, an MCDM framework was employed to obtain the overall ranking of the different alternatives and identify the optimal combination of retrofitting schemes, again using both detailed and simplified approaches.

The preliminary assessment of the structural retrofit models resulted in an effectiveness ranking of the retrofit alternatives as $S_4 > S_1 > S_3 > S_2$ and $S_1 > S_4 > S_3 > S_2$ for the medium and high hazard sites, respectively, for the Life Safety limit state. Regarding the APF values, notable differences were obtained. While the approaches yielded similar results for medium-hazard levels, for the high-hazard level, the simplified approach produces lower APF values than the detailed one in high-hazard sites, which needs to be considered as a trade-off for computational efficiency. Regarding the EAL and EAEI, the simplified approach tends to overestimate EAL with respect to the detailed one. Such overestimation can be attributed to the simplified nature of the Sismabonus procedure, which needed to be incorporated into the current Italian seismic risk guidelines in order to enhance its usability by practitioners. Nevertheless, the order of magnitude is kept the same between the different methodologies. When employing the MCDM framework to obtain the overall ranking of the different alternatives and identify the optimal combination of retrofitting schemes combined with the different detailed and simplified approaches, similar relative closeness values among several alternatives pointed towards the identification of a group of preferable alternatives, instead of the most preferable one. By quantifying the 25_{th} and 75^{th} percentiles of the relative closeness (RC) values for both detailed and simplified approaches, three distinct groups of alternatives were identified: less preferable (RC value below the 25^{th} percentile), relatively preferable (RC value between the 25^{th} and the 75^{th} percentile), and most preferable (RC value above the 75^{th} percentile). When the relative closeness values of different alternatives are very similar, instead of selecting the optimal solution, this approach allows decision-makers to pick the solution to adopt from a group of alternatives with similar relative performance, depending on specific needs and objectives.

Globally, the results showed distinct classifications for medium- and high-seismic hazard sites. For high-hazard ones, the influence of the seismic hazard is highly present since rankings tend to be grouped by the structural retrofit scheme, and, in

most cases, the most severe energy retrofit alternative was generally preferred over the other alternatives. In medium-seismic hazard sites, rankings are equally affected by both types of retrofit intervention. For both levels of hazard, S_1 is consistently the least preferable structural retrofit alternative. Even though its seismic performance is relatively better than alternatives S_2 and S_3, its high cost tends to penalize it on the MCDM framework. Comparing both approaches, results show that in high-hazard areas, rankings stay consistent, while in medium-hazard sites, detailed and simplified approaches yield different results. In the detailed one, both energy and seismic retrofit play crucial roles, leading to varied rankings, where the simplified method aligns rankings based on the structural retrofit scheme. Despite similar performance values (APF, EAL, and EAEI), the MCDM struggles to point clear preferable alternatives. Nevertheless, the results obtained through the simplified approach are promising, given that the differences observed in the optimal combination ranking, compared to the detailed counterpart, are mainly justified by the relative distance between different alternatives that affect the mathematical process of the MCDM procedure. In fact, although further investigations will support more general conclusions on the reliability of the simplified, practice-oriented approach, from an overall perspective, the employment of the detailed and simplified approaches led to similar results in the obtained ranking, showing the benefits of employing tools that require less time and computational demand.

This chapter also highlighted the importance of incorporating post-earthquake downtime as an additional decision variable in the MCDM framework for selecting optimal seismic retrofitting interventions. By introducing a downtime-based metric, namely the expected annual downtime (EAD), the evaluation of retrofitting alternatives became more comprehensive, capturing the ability of the building to restore occupancy and functional use after an earthquake. In the considered case-study, all retrofitting solutions substantially reduced median downtime for both re-occupancy (RO) and functional recovery (FR) states compared to the as-built configuration. The effect of downtime on the preference ranking of retrofitting alternatives was particularly evident under high seismic hazard conditions, where achieving full recovery was generally impeded and the probability of functional recovery decreased with increasing hazard intensity. Integrating EAD into the MCDM framework therefore allows decision-makers to consider both the resilience and usability if building post-event, providing a more realistic basis for prioritising retrofit interventions.

CHAPTER 6

Conclusions

6 CONCLUSIONS

6.1 SUMMARY

This thesis addressed the urgent need for integrated and scalable methodologies capable of supporting large-scale decision making for the renovation and seismic retrofitting of existing buildings. Based on the results presented in the previous chapters, the main contributions, corresponding to the objectives initially set (Section 1.2), can be summarised as follows:

1) **Integrated national-scale prioritisation**: the proposed framework effectively identified priority areas for combined seismic and energy retrofitting by integrating technical, socio-economic, and equity concerns. This comprehensive approach not only highlights regions where interventions are most urgently needed, but also provides policymakers with clear, evidence-based guidance for allocating resources in an equitable and efficient manner. By capturing the interplay between different vulnerability and performance indicators, the framework ensures that large-scale renovation strategies are both targeted and balanced, supporting resilient and sustainable decision-making across large building stocks.
2) **Regional-scale renovation planning:** targeted retrofit interventions applied to the higher-risk building taxonomy classes within the highest-priority region can achieve substantial and measurable reductions in seismic risk at the urban scale. Retrofit viability is strongly governed by design code level and building height. Sequencing investments by decreasing risk level class ensures that the greatest risk reduction is concentrated in the earliest intervention phases, maximising the efficiency of resource allocation across the building stock.
3) **Generalised loss and impact assessment functions**: their development overcame the limitations of building-specific, computationally intensive risk assessment methodologies. These functions enable rapid and reliable estimation of expected economic losses and environmental impacts, making them suitable for both regional-scale studies and single-building evaluations. Their computational efficiency and flexibility also allow their application in large-scale risk assessment studies or research applications that require the assessment of numerous intervention alternatives, such as optimisation approaches involving a large initial population of feasible

solutions, where the use of detailed component-based approaches would be impractical.

4) **Optimal selection of retrofitting strategies**: by employing a multi-criteria decision-making (MCDM) framework, this research demonstrated how variations in seismic hazard and climatic conditions can significantly influence the ranking of combined seismic and energy retrofit alternatives. The findings also confirmed that the proposed framework effectively captures the complex trade-offs among technical, economic, environmental, and social variables, enabling the identification of the most suitable retrofit solutions. Furthermore, the MCDM approach proved particularly valuable in cases where multiple alternatives exhibit similar performance, allowing decision-makers to select among a group of almost comparably effective strategies rather than having to opt for a single optimal solution.
5) **Bridging research and practice**: the simplified, practice-oriented approach developed herein proved suitable for professional application, enabling practitioners to estimate key decision variables and make informed choices for real-world retrofitting projects, thereby enhancing both feasibility and impact of interventions. Moreover, these functions can support research applications that require the assessment of numerous intervention alternatives, such as optimisation approaches involving a large initial population of feasible solutions, where traditional component-based assessment methodologies would be computationally unfeasible.

Together, these contributions provide a consistent body of work that enhances the efficiency, scalability, and applicability of integrated seismic and energy assessment tools, while supporting sustainable and socially informed decision-making.

It is also worth noting the role of national context in shaping and transferring the proposed frameworks. The work spans two country settings: i. Portugal, for the national prioritisation, regional renovation scenarios, and development of storey loss and environmental impact functions, and ii. Italy, for the single-building retrofit decision-making case study. While Italy is many times seen as a benchmark in Europe regarding seismic risk, with vast post-earthquake data, validated tools, and an established seismic risk classification framework, Portugal has a comparatively limited body of research in this area, lacking the depth of post-earthquake observational data and component-level consequence functions, needed to fully support building-scale loss assessment without relying on proxy data from

analogous contexts. Nevertheless, both countries share similar building stock characteristics, share similar regulations, and face comparable challenges of seismic vulnerability and energy inefficiency, making the Italian data directly relevant to the Portuguese context. Moreover, the experience of working across two European contexts provides useful insight for future efforts to extend these frameworks elsewhere, particularly in Southern and Eastern Europe where seismic vulnerability, energy inefficiency, and socioeconomic disparity often coincide.

6.2 RESEARCH FINDINGS

6.2.1 Priority analysis framework for equitable seismic and energy-efficiency renovation of residential buildings applied to mainland Portugal

Chapter 2 proposed a holistic prioritisation framework that integrates seismic risk, energy performance, and socioeconomic vulnerability to identify where retrofitting or renovation efforts should be targeted. The framework relies on engineering-based, state-of-the-art indicators, is scalable to other countries, and enables national-scale strategies aligned with resilience, sustainability, and equity objectives. The major findings are summarised as follows:

- Prioritisation patterns vary significantly depending on the combination of indicators considered, which highlights the importance of avoiding single-sector approaches, as focusing solely on energy or seismic needs can lead to sub-optimal long-term outcomes.
- From a seismic perspective, the Lisbon Metropolitan Area (AML) and the Algarve regions were identified as the most critical areas, while most regions in Norte and Centro exhibited lower seismic vulnerability.
- In terms of energy performance-based prioritisation, the AML, Algarve, Norte, Lisboa, and Castelo Branco showed significant inefficiencies, whereas districts in the Centro region ranked lower, indicating better efficiency and reduced urgency for interventions.
- Considering socioeconomic vulnerability-based prioritisation, Faro, Viana do Castelo, and Castelo Branco emerged as critical due to social challenges, while Centro regions districts displayed greater resilience.
- An integrated assessment combining seismic, energy, and socioeconomic indicators highlighted Algarve, AML, and some districts in Norte as top

priorities, whereas districts such as Coimbra and Viseu ranked lower, supporting a balanced retrofitting strategy across physical, energy, and social dimensions.

- The framework also provided guidance for identifying the most critical building taxonomy classes, supporting the planning of national-scale renovation scenarios.

6.2.2 Regional renovation scenarios for seismic upgrading of RC buildings

Chapter 3 proposed a comprehensive methodology for seismic risk assessment and retrofit evaluation of the Lisbon RC building stock, integrating structural analysis, loss estimation, and economic feasibility assessment to support retrofit policy in Portugal. The major findings are summarised as follows:

- No code (CDN) and low code (CDL) RC buildings of one to six storeys were identified as the primary targets for seismic interventions, with single-storey CDN emerging as the most vulnerable and the most responsive to retrofit in terms of loss reduction.
- Both retrofit strategies - RC jacketing combined with FRP wrapping (RCJ+FRP) and steel jacketing combined with FRP wrapping (STJ+FRP) - effectively reduce seismic risk across all taxonomies. RCJ+FRP consistently outperformed STJ+FRP in structural improvement and loss reduction and should be preferred where maximum risk mitigation is the objective.
- STJ+FRP enabled a more rapid recovery of its investment due to lower upfront costs, making it a viable option where budget constraints or shorter planning horizons apply.
- Retrofit feasibility is strongly governed by design code level and building height: low-rise CDN buildings offer the most favourable cost-benefit ratios and shortest payback times, while retrofitting mid- and high-rise CDL buildings remains economically marginal or unfeasible within the assumed planning horizon.
- The phased intervention scenario confirmed that the greatest risk reduction per unit of investment is concentrated in the earliest phases, underscoring the importance of prioritising the most vulnerable taxonomies first.
- The derived fragility and vulnerability functions are directly applicable to national risk models, and the methodology is transferable to other

Portuguese regions and international contexts facing similar challenges of ageing building stocks and elevated seismic exposure.

6.2.3 Storey loss and environmental impact functions for existing reinforced concrete buildings

In Chapter 4, storey loss and environmental impact functions were developed for reinforced concrete buildings with limited seismic capacity. The methodology combined typical components, corresponding fragility curves, and repair costs and environmental impact consequence functions. The proposed functions provide a computationally efficient alternative to detailed component-based assessment such as FEMA P-58 (FEMA 2018a). The major findings are summarised as follows:

- Storey-based loss and impact functions offers a robust and scalable solution for large-scale seismic risk studies, significantly reducing computational demand while maintaining a high degree of accuracy.
- Generalised functions were successfully adapted to the Portuguese context, confirming their applicability across different national datasets and construction practice.
- A comparative application using a typical Portuguese RC building further showed a strong agreement between the storey-based estimates and the FEMA P-58 component-based ones, both in terms of loss curves and annualised metrics. This consistency further validates the reliability of the proposed method as an effective alternative where detailed structural information is limited or where large portfolios of buildings need to be assessed.

6.2.4 Retrofitting decision making for single buildings

Chapter 5 investigated how different seismic hazard levels, climatic conditions, and methodological choices influence the prioritisation of combined seismic and energy retrofitting interventions. Using a reinforced concrete school building, belonging to the Italian school building stock, the analysis explored nine distinct site scenarios defined by the combination of three seismic hazard levels (low, moderate, and high) and three climate zones (cold, moderate, and warm). For the scenarios considering moderate and high hazard levels, the building was assessed in both its as-built and retrofitted configurations, using four seismic retrofitting strategies and three energy renovation solutions. A wide set of decision variables (economic, environmental,

technical) were considered and the ones associated with the seismic performance of the building were estimated using both a detailed performance-based and a simplified approach. The results were subsequently incorporated into a Multi Criteria Decision Maling (MCDM) framework to understand how different locations and different assessment method influence the final ranking of retrofit alternatives. The major findings are summarised as follows:

- In high seismic hazard sites, structural retrofit dominates the ranking, with energy retrofit preferences varying with climate conditions. In medium seismic hazard sites, both energy and structural retrofits contribute equally to decision-making. In general, in colder climates, energy retrofit alternatives with better performance are generally preferred, whereas in warmer climates preference shifts toward structural retrofitting, with the type depending on the seismic hazard level.
- The comparison between simplified and detailed methodologies showed consistent trends but also highlighted systematic differences, where the simplified approach tends to underestimate the annual probability of failure in high-hazard areas and overestimate the expected annual losses, owing to the conservative and aggregated nature of its assumptions. For high-hazard regions, both the simplified and detailed approaches led to very similar prioritisation patters, indicating that simplified tools can be confidently used in contexts where seismic demand dominates the decision process. In moderate hazard regions, however, rankings obtained from the two approaches diverged more noticeably, reflecting the fact that both seismic and energy factors contribute comparably to the overall performance. In these cases, the simplified method tended to cluster alternatives according to the structural retrofit scheme, while the detailed method captured more nuances interactions between energy and seismic improvements.
- In the case of retrofit alternatives exhibiting very similar performance values, the MCDM framework is more effective at identifying groups of preferable options rather than isolating a single optimal solution. This offers decision makers greater flexibility, allowing them to select among several comparably performing strategies.
- Considering downtime, alongside traditional decision variables, allows decision-makers to capture not only structural and energy performance but also post-event usability, offering a more comprehensive basis for prioritising retrofit interventions. The impact of downtime on the preference ranking of

retrofitting alternatives was especially pronounced in high seismic hazard scenarios, where full recovery was often unattainable and the likelihood of functional restoration diminished as hazard intensity increased.

6.3 FUTURE DEVELOPMENTS

The findings obtained from this doctoral research point to several promising steps for future research and developments in the field of integrated seismic, environmental and energy assessment and decision-making. Hence, as a final remark, suggestions for future works are identified and listed as follow:

- **Framework and data improvements.** To ensure that the proposed frameworks remain relevant and reliable, it is essential to regularly update all input datasets. This is not only due to the time-dependence of the data but also to the likelihood that new data sources will emerge over time. Although most of the information used in this study originates from official government data (i.e., typically collected and published by governmental agencies) or obtained through rigorous research methodologies, maximising their reliability and relevance, some variables (i.e., energy poverty and risk awareness) were derived from other studies. Once officially published data becomes available, the framework should be updated to further enhance the accuracy and robustness of the results. The proposed framework is scalable to different analysis contexts, i.e., the same priority analysis rationale can be applied to different municipalities within a region or different parishes within a municipality. The same reasoning can also be applied to building typologies, i.e., the priority analysis results could be disaggregated and analysed from a building taxonomy viewpoint, comparing different classes. Consequently, future studies could focus on higher-resolution analyses, enabling a deeper understanding of vulnerabilities linked to specific building typologies, demographic factors, and social context. This would facilitate more precise decision-making at the local level, helping to identify targeted interventions and develop more effective, tailored mitigation strategies. Moreover, by linking building exposure data with optimisation algorithms, this framework can efficiently identify high-priority targets and determine the most effective combination of retrofitting measures. The framework can also be expanded to include additional hazards, such as floods, windstorms, or wildfire, allowing for a more thorough risk assessment and priority analysis to guide decision makers.

- **Advancements of storey loss and environmental impact function modelling.** While the developed storey loss functions (SLF) and storey environmental impact functions (SEIF) models provide a robust foundation, further validation across a broader range of building typologies (including also other construction materials) and construction periods would strengthen their generality and wider application. Future work could also expand the employed consequence models by incorporating more comprehensive post-earthquake repair costs and refining environmental impact estimates associated with both damage and retrofit interventions. In particular, the development of storey repair time and downtime functions would complete the suite of decision variables required for a fully resilience-based assessment framework, providing a more comprehensive evaluation of post-earthquake recovery and supporting the prioritisation of retrofit interventions as well as the design of new buildings.
- **Further exploration of MCDM under simplified approaches.** To fully assess the reliability and limitations of simplified seismic performance metrics, additional validation is needed across different building types, retrofit strategies, and locations. Scenario-based analysis, combining different seismic hazard conditions with anticipated climate evolution, would further support long-term planning by helping stakeholders understand how retrofit priorities might shift over time. Additionally, the MCDM framework, currently tailored to seismic hazard, can be extended in the future to accommodate multiple perils, in alignment with the growing need for resilient design in multi-hazard environments.
- **Integrated decision tool.** Building upon the methods developed in this dissertation, an important direction for future work lies in the creation of a unified digital tool/platform that seamlessly integrates hazard, exposure, vulnerability, energy performance, environmental impacts, and socioeconomic data. Such an integrated risk platform would provide a coherent environment for managing the full decision-making process, from data acquisition to intervention planning. Within this framework, the platform would incorporate a risk-assessment module that dynamically updates risk levels in line with new information, a prioritisation module capable of evaluating renovation needs across multiple metrics, and a renovation-scenario component that supports the simulation and comparison of alternative strategies. By allowing decision-makers to revise system inputs according to the evolving status of renovation interventions, the tool would

ensure that assessments remain aligned with current building conditions and with updated prioritisation outcomes, ultimately enabling more transparent, effective and adaptive planning.

- **Towards practical implementation:** Beyond research directions, it is worth reflecting on how the tools and frameworks developed in this thesis could be implemented in practice. For the national prioritisation framework, a natural next step would be its integration into national renovation planning processes, to help inform how public funding is allocated across regions. For the renovation scenarios, future developments could include extending the analysis to other building taxonomies and regions, and evaluating multiple intervention options through multi-criteria decision making or multi-objective optimisation approaches. Reinforcement learning techniques could also be explored to derive long-term optimal renovation policies, enabling dynamic adaptation of investment strategies as new data and updated risk assessments become available. For the storey loss and environmental impact functions, packaging them into accessible tools would allow practitioners to run rapid loss and embodied carbon assessments without needing detailed component-level data. Moreover, a simple web-based interface with default settings for the Portuguese context would make their adoption much more straightforward. For the single-building MCDM framework, a promising pathway would be its integration into national retrofit incentive schemes, along the lines of the Italian Sismabonus, where a structured but streamlined decision procedure could help both engineers and building owners identify and justify the most suitable intervention. Across all these tools, engagement with professional engineering bodies, public authorities responsible for building safety and energy policy, and continuing education programmes would be key to ensuring they actually reach the people they are designed to assist.

REFERENCES

Ademovic N, Formisano A, Penazzato L, Oliveira DV (2022) Seismic and energy integrated retrofit of buildings: A critical review. Front Built Environ 8:963337. https://doi.org/10.3389/fbuil.2022.963337

Akhoundi F, Vasconcelos G, Lourenço P, et al (2018) In-plane behavior of cavity masonry infills and strengthening with textile reinforced mortar. Engineering Structures 156:145–160. https://doi.org/10.1016/j.engstruct.2017.11.002

Aljawhari K, Gentile R, Galasso C (2023a) Simulation-based consequence models of seismic direct loss and repair time for archetype reinforced concrete frames. Soil Dynamics and Earthquake Engineering 172:107979. https://doi.org/10.1016/j.soildyn.2023.107979

Aljawhari K, Gentile R, Galasso C (2024) Earthquake-induced environmental impacts for residential Italian buildings: Consequence models and risk assessment. Journal of Building Engineering 84:108149. https://doi.org/10.1016/j.jobe.2023.108149

Aljawhari K, Gentile R, Galasso C (2022) A fragility-oriented approach for seismic retrofit design. Earthquake Spectra 38:1813–1843. https://doi.org/10.1177/87552930221078324

Aljawhari K, Gentile R, Galasso C (2023b) Simulation-based consequence models of seismic direct loss and repair time for archetype reinforced concrete frames. Soil Dynamics and Earthquake Engineering 172:107979. https://doi.org/10.1016/j.soildyn.2023.107979

Aljawhari K, Gentile R, Galasso C (2025) Beyond Direct Economic Losses: An Integrated Approach to Seismic Retrofit Considering Sustainability and Indirect Losses. Earthq Engng Struct Dyn 54:1737–1758. https://doi.org/10.1002/eqe.4324

Almufti I, Willford M (2013) Resilience-based Earthquake Design Initiative for the Next Generation of Buildings. REDi™ Rating System 1–133

Ancheta TD, Darragh RB, Stewart JP, et al (2014) NGA-West2 Database. Earthquake Spectra 30:989–1005. https://doi.org/10.1193/070913EQS197M

Anelli A, Mori F, Moscatelli M (2023) Seismic fragility and vulnerability curves for the Italian residential building stock. Structure and Infrastructure Engineering 19:113–133. https://doi.org/10.1080/15732479.2021.1936568

ANIA (2024) AllontAniamo i rischi, RimAniamo protetti. Edition (2024). https://www.ania.it/allontaniamo-i-rischi

APA (2024) Fator de Emissão da Eletricidade - 2024 (Ficha técnica)

Applied Technology Council (ATC) (1996) Seismic Evaluation and Retrofit of Concrete Buildings. Report No. ATC-40: 1–2

Arroyo D, Ordaz M, Teran-Gilmore A (2015) Seismic Loss Estimation and Environmental Issues. Earthquake Spectra 31:1285–1308. https://doi.org/10.1193/020713EQS023M

Asadi E, Salman AM, Li Y (2019) Multi-criteria decision-making for seismic resilience and sustainability assessment of diagrid buildings. Engineering Structures 191:229–246. https://doi.org/10.1016/j.engstruct.2019.04.049

Aslani H, Miranda E (2005) Probabilistic earthquake loss estimation and loss deaggregation in buildings. Stanford University, Stanford University

Baggio C, Bernardini A, Colozza R, et al (2007) Field Manual for post-earthquake damage and safety assessment and short term countermeasures (AeDES)

Bal İE, Crowley H, Pinho R, Gülay FG (2008) Detailed assessment of structural characteristics of Turkish RC building stock for loss assessment models. Soil Dynamics and Earthquake Engineering 28:914–932. https://doi.org/10.1016/j.soildyn.2007.10.005

Baltzopoulos G, Baraschino R, Iervolino I, Vamvatsikos D (2017) SPO2FRAG: software for seismic fragility assessment based on static pushover. Bulletin of Earthquake Engineering 15:4399–4425. https://doi.org/10.1007/s10518-017-0145-3

Belleri A, Marini A (2016) Does seismic risk affect the environmental impact of existing buildings? Energy and Buildings 110:149–158. https://doi.org/10.1016/j.enbuild.2015.10.048

Bernardo V, Campos Costa A, Candeias P, Costa A (2022) Seismic vulnerability assessment and fragility analysis of pre-code masonry buildings in Portugal. Bulletin of Earthquake Engineering 20:6229–6265. https://doi.org/10.1007/s10518-022-01434-8

Binici B, Yakut A, Kadas K, et al (2023) Performance of RC buildings after Kahramanmaraş Earthquakes: lessons toward performance based design. Earthq Eng Eng Vib 22:883–894. https://doi.org/10.1007/s11803-023-2206-8

Bournas DA (2018) Concurrent seismic and energy retrofitting of RC and masonry building envelopes using inorganic textile-based composites combined with insulation materials: A new concept. Composites Part B: Engineering 148:166–179. https://doi.org/10.1016/j.compositesb.2018.04.002

Braga F, Manfredi V, Masi A, et al (2011) Performance of non-structural elements in RC buildings during the L'Aquila, 2009 earthquake. Bull Earthquake Eng 9:307–324. https://doi.org/10.1007/s10518-010-9205-7

Brzev S, Scawthorn C, Charleson AW, et al (2013) GEM Building Taxonomy Version 2.0. GEM Technical Report 02:188. https://doi.org/doi:%2010.13117/GEM.EXP-MOD.TR2013.02.

Burton CG, Silva V (2016) Assessing integrated earthquake risk in OpenQuake with an application to Mainland Portugal. Earthquake Spectra 32:1383–1403. https://doi.org/10.1193/120814EQS209M

Calvi GM (2013) Choices and criteria for seismic strengthening. Journal of Earthquake Engineering 17:769–802. https://doi.org/10.1080/13632469.2013.781556

Calvi GM (2025) Mallet–Milne lecture 2025: risk management and rehousing of people displaced by earthquake disasters. Bulletin of Earthquake Engineering 23:2961–3041

Calvi GM, O'Reilly GJ, Andreotti G (2021) Towards a practical loss-based design approach and procedure. Earthquake Engineering & Structural Dynamics

50:3741–3753. https://doi.org/https://doi.org/10.1002/eqe.3530Digital Object Identifier (DOI)

Calvi GM, Sousa L, Ruggeri C (2016) Energy Efficiency and Seismic Resilience: A Common Approach. In: Multi-hazard Approaches to Civil Infrastructure Engineering. Springer International Publishing, Cham, pp 165–208

Cardone D (2016a) Fragility curves and loss functions for RC structural components with smooth rebars. Earthquakes and Structures 10:1181–1212. https://doi.org/10.12989/EAS.2016.10.5.1181

Cardone D (2016b) Fragility curves and loss functions for RC structural components with smooth rebars. Earthquake and Structures 10:1181–1212. https://doi.org/10.12989/eas.2016.10.5.1181

Cardone D, Gesualdi G, Perrone G (2019) Cost-Benefit Analysis of Alternative Retrofit Strategies for RC Frame Buildings. Journal of Earthquake Engineering 23:208–241. https://doi.org/10.1080/13632469.2017.1323041

Cardone D, Perrone G (2015) Developing fragility curves and loss functions for masonry infill walls. Earthquakes and Structures 9:257–279. https://doi.org/10.12989/EAS.2015.9.1.257

Carofilis W, Clemett N, Gabbianelli G, et al (2022a) Influence of Parameter Uncertainty in Multi-Criteria Decision-Making When Identifying Optimal Retrofitting Strategies for RC Buildings. Journal of Earthquake Engineering. https://doi.org/10.1080/13632469.2022.2087794

Carofilis W, Gabbianelli G, Monteiro R (2021) Assessment of Multi-Criteria Evaluation Procedures for Identification of Optimal Seismic Retrofitting Strategies for Existing RC Buildings. Journal of Earthquake Engineering 26:5539–5572. https://doi.org/10.1080/13632469.2021.1878074

Carofilis W, Gabbianelli G, Monteiro R (2022b) Assessment of Multi-Criteria Evaluation Procedures for Identification of Optimal Seismic Retrofitting Strategies for Existing RC Buildings. Journal of Earthquake Engineering 26:5539–5572. https://doi.org/10.1080/13632469.2021.1878074

Carpanese P, Follador V, Donà M, Da Porto F (2025) A methodology for selecting optimal seismic risk mitigation strategies for the Italian residential masonry

built heritage. International Journal of Disaster Risk Reduction 105897. https://doi.org/10.1016/j.ijdrr.2025.105897

Carreño ML, Cardona OD, Barbat AH (2012) New methodology for urban seismic risk assessment from a holistic perspective. Bull Earthquake Eng 10:547–565. https://doi.org/10.1007/s10518-011-9302-2

Caruso M, Couto R, Pinho R, Monteiro R (2023a) Decision-making approaches for optimal seismic/energy integrated retrofitting of existing buildings. Frontiers in Built Environment 9:1–12. https://doi.org/10.3389/fbuil.2023.1176515

Caruso M, Pinho R, Bianchi F, et al (2021) Integrated economic and environmental building classification and optimal seismic vulnerability/energy efficiency retrofitting. Bulletin of Earthquake Engineering 19:3627–3670. https://doi.org/10.1007/s10518-021-01101-4

Caruso M, Pinho R, Bianchi F, et al (2023b) Multi-criteria decision-making approach for optimal seismic/energy retrofitting of existing buildings. Earthquake Spectra 39:191–217. https://doi.org/10.1177/87552930221141917

Caruso M, Pinho R, Bianchi F, et al (2020) A life cycle framework for the identification of optimal building renovation strategies considering economic and environmental impacts. Sustainability (Switzerland) 12:1–20. https://doi.org/10.3390/su122310221

Caruso M, Silva V, Aljawhari K, et al (2024) Unveiling the Environmental Impact of Earthquakes in Europe

Carvalho BP, Fonseca M, Peralta S (2023) Pobreza Energética em Portugal: Uma análise municipal. Portugal, Balanço Social

Caterino N, Iervolino I, Manfredi G, Cosenza E (2008) Multi-Criteria Decision Making for Seismic Retrofitting of RC Structures. Journal of Earthquake Engineering 12:555–583. https://doi.org/10.1080/13632460701572872

CEN (2005) Norma Portuguesa. Eurocódigo 8 – Projeto de estruturas para resistência aos sismos Parte 3: Avaliação e reabilitação de edifícios

CEN (2009) Eurocódigo 8: Projecto de estruturas para resistência aos sismos Parte 1: Regras gerais, acções sísmicas e regras para edifícios

Chhabra JPS, Hasik V, Bilec MM, Warn GP (2018) Probabilistic Assessment of the Life-Cycle Environmental Performance and Functional Life of Buildings due to Seismic Events. J Archit Eng 24:04017035. https://doi.org/10.1061/(ASCE)AE.1943-5568.0000284

Chiozzi A, Miranda E (2017) Fragility functions for masonry infill walls with in-plane loading. Earthq Engng Struct Dyn 46:2831–2850. https://doi.org/10.1002/eqe.2934

Chopra AK, Goel RK (2000) Evaluation of NSP to Estimate Seismic Deformation: SDF Systems. Journal of Structural Engineering 126:482–490. https://doi.org/10.1061/(ASCE)0733-9445(2000)126:4(482)

Cimellaro G (2013) Resilience-based design (RBD) modelling of civil infrastructure to assess seismic hazards. In: Elsevier (ed) Seismic Risk Analysis and Management of Civil Infrastructure Systems. pp 268–303

Clemett N, Carofilis Gallo WW, O'Reilly GJ, et al (2022) Optimal seismic retrofitting of existing buildings considering environmental impact. Engineering Structures 250:113391. https://doi.org/10.1016/j.engstruct.2021.113391

Clemett N, Carofilis W, Gabbianelli G, et al (2023) Optimal Combined Seismic and Energy Efficiency Retrofitting for Existing Buildings in Italy. Journal of Structural Engineering 149:1–16. https://doi.org/10.1061/(asce)st.1943-541x.0003500

Comber MV, Poland C, Sinclair M (2012) Environmental Impact Seismic Assessment: Application of Performance-Based Earthquake Engineering Methodologies to Optimize Environmental Performance. In: Structures Congress 2012. American Society of Civil Engineers, Chicago, Illinois, United States, pp 910–921

Cosenza E, Del Vecchio C, Di Ludovico M, et al (2018) The Italian guidelines for seismic risk classification of constructions: technical principles and validation. Bull Earthquake Eng 16:5905–5935. https://doi.org/10.1007/s10518-018-0431-8

Costa AC, Carvalho MLSA, Coelho E, et al (2010) Evaluation of seismic risk and mitigation strategies for the existing building stock: Application of LNECloss

to the metropolitan area of Lisbon. Bulletin of Earthquake Engineering 8:119–134. https://doi.org/10.1007/s10518-009-9160-3

Costa R, Haukaas T, Chang S (2021) Agent-based model for post-earthquake housing recovery. Earthquake Spectra 37:46–72

Couto R, Mucedero G, Bento R, Monteiro R (2024) A Practice-Oriented Approach for Seismic and Energy Performance Upgrading of Existing Buildings. Journal of Earthquake Engineering 1–28. https://doi.org/10.1080/13632469.2024.2382474

Couto R, Mucedero G, Bento R, Monteiro R (2025) Priority analysis framework for equitable seismic and energy-efficiency renovation of residential buildings applied to mainland Portugal. Earthquake Spectra. https://doi.org/10.1177/87552930251335282

Couto R, Mucedero G, Bento R, Monteiro R (2023) On the Influence of Climate and Seismic Hazard Conditions in the Identification of Optimal Retrofitting Strategies for RC Buildings. COMPDYN Proceedings 2070–2084. https://doi.org/10.7712/120123.10543.20474

Crowley, Dabbeek, Despotaki, et al (2021a) European Seismic Risk Model (ESRM20). EFEHR Technical Report 002 V100. https://doi.org/https://doi.org/10.7414/EUC-EFEHR-TR002-ESRM20

Crowley H, Despotaki V, Rodrigues D, et al (2020) Exposure model for European seismic risk assessment. Earthquake Spectra 36:252–273. https://doi.org/10.1177/8755293020919429

Crowley H, Despotaki V, Silva V, et al (2021b) Model of seismic design lateral force levels for the existing reinforced concrete European building stock. Bull Earthquake Eng 19:2839–2865. https://doi.org/10.1007/s10518-021-01083-3

Crowley H, Rodrigues D, Silva V, et al The European Seismic Risk Model 2020 (ESRM 2020)

Cruz CO, Branco F (2020) Reconstruction Cost Model for Housing Insurance. J Leg Aff Dispute Resolut Eng Constr 12:05020007. https://doi.org/10.1061/(ASCE)LA.1943-4170.0000408

Da Porto F, Donà M, Rosti A, et al (2021) Comparative analysis of the fragility curves for Italian residential masonry and RC buildings. Bull Earthquake Eng 19:3209–3252. https://doi.org/10.1007/s10518-021-01120-1

Danciu L, Giardini D, Weatherill G, et al (2024) The 2020 European Seismic Hazard Model: Overview and Results. Natural Hazards and Earth System Sciences 24:3049–3073. https://doi.org/10.5194/egusphere-2023-3062

Danciu L, Nandan S, Reyes C, et al (2021) The 2020 update of the European Seismic Hazard Model: Model Overview. EFEHR Technical Report 001. https://doi.org/https://doi.org/10.12686/a15

Daniel S, Ghiaus C (2023) Multi-Criteria Decision Analysis for Energy Retrofit of Residential Buildings: Methodology and Feedback from Real Application. Energies 16:902. https://doi.org/10.3390/en16020902

De Risi MT, Angelucci G, Manfredi V, et al (2025) Seismic performance of Italian pre-code RC buildings strengthened via local interventions: Fragility curves and failure rates. Structures 80:109756. https://doi.org/10.1016/j.istruc.2025.109756

De Risi MT, Del Gaudio C, Verderame GM (2020) A component-level methodology to evaluate the seismic repair costs of infills and services for Italian RC buildings. Bull Earthquake Eng 18:6533–6570. https://doi.org/10.1007/s10518-020-00944-7

Decree–Law No 95/2019 of 18 July (2019) Regime aplicável à reabilitação de edifícios ou frações autónomas (Regime applicable to the rehabilitation of buildings or autonomous fractions)'. Republic Diary, 136:35–45

Decreto Ministeriale (2020) DM n. 58/2020. Linee Guida per la Classificazione del Rischio Sismico delle Costruzioni. Rome, Italy

Del Gaudio C, De Martino G, Di Ludovico M, et al (2017) Empirical fragility curves from damage data on RC buildings after the 2009 L'Aquila earthquake. Bull Earthquake Eng 15:1425–1450. https://doi.org/10.1007/s10518-016-0026-1

Del Gaudio C, De Risi MT, Ricci P, Verderame GM (2019) Empirical drift-fragility functions and loss estimation for infills in reinforced concrete frames under

seismic loading. Bull Earthquake Eng 17:1285–1330. https://doi.org/10.1007/s10518-018-0501-y

Del Vecchio C, Di Ludovico M, Pampanin S, Prota A (2018) Repair Costs of Existing RC Buildings Damaged by the L'Aquila Earthquake and Comparison with FEMA P-58 Predictions. Earthquake Spectra 34:237–263. https://doi.org/10.1193/122916EQS257M

Del Vecchio C, Ludovico MD, Prota A (2020) Repair costs of reinforced concrete building components: from actual data analysis to calibrated consequence functions. Earthquake Spectra 36:353–377. https://doi.org/10.1177/8755293019878194

DGEG (2022a) Consumo de electricidade por município e setor de atividade. https://www.dgeg.gov.pt/pt/estatistica/energia/eletricidade/consumo-por-municipio-e-setor-de-atividade/

DGEG (2022b) Consumo de gás natural por município e por setor de atividade. https://www.dgeg.gov.pt/pt/estatistica/energia/gas-natural/consumos/

DGEG (2024) Ficha Técnica. Lisbom

Di Ludovico M, Prota A, Moroni C, et al (2017) Reconstruction process of damaged residential buildings outside historical centres after the L'Aquila earthquake: part II—"heavy damage" reconstruction. Bulletin of Earthquake Engineering 15:667–692. https://doi.org/10.1007/s10518-016-9877-8

Di Trapani F, Di Benedetto M, Petracca M, Camata G (2024) Local infill-frame interaction under seismic loads: Investigation through refined micro-modeling. Engineering Structures 315:

Dolce M, Prota A, Borzi B, et al (2021) Seismic risk assessment of residential buildings in Italy. Bull Earthquake Eng 19:2999–3032. https://doi.org/10.1007/s10518-020-01009-5

Dolšek M, Fajfar P (2008) The effect of masonry infills on the seismic response of a four-storey reinforced concrete frame — a deterministic assessment. Engineering Structures 30:1991–2001. https://doi.org/10.1016/j.engstruct.2008.01.001

Donà M, Bizzaro L, Carturan F, Da Porto F (2019) Effects of Business Recovery Strategies on Seismic Risk and Cost-Effectiveness of Structural Retrofitting for Business Enterprises. Earthquake Spectra 35:1795–1819. https://doi.org/10.1193/041918EQS098M

Economico IMDS (2015) Decreto interministeriale 26 Giugno 2015, Applicazione delle metodologie di calcolo delle prestazioni energetiche e definizione delle prescrizioni e dei requisiti minimi degli edifici. Rome: Italian Government

Edilclima (2022) EC700 Calcolo Prestazioni Energetiche Degli Edifici—Versione 11.

Elkady A, Lignos DG (2020) EaRL—Software for Earthquake Risk, Loss and Lifecycle Analysis. SoftwareX 12:100607. https://doi.org/10.1016/j.softx.2020.100607

European Comission (2024) EU Social Progress Index 2.0 - 2024 edition. https://ec.europa.eu/regional_policy/information-sources/maps/social-progress_en

European Union (2023) Directive (EU) 2023/1791 of the European Parliament and of the Council of 13 September 2023 on energy efficiency and amending Regulation (EU) 2023/955. Official Jounral of the European Union 66:

Eurostat (2023a) Energy Statistics - Cooling and Heating Degree Days. https://ec.europa.eu/eurostat/web/energy/database

Eurostat (2024a) Cooling and heating degree days by NUTS 3 region - annual data. https://doi.org/https://doi.org/10.2908/NRG_CHDDR2_A

Eurostat (2023b) Inability to keep home adequately warm - EU-SILC survey. https://ec.europa.eu/eurostat/databrowser/view/ilc_mdes01/default/table?lang=en. Accessed 3 Oct 2024

Eurostat (2024b) Labour cost levels by NACE Rev. 2 activity

Eurostat (2024c) Enterprises by detailed NACE Rev. 2 activity and special aggregates (sbs_ovw_act)

Fajfar P (2000) A Nonlinear Analysis Method for Performance-Based Seismic Design. Earthquake Spectra 16:573–592. https://doi.org/10.1193/1.1586128

FEMA (2003) HAZUS-MH technical manual

FEMA (2018a) Seismic Performance Assessment of Buildings, Volume 1 - Methodology

FEMA (2024) Hazus Earthquake Model Technical Manual. Hazus 6.1

FEMA (2018b) Seismic Performance Assessment of Buildings, Volume 3 – Supporting Electronic Materials and Background Documentation. Fema P-58

FEMA (2018c) Seismic Performance Assessment of Buildings, Volume 3 - Supporting Electronic Materials and Background Documentation. Rep. No. FEMA P-58-3

Follador V, Carpanese P, Donà M, Da Porto F (2023) Effect of retrofit interventions on seismic fragility of Italian residential masonry buildings. International Journal of Disaster Risk Reduction 91:103668. https://doi.org/10.1016/j.ijdrr.2023.103668

Formisano A, Vaiano G, Fabbrocino F (2019) Seismic and Energetic Interventions on a Typical South Italy Residential Building: Cost Analysis and Tax Detraction. Frontiers in Built Environment 5:. https://doi.org/10.3389/fbuil.2019.00012

Freddi F, Novelli V, Gentile R, et al (2021) Observations from the 26th November 2019 Albania earthquake: the earthquake engineering field investigation team (EEFIT) mission. Bull Earthquake Eng 19:2013–2044. https://doi.org/10.1007/s10518-021-01062-8

Furtado A, Costa C, Arêde A, Rodrigues H (2016) Geometric characterisation of Portuguese RC buildings with masonry infill walls. European Journal of Environmental and Civil Engineering 20:396–411. https://doi.org/10.1080/19648189.2015.1039660

Gencturk B, Elnashai AS (2008) Development and application of an advanced capacity spectrum method. Engineering Structures 30:3345–3354. https://doi.org/10.1016/j.engstruct.2008.05.008

Gentile R, Calvi GM (2023) Direct loss-based seismic design of reinforced concrete frame and wall structures. Earthq Engng Struct Dyn 52:4395–4415. https://doi.org/10.1002/eqe.3955

Gentile R, Galasso C (2021) Simplified seismic loss assessment for optimal structural retrofit of RC buildings. Earthquake Spectra 37:346–365. https://doi.org/10.1177/8755293020952441

Gervásio H, Dimova S (2018) Model for life cycle assessment (LCA) of buildings: EFIResources: resource efficient construction towards sustainable design. Publications Office of the European Union, Luxembourg

Gkatzogias K, Crowley H, Veljkovic A, et al (2022a) Prioritising EU regions for building renovation: seismic risk, energy efficiency, socioeconomic vulnerability – REEBUILD: Integrated techniques for the seismic strengthening and energy efficiency of existing buildings. Publications Office of the European Union. https://doi.org/10.2760/263803,%20JRC128988

Gkatzogias K, Pohoryles DA, Romano E, Bournas DA (2023) Integrated seismic and energy renovation of buildings. Publications Office of the European Union. https://doi.org/10.2760/346428,%20JRC132940

Gkatzogias K, Tsionis G, Crowley H, et al (2022b) Building renovation in the EU: scenarios and impact assessment. Publications Office of the European Union, Luxembourg

Global Data Lab (2023) Subnational HDI. https://globaldatalab.org

Gonzalez RE, Stephens MT, Toma C, et al (2021) Post-earthquake Demolition in Christchurch, New Zealand: A Case-Study Towards Incorporating Environmental Impacts in Demolition Decisions. In: Akkar S, Ilki A, Goksu C, Erdik M (eds) Advances in Assessment and Modeling of Earthquake Loss. Springer International Publishing, Cham, pp 47–64

Gusella F, Bartoli G, Pintucchi B (2025) A simplified loss-based procedure for seismic risk mitigation at a territorial scale. Bull Earthquake Eng 23:1941–1968. https://doi.org/10.1007/s10518-025-02117-w

Hak S, Morandi P, Magenes G (2014) Local Effects in the Seismic Design of RC Frame Structures with Masonry Infills. In: Proceedings of the 4th International Conference on Computational Methods in Structural Dynamics and Earthquake Engineering (COMPDYN 2013). Institute of Structural Analysis and Antiseismic Research School of Civil Engineering National Technical University of Athens (NTUA) Greece, Kos Island, Greece, pp 2931–2943

Hak S, Morandi P, Magenes G, Sullivan TJ (2012) Damage Control for Clay Masonry Infills in the Design of RC Frame Structures. Journal of Earthquake Engineering 16:1–35. https://doi.org/10.1080/13632469.2012.670575

Hallegatte S, Walsh B (2021) Disasters, Poverty and Inequality - World Bank. In: The Routledge Handbook of the Political Economy of the Environment. Routledge, London

Hammond G, Jones C, Lowrie F, Tse P (2011) Embodied carbon: the Inventory of Carbon and Energy (ICE). BSRIA, Bracknell

Harati M, Van De Lindt JW (2024) Data-driven machine learning for multi-hazard fragility surfaces in seismic resilience analysis. Computer aided Civil Eng 40:698–720. https://doi.org/10.1111/mice.13356

Hasanoğlu S, Ozsarac V, O'Reilly GJ (2025) A model for the simulated design of Turkish RC frame buildings in seismic vulnerability analysis. Bull Earthquake Eng. https://doi.org/10.1007/s10518-025-02301-y

Hasik V, Chhabra JPS, Warn GP, Bilec MM (2018) Review of approaches for integrating loss estimation and life cycle assessment to assess impacts of seismic building damage and repair. Engineering Structures 175:123–137. https://doi.org/10.1016/j.engstruct.2018.08.011

Homewyse (2021) "Homewyse Material Cost Calculators." https://www.homewyse.com/costs/index.html. Il. Accessed 12 Aug 2021

Ilic JM, Bento R, Cattari S (2020) 3DGIS representation for supporting seismic mitigation policies at urban scale: The case study of Lisbon. Journal of Cultural Heritage 45:265–278. https://doi.org/10.1016/j.culher.2020.04.001

Ilki A, Celep Z (2012) Earthquakes, Existing Buildings and Seismic Design Codes in Turkey. Arab J Sci Eng 37:365–380. https://doi.org/10.1007/s13369-012-0183-8

Jalayer F, Ebrahimian H, Miano A, et al (2017a) Analytical fragility assessment using unscaled ground motion records. Earthquake Engng Struct Dyn 46:2639–2663. https://doi.org/10.1002/eqe.2922

Jalayer F, Ebrahimian H, Miano A, et al (2017b) Analytical fragility assessment using unscaled ground motion records. Earthquake Engineering and Structural Dynamics 46:2639–2663. https://doi.org/10.1002/eqe.2922

Kappos AJ (2013) Seismic Vulnerability and Loss Assessment for Buildings in Greece. In: Gueguen P (ed) Seismic Vulnerability of Structures, 1st edn. Wiley, pp 111–160

Kappos AJ, Dimitrakopoulos EG (2008) Feasibility of pre-earthquake strengthening of buildings based on cost-benefit and life-cycle cost analysis, with the aid of fragility curves. Nat Hazards 45:33–54. https://doi.org/10.1007/s11069-007-9155-9

Kappos AJ, Panagopoulos G, Panagiotopoulos C, Penelis G (2006) A hybrid method for the vulnerability assessment of R/C and URM buildings. Bull Earthquake Eng 4:391–413. https://doi.org/10.1007/s10518-006-9023-0

Liel AB, Deierlein GG (2013) Cost-Benefit Evaluation of Seismic Risk Mitigation Alternatives for Older Concrete Frame Buildings. Earthquake Spectra 29:1391–1411. https://doi.org/10.1193/030911EQS040M

LNEC (2005) Building Stock Inventory and Vulnerability Data for Lisbon Metropolitan Area. RELATÓRIO 423/2005 - NESDE Lisbon,

Lopes GC, Silva V, Costa C, et al (2024a) Advancing the understanding of earthquake risk in Portugal. Bulletin of Earthquake Engineering. https://doi.org/10.1007/s10518-024-01975-0

Lopes GC, Silva V, Costa C, et al (2024b) Advancing the understanding of earthquake risk in Portugal. Bull Earthquake Eng 22:5379–5401. https://doi.org/10.1007/s10518-024-01975-0

Lovon H, Silva V, Vicente R, Miguel T (2023) Seismic vulnerability assessment of Portuguese masonry buildings. Structures 55:853–865. https://doi.org/10.1016/j.istruc.2023.06.083

Luzi L, Lanzano G, Felicetta C, et al (2020) Engineering Strong Motion Database (ESM) (Version 2.0). Istituto Nazionale di Geofisica e Vulcanologia (INGV). https://doi.org/https://doi.org/10.13127/ESM.2

Mahbubur Rahman Md, Sadequr Rahman Md, Jerin T (2023) Social vulnerability to earthquake disaster: insights from the people of 48th ward of Dhaka South City, Bangladesh. Environmental Hazards 22:116–135. https://doi.org/10.1080/17477891.2022.2085075

Manfredi G, Prota A, Verderame GM, et al (2014) 2012 Emilia earthquake, Italy: reinforced concrete buildings response. Bull Earthquake Eng 12:2275–2298. https://doi.org/10.1007/s10518-013-9512-x

Manfredi V, Masi A (2018) Seismic Strengthening and Energy Efficiency: Towards an Integrated Approach for the Rehabilitation of Existing RC Buildings. Buildings 8:36. https://doi.org/10.3390/buildings8030036

Manfredi V, Masi A, Nicodemo G, Digrisolo A (2023a) Seismic fragility curves for the Italian RC residential buildings based on non-linear dynamic analyses. Springer Netherlands

Manfredi V, Masi A, Nicodemo G, Digrisolo A (2023b) Seismic fragility curves for the Italian RC residential buildings based on non-linear dynamic analyses. Bull Earthquake Eng 21:2173–2214. https://doi.org/10.1007/s10518-022-01605-7

Marini A, Passoni C, Belleri A, et al (2022) Combining seismic retrofit with energy refurbishment for the sustainable renovation of RC buildings: a proof of concept. European Journal of Environmental and Civil Engineering 26:2475–2495. https://doi.org/10.1080/19648189.2017.1363665

Martins L, Silva V (2021a) Development of a fragility and vulnerability model for global seismic risk analyses. Bulletin of Earthquake Engineering 19:6719–6745. https://doi.org/10.1007/s10518-020-00885-1

Martins L, Silva V (2021b) Development of a fragility and vulnerability model for global seismic risk analyses. Bull Earthquake Eng 19:6719–6745. https://doi.org/10.1007/s10518-020-00885-1

Mauro G, Menna C, Vitiello U, et al (2017) A Multi-Step Approach to Assess the Lifecycle Economic Impact of Seismic Risk on Optimal Energy Retrofit. Sustainability 9:989. https://doi.org/10.3390/su9060989

Mazzolani FM, Formisano A, Vaiano G (2018) “Adeguamento sismico di edifici in cemento aramato: BRB e FRP.” Costruzioni metalliche 1 25–50

McKenna F, Scott MH, Fenves GL (2010a) Nonlinear Finite-Element Analysis Software Architecture Using Object Composition. Journal of Computing in Civil Engineering 24:95–107

McKenna F, Scott MH, Fenves GL (2010b) Nonlinear Finite-Element Analysis Software Architecture Using Object Composition. Journal of Computing in Civil Engineering 24:95–107. https://doi.org/10.1061/(ASCE)CP.1943-5487.0000002

Menna C, Del Vecchio C, Di Ludovico M, et al (2021) Conceptual design of integrated seismic and energy retrofit interventions. Journal of Building Engineering 38:102190. https://doi.org/10.1016/j.jobe.2021.102190

Menna C, Vitiello U, Mauro G, et al (2019) Integration of Seismic Risk into Energy Retrofit Optimization Procedures: A Possible Approach Based on Life Cycle Evaluation. IOP Conference Series: Earth and Environmental Science 290:012022. https://doi.org/10.1088/1755-1315/290/1/012022

Ministery of the Environment and Energy Transition (2019) Roadmap for Carbon Neutrality 2050 (RNC2050) Long-Term Strategy for Carbon Neutrality of the Portuguese Economy by 2050. Report R 262/2019 102

MIT (2018) NTC 2018: D.M. del Ministero delle Infrastrutture e dei trasporti del 17/01/2018. Aggiorna- mento delle Norme Tecniche per le Costruzioni (in Italian)

Moehle J, Deierlein GG (2004) A Framework Methodology for Performance-Based Earthquake Engineering. Vancouver, B.C., Canada

Molina C, Eeri HM, Vahanvaty T, et al (2022) An analytical framework to assess earthquake-induced downtime and model recovery of buildings. Earthquake Spectra. https://doi.org/10.1177/87552930211060856

Mucedero G, Couto R, Clemett N, Monteiro R (2023) Implications of masonry infill – related uncertainty on the optimal seismic retrofitting of existing buildings. 14th International Conference on Applications of Statistics and Probability in Civil Engineering 1–8

Mucedero G, Couto R, Yükselen B, Monteiro R (2025a) Estimation of seismic downtime for building retrofitting decision-making. Resilient Cities and Structures

Mucedero G, Monteiro R (2024a) An integrated regional prioritisation framework for seismic and energy-efficiency performance upgrading of residential buildings. International Journal of Disaster Risk Reduction 103:104341. https://doi.org/10.1016/j.ijdrr.2024.104341

Mucedero G, Monteiro R (2024b) An integrated regional prioritisation framework for seismic and energy-efficiency performance upgrading of residential buildings. International Journal of Disaster Risk Reduction 103:104341. https://doi.org/10.1016/j.ijdrr.2024.104341

Mucedero G, Perrone D, Brunesi E, Monteiro R (2020) Numerical Modelling and Validation of the Response of Masonry Infilled RC Frames Using Experimental Testing Results. Buildings 10:182. https://doi.org/10.3390/buildings10100182

Mucedero G, Perrone D, Monteiro R (2024a) Generalised Storey Loss Functions for Seismic Loss Assessment of Italian Residential Buildings. Journal of Earthquake Engineering 28:451–474. https://doi.org/10.1080/13632469.2023.2218491

Mucedero G, Perrone D, Monteiro R (2021) Nonlinear static characterisation of masonry-infilled RC building portfolios accounting for variability of infill properties. Bull Earthquake Eng 19:2597–2641. https://doi.org/10.1007/s10518-021-01068-2

Mucedero G, Perrone D, Monteiro R (2024b) Generalised Storey Loss Functions for Seismic Loss Assessment of Italian Residential Buildings. Journal of Earthquake Engineering 28:451–474. https://doi.org/10.1080/13632469.2023.2218491

Mucedero G, Perrone D, Monteiro R (2022a) Infill Variability and Modelling Uncertainty Implications on the Seismic Loss Assessment of an Existing RC Italian School Building. Applied Sciences (Switzerland) 12:. https://doi.org/10.3390/app122312002

Mucedero G, Perrone D, Monteiro R (2022b) Epistemic uncertainty in poorly detailed existing frames accounting for masonry infill variability and RC shear failure. Earthquake Engineering and Structural Dynamics 51:3755–3778. https://doi.org/10.1002/eqe.3748

Mucedero G, Yükselen B, Couto R, et al (2025b) Beyond structural safety: downtime-based performance criteria as future design objectives for Italian buildings (under review). Journal of Building Engineering

Nafeh AMB, O'Reilly GJ (2024a) Fragility functions for non-ductile infilled reinforced concrete buildings using next-generation intensity measures based on analytical models and empirical data from past earthquakes. Bull Earthquake Eng 22:4983–5021. https://doi.org/10.1007/s10518-024-01955-4

Nafeh AMB, O'Reilly GJ (2024b) Simplified pushover-based seismic loss assessment for existing infilled frame structures. Bulletin of Earthquake Engineering 22:951–995. https://doi.org/https://doi.org/10.1007/s10518-023-01792-x

Nafeh AMB, O'Reilly GJ (2022) Unbiased simplified seismic fragility estimation of non-ductile infilled RC structures. Soil Dynamics and Earthquake Engineering 157:107253. https://doi.org/10.1016/j.soildyn.2022.107253

Natale A, Del Vecchio C, Di Ludovico M (2021) Seismic retrofit solutions using base isolation for existing RC buildings: economic feasibilty and pay-back time. Bull Earthquake Eng 19:483–512. https://doi.org/10.1007/s10518-020-00988-9

Nettis A, Gentile R, Raffaele D, et al (2021a) Cloud Capacity Spectrum Method: Accounting for record-to-record variability in fragility analysis using nonlinear static procedures. Soil Dynamics and Earthquake Engineering 150:106829. https://doi.org/10.1016/j.soildyn.2021.106829

Nettis A, Gentile R, Raffaele D, et al (2021b) Cloud Capacity Spectrum Method: Accounting for record-to-record variability in fragility analysis using nonlinear static procedures. Soil Dynamics and Earthquake Engineering 150:106829. https://doi.org/10.1016/j.soildyn.2021.106829

Oliveira C, Costa A (1984) Updating seismic hazard maps. 8th WCEE

O'Reilly GJ (2016) Performance-based seismic assessment and retrofit of existing RC frame buildings in Italy. PhD Thesis

O'Reilly GJ, Perrone D, Fox M, et al (2018) Seismic assessment and loss estimation of existing school buildings in Italy. Engineering Structures 168:142–162. https://doi.org/10.1016/j.engstruct.2018.04.056

O'Reilly GJ, Shahnazaryan D (2024) On the utility of story loss functions for regional seismic vulnerability modeling and risk assessment. Earthquake Spectra 40:1933–1955. https://doi.org/10.1177/87552930241245940

O'Reilly GJ, Sullivan TJ (2019) Modeling Techniques for the Seismic Assessment of the Existing Italian RC Frame Structures. Journal of Earthquake Engineering 23:1262–1296. https://doi.org/10.1080/13632469.2017.1360224

O'Reilly GJ, Sullivan TJ (2018) Quantification of modelling uncertainty in existing Italian RC frames. Earthquake Engineering and Structural Dynamics 47:1054–1074. https://doi.org/10.1002/eqe.3005

Ozkula G, Dowell RK, Baser T, et al (2023) Field reconnaissance and observations from the February 6, 2023, Turkey earthquake sequence. Springer Netherlands

Ozsarac V, Pereira N, Mohamed H, et al (2025) The Built Environment Data Framework for Simulated Design and Vulnerability Modelling in Earthquake Engineering. Earthq Engng Struct Dyn eqe.4378. https://doi.org/10.1002/eqe.4378

Pagani M, Monelli D, Weatherill G, et al (2014) OpenQuake Engine: An Open Hazard (and Risk) Software for the Global Earthquake Model. Seismological Research Letters 85:692–702. https://doi.org/10.1785/0220130087

Pagni CA, Lowes LN (2006) Fragility Functions for Older Reinforced Concrete Beam-Column Joints. Earthquake Spectra 22:215–238. https://doi.org/10.1193/1.2163365

Pan C, Wang H, Huang S, Zhang H (2014) The Great East Japan Earthquake and Tsunami Aftermath: Preliminary Assessment of Carbon Footprint of Housing Reconstruction. In: Kontar YA, Santiago-Fandiño V, Takahashi T (eds) Tsunami Events and Lessons Learned. Springer Netherlands, Dordrecht, pp 435–450

Papadopoulos AN, Roth P, Danciu L, et al (2024) The Earthquake Risk Model of Switzerland, ERM-CH23. Nat Hazards Earth Syst Sci 24:3561–3578. https://doi.org/10.5194/nhess-24-3561-2024

Papadopoulos AN, Vamvatsikos D, Kazantzi AK (2019) Development and Application of FEMA P-58 Compatible Story Loss Functions. Earthquake Spectra 35:95–112. https://doi.org/10.1193/102417EQS222M

Passoni C, Marini A, Belleri A, Menna C (2021) Redefining the concept of sustainable renovation of buildings: State of the art and an LCT-based design framework. Sustainable Cities and Society 64:102519. https://doi.org/10.1016/j.scs.2020.102519

Paul N, Lee JS, Mieler M, Almufti I (2018) Improving Estimates of Earthquake-Induced Downtime in Individual Buildings Using the REDi Methodology. Structures Congress 2018: Blast, Impact Loading, and Response; and Research and Education - Selected Papers from the Structures Congress 2018 2018-April:77–86. https://doi.org/10.1061/9780784481349.008

Peres R, Couto R, Sousa I, et al (2023) Modelling and evaluation of brittle shear effects on the seismic performance and loss assessment of RC buildings. Engineering Structures 275:115–230. https://doi.org/https://doi.org/10.1016/j.engstruct.2022.115230

Pohoryles D, Bournas D, Da Porto F, et al (2022) Technologies for the combined seismic and energy upgrading of existing buildings. Publications Office of the European Union. https://doi.org/10.2760/86567,%20JRC128458.

Pohoryles DA, Maduta C, Bournas DA, Kouris LA (2020) Energy performance of existing residential buildings in Europe: A novel approach combining energy with seismic retrofitting. Energy and Buildings 223:. https://doi.org/10.1016/j.enbuild.2020.110024

Portuguese Republic (2019) National Energy and Climate Plan 2021-2030 (NECP 2030). Portugal 1–293

Presidência do Conselho de Ministros (2024) Resolução do Conselho de Ministros n.º 11/2024, de 8 de janeiro. Diário da República nº 5/2024 Série I:

Prota A, Di Ludovico M, Vecchio C, Menna C (2020) Progetto DPC-ReLUIS 2019-2021 WP5: Interventi di rapida esecuzione a basso impatto ed integrati. 72:

Ramirez CM, Miranda E (2009) Building-specific loss estimation methods & tools for simplified performance-based earthquake. Stanford University, Department of Civil and Environmental Engineering

REBA (1967) Regulamento de estruturas de betão armado, Decreto-Lei No. 47723

Reinoso E, Jaimes MA, Esteva L (2018) Estimation of life vulnerability inside buildings during earthquakes. Structure and Infrastructure Engineering 14:1140–1152. https://doi.org/10.1080/15732479.2017.1401097

Reis A, Heleno L, Monteiro S, Oliveira NS (2024) Sustainability Assessment of Building Rehabilitation Solutions: The Mid 70s Portuguese Building. pp 555–564

Rennert K, Errickson F, Prest BC, et al (2022) Comprehensive evidence implies a higher social cost of CO2. Nature 610:687–692. https://doi.org/10.1038/s41586-022-05224-9

Repapis C, Zeris CA (2019) Seismic Assessment of Non-conforming Infilled RC Buildings Using IDA Procedures. Front Built Environ 4:88. https://doi.org/10.3389/fbuil.2018.00088

Requena-Garcia-Cruz MV, Morales-Esteban A, Durand-Neyra P (2022) Assessment of specific structural and ground-improvement seismic retrofitting techniques for a case study RC building by means of a multi-criteria evaluation. Structures 38:265–278. https://doi.org/10.1016/j.istruc.2022.02.015

Requena-García-Cruz MV, Morales-Esteban A, Durand-Neyra P, Estêvão JMC (2020) An index-based method for evaluating seismic retrofitting techniques. Application to a reinforced concrete primary school in Huelva. In: Earth and its Atmosphere. Hyderabad, India

Retamales R, Davies R, Mosqueda G, Filiatrault A (2013) Experimental Seismic Fragility of Cold-Formed Steel Framed Gypsum Partition Walls. J Struct Eng 139:1285–1293. https://doi.org/10.1061/(ASCE)ST.1943-541X.0000657

Ricci P, De Luca F, Verderame GM (2011) 6th April 2009 L'Aquila earthquake, Italy: reinforced concrete building performance. Bull Earthquake Eng 9:285–305. https://doi.org/10.1007/s10518-010-9204-8

Romão X, Pereira N, Castro JM, et al (2021) European Building Vulnerability Data Repository (v2.1). Zenodo. https://doi.org/https://doi.org/10.5281/zenodo.5639318

Rossi A, Morandi P, Magenes G (2021) A novel approach for the evaluation of the economical losses due to seismic actions on RC buildings with masonry infills. Soil Dynamics and Earthquake Engineering 145:106722. https://doi.org/10.1016/j.soildyn.2021.106722

Rosti A, Del Gaudio C, Rota M, et al (2021) Empirical fragility curves for Italian residential RC buildings. Bulletin of Earthquake Engineering 19:3165–3183. https://doi.org/10.1007/s10518-020-00971-4

Rovai E (1994) The Social Geography of Disaster Recovery: Differential Community Response to the North Coast Earthquakes. Yearbook of the Association of Pacific Coast Geographers 56:49–74

RSA (1983) Regulamento de Segurança e Acções para Estruturas de Edifícios e Pontes. Decreto-Lei n.º 235/83. Diário da República: Lisbon, Portugal

RSCCS (1958a) Regulamento de Segurança das Construções Contra os Sismos, Decreto-Lei n.º 41658 de 31 de Maio de 1958. Diário da República: Lisbon, Portugal

RSCCS (1958b) Regulamento de segurança das construções contra os sismos, Decreto Lei No. 41658

RSEP (1961a) Regulamento de Solicitações em Edifícios e Pontes (RSEP). Decreto nº 44041 de 18 de Novembro. Diário da República: Lisbon, Portugal

RSEP (1961b) Regulamento de solicitações em edifício e pontes, Decreto-Lei No. 44041

Ruggieri S, Porco F, Uva G, Vamvatsikos D (2021) Two frugal options to assess class fragility and seismic safety for low-rise reinforced concrete school buildings in Southern Italy. Bulletin of Earthquake Engineering 19:1415–1439. https://doi.org/10.1007/s10518-020-01033-5

Ruiz-García J, Ramos-Cruz JM (2024) Drift-based fragility assessment of nonductile reinforced concrete columns failing in shear under cyclic loading. Engineering Structures 302:117378. https://doi.org/10.1016/j.engstruct.2023.117378

Ruiz-Pinilla JG, Adam JM, Pérez-Cárcel R, et al (2016) Learning from RC building structures damaged by the earthquake in Lorca, Spain, in 2011. Engineering

Failure Analysis 68:76–86. https://doi.org/10.1016/j.engfailanal.2016.05.013

Saler E, Gattesco N, da Porto F (2023) A new combined approach to prioritise seismic retrofit interventions on stocks of r.c. school buildings. International Journal of Disaster Risk Reduction 93:103767. https://doi.org/10.1016/j.ijdrr.2023.103767

Sarchi L, Varum H, Monteiro R, Silveira D (2018) Seismic behavior of two Portuguese adobe buildings: part II —numerical modeling and fragility assessment. International Journal of Architectural Heritage 12:936–950. https://doi.org/10.1080/15583058.2017.1423132

Sassun K, Sullivan TJ, Morandi P, Cardone D (2016a) Characterising the in-plane seismic performance of infill masonry. BNZSEE 49:98–115. https://doi.org/10.5459/bnzsee.49.1.98-115

Sassun K, Sullivan TJ, Morandi P, Cardone D (2016b) Characterising the in-plane seismic performance of infill masonry. Bulletin of the New Zealand Society for Earthquake Engineering 49:98–115. https://doi.org/10.5459/bnzsee.49.1.98-115

Scott MH, Fenves GL (2006) Plastic hinge integration methods for force-based beam-column elements. Journal of Structural Engineering 132:. https://doi.org/10.1061/(ASCE)0733-9445(2006)132:2(244)

Sediek OA, Roohi M, van de Lindt JW (2024) A genetic algorithm framework for seismic retrofit of building portfolios to enhance community resilience. International Journal of Disaster Risk Reduction 108:104570. https://doi.org/https://doi.org/10.1016/j.ijdrr.2024.104570

Sengupta P, Li B (2014) Seismic Fragility Evaluation of Lightly Reinforced Concrete Beam-Column Joints. Journal of Earthquake Engineering 18:1102–1128. https://doi.org/10.1080/13632469.2014.919890

Shahnazaryan D, O'Reilly GJ, Monteiro R (2021) Story loss functions for seismic design and assessment: Development of tools and application. Earthquake Spectra 37:2813–2839. https://doi.org/10.1177/87552930211023523

Silva A, Castro JM, Monteiro R (2020) A rational approach to the conversion of FEMA P-58 seismic repair costs to Europe. Earthquake Spectra 36:1607–1618. https://doi.org/10.1177/8755293019899964

Silva LM, Vasconcelos G, Lourenço PB (2021) Innovative systems for earthquake-resistant masonry infill walls: Characterization of materials and masonry assemblages. Journal of Building Engineering 39:102195. https://doi.org/10.1016/j.jobe.2021.102195

Silva V, Crowley H, Varum H, et al (2015a) Investigation of the characteristics of Portuguese regular moment-frame RC buildings and development of a vulnerability model. Bulletin of Earthquake Engineering 13:1455–1490. https://doi.org/10.1007/s10518-014-9669-y

Silva V, Crowley H, Varum H, Pinho R (2015b) Seismic risk assessment for mainland Portugal. Bulletin of Earthquake Engineering 13:429–457. https://doi.org/10.1007/s10518-014-9630-0

Silva V, Crowley H, Varum H, Pinho R (2015c) Seismic risk assessment for mainland Portugal. Bull Earthquake Eng 13:429–457. https://doi.org/10.1007/s10518-014-9630-0

Simões AG, Bento R, Lagomarsino S, et al (2019) Seismic assessment of nineteenth and twentieth centuries URM buildings in Lisbon: structural features and derivation of fragility curves. Bulletin of Earthquake Engineering. https://doi.org/10.1007/s10518-019-00618-z

Simonen K, Huang M, Aicher C, Morris P (2018) Embodied carbon as a proxy for the environmental impact of earthquake damage repair. Energy and Buildings 164:131–139. https://doi.org/10.1016/j.enbuild.2017.12.065

Sousa L (2016) Development of Innovative Methodologies for the Treatment of Uncertainties in the Earthquake Loss Assessment of Building Portfolios. FEUP

Sousa L, Monteiro R (2018a) Seismic retrofit options for non-structural building partition walls: Impact on loss estimation and cost-benefit analysis. Engineering Structures 161:8–27. https://doi.org/10.1016/j.engstruct.2018.01.028

Sousa L, Monteiro R (2018b) Seismic retrofit options for non-structural building partition walls: Impact on loss estimation and cost-benefit analysis. Engineering Structures 161:8–27. https://doi.org/10.1016/j.engstruct.2018.01.028

Sousa ML (2007) Hierarquização das regiões de Portugal continental em função do seu risco sísmico. Sísmica 2007 - 7º Congresso de sismologia e engenharia sísmica 1–12

Sousa ML (2006) Risco sísmico em Portugal continenal. Instituto Superior Técnico

Sousa ML, Costa AC (2016) Evolution of earthquake losses in Portuguese residential building stock. Bulletin of Earthquake Engineering 14:2009–2029. https://doi.org/10.1007/s10518-015-9809-z

Sousa ML, Oliveira CS, Costa AC (2006) Caracterização do Parque Habitacional de Portugal Continental para estudos de Risco Sísmico (in portuguese). Revista Portuguesa de Engenharia de Estruturas 55:35–50

SPUR (2012) Safe enough to stay. Report. San Francisco, C

Takeuchi T, Yasuda K, Iwata M (2009) Seismic Retrofitting Using Energy Dissipation Façades. In: Improving the Seismic Performance of Existing Buildings and Other Structures. American Society of Civil Engineers, Reston, VA, pp 1000–1009

Takeuchi T, Yasuda K, Iwata M (2006) Studies on Integrated Building Facade Engineering with High-Performance Structural Elements. In: IABSE Symposium, Budapest 2006: Responding to Tomorrow's Challenges in Structural Engineering. International Association for Bridge and Structural Engineering (IABSE), Zurich, Switzerland, pp 33–40

Tavares AO, Mendes JM, Basto E (2011) Percepção dos riscos naturais e tecnológicos, confiança institucional e preparação para situações de emergência: O caso de Portugal continental. Revista Crítica de Ciências Sociais 167–193. https://doi.org/10.4000/rccs.1380

Thomas K, Hardy RD, Lazrus H, et al (2019) Explaining differential vulnerability to climate change: A social science review. WIREs Climate Change 10:e565. https://doi.org/10.1002/wcc.565

Ugalde D, Lopez-Garcia D, Parra PF (2020) Fragility-based analysis of the influence of effective stiffness of reinforced concrete members in shear wall buildings. Bulletin of Earthquake Engineering 18:2061–2082. https://doi.org/10.1007/s10518-020-00786-3

UNI (2016) Riscaldamento e raffrescamento degli edifici—Dati climatici. Milan, Italy

UNI (2014a) Prestazioni energetiche degli edifici Parte 1: Determinazione del fabbisogno di energia termica dell'edificio per la climatizzazione estiva ed invernale. Milan, Italy

UNI (2014b) Prestazioni energetiche degli edifici Parte 2: Determinazione del fabbisogno di energia primaria per la climatizzazione invernale, per la produzione di acqua calda sanitaria, per la ventilazione e per l'illuminazione in edifici non residenziali. Milan, Italy

U.S. Environmental Protection Agency, (2022) Supply Chain Greenhouse Gas Emission Factors v1.3 by NAICS-6

Vamvatsikos D, Cornell CA (2005) Direct Estimation of Seismic Demand and Capacity of Multidegree-of-Freedom Systems through Incremental Dynamic Analysis of Single Degree of Freedom Approximation. Journal of Structural Engineering 131:589–599. https://doi.org/10.1061/(ASCE)0733-9445(2005)131:4(589)

Varela L, Correia AA, Guerreiro L (2024) Influence of masonry infill walls on the seismic response of existing RC frames buildings - application to Portugal. In: 18th World Conference on Earthquake Engineering (WCEE2024), Milan. Milan, Italy, pp 1–12

Verderame GM, De Luca F, Ricci P, Manfredi G (2011) Preliminary analysis of a soft-storey mechanism after the 2009 L'Aquila earthquake. Earthquake Engineering and Structural Dynamics 40:925–944. https://doi.org/10.1002/eqe.1069

Vicente R, Ferreira TM, Maio R (2015) Mitigação do risco sísmico de núcleos urbanos antigos: caracterização e avaliação da vulnerabilidade sísmica do bairro ribeirinho de Faro. TER 283–290. https://doi.org/10.14195/1647-7723_22_22

Vilanova SP, Fonseca JFBD (2007) Probabilistic seismic-hazard assessment for Portugal. Bulletin of the Seismological Society of America 97:1702–1717. https://doi.org/10.1785/0120050198

Wei H-H, Skibniewski MJ, Shohet IM, Yao X (2016) Lifecycle Environmental Performance of Natural-Hazard Mitigation for Buildings. J Perform Constr Facil 30:. https://doi.org/10.1061/(asce)cf.1943-5509.0000803

Woessner J, Laurentiu D, Giardini D, et al (2015) The 2013 European Seismic Hazard Model : key components and results. 3553–3596. https://doi.org/10.1007/s10518-015-9795-1

Xavier V, Couto R, Monteiro R, et al (2022) Detailed Structural Characterization of Existing RC Buildings for Seismic Exposure Modelling of the Lisbon Area. Buildings 12:642. https://doi.org/10.3390/buildings12050642

Xofi M, Ferreira TM, Domingues JC, et al (2024) On the Seismic Vulnerability Assessment of Urban Areas Using Census Data: The Lisbon Metropolitan Area as a Pilot Study Area. Journal of Earthquake Engineering 28:242–265. https://doi.org/10.1080/13632469.2023.2197078

Yepes-Estrada C, Calderon A, Costa C, et al (2023) Global building exposure model for earthquake risk assessment. Earthquake Spectra 39:2212–2235. https://doi.org/10.1177/87552930231194048

Yükselen B, Mucedero G, Monteiro R (2025a) Evaluation and Enhancement of Optimisation Algorithms for Automated Seismic Retrofitting of Existing Buildings. Journal of Earthquake Engineering 1–34. https://doi.org/10.1080/13632469.2025.2541237

Yükselen B, Mucedero G, Monteiro R (2025b) Multi-variable optimisation of building seismic retrofitting. Rhodes Island, Greece, pp 3602–3616

Zsarnoczay A, Manousakis JV, Kourehpaz P, et al (2024) NHERI-SimCenter/pelicun: v3.3 (v3.3). ZENODO

APPENDICES

Appendices

APPENDIX A.1 – FRAGILITY MAPPING

Table A. 1 Mapping of building taxonomy from the exposure model to corresponding sources of fragility curves

Building Taxonomy	Silva et al. (2015a,b)	Romão et al. (2021)	Martins and Silva (2021)
CR/LFINF+CDL+LFC:0.0/H:1	CR_MC_C_1	CR_LFINF-CDL-0_H1	CR_LFINF+CDL+DUL_H1
CR/LFINF+CDL+LFC:0.0/H:2	CR_MC_C_2	CR_LFINF-CDL-0_H2	CR_LFINF+CDL+DUL_H2
CR/LFINF+CDL+LFC:0.0/H:3	CR_MC_C_3	CR_LFINF-CDL-0_H3	CR_LFINF+CDL+DUL_H3
CR/LFINF+CDL+LFC:0.0/H:4	CR_MC_C_4	CR_LFINF-CDL-0_H4	CR_LFINF+CDL+DUL_H4
CR/LFINF+CDL+LFC:0.0/H:5	CR_MC_C_5-7	CR_LFINF-CDL-0_H5	CR_LFINF+CDL+DUL_H5
CR/LFINF+CDL+LFC:0.0/H:6	CR_MC_C_5-7	CR_LFINF-CDL-0_H6	CR_LFINF+CDL+DUL_H6
CR/LFINF+CDL+LFC:0.0/HBET:7-20	CR_MC_C_>8	CR_LFINF-CDL-0_H6	CR_LFINF+CDL+DUL_H7
CR/LFINF+CDL+LFC:5.0/H:1	CR_MC_B_1	CR_LFINF-CDL-5_H1	CR_LFINF+CDL+DUL_H1
CR/LFINF+CDL+LFC:5.0/H:2	CR_MC_B_2	CR_LFINF-CDL-5_H2	CR_LFINF+CDL+DUL_H2
CR/LFINF+CDL+LFC:5.0/H:3	CR_MC_B_3	CR_LFINF-CDL-5_H3	CR_LFINF+CDL+DUL_H3
CR/LFINF+CDL+LFC:5.0/H:4	CR_MC_B_4	CR_LFINF-CDL-5_H4	CR_LFINF+CDL+DUL_H4
CR/LFINF+CDL+LFC:5.0/H:5	CR_MC_B_5-7	CR_LFINF-CDL-5_H5	CR_LFINF+CDL+DUL_H5
CR/LFINF+CDL+LFC:5.0/H:6	CR_MC_B_5-7	CR_LFINF-CDL-5_H6	CR_LFINF+CDL+DUL_H6
CR/LFINF+CDL+LFC:5.0/HBET:7-20	CR_MC_B_>8	CR_LFINF-CDL-5_H6	CR_LFINF+CDL+DUL_H7
CR/LFINF+CDL+LFC:10.0/H:1	CR_MC_A_1	CR_LFINF-CDL-10_H1	CR_LFINF+CDL+DUL_H1
CR/LFINF+CDL+LFC:10.0/H:2	CR_MC_A_2	CR_LFINF-CDL-10_H2	CR_LFINF+CDL+DUL_H2
CR/LFINF+CDL+LFC:10.0/H:3	CR_MC_A_3	CR_LFINF-CDL-10_H3	CR_LFINF+CDL+DUL_H3
CR/LFINF+CDL+LFC:10.0/H:4	CR_MC_A_4	CR_LFINF-CDL-10_H4	CR_LFINF+CDL+DUL_H4
CR/LFINF+CDL+LFC:10.0/H:5	CR_MC_A_5-7	CR_LFINF-CDL-10_H5	CR_LFINF+CDL+DUL_H5
CR/LFINF+CDL+LFC:10.0/H:6	CR_MC_A_5-7	CR_LFINF-CDL-10_H6	CR_LFINF+CDL+DUL_H6

CR/LFINF+CDL+LFC:10.0/HBET:7-20	CR_MC_A_>8	CR_LFINF-CDL-10_H6	CR_LFINF+CDL+DUL_H7
CR/LFINF+CDM/H:1	CR_C_D_1	CR_LFINF-CDM-0_H1	CR_LFINF+CDM+DUL_H1
CR/LFINF+CDM/H:2	CR_C_D_2	CR_LFINF-CDM-0_H2	CR_LFINF+CDM+DUL_H2
CR/LFINF+CDM/H:3	CR_C_D_3	CR_LFINF-CDM-0_H3	CR_LFINF+CDM+DUL_H3
CR/LFINF+CDM/H:4	CR_C_D_4	CR_LFINF-CDM-0_H4	CR_LFINF+CDM+DUL_H4
CR/LFINF+CDM/H:5	CR_C_D_5-7	CR_LFINF-CDM-0_H5	CR_LFINF+CDM+DUL_H5
CR/LFINF+CDM/H:6	CR_C_D_5-7	CR_LFINF-CDM-0_H6	CR_LFINF+CDM+DUL_H6
CR/LFINF+CDM/HBET:7-20	CR_C_D_>8	CR_LFINF-CDM-0_H6	CR_LFINF+CDM+DUL_H7
CR/LFINF+CDM+LFC:4.5/H:1	CR_C_D_1	CR_LFINF-CDM-5_H1	CR_LFINF+CDM+DUL_H1
CR/LFINF+CDM+LFC:4.5/H:2	CR_C_D_2	CR_LFINF-CDM-5_H2	CR_LFINF+CDM+DUL_H2
CR/LFINF+CDM+LFC:4.5/H:3	CR_C_D_3	CR_LFINF-CDM-5_H3	CR_LFINF+CDM+DUL_H3
CR/LFINF+CDM+LFC:4.5/H:4	CR_C_D_4	CR_LFINF-CDM-5_H4	CR_LFINF+CDM+DUL_H4
CR/LFINF+CDM+LFC:4.5/H:5	CR_C_D_5-7	CR_LFINF-CDM-5_H5	CR_LFINF+CDM+DUL_H5
CR/LFINF+CDM+LFC:4.5/H:6	CR_C_D_5-7	CR_LFINF-CDM-5_H6	CR_LFINF+CDM+DUL_H6
CR/LFINF+CDM+LFC:4.5/HBET:7-20	CR_C_D_>8	CR_LFINF-CDM-5_H6	CR_LFINF+CDM+DUL_H7
CR/LFINF+CDM+LFC:9.0/H:1	CR_C_C_1	CR_LFINF-CDM-10_H1	CR_LFINF+CDM+DUM_H1
CR/LFINF+CDM+LFC:9.0/H:2	CR_C_C_2	CR_LFINF-CDM-10_H2	CR_LFINF+CDM+DUM_H2
CR/LFINF+CDM+LFC:9.0/H:3	CR_C_C_3	CR_LFINF-CDM-10_H3	CR_LFINF+CDM+DUM_H3
CR/LFINF+CDM+LFC:9.0/H:4	CR_C_C_4	CR_LFINF-CDM-10_H4	CR_LFINF+CDM+DUM_H4
CR/LFINF+CDM+LFC:9.0/H:5	CR_C_C_5-7	CR_LFINF-CDM-10_H5	CR_LFINF+CDM+DUM_H5
CR/LFINF+CDM+LFC:9.0/H:6	CR_C_C_5-7	CR_LFINF-CDM-10_H6	CR_LFINF+CDM+DUM_H6
CR/LFINF+CDM+LFC:9.0/HBET:7-20	CR_C_C_>8	CR_LFINF-CDM-10_H6	CR_LFINF+CDM+DUM_H7
CR/LFINF+CDM+LFC:12.0/H:1	CR_C_B_1	CR_LFINF-CDM-10_H1	CR_LFINF+CDM+DUM_H1

CR/LFINF+CDM+LFC:12.0/H:2	CR_C_B_2	CR_LFINF-CDM-10_H2	CR_LFINF+CDM+DUM_H2
CR/LFINF+CDM+LFC:12.0/H:3	CR_C_B_3	CR_LFINF-CDM-10_H3	CR_LFINF+CDM+DUM_H3
CR/LFINF+CDM+LFC:12.0/H:4	CR_C_B_4	CR_LFINF-CDM-10_H4	CR_LFINF+CDM+DUM_H4
CR/LFINF+CDM+LFC:12.0/H:5	CR_C_B_5-7	CR_LFINF-CDM-10_H5	CR_LFINF+CDM+DUM_H5
CR/LFINF+CDM+LFC:12.0/H:6	CR_C_B_5-7	CR_LFINF-CDM-10_H6	CR_LFINF+CDM+DUM_H6
CR/LFINF+CDM+LFC:12.0/HBET:7-20	CR_C_B_>8	CR_LFINF-CDM-10_H6	CR_LFINF+CDM+DUM_H7
CR/LFINF+CDM+LFC:16.5/H:1	CR_C_A_1	CR_LFINF-CDM-15_H1	CR_LFINF+CDM+DUM_H1
CR/LFINF+CDM+LFC:16.5/H:2	CR_C_A_2	CR_LFINF-CDM-15_H2	CR_LFINF+CDM+DUM_H2
CR/LFINF+CDM+LFC:16.5/H:3	CR_C_A_3	CR_LFINF-CDM-15_H3	CR_LFINF+CDM+DUM_H3
CR/LFINF+CDM+LFC:16.5/H:4	CR_C_A_4	CR_LFINF-CDM-15_H4	CR_LFINF+CDM+DUM_H4
CR/LFINF+CDM+LFC:16.5/H:5	CR_C_A_5-7	CR_LFINF-CDM-15_H5	CR_LFINF+CDM+DUM_H5
CR/LFINF+CDM+LFC:16.5/H:6	CR_C_A_5-7	CR_LFINF-CDM-15_H6	CR_LFINF+CDM+DUM_H6
CR/LFINF+CDM+LFC:16.5/HBET:7-20	CR_C_A_>8	CR_LFINF-CDM-15_H6	CR_LFINF+CDM+DUM_H7
CR/LFINF+CDN/H:1	CR_PC_1	CR_LFINF-CDN-0_H1	CR_LFINF+CDN+DNO_H1
CR/LFINF+CDN/H:2	CR_PC_2	CR_LFINF-CDN-0_H2	CR_LFINF+CDN+DNO_H2
CR/LFINF+CDN/H:3	CR_PC_3	CR_LFINF-CDN-0_H3	CR_LFINF+CDN+DNO_H3
CR/LFINF+CDN/H:4	CR_PC_4	CR_LFINF-CDN-0_H4	CR_LFINF+CDN+DNO_H4
CR/LFINF+CDN/H:5	CR_PC_5-7	CR_LFINF-CDN-0_H5	CR_LFINF+CDN+DNO_H5
CR/LFINF+CDN/H:6	CR_PC_5-7	CR_LFINF-CDN-0_H6	CR_LFINF+CDN+DNO_H6
CR/LFINF+CDN/HBET:7-20	CR_PC_>8	CR_LFINF-CDN-0_H6	CR_LFINF+CDN+DNO_H7
MUR/LWAL+CDN/H:1	M3_1	MUR/LWAL-DNO_H1	MUR+STRUB_LWAL+DNO_H1
MUR/LWAL+CDN/H:1/FC	M0_PC_1	MUR/LWAL-DNO_H1	MUR+STRUB_LWAL+DNO_H1
MUR/LWAL+CDN/H:1/FW	M0_PC_1	MUR/LWAL-DNO_H1	MUR+STRUB_LWAL+DNO_H1

MUR/LWAL+CDN/H:2	M3_2	MUR/LWAL-DNO_H2	MUR+STRUB_LWAL+DNO_H2
MUR/LWAL+CDN/H:2/FC	M0_PC_2	MUR/LWAL-DNO_H2	MUR+STRUB_LWAL+DNO_H2
MUR/LWAL+CDN/H:2/FW	M0_PC_2	MUR/LWAL-DNO_H2	MUR+STRUB_LWAL+DNO_H2
MUR/LWAL+CDN/H:3	M3_3	MUR/LWAL-DNO_H3	MUR+STRUB_LWAL+DNO_H3
MUR/LWAL+CDN/H:3/FC	M0_PC_3	MUR/LWAL-DNO_H3	MUR+STRUB_LWAL+DNO_H3
MUR/LWAL+CDN/H:3/FW	M0_PC_3	MUR/LWAL-DNO_H3	MUR+STRUB_LWAL+DNO_H3
MUR/LWAL+CDN/H:4/FC	M0_PC_4	MUR/LWAL-DNO_H4	MUR+STRUB_LWAL+DNO_H4
MUR/LWAL+CDN/H:4/FW	M0_PC_4	MUR/LWAL-DNO_H4	MUR+STRUB_LWAL+DNO_H4
MUR/LWAL+CDN/H:5/FC	M0_PC_5-7	MUR/LWAL-DNO_H5	MUR+STRUB_LWAL+DNO_H5
MUR/LWAL+CDN/H:5/FW	M0_PC_5-7	MUR/LWAL-DNO_H5	MUR+STRUB_LWAL+DNO_H5
MUR/LWAL+CDN/H:6/FC	M0_PC_5-7	MUR/LWAL-DNO_H6	MUR+STRUB_LWAL+DNO_H5
MUR/LWAL+CDN/HBET:7-20/FC	M0_PC_5-7	MUR/LWAL-DNO_H6	MUR+STRUB_LWAL+DNO_H5
UNK/CDL/H:1	M0_MC_1	MUR/LWAL-DNO_H1	MUR+STRUB_LWAL+DNO_H1
UNK/CDL/H:2	M0_MC_2	MUR/LWAL-DNO_H2	MUR+STRUB_LWAL+DNO_H2
UNK/CDL/H:3	M0_MC_3	MUR/LWAL-DNO_H3	MUR+STRUB_LWAL+DNO_H3
UNK/CDL/H:4	M0_MC_4	MUR/LWAL-DNO_H4	MUR+STRUB_LWAL+DNO_H4
UNK/CDL/H:5	M0_MC_5-7	MUR/LWAL-DNO_H5	MUR+STRUB_LWAL+DNO_H5
UNK/CDL/H:6	M0_MC_5-7	MUR/LWAL-DNO_H6	MUR+STRUB_LWAL+DNO_H5
UNK/CDL/HBET:7-20	M0_MC_5-7	MUR/LWAL-DNO_H6	MUR+STRUB_LWAL+DNO_H5
UNK/CDM/H:1	M0_C_1	MUR/LWAL-DNO_H1	MUR+STRUB_LWAL+DNO_H1
UNK/CDM/H:2	M0_C_2	MUR/LWAL-DNO_H2	MUR+STRUB_LWAL+DNO_H2
UNK/CDM/H:3	M0_C_3	MUR/LWAL-DNO_H3	MUR+STRUB_LWAL+DNO_H3
UNK/CDM/H:4	M0_C_4	MUR/LWAL-DNO_H4	MUR+STRUB_LWAL+DNO_H4

UNK/CDM/H:5	M0_C_5-7	MUR/LWAL-DNO_H5	MUR+STRUB_LWAL+DNO_H5
UNK/CDM/H:6	M0_C_5-7	MUR/LWAL-DNO_H6	MUR+STRUB_LWAL+DNO_H5
UNK/CDM/HBET:7-20	M0_C_5-7	MUR/LWAL-DNO_H6	MUR+STRUB_LWAL+DNO_H5
UNK/CDN/H:1	M0_PC_1	MR_LWAL-DUM_H1	MR_LWAL+DUM_H1
UNK/CDN/H:2	M0_PC_2	MR_LWAL-DUM_H2	MR_LWAL+DUM_H2
UNK/CDN/H:3	M0_PC_3	MR_LWAL-DUM_H3	MR_LWAL+DUM_H3
UNK/CDN/H:4	M0_PC_4	MR_LWAL-DUM_H4	MR_LWAL+DUM_H4
UNK/CDN/H:5	M0_PC_5-7	MR_LWAL-DUM_H5	MR_LWAL+DUM_H5
UNK/CDN/H:6	M0_PC_5-7	MR_LWAL-DUM_H5	MR_LWAL+DUM_H5
UNK/CDN/HBET:7-20	M0_PC_5-7	MR_LWAL-DUM_H5	MR_LWAL+DUM_H5

APPENDIX A.2 – DAMAGE TO LOSS MODEL PARAMETERS

Table A. 2 Damage to loss model parameters by building taxonomy

Building Taxonomy	$P_{lethal,dscollapse}$	c_f	$P_{entrapment,day}$	$P_{entrapment,night}$	$P_{LL,entrapment}$
CR_LFINF_CDN_0_H1	0.01	1	0.25	0.95	0.4
CR_LFINF_CDN_0_H2	0.01	1	0.5	0.95	0.4
CR_LFINF_CDN_0_H3	0.01	1	0.75	0.95	0.4
CR_LFINF_CDN_0_H4	0.01	1	0.75	0.95	0.4
CR_LFINF_CDN_0_H5	0.01	1	0.95	0.95	0.7
CR_LFINF_CDN_0_H6	0.01	1	0.95	0.95	0.7
CR_LFINF_CDN_0_HBET7-20	0.01	1	0.95	0.95	0.7
CR_LFINF_CDL_5_H1	0.01	2	0.25	0.95	0.4
CR_LFINF_CDL_5_H2	0.01	2	0.5	0.95	0.4
CR_LFINF_CDL_5_H3	0.01	2	0.75	0.95	0.4
CR_LFINF_CDL_5_H4	0.01	2	0.75	0.95	0.4
CR_LFINF_CDL_5_H5	0.01	2	0.95	0.95	0.7
CR_LFINF_CDL_5_H6	0.01	2	0.95	0.95	0.7
CR_LFINF_CDL_5_HBET7-20	0.01	2	0.95	0.95	0.7
CR_LFINF_CDL_10_H1	0.01	2	0.25	0.95	0.4
CR_LFINF_CDL_10_H2	0.01	2	0.5	0.95	0.4
CR_LFINF_CDL_10_H3	0.01	2	0.75	0.95	0.4
CR_LFINF_CDL_10_H4	0.01	2	0.75	0.95	0.4
CR_LFINF_CDL_10_H5	0.01	2	0.95	0.95	0.7
CR_LFINF_CDL_10_H6	0.01	2	0.95	0.95	0.7
CR_LFINF_CDL_10_HBET7-20	0.01	2	0.95	0.95	0.7
CR_LFINF_CDM_5_H1	0.01	1	0.25	0.95	0.4
CR_LFINF_CDM_5_H2	0.01	1	0.5	0.95	0.4
CR_LFINF_CDM_5_H3	0.01	1	0.75	0.95	0.4
CR_LFINF_CDM_5_H4	0.01	1	0.75	0.95	0.4
CR_LFINF_CDM_5_H5	0.01	1	0.95	0.95	0.7
CR_LFINF_CDM_5_H6	0.01	1	0.95	0.95	0.7
CR_LFINF_CDM_5_HBET7-20	0.01	1	0.95	0.95	0.7
CR_LFINF_CDM_10_H1	0.01	1	0.25	0.95	0.4
CR_LFINF_CDM_10_H2	0.01	1	0.5	0.95	0.4
CR_LFINF_CDM_10_H3	0.01	1	0.75	0.95	0.4
CR_LFINF_CDM_10_H4	0.01	1	0.75	0.95	0.4

CR_LFINF_CDM_10_H5	0.01	1	0.95	0.95	0.7
CR_LFINF_CDM_10_H6	0.01	1	0.95	0.95	0.7
CR_LFINF_CDM_10_HBET7-20	0.01	1	0.95	0.95	0.7
MUR_STDRE-LWAL_CDN_H1	0.01	3	0.25	0.95	0.4
MUR_STDRE-LWAL_CDN_H2	0.01	3	0.5	0.95	0.4
MUR_STDRE-LWAL_CDN_H3	0.01	3	0.75	0.95	0.4
MUR_STDRE-LWAL_CDN_H4	0.01	3	0.75	0.95	0.4
MUR_STDRE-LWAL_CDN_H5	0.01	3	0.95	0.95	0.7
MUR_STRUB-LWAL_CDN_H1	0.01	5	0.25	0.95	0.4
MUR_STRUB-LWAL_CDN_H2	0.01	5	0.5	0.95	0.4
MUR_STRUB-LWAL_CDN_H3	0.01	5	0.75	0.95	0.4
MUR_STRUB-LWAL_CDN_H4	0.01	5	0.75	0.95	0.4
MUR_STRUB-LWAL_CDN_H5	0.01	5	0.95	0.95	0.7

APPENDIX B.1 – FRAGILITY SOURCE

Table B. 1 Summary of fragility parameters for all building components

Category	Comp.	EDP	Source	DS1		DS2		DS3		DS4		DS5	
				θ	β	θ	β	θ	β	θ	β	θ	β
1	Interior beam-column joints	PSD	(Sengupta and Li 2014)	0.74	0.31	2.50	0.24	4.60	0.25	5.58	0.25		
			(Cardone 2016a)	0.65	0.40	1.75	0.35	3.00	0.30	0.65	0.40		
			(Pagni and Lowes 2006)	0.57	0.47	1.27	0.49	2.44	0.37	3.01	0.27	3.54	0.26
	Exterior beam-column joints		(Sengupta and Li 2014)	0.57	0.49	2.06	0.50	3.66	0.51	4.54	0.52	0.57	0.49
			(Cardone 2016a)	0.75	0.40	1.25	0.40	2.00	0.40	0.75	0.40	1.25	0.40
			(Cardone 2016a)	0.55	0.40	1.50	0.40	2.75	0.40	0.55	0.40	1.50	0.40
			(Pagni and Lowes 2006)	0.57	0.47	1.27	0.49	2.44	0.37	3.01	0.27	3.54	0.26
	Brittle columns		(Cardone 2016a)	0.95	0.30	1.25	0.40	2.00	0.40				
				0.65	0.30	0.85	0.40	1.50	0.40				
			(Ruiz-García and Ramos-Cruz 2024)	0.14	1.09	0.93	0.55	1.40	0.43	2.91	0.71		
			(Aslani and Miranda 2005)	0.35	0.37	0.71	0.44	2.00	0.58	3.10	0.63		
2	Infills	PSD		0.15	0.5	0.4	0.5	1	0.4	1.75	0.35		

		(Cardone and Perrone 2015)	0.1	0.5	0.3	0.5	0.75	0.4	1.75	0.35
			0.075	0.5	0.2	0.5	0.5	0.4	1.75	0.35
		(Sassun et al. 2016a)	0.18	0.52	0.46	0.54	1.05	0.4	1.88	0.38
			0.14	0.36	0.33	0.48	0.96	0.21	2	0.28
			0.16	0.68	0.44	0.7	0.97	0.58	1.33	0.55
		(Chiozzi and Miranda 2017)	0.10	0.11	0.30	0.26	0.80	0.34		
			0.14	0.33	0.34	0.29	0.84	0.33		
			0.12	0.30	0.34	0.30	0.88	0.26		
			0.12	0.36	0.32	0.30	0.74	0.29		
			0.14	0.27	0.33	0.22	0.85	0.33		
			0.11	0.30	0.28	0.29	0.81	0.37		
			0.13	0.33	0.35	0.26	0.84	0.29		
			0.15	0.22	0.35	0.22	0.87	0.35		
			0.10	0.11	0.30	0.26	0.80	0.34		
			0.14	0.33	0.34	0.29	0.84	0.33		
		(Del Gaudio et al. 2019)	0.08	0.8	0.33	0.4	0.89	0.5	1.59	0.4
			0.11	0.8	0.33	0.6	1.04	0.4	2.5	0.4
		Rossi et al. (2021)	0.2	0.35	0.3	0.35	1	0.35		
			0.2	0.35	0.3	0.35	1	0.35		
			0.3	0.35	0.5	0.35	1.75	0.35		
	PFA	Cardone and Perrone (2015)	0.65	0.35						
Partitions	PSD	Aslani and Miranda (2005)	0.4	0.56	0.78	0.27	1.1	0.25		
		(Retamales et al. 2013)	0.35	0.52	0.67	0.39	1.05	0.52		
			0.15	0.5	0.4	0.5	1	0.4		

			(Cardone and Perrone 2015, p. 201)	0.075	0.5	0.2	0.5	0.5	0.4
			(FEMA 2018a)	0.35	0.6	0.95	0.45	2.1	0.2
		PFA	(Cardone and Perrone 2015, p. 201)	0.65	0.21				
3	Plumbing and electrical system	PSD/PFA	*						
4	Windows and doors	PSD/PFA	*						
5	Concrete tiles	PFA	(FEMA 2018a)	0.5	0.4	0.7	0.4		
	Lighting			1	0.6				
	Sanitary Waste piping			1.2	0.5	2.4	0.5		

APPENDIX B.2 – WEIBULL FITTING COEFFICIENTS

Table B. 2 Weibull fitting coefficients (α, β and γ) derived for Storey Loss Functions (SLFs) by component category, expressed as a function of the Engineering Demand Parameter (EDP): Peak Storey Drift (PSD) and Peak Floor Acceleration (PFA)

Cat.		**1**	**2**		**3**		**4**	**5**
EDP		PSD	PSD	PFA	PSD	PFA	PSD	PFA
16th	α	1.00	0.99	0.90	0.93	0.81	0.93	0.90
	β	0.03	0.01	0.89	0.01	1.00	0.02	3.40
	γ	1.57	1.31	5.39	1.28	5.48	1.62	3.05
50th	α	0.98	0.99	0.93	0.98	0.91	0.98	0.94
	β	0.03	0.01	0.71	0.01	0.87	0.01	2.64
	γ	1.46	1.15	4.36	1.47	3.51	1.61	2.54
84th	α	0.98	0.99	0.93	0.97	0.89	0.97	0.94
	β	0.02	0.01	0.57	0.01	0.68	0.01	2.04
	γ	1.34	0.99	3.66	1.65	3.50	1.50	2.08
Mean	α	0.99	0.99	0.95	0.98	0.92	0.98	0.95
	β	0.02	0.01	0.70	0.01	0.78	0.01	2.57
	γ	1.38	1.07	3.26	1.35	3.01	1.31	2.11

Table B. 3 Weibull fitting coefficients (α, β and γ) derived for Storey Environmental Impact Functions (SEIFs) by component category, expressed as a function of the Engineering Demand Parameter (EDP): Peak Storey Drift (PSD) and Peak Floor Acceleration (PFA)

Cat.		**1**	**2**		**3**		**4**	**5**
EDP		PSD	PSD	PFA	PSD	PFA	PSD	PFA
16^{th}	α	0.95	0.98	0.92	0.92	0.83	0.95	0.91
	β	0.03	0.01	0.87	0.02	1.09	0.02	3.01
	γ	1.56	1.55	5.94	1.31	4.67	1.68	2.85
50^{th}	α	1.00	0.99	0.92	1.00	0.92	0.99	0.94
	β	0.02	0.00	0.72	0.01	0.89	0.01	2.34
	γ	1.37	1.32	4.42	1.14	3.48	1.54	2.38
84^{th}	α	0.98	1.00	0.95	0.98	0.94	0.98	0.95
	β	0.02	0.00	0.58	0.01	0.68	0.01	1.82
	γ	1.32	1.08	3.59	0.92	3.75	1.51	1.91
Mean	α	0.99	0.99	0.96	0.99	0.95	0.99	0.95
	β	0.02	0.00	0.70	0.01	0.80	0.01	2.28
	γ	1.31	1.18	3.25	1.01	2.86	1.33	2.00

Table B. 4 Weibull fitting coefficients (α, β and γ) derived for Portuguese Storey Loss Functions (SLFs) by component category, expressed as a function of the Engineering Demand Parameter (EDP): Peak Storey Drift (PSD) and Peak Floor Acceleration (PFA)

Cat.		**1**	**2**		**3**		**4**	**5**
EDP		PSD	PSD	PFA	PSD	PFA	PSD	PFA
16th	α	0.97	0.98	0.93	0.95	0.84	0.99	0.90
	β	0.03	0.01	0.87	0.01	1.10	0.02	3.34
	γ	1.61	1.36	6.66	1.35	3.75	1.60	2.99
50th	α	1.00	0.99	0.95	0.99	0.92	0.97	0.95
	β	0.03	0.01	0.72	0.01	0.90	0.01	2.63
	γ	1.46	1.17	4.34	1.47	3.03	1.67	2.44
84th	α	0.98	0.99	0.95	0.99	0.94	0.98	0.96
	β	0.02	0.01	0.59	0.01	0.67	0.01	2.03
	γ	1.38	1.02	3.83	1.63	4.01	1.52	2.05
Mean	α	0.99	0.99	0.97	0.99	0.95	0.99	0.96
	β	0.03	0.01	0.70	0.01	0.80	0.01	2.55
	γ	1.40	1.11	3.26	1.37	2.82	1.33	2.05

Table B. 5 Weibull fitting coefficients (α, β and γ) derived for Portuguese Storey Environmental Impact Functions (SEIFs) by component category, expressed as a function of the Engineering Demand Parameter (EDP): Peak Storey Drift (PSD) and Peak Floor Acceleration (PFA)

Cat.		**1**	**2**		**3**		**4**	**5**
EDP		PSD	PSD	PFA	PSD	PFA	PSD	PFA
16th	α	0.89	0.97	0.92	0.92	1.00	0.81	1.00
	β	0.03	0.01	0.85	0.85	0.02	1.09	0.02
	γ	1.76	1.60	6.39	6.39	1.28	4.47	1.93
50th	α	1.00	0.98	0.95	0.95	1.00	0.89	1.00
	β	0.03	0.00	0.71	0.71	0.01	0.89	0.01
	γ	1.42	1.31	4.66	4.66	1.14	3.79	1.63
84th	α	0.99	1.00	0.95	0.95	0.97	0.95	1.00
	β	0.02	0.00	0.58	0.58	0.01	0.68	0.01
	γ	1.28	1.09	3.78	3.78	0.93	4.00	1.50
Mean	α	0.99	0.99	0.96	0.96	0.98	0.94	0.98
	β	0.02	0.00	0.69	0.69	0.01	0.80	0.01
	γ	1.33	1.19	3.40	3.40	1.01	2.90	1.33

APPENDIX B.3 – REPAIR COST CONVERSION FACTOR (RCCF)

Table B. 6 Repair Cost Conversion Factor for all European Union countries having Italy as the reference country, adjusted to 2022 price levels

Country	r_{lab}	r_{mat}	$r_{m,p}$	r_{prod}	RCCF	
					Structural & architectural components	Non-structural components
Austria	1.54	1.08	1.00	0.82	1.46	1.14
Belgium	1.54	0.95	1.00	0.82	1.43	1.06
Bulgaria	0.26	0.52	1.00	1.22	0.44	0.61
Croatia	0.44	0.59	1.00	0.91	0.60	0.68
Cyprus	0.62	0.64	1.00	1.16	0.64	0.72
Czechia	0.59	0.65	1.00	0.80	0.75	0.75
Denmark	1.78	1.55	1.00	0.72	1.92	1.51
Estonia	0.66	0.63	1.00	0.86	0.76	0.74
Finland	1.49	1.22	1.00	0.83	1.47	1.22
France	1.45	1.11	1.00	0.74	1.51	1.17
Germany	1.38	1.03	1.00	0.83	1.35	1.09
Greece	0.47	0.68	1.00	0.80	0.68	0.75
Hungary	0.36	0.57	1.00	1.11	0.51	0.65
Ireland	1.42	0.85	1.00	0.82	1.31	0.97
Latvia	0.47	0.62	1.00	0.78	0.67	0.71
Lithuania	0.46	0.63	1.00	0.88	0.63	0.71
Luxembourg	1.30	1.05	1.00	1.02	1.15	1.06
Malta	0.50	0.85	1.00	1.51	0.61	0.84
Netherlands	1.61	0.88	1.00	0.91	1.34	1.00
Poland	0.43	0.70	1.00	1.00	0.61	0.75
Portugal	0.51	0.54	1.00	0.90	0.62	0.66
Romania	0.29	0.50	1.00	1.51	0.42	0.59
Slovakia	0.54	0.55	1.00	0.56	0.83	0.71
Slovenia	0.77	0.85	1.00	0.80	0.93	0.90
Spain	0.85	0.75	1.00	0.89	0.89	0.83
Sweden	1.59	1.43	1.00	0.86	1.58	1.37

Note: Cost fractions were defined as $f_{lab} = 0.15$(0.25), $f_{mat} = 0.50$(0.10), and $f_{m,p} = 0.35$(0.65), for structural/architectural and non-structural components, respectively.

APPENDIX C.1 – BUILDING INVENTORY

Table C. 1 Inventory of building components and their fragility function parameters

ID	Component	Source	EDP	Units	S_0	S_1	S_2	S_3	S_4
B1033.013a	Special Concentric Braced Frame w HSS braces, balanced design criteria, X Brace, Brace w < 40 PLF	(FEMA 2018b)	PSD	each	-	-	X	X	-
B1041.001a	Ductile Weak Column with lapped bars - Pre-1970's construction	(Cardone 2016b)		each	X	-	-	X	-
B1041.001b[a]	Ductile Weak Column retrofitted with FRP wrap	(FEMA 2018b)		each	-	X	X	X	X
B1046.001a	Non-Ductile Exterior Weak Beam-Column Joint with hooked round bars - Pre-1970's construction	(Cardone 2016b)		each	X	X	X	X	X
B1046.001c[b]	Exterior Beam Column Joint retrofitted with CFRP	(FEMA 2018b)		each	-	X	-	X	X
B1046.002a	Non-Ductile Interior Beam-Column Joint with Weak Column - Pre-1970's construction	(Cardone 2016b)		each	X	X	X	X	X
B1046.002c[b]	Interior Beam Column Joint retrofitted with CFRP	(FEMA 2018b)		each	-	X	-	X	X
B1051.001a	Unreinforced Masonry Infill - no windows, 100% masonry	(Sassun et al. 2016b)		m^2	X	-	-	-	-
B1051.001b[c]	Unreinforced Masonry Infill - no windows, 100% masonry - 1.3% drift seismic gap			m^2	-	X	X	X	X
B1051.002a	Unreinforced Masonry Infill - 34% windows, 66% masonry			m^2	X	X	-	-	X
B1051.002b[c]	Unreinforced Masonry Infill - 34% windows, 66% masonry - 1.3% drift seismic gap			m^2	-	-	X	X	-
B1051.003a	Unreinforced Masonry Infill - 66% windows, 34% masonry			m^2	X	-	-	-	-
B1051.003b[c]	Unreinforced Masonry Infill - 66% windows, 34% masonry - 1.3% drift seismic gap			m^2	-	X	-	-	X

B1051.003d	Unreinforced Masonry Infill - 66% windows, 34% masonry - 100mm EPS insulation - 1.3% drift seismic gap			m^2	-	-	X	X	-
B2021.001a[d]	Window in URM infill			m^2	X	-	-	-	-
B2021.001b[c,d]	Window in URM infill - 1.3% drift seismic gap				-	X	X	X	X
B2022.001	Curtain Walls - Generic Midrise Stick-Built Curtain wall, Config: Monolithic, Lamination: Unknown, Glass Type: Unknown, Details: Aspect ratio = 6:5, Other details Unknown	(FEMA 2018b)		m	X	X	X	X	X
C1021.001a[d]	Doors - subject to infill collapse	(Sassun et al. 2016b)		each	X	-	-	-	-
C1021.001b[c,d]	Doors - subject to infill collapse - 1.3% drift seismic gap			each	-	X	X	X	X
C2011.011b	Non-monolithic precast concrete stair assembly with concrete stringers and treads with no seismic joint.			each	X	-	-	-	-
C2011.011c[c]	Non-monolithic precast concrete stair assembly with concrete stringers and treads with 1.3% drift seismic gap			each	-	X	X	X	X
C3032.001b	Suspended Ceiling, SDC A,B,C, Area (A): 250 < A < 1000, Vert support only			m	X	X	X	X	X
C3034.001	Independent Pendant Lighting - non seismic			each	X	X	X	X	X
D2022.011a	Cold Water Piping - Small Diameter Threaded Steel - (2.5 inches in diameter or less), SDC A or B	(FEMA 2018b)	PFA	m	X	X	X	X	X
D2022.011a	Heating hot Water Piping - Small Diameter Threaded Steel - (2.5 inches in diameter or less), SDC A or B			m	X	X	X	X	X
D3021.001	Traditional Gas-Powered Boiler			each	X	X	X	X	X
D3041.101a	HVAC Fan - Capacity: all - Unanchored equipment that is not vibration isolated - Equipment fragility only		PFA	m	X	X	X	X	X
D3067.011a	Control Panel - Capacity: all - Unanchored equipment that is not vibration isolated - Equipment fragility only		PFA	each	X	X	X	X	X
E2022.020	Mobile Blackboards		PFA	each	X	X	X	X	X
E2022.021a	Electronic Blackboards		PFA	each	X	X	X	X	X

E2022.023	Desktop electronics including computers, monitors, stereos, etc, smooth surface		PFA	each	X	X	X	X	X
E2022.024a	Projector - suspended - non seismic		PFA	each	X	X	X	X	X
E2022.104a	Bookcase, 4 shelves, unanchored laterally		PFV	each	X	X	X	X	X
E2022.200a[d]	Chairs - subject to infill collapse	(Sassun et al. 2016b)	PSD	each	X	-	-	-	-
E2022.200b[c,d]	Chairs - subject to infill collapse - 1.3% drift seismic gap			each	-	X	X	X	X
E2022.201a[d]	Desks - subject to infill collapse			each	X	-	-	-	-
E2022.201b[c,d]	Desks - subject to infill collapse - 1.3% drift seismic gap			each	-	X	X	X	X

Note: PSD: Peak Storey Drift; PFA: Peak Floor Acceleration; PFV: Peak Floor Velocity

[a] *fragility based on FEMA B1041.001a - assumes that FRP wrapped column has similar performance to well detailed columns*

[b] *fragility based on FEMA 1041.001a - assumes that joint performs similarly to a code detailed joint.*

[c] *median plus 0.013 for seismic gap*

[d] *based on the DS4 of fragility B1051.001a.*